The Development of Phenotypic Screening Methods for Drug Discovery in Mitochondrial Dysfunction

Gareth Ettridge

BSc (Hons) MSc

Supervisors

Professor Robert Lightowlers

Professor Doug Turnbull

Doctor Oliver Russell

Thesis submitted for the degree of Doctor of Philosophy

Wellcome Centre for Mitochondrial Research

Newcastle University

June 2021

Abstract

This project both develops and employs high throughput phenotypic screening in the mitochondrial dysfunction research space. Initially, mitochondrial proliferation was investigated as it has emerged as a potential therapeutic pathway of interest. Collaborative efforts with the small biotechnology company, Nanna Therapeutics, have resulted in the screening of millions of bacterial natural product extracts for mitochondrial proliferation. The current project develops a multi-stage assay pipeline for the further screening of the hits identified in the work conducted by Nanna Therapeutics. A total of 10 hit extracts were identified, each capable of inducing increases in multiple parameters associated with mitochondrial biogenesis, in human cell lines. Four of the hits were selected for further investigation, as a result of maximal mitochondrial density increases being achieved with the minimum dose - in comparison with the remaining hit population.

Mutations affecting the assembly of mitochondrial complexes were also investigated in the project. Mitochondrial Complex I (CI) deficiency is the leading biological hallmark of mitochondrial disease. As such, a high throughput screen has been optimised for the identification of novel therapeutic agents for the rescue of CI deficiency. As a result of the screen optimisation process, the current project also demonstrates the activity of lead compound for CI deficiency rescue, MOA2. The developed CI immunofluorescent staining protocol was also applied to Mitochondrial Complex IV (CIV) and Mitochondrial Complex II. Successful optimisation of a quadruple immunofluorescent technique targeting CI, CII and CIV followed, which was used to further show novel effects of MOA2.

This project has given rise to multiple outputs. This thesis details the development of a high throughput assay pipeline for the discovery of small molecules capable of inducing mitochondrial proliferation, identifying ten hits. It has also demonstrated the effects of mitochondrial biogenesis on mitophagy. Finally, the current project has developed a novel *in* vitro method for the assessment of mitochondrial complex deficiencies in cells using immunofluorescent staining, with potential applications to the mitochondrial disease diagnostic space with further validation.

Acknowledgements

This Ph.D. was started with the single goal of improving the lives of those dealt an unfair genetic hand in the card game that is human existence. An insurmountable task for one person, but surrounded by an array of colleagues, friends and loved ones I believe that, thanks to this work, a new dent has appeared in the armour of mitochondrial diseases and metabolic dysfunction.

Firstly, I thank my supervisors Prof. R. Lightowlers, Prof. D. Turnbull and Dr. O. Russell for their guidance, patience and encouragement throughout the project.

Secondly, I thank my laboratory colleagues, fellow Ph.D. candidates and post-docs alike, for the comradery and support everyone at WCMR benefits from. Specifically, I would like to thank Mr. A. Creigh and Dr. S. Bell for their early practical tuition and later fruitful collaborations. I would also like to thank Dr. I. Ghouri, Dr. S. Ayyub and Dr. R. Temperley for their valuable scientific guidance and support, as well as tolerating my all too frequent “have a look at this awesome microscopy image/data set” moments and my many joyous outbursts, upon my successful data processing, right when they were trying to concentrate on their own work in the “Fishbowl” office.

This Ph.D. project has not only been an academic journey but one of great personal growth and development. For that reason, I finally, but most significantly, present my gratitude to one Miss Jennifer Howard:

Jen, you have been the constant source of support, courage and motivation throughout this toughest of academic endeavours, all while completing your own postgraduate qualifications and striding out into the tumultuous quagmire that is the working world. You are my equal and opposite, the steel that sharpens my own and the one person I could not live without. I owe my academic and personal successes in every capacity, present and future, to your support. Our love has grown since the moment we met. I am sure we will look back on this time and reminisce about the early days of the flat share, the day trips, the Oxford move as well as (at the time of writing) the eagerly anticipated best day of our lives. I will be forever grateful that we chose to do it all together, one step at a time, just you and I.

Author Declaration

This thesis is submitted for the degree of Doctor of Philosophy at Newcastle University. The research was conducted at the Wellcome Centre for Mitochondrial Research, under the supervision of Professor Robert N. Lightowlers, Professor Doug M. Turnbull, and Doctor Oliver Russell. All research is my own unless stated otherwise.

I certify that the research material in this thesis has not been previously submitted by me for a degree or any other qualification at this or any other University.

Chapter Specific Declarations and Comments

Chapter 3, bacterial extract libraries, used in mitochondrial biogenesis screening, were produced exclusively by the efforts of the staff at Nanna Therapeutics. Primary screens for inducers of mitochondrial biogenesis were also carried out by staff at Nanna Therapeutics.

Chapter 3 and Appendix A. Data processing R code used for flow cytometry analysis was originally authored by Doctor John Grady (Institute of Neuroscience, Newcastle University) and adapted for use in this project.

Chapter 4, mitoQC data analysis, and chapter 5, western blot analysis of steady-state mitochondrial complex levels, were kindly carried out by Dr. S. Bell (Wellcome Centre for Mitochondrial Research).

Chapter 5, maximal mitochondrial complex activity assays were kindly carried out by The Newcastle Highly Specialised Mitochondrial Diagnostic Service.

Chapter 5, the author acknowledges the omission of details pertaining to a lead compound of pharmacological interest for the future treatment of mitochondrial diseases. Such omissions were made to preserve the status of intellectual property surrounding the compound.

Table of Contents

Index of Tables

Index of Figures

Index of Abbreviations

ADP: Adenosine Diphosphate

AF: Alexa-Flour

ATP: Adenosine Triphosphate

BSA: Bovine Serum Albumin

CCCP: Cyanide m-chlorophenylhydrazone

CI, II, III, IV, V: Mitochondrial Complex I, II, III, IV, V

CNS: Central Nervous System

COX: Cytochrome Oxidase

DdCBEs: DddA-derived Cytosine Base Editors

DMSO: Dimethyl Sulphoxide

DNA: Deoxyribonucleic acid

ER: Endoplasmic Reticulum

FAD: Flavin Adenine Dinucleotide

$FADH_2$: Flavin Adenine Dinucleotide - Reduced

FAM: 6-carboxyfluorescein

FCCP: Cyanide-p-trifluoromethoxyphenylhydrazone

FeS: Iron-Sulphur (referring to Iron-Sulphur Clusters)

gRNA: Guide RNA

HT: High Throughput

HTS: High Throughput Screen

IBM: Inner Boundary Membrane

IMS: Intermembrane Space

KD: Knockdown

KO: Knockout

LHON: Leber's hereditary optic neuropathy

m-GFP: Mitochondrially Localising Green Fluorescent Protein

MAM: Mitochondria Associated Membrane

MCU: Mitochondrial Ca^{2+} Uniporter

MELAS: Mitochondrial Encephalopathy, Lactic Acidosis and Stroke-like episodes

MGB: Minor Grove Binder

MICOS: Mitochondrial Contact Site and Cristae Organizing System

MIM: Mitochondrial Inner Membrane

Mitochondrial Biogenesis: MB

MOA2: Mechanism of Action 2 – A lead compound for the rescue of mitochondrial complex I deficiency

MOM: Mitochondrial Outer Membrane

mtDNA: Mitochondrial DNA

mtTALENs: Mitochondrially localising Transcription Activator-Like Effector Nucleases

mtZFNs: Mitochondrially localising Zinc Finger Nucleases

NAD: Nicotinamide Adenine Dinucleotide

NADH: Nicotinamide Adenine Dinucleotide – Reduced

NARP: Neurogenic Muscle Weakness, Ataxia, and Retinitis Pigmentosa

NGS: Normal Goat Serum

NMDAS: Newcastle Mitochondrial Disease Scale for Adults

OR-1: Oliver Russel Extract 1 – A bacterial extract used as a positive control for mitochondrial biogenesis

OXPHOS: Oxidative Phosphorylation

PBS: Phosphate Buffered Saline

PBST: Phosphate Buffered Saline with TritonX100

P_i: Inorganic Phosphate

POI: Protein of Interest

rAAV: Recombinant Adeno-Associated Virus

RNA: Ribonucleic Acid

ROI: Region of Interest

ROS: Reactive Oxygen Species

rRNA: Ribosomal RNA

SEFA: Seahorse Extracellular Flux Analysis

TBS: Tris Buffered Saline

TBST: Tris Buffered Saline with Tween20

TCA: Tricarboxylic Acid

TFAM: Transcription Factor A Mitochondrial

TIM: Translocase of the Inner Membrane

TMRM: Tetramethylrhodamine

TOM20: Translocase of the Outer Membrane Subunit 20

tRNA: Transfer RNA

VIC: 2′-chloro-7′phenyl-1,4-dichloro-6-carboxy-fluorescein

WCMR: Wellcome Centre for Mitochondrial Research

WGS: Whole Genome Sequencing

Chapter 1:

Introduction

Mitochondria are double membrane bound organelles vital for the survival of complex eukaryotic cells. Formed from four distinct compartments, the outer and inner membranes, intermembrane space and matrix; mitochondria produce the majority of the cellular energy carrier molecule, adenosine triphosphate (ATP), through oxidative phosphorylation (OXPHOS). This is achieved through the utilisation of an electrochemical gradient of hydrogen ions (protons), and subsequent membrane potential, which is formed by the action of the three respiratory complexes pumping protons from the matrix into the intermembrane space. The active movement of protons from the matrix, across the mitochondrial inner membrane (MIM) into the intermembrane space (IMS), results in an increase in pH within the matrix relative to the IMS and cytosol, as well as a localised relative negative charge within the matrix - the membrane potential.

The establishment and maintenance of the membrane potential not only supports the OXPHOS process, but it is critical for an array of additional mitochondrial functions – both directly and indirectly through the support of mitochondrial protein import. These functions include calcium homeostasis, reactive oxygen species (ROS) signalling, steroid synthesis, Iron-Sulphur (FeS) cluster synthesis and apoptotic regulation.

Due to their vital importance in multiple essential cellular pathways, mitochondria present as vulnerable targets of disease. As mitochondria harbour their own DNA, genetic mutations can arise in either nuclear or mitochondrially encoded proteins. This is only one of the complicating factors that impacts the clinical presentation of mitochondrial diseases, and the efforts being made to discover much needed therapeutic options for patients.

The following chapter details current knowledge surrounding mitochondria, their form, function and dysfunctions, as well as currently available therapeutic options and treatments under research.

1.1 Mitochondrial Evolution

The development of the mitochondrion as an intracellular organelle in the eukaryotic cell has been recognised as a vital turning point in the evolution of complex life (Margulis, 1971, Gray et al., 1999, Gray et al., 2001, Falkenberg et al., 2007, Blackstone, 2015). The most widely accepted theory explaining this energetic breakthrough is that of endosymbiosis - the engulfment and assimilation of one organism into another for their mutual benefit. The most likely partners for endosymbiosis are an α-proteobacteria (pre-mitochondria) and an archaean (pre-eukaryotic host). Evolutionary advantage is thought to have emerged as a result of pre-mitochondria specialising into metabolic roles, while the pre-eukaryotic host ensured survival (Lane and Martin, 2010, Blackstone, 2015, Martin et al., 2015).

The size of the mitochondrial genome, its mechanism of replication and gene expression bear striking similarities to bacterial processes. The simplicity of mtDNA structure and packaging, the nature of the mtDNA replication, a lack of introns in RNA's and (initially) polycistronic transcripts all indicate a prokaryotic origin (these topics are explored in depth in section 1.4). These observations provide evidence supporting the widely accepted theory of the ancient endosymbiotic origin of mitochondria.

1.2 Mitochondrial Structure

The hallmark of mitochondrial structure is an envelope of lipid bilayer membranes. Individual mitochondria exhibit continual fusion and fission activity in the cell, creating a dynamic network of interconnected mitochondria and individual puncta. Three respiratory complexes of the inner membrane contribute to the creation of the proton motive force, through the pumping of hydrogen ions from the matrix into the inter-membrane space (IMS), which is maintained by the impermeable nature of the mitochondrial inner membrane. The movement of hydrogen ions out of the matrix results in a higher pH in the matrix, relative to the IMS, which generates a potential difference of approximately 180mV across the inner membrane (Chen, 1988). The resulting disparity in pH between the IMS and the matrix is the single most important property of mitochondria, as it directly facilitates all mitochondrial functions. The mitochondrion consists of a total of two membranes and two compartments, each of which are briefly outlined below.

1.2.1 Composition of the Mitochondrial Outer Membrane

The mitochondrial outer membrane (MOM) largely separates the whole mitochondrion from the cytosol, though it remains permeable to any molecules smaller than 5kDa and allows the passage of small molecule metabolites through the Voltage Dependent Anion Channel (VDAC). The regulation of ions through VDAC has been shown to mediate mitochondrially driven apoptosis (Shoshan-Barmatz et al., 2010).

The MOM itself comprises a wide variety of phospholipids, though phosphatidylcholine (40%) and phosphatidylethanolamine (26%) are the largest contributors to the MOM (Zinser et al., 1991). These, and low levels of cardiolipin, have been shown to aid in the formation of membrane-embedded complexes such as the translocase of the outer membrane (TOM) complex (Gebert et al., 2009, Osman et al., 2011, Aaltonen et al., 2016). The majority of phospholipids that make up the mitochondrial membranes are synthesised in the endoplasmic reticulum (ER) (Kennedy, 1958, Cigana and Bakovic, 2014, Schenkel and Bakovic, 2014), which are directly transferred from ER membranes to the MOM at ER-MOM interface sites – shown in yeast to be tethered by complexes of ER proteins (Mmm1) and MOM proteins (Mdm34, Mdm10, and Mdm12) (Osman et al., 2011). Recent advances have identified the mammalian ortholog of Mmm1 as PDZD8 (Hirabayashi et al., 2017). Mitochondria are known to synthesise a wide range of phospholipids and small molecules to maintain membrane

composition (Osman et al., 2011, Schenkel and Bakovic, 2014). The MOM plays a vital role in the dynamic nature of the structure of the mitochondrial network and the import of mitochondrial proteins from the cytosol – detailed in sections 1.3 and 1.5 respectively.

1.2.2 Composition of the Mitochondrial Inner Membrane

Much like the MOM, the mitochondrial inner membrane (MIM) is composed of phospholipids synthesised in both the ER and mitochondrial matrix (Zinser et al., 1991). Phospholipids are first transferred to the MOM from the ER, then transported to the MIM by SLMO2-TRIAP1 complexes (Aaltonen et al., 2016). Cardiolipin, a phospholipid concentrated in the MIM, plays an important structural role in protein complexes, with evidence suggesting that protein super-complexes - higher order structures of CI, CIII and CIV bound together (Dudkina et al., 2010) discussed in section 1.6.1 - are destabilised in mitochondria deficient in cardiolipin (Pfeiffer et al., 2003, Mileykovskaya and Dowhan, 2014, Paradies et al., 2014).

A key feature of the MIM is multiple densely packed invaginations, known as cristae (Stephan T et al., 2019). Cristae project into the interior space of the mitochondrion (the matrix) and act to maximise the surface area available for components of the respiratory chain. This compartmentalises in MIM into two distinct sub-sections: the inner boundary membrane and the cristae membrane. Cristae are formed by the mitochondrial cristae organizing system (MICOS) complexes constructing rings in the inner membrane – from which a phospholipid bilayer can project (Rampelt H et al., 2017, Kondadi et al., 2020). Oligomers of dimeric mitochondrial Complex V (CV) act to provide structure to the cristae membranes, defining the curvature of the structure (Strauss et al., 2008, Rampelt H et al., 2017, Spikes et al., 2020). MICOS complexes have been shown to completely separate the inner boundary membrane from the intra-cristae space, forming cristae junctions, and thereby allow each crista to form a proton motive force that is independent of its' neighbours (Wolf et al., 2019). Cristae are by no means static and have been shown to continuously remodel to best meet the needs of the cell at a given moment (Kondadi et al., 2020). The MICOS complexes also act as contact sites between the MOM and the MIM to contribute to overall mitochondrial structure and allow the formation of complexes of protein import machinery; discussed in section 1.6 (Hoppins et al., 2011, Hovarth et al., 2015).

The MIM is one of the most protein rich biological membranes, with a protein:lipid ratio of 3:1 (Vogel et al., 2006). The cristae exhibit a significantly different protein population than the inner boundary membrane (IBM) - the cristae contain the majority of the respiratory complexes, while the IBM holds more protein import machinery (e.g. TIM subunits) (Vogel et al., 2006). The TIM complex acts in concert with the TOM complex to facilitate protein translocation from the cytosol to the mitochondrial matrix (Wiedemann and Pfanner, 2017) - outlined in forthcoming sections.

1.2.3 The Intermembrane Space

The intermembrane space (IMS) has been recently shown to be divided into two distinct regions – the boundary membrane space and multiple sub-compartments: the intra-cristae spaces (Wolf et al., 2019, Kondadi et al., 2020). While the boundary membrane space is in equilibrium with the cytosol, the intra-cristae spaces, surrounded by impermeable MIM, allow for the accumulation of protons that provide the electrochemical gradient to drive ATP synthesis through Complex V, via the process of oxidative phosphorylation. A large stress placed upon mitochondria, such as inhibition of Complex I, using the small molecule rotenone or the mitochondrial uncoupler carbonyl cyanide-p-trifluoromethoxyphenylhydrazone (FCCP), is known to induce mitochondrial fragmentation (De Vos et al., 2005, Tauber et al., 2013) through mitochondrial fission (discussed in section 1.3.1). The risk of membrane potential loss is divided amongst multiple units through the creation of small mitochondrial puncta. This also more easily facilitates the targeted degradation of dysfunctional mitochondrial material, mitophagy (discussed in section 1.5.2), to allow for the re-formation of the mitochondrial network with remaining healthy mitochondrial matter.

The IMS also plays a role in the import of proteins from the cytosol, harbouring multiple chaperone proteins for the trafficking of mitochondrial proteins to appropriate compartments of the mitochondrion. Protein import to mitochondria relies on contact sites between the MOM and the MIM across the IMS. Protein import is discussed in greater detail in section 1.5.2.

1.2.4 Mitochondrial Matrix

The aqueous space enclosed by the MIM is known as the mitochondrial matrix. Cristae project into the matrix creating densely packed lamella-like plate structures along lengths of mitochondria (Stephan T et al., 2019). The mitochondrial matrix plays host to all proteins involved in mitochondrial gene expression, housing mtDNA nucleoids, RNA granules and ribosomes within spaces between these large cristae structures (Tauber et al., 2013, Stephan T et al., 2019). Mitochondrial DNA and gene expression are discussed in section 1.4.

The mitochondrial matrix is the site of the Krebs cycle – a large interconnected series of redox reactions that generate reduced electron carriers (NADH and $FADH_2$), to be oxidised by the respiratory chain complexes to provide protons for the formation of the proton motive force (Robinson et al., 1987, Schroeder et al., 2009). The matrix also houses all enzymes necessary for an array of additional mitochondrial functions, including β-oxidation of fatty acids, the urea cycle, and the formation of iron-sulphur (FeS) clusters. These multiple functions of the mitochondrial are discussed in section 1.6.

1.3 Mitochondrial Morphology and Dynamics

Mitochondria often exist within the cell as an extensive dynamic network (Bereiter-Hahn and Voth, 1994, Chan, 2012, Youle and Bliek, 2012). The two extremes of multiple punctate spheroids and one complete interconnected network are balanced using fission and fusion mechanisms. These act in combination to bring about optimal mitochondrial morphology in a given environment (Sukhorukov et al., 2012, Rafelski, 2013).

Inhibition of fission machinery leaves the mitochondrion in a more interconnected network, while a reduction in the levels of fusion results in the fragmentation of the network into small puncta (Chan, 2012). These findings suggest that the two processes are constantly acting antagonistically to each other, rather than one or the other being activated as required.

1.3.1 Mitochondrial Fission

Human mitochondrial fission is brought about by the action of the cytosolic GTP-ase Dynamin Related Protein 1 (Drp1) (Elgass et al., 2013, Prudent and McBride, 2016). Drp1 is recruited to the MOM by MiD51, a receptor on the cytosolic surface of the MOM (Ma et al., 2019). Under basal conditions, MiD51 is monomeric in the MOM resulting in GTP-bound Drp1 being minimally recruited. The dimerisation of MiD51 increases its binding affinity for Drp1, recruiting oligomeric Drp1 (Ma et al., 2019). Hydrolysis of GTP by Drp1 further increases interaction strength between MiD51 and Drp1, allowing the formation of a fission complex of Drp1 which encircles the targeted mitochondrion leading to fission (Youle and Bliek, 2012, Prudent and McBride, 2016, Ma et al., 2019). The constriction of Drp1 around the circumference of the mitochondrion is sufficient to cleave both the MOM and the MIM. The exact mechanism behind the targeting of specific fission sites remains elusive, however links have been drawn between ER-mitochondrial contact sites stimulating fission events (Prudent and McBride, 2016).

1.3.2 Mitochondrial Fusion

Fusion is mediated using three proteins, mitofusin (Mfn) 1 and 2, responsible for outer membrane fusion, and Optic Atrophy Protein 1 (OPA1) which controls inner membrane fusion (Chan, 2012, Youle and Bliek, 2012).

Mfn1 and 2 are functionally degenerate MOM spanning proteins, which contain a GTP-ase domain and two hydrophobic repeat domains. Mfn1 and Mfn2 KO cells exhibit fragmented mitochondria and a lack of fusion activity; the overexpression of either protein is sufficient to restore healthy mitochondrial morphology (Griffin et al., 2006). Mfn positive mitochondria cannot fuse with Mfn null mitochondria, thus the presence of either mitofusin protein, but not necessarily both forms, is required for mitochondrial fusion (Koshiba et al., 2004). All domains of the Mfn proteins are required for mitochondrial fusion, truncated Mfn lacking the GTP-ase domain results in tightly grouped clumps of punctate mitochondria (Koshiba et al., 2004). This is because GTP-ase activity is required to induce the oligomerisation of mitofusin proteins (Chan, 2012, Ranieri et al., 2013). The hydrophobic domains of Mfns are instrumental in tethering mitochondrial membranes together, forming dimers across trans-MOM spaces to allow fusion (Koshiba et al., 2004, Ranieri et al., 2013).

The fusion of the MIMs of two mitochondria is dependent on the successful fusion of the two MOMs. OPA1 is a member of the dynamin protein family found in the MIM which, like Drp1, contains a GTP-ase domain (Guillery et al., 2008, Chan, 2012). The GTP-ase activity of OPA1 increases upon the formation of homo-multimeric complexes, which lead to membrane fusion (Chan, 2012). Unlike mitofusin proteins, OPA1 is not required on both MIMs of fusing mitochondria – only one OPA1 positive MIM is required (Song et al., 2009). Despite this, OPA1 has been shown to interact with Mfn1/2, mechanistically linking outer and inner mitochondrial membrane fusion to complete the fusion process (Guillery et al., 2008).

As well as being essential for MIM fusion, OPA1 has also been linked to the formation of mitochondrial cristae, with knockdowns of OPA1 resulting in abnormal cristae morphology and a reduction in respiration rate (Frezza et al., 2006, Chan, 2012, Ranieri et al., 2013).

The dynamic nature of the mitochondrial network serves to optimise the activity of the organelles and allow for the selective degradation of dysfunctional material. The fission of an area of network with a reduced membrane potential allows for its targeted

degradation, without affecting the remaining material. Highly fractured networks also spread the burden of chemical insults and mitochondrial stress across multiple smaller units, limiting their deleterious effects on the cell. Highly fused networks have been found to exhibit greater ATP output than equivalent areas of punctate spheroids, having a greater internal surface area suitable to be used to house crista membranes. Extensive networks also facilitate improved translocation of material within networks – allowing the distribution of mitochondrially synthesised proteins (Hoitzing et al., 2015).

Hyper-fusion of mitochondria is noted in cells under starvation conditions, hypothesised to be an attempt to best optimise nutrient use given limited availability and protect them from autophagosome engulfment to maintain cell viability (Gomes et al., 2011). This hypothesis is linked to calcium ion handling (discussed in section 1.6.5), in that fused networks have been modelled to show that calcium diffuses from the endoplasmic reticulum (ER) into a greater mitochondrial area in comparison to fissile mitochondria. This is proposed to allow for the control of calcium concentrations to optimise ATP synthesis: calcium does not reach fragmented material, while hyper-fusion serves to 'dilute' calcium in a greater volume of mitochondria. Optimum calcium handling, under basal conditions, is proposed to occur when mitochondria exhibit both fusile and fissile behaviour (Hoitzing et al., 2015).

It can be concluded that a balance of fusion and fission, resulting in a dynamic mitochondrial network, is required for healthy cellular responses to ever-changing environmental stimuli and challenges.

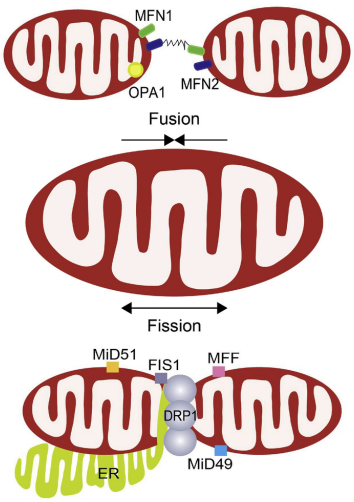

Fig 1.1 *A schematic of the basic processes of mitochondrial fission and fusion (Liu et al., 2020)*

1.4 Mitochondrial DNA and Protein Expression

1.4.1 The Mitochondrial Genome

Mitochondrial DNA is held within the mitochondrial matrix, as single molecules of DNA arranged as loops, similar to prokaryotes. Mitochondria are polyploid: the copy number of the mitochondrial genome present in a single cell can range from 100 to 500,000, dependent on cell type (Reynier et al., 2001, Zhang et al., 2017b). mtDNA molecules are packaged in a coat of Mitochondrial Transcription Factor A (TFAM), essential for mtDNA replication and transcription (Alam et al., 2003). Again, similar to prokaryotic DNA and unlike eukaryotic DNA, which is abundant in non-coding regulatory regions, the vast majority of mtDNA is coding. Each mitochondrial genome molecule contains 37 genes, formed from 16,569 base-pairs, of which 13 encode proteins; subunits of the components of the oxidative phosphorylation (OXPHOS) machinery (Anderson et al., 1981, Gustafsson et al., 2016). The remaining 24 mtDNA gene products consist of 22 transfer RNAs (tRNAs) and 2 ribosomal RNAs, which are essential for the translation of the afore mentioned 13 mitochondrial proteins (Anderson et al., 1981, Lightowlers et al., 2015). The two mtDNA strands have been named “Heavy” and “Light”, due to markedly different total molecular masses; the heavy strand contains more purine bases than the light strand. Both the heavy and light stands of mtDNA code for genes. The light strand codes for MT-ND6, and eight of the 22 mt-tRNA’s (Anderson et al., 1981), while the heavy strand codes for the remainder of the mt-tRNA’s (Falkenberg et al., 2007, Temperley et al., 2010).

1.4.2 Mitochondrial DNA Inheritance

Mitochondrial DNA is inherited exclusively through the maternal line in humans (Wei and Chinnery, 2020). Examples of non-maternal mtDNA inheritance have been shown in other species; some plants acquire DNA from pollen, while some molluscs exhibit doubly uniparental inheritance - males of the species inherit mtDNA solely from the paternal line (Ladoukakis and Zouros, 2017). Mammalian mtDNA maternal inheritance is enforced through the rapid ubiquitination and degradation of sperm mitochondria, upon fertilisation of the oocyte (Sutovsky et al., 1999). Before fertilisation, mtDNA is subject to a bottleneck, in that all cells in the resulting human originate from one oocyte, containing select mitochondria. In the case of healthy mothers, this effect is irrelevant, however, there are great implications for female mitochondrial disease patients seeking to have children (Carling et al., 2011) – discussed in section 1.8.2.

1.4.3 Mitochondrial DNA Replication

The core protein of mtDNA replication is DNA Polymerase γ (POLγ), which in humans is a heterotrimer between one POLγA, and two copies of POLγB (Fan et al., 2006). The machinery of mtDNA replication as a whole resembles those found in bacteriophages, potentially indicating bacterial origin, having acquired genes from bacteriophage attack, while human POLγA shares its family with bacterial DNA polymerase I (Shutt and Gray, 2006, Gustafsson et al., 2016).

The majority of regulatory elements in mtDNA are contained in a single non-coding region: the D Loop, with the notable exception of the Light Strand Origin of Replication (O_L) at approximately 11,000bp downstream of the D-Loop (Falkenberg et al., 2007). The D Loop is flanked on at the 5' end by the three CSBs and on the 3' end by the Termination Associated Sequence (TAS) site. The exact mechanism of mtDNA replication remains contested, however, the single strand displacement model predominates over others (Robberson et al., 1972, Clayton, 1982, Gustafsson et al., 2016).

In this model, mtDNA replication begins with RNA primer formation facilitated by POLRMT, TFAM and TFB2 at the light strand promoter (LSP), spanning three Conserved Sequence Boxes (CSBs). The RNA primer is required for the initiation of replication at the Heavy Strand Origin of Replication (O_H) (Gustafsson et al., 2016). Transcription proceeds from the LSP forming a G-quadruplex structure of nascent RNA and non-template DNA strand between CSBs 3 and 1, resulting in premature transcription termination at CSB2 giving the RNA primer (Falkenberg, 2018). Mitochondrial Transcription Elongation Factor is proposed to act as a regulator in this process, its activity is hypothesised to prevent or allow the continuation of transcription, covered in section 1.4.5 (Agaronyan et al., 2015). Initiation of replication from the RNA primer in the D Loop often terminates at the TAS site, producing a 650 nucleotide long section of DNA known as 7S DNA, which remains bound to the L-Strand forming a short triplex stretch, which displaces the nascent H-Strand and gives the D Loop its name (Falkenberg, 2018). With this structure in place, DNA replicating POLγ stalls at the 3' end of the D Loop; the mtDNA helicase TWINKLE then acts as a key regulator in allowing DNA replication to move past the TAS, through a currently unelucidated mechanism (Falkenberg, 2018). TWINKLE occupancy in the D-Loop is low under basal conditions but increases with low mtDNA copy number to remove the 7S DNA and allow POLγ to bind and continue DNA synthesis (Jemt et al., 2015).

DNA replication facilitated by POLγ proceeds as the mtDNA helicase TWINKLE unwinds the mtDNA double helix, traveling in the 5' to 3' direction with POLγ (Korhonen et al., 2004). During this process, the parental H strand exists as a single strand, vulnerable to sporadic and unregulated transcription. This is prevented by the association of mitochondrial single-stranded DNA-binding protein (mtSSB) (Miralles Fuste et al., 2014). Once DNA replication reaches the Light Strand Origin of Replication (O_L), the parental Heavy Strand forms a stem-loop at the O_L site, preventing the association of mtSSB. This action allows POLRMT to bind and produce the primer required for DNA synthesis of a new light strand (Gustafsson et al., 2016). The synthesis of daughter strands of DNA continues until both have completed a full copy of the mtDNA genome. As replication proceeds, daughter strand synthesis is proofread by an exonuclease domain of POLγA; incorrect base pairing results in the reversal of POLγ progression, the excision and replacement of falsely bound nucleotides (Macao et al., 2015). For DNA synthesis to complete a circuit of the genome, RNA primers, used to initiate DNA replication, are removed by RNase H1 and MGME1 (Gustafsson et al., 2016, Nicholls and Gustafsson, 2018). Upon a complete cycle of the mtDNA genome POLγ exhibits idling activity; the synthesis and subsequent excision of a small number of nucleotides in the region preceding the 5' end of newly synthesised DNA (Macao et al., 2015, Gustafsson et al., 2016). DNA ligase III then creates a phosphodiester bond between juxtaposed 3' and 5' ends of daughter DNA strands. Effective termination of mtDNA replication is dependent on exonuclease activity of POLγ, without such activity DNA synthesis proceeds into duplex DNA, creating a substrate incompatible for DNA ligase III (Macao et al., 2015).

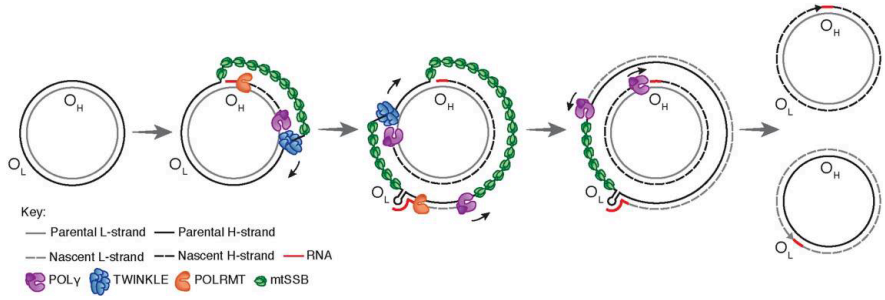

Fig 1.2. *The strand displacement model of mtDNA replication (Falkenberg, 2018).*

This mode of replication results in the concatenation of the two daughter mtDNA molecules at O_H (Nicholls and Gustafsson, 2018, Nicholls et al., 2018). This complex of mtDNA molecules, interlinked by a single strand, is resolved by Top3α – a type IA topoisomerase localised to both the nucleus and mitochondrial matrix (Nicholls et al., 2018). Cells subject to a knockdown of Top3α exhibit reduced mtDNA copy number highly concatenated nucleoids by EM (Nicholls et al., 2018).

1.4.4 Mitochondrial Transcription

Mitochondrial RNAP (POLRMT) is a single polypeptide, which contains several conserved motifs shared with bacteriophage RNAP enzymes (Masters et al., 1987, Titranti et al., 1997). The small size of POLRMT further contrasts the much larger complexes observed in eukaryotes (Nogales et al., 2017). POLRMT only becomes transcriptionally active when associated with TFAM and mitochondrial transcription factor 2 (TFB2M) (Falkenberg et al., 2002, McCulloch et al., 2002). All transcription of mtDNA begins within the D Loop (Falkenberg et al., 2007, Gustafsson et al., 2016). The distinct absence of multiple regions of non-coding DNA, serving as binding sites for activators or repressors for gene expression regulation, contrasts its eukaryotic nuclear counterpart (Lee and Young, 2000). Again resembling prokaryotic systems, transcription from mtDNA initially results in polycistronic RNA (Sarkar, 1997, Falkenberg et al., 2007). Transcription which commences on the Light Strand Promotor (LSP) in the D-Loop, when facilitated by active Mitochondrial Transcription Elongation Factor (TEFM) (Agaronyan et al., 2015), results in the synthesis of a single polycistronic RNA molecule encoding one mRNA encoding MT-ND6, and eight of the 22 mt-tRNA's (Falkenberg et al., 2007, Temperley et al., 2010). Transcription initiation at the H site promoter (HSP) generates a large polycistronic RNA molecule encoding all genes on the heavy strand of mtDNA (Falkenberg et al., 2007, Temperley et al., 2010). The polycistronic RNAs are immediately processed in RNA granules in close proximity to mtDNA nucleoids (Jourdain et al., 2013, Jourdain et al., 2016): RNA cleavage normally occurs at 5' and 3' ends of tRNA genes, by RNases P and Z respectively, resulting in monocistronic mt-mRNAs, with the notable exceptions of ATP6/8 and ND4/ND4L (Sarkar, 1997, Temperley et al., 2010, Hallberg and Larsson, 2014). The majority of mt-mRNA species are then polyadenylated, adding approximately 50 nucleotides to each molecule, with two exceptions of ND5 and the mt-rRNAs – gaining <10 nucleotides each (Temperley et al., 2010).

1.4.5 Mitochondrial Translation

Mitochondria contain all the machinery necessary for functional protein synthesis, though all protein components are encoded by the nucleus (Roodyn et al., 1961, Lightowlers et al., 2014). The Svedberg value, a measure of ribosomal density, for the mitochondrial ribosome (mitoribosome), is 55S, lower than both prokaryotic ribosomes (the 70S) and eukaryotic ribosomes (80S) (Kapp and Lorsch, 2004, Rodnina, 2018). Mitoribosomes are composed of a 28S small subunit, containing one rRNA (12S) and 30 proteins, and a 39S large subunit formed from one rRNA (16S), 53 proteins and a structural tRNAVal (Greber et al., 2015, Amunts et al., 2015). The lower Svedberg value, indicative of a reduced density, of the mitoribosome, is due in part to the inversion of the ratio of RNA:Protein relative to others: from 2:1 in the cytosol to 1:2 in the mitochondrial matrix (Lightowlers et al., 2014). Much of the rRNA, present in other examples of ribosomes, has been lost in mitoribosomes, with some spatial voids filled with additional polypeptides with no orthologs – other voids remain resulting in a relatively porous structure relative to other ribosomes, which further contributes to the low density of mitoribosomes (Sharma et al., 2003, Greber et al., 2014, Lightowlers et al., 2014). Despite clear similarities to bacterial translation systems, distinct differences are apparent. Newly transcribed mRNA enters into RNA granules, found adjacent to mtDNA nucleoids (Iborra et al., 2004, Pearce et al., 2017), for processing and maturation (Antonicka and Shoubridge, 2015, Jourdian et al., 2016). Therefore, co-transcriptional translation - common in prokaryotes - is highly unlikely to occur in mitochondria (Kohler et al., 2017). Many other features present in bacteria, such as Shine-Dalgarno sequences to aid with the correct loading of mRNA to ribosomes, are not found in mitochondrial translation (Ma et al., 2002, Lightowlers et al., 2014). Sites of mitochondrial translation from mature mt-mRNAs, from RNA granules, are localised at cristae membranes and are spatially distinct from RNA granules themselves (Zorkau et al., 2021).

All proteinaceous translational machinery is coded for in the nucleus and imported into mitochondria from the cytosol, with the notable exceptions of mt-tRNA's and both mt-rRNAs (Temperley et al., 2010). As well as all mitochondrial ribosomal proteins, these imported proteins include two initiation and two elongation factors, as well as one canonical termination factor and all enzymes required for post-transcriptional modification of proteins, mitoribosome assembly, mitoribosome turnover and all required tRNA synthetases (Gray, 2012, Lightowlers et al., 2014).

1.5 Mitochondrial Turnover and Degradation of Aberrant Mitochondrial Proteins

Mitochondrial material is in a state of constant turnover. New mitochondrial material is synthesised (mitochondrial biogenesis) while dysfunctional mitochondria are degraded (mitophagy). This turnover allows the cell to maintain a healthy population of mitochondria, and so is critical to the adaptation of cells to a dynamic environment (Zhu et al., 2013).

1.5.1. Mitochondrial Biogenesis

Mitochondrial biogenesis (MB) requires the co-ordinated action of both nuclear and mitochondrial genomes, as well as the *de-novo* synthesis of lipids for the formation of new mitochondria.

Several transcription factors and co-activators have been identified that are associated with mitochondrial biogenesis. These include Nuclear Respiratory Factor (NRF)-1, NRF-2 (also referred to as FA-Binding Protein, GABP), the Peroxisome Proliferator-Activated Receptor (PPAR) proteins and their co-activators, and the oestrogen related receptors (ERRs) (Scarpulla, 2002, Hock and Kralli, 2009, Eichner and Giguère, 2011).

Nuclear Respiratory Factors and Peroxisome Proliferator-Activated Receptors

NRF-1 is responsible for the downstream expression of the mitochondrial genome, through the induction of Mitochondrial Transcription Factor A (TFAM) (Hock and Kralli, 2009) – which also plays a pivotal role in mtDNA replication and MB (Scarpulla, 2008). The overexpression of NRF-1 in transgenic mice alone does not give rise to an increased respiratory capacity or MB (Baar et al., 2003). This finding indicates that other factors are required to work in concert with NRF-1 to bring about MB. NRF-2 partially fulfils this role, possessing DNA binding domains, which recognise elements in nuclear genes encoding OXPHOS components, TFAM and mitochondrial import proteins (Scarpulla, 2008) as well as multiple anti-oxidant enzymes (Dong et al., 2008).

The Peroxisome Proliferator Activator Receptor (PPAR) proteins regulate the expression of proteins associated with fatty acid oxidation, having direct implications for mitochondrial function (Hock and Kralli, 2009). PPARα and β/δ are associated with fatty acid oxidation and catabolism, while PPARγ promotes lipid anabolism and accumulation. High levels of PPARα and β/δ have been reported in metabolically active

liver and heart tissue; whereas high levels of PPARγ is observed in white adipose tissue (WAT) – highly anabolic lipid storage tissue (Evans et al., 2004, Hock and Kralli, 2009).

PPARγ has also been shown to control the translation of mitochondrial uncoupler proteins 1 (UCP1) (Sears et al., 1996). UCP1 has been shown to deplete the mitochondrial membrane potential by partially permeabilising mitochondrial membranes, releasing protons from the IMS allowing them to bypass CV (Demine et al., 2019). UCP1 is stringently regulated by GDP and Free Fatty Acid (FFA) concentrations; GDP binding inhibits UCP1 activity, while FFAs are known to promote membrane potential depletion and further increased by phosphorylation at serine residue at positions 3, 4 and 51, by Cyclin Dependent Kinase 2 (CDK2) and Protein Kinase C (PKC) (Carroll et al., 2008, Demine et al., 2019). The respiratory chain acts to re-establish the membrane potential, generating excess heat as a product of electron transport reactions. Mitochondria are most commonly uncoupled, and are consequently highly catabolic, in brown adipose tissue (BAT) (Handschin and Spiegelman, 2006).

PPARγ is expressed in both BAT and WAT, though these tissues exhibit drastically contrasting metabolic activity. This functional specificity between tissue types is brought about in part by differing levels and activities of PPARγ Coactivator-1α (PGC-1α) (Handschin and Spiegelman, 2006). The exposure of cells to PPARγ agonists has been shown to increase the expression of PGC-1α, the binding of PGC-1α to PPARγ changes the transcriptional behaviour of PPARγ to bring about the markedly contrasting phenotypes of WAT and BAT (Hock and Kralli, 2009).

Oestrogen Related Receptors

The oestrogen related receptors (ERRs) α, β and γ, regulate the transcription of tricarboxylic acid cycle, OXPHOS and fatty acid oxidation genes (Eichner and Giguère, 2011, Scarpulla et al., 2012). The ERRs are expressed in tissues associated with elevated metabolic activity: cardiac, renal, and skeletal muscle tissues. ERRα levels are also high in BAT, while both ERRα and γ are expressed in the brain (Eichner and Giguère, 2011). ERRs are associated with a number of co-regulators, including PGC-1α, which significantly alter target genes (Hock and Kralli, 2009, Eichner and Giguère, 2011). ERRα/ PGC-1α association has been linked to ATP and nucleotide synthesis as well as amino acid and lipid metabolism, AMPK signalling and heme biosynthesis (Eichner and Giguère, 2011).

PGC-1α

Of all relevant co-regulators of transcription, PGC-1α is the most prominent, interacting with, and increasing the activity of: NRF-1, NRF-2, ERRα and PPARβ/δ. This array of efficacy has resulted in PGC-1α being widely renowned as the master regulator of MB (Handschin and Spiegelman, 2006, Giguère, 2008, Hock and Kralli, 2009, Wallace et al., 2010, Eichner and Giguère, 2011, Komen and Thorburn, 2014, Lightowlers et al., 2015, Rai et al., 2015, Ploumi et al., 2017).

Transcriptional Control of PGC-1α

PGC-1α is under the transcriptional control of cAMP response element-binding protein (CREB); the activity of which is increased by protein kinase A (PKA) as cAMP levels increase (Herzig et al., 2001, Hock and Kralli, 2009). CREB activity in muscle can also be induced by an increase in intracellular calcium, as a result of prolonged exercise. The increase is detected by Ca^{2+}/calmodulin-dependent protein kinase (CAMK), which phosphorylates p38 mitogen-activated protein kinase (MAPK) and CREB via protein kinase A (Röckl et al., 2008, Hock and Kralli, 2009, Fernandez-Marcos and Auwerx, 2011). PGC-1α transcription is also regulated by Tfe3 and Tfeb of the MiT family of transcription factors. These transcription factors recognise three E-box motifs within the PGC-1α gene to upregulate transcription (Salma et al., 2015). The knockdown and overexpression of Tfe3 results in reduced and raised levels of PGC-1α respectively; the effects of which are reflected in PGC-1α target genes (Salma et al., 2015).

The yin-yang 1 (YY1) transcription factor binds PGC-1α, forming a complex that promotes transcription of both cytochrome c and PGC-1α, forming a positive feedback loop for PGC-1α expression (Cunningham et al., 2007). YY1/PGC-1α function is under the regulatory control of mTORC1; rapamycin inhibition of mTOR results in a decrease in the transcription of YY1 associated genes (Cunningham et al., 2007). This branch of control over PGC-1α expression via YY1 and mTOR allows for nutrient sensing in the cellular environment (Foster and Fingar, 2010). PGC-1α expression is further mediated by activation transcription factor 2 (ATF2 – of the p38MAPK pathway) which acts as a co-activator for CREB (Fernandez-Marcos and Auwerx, 2011, Salma et al., 2015). Myocyte enhancer factor 2 (MEF2), also part of the p38MAPK pathway, acts as an autoregulatory feed-forward loop for PGC-1α (Czubryt et al., 2003, Fernandez-Marcos and Auwerx, 2011).

Transcriptional repression provides an additional arm of expression control. RIP140 is a co-repressor of the NRFs and ERRs involved in the repression of catabolism in WAT and muscle (Powelka et al., 2006, Hallberg et al., 2008). RIP140 has been shown to bind repressor regions in genes associated with MB, fatty acid oxidation and OXPHOS (Powelka et al., 2006). Furthermore, RIP140 binds and inhibits the co-transcriptional activity of PGC-1α (Hallberg et al., 2008). Knockdowns of RIP140 result in muscle fibre type switch, from fast-twitch anaerobic to slow-twitch aerobic respiratory pathways (Seth et al., 2007). Seth et al., 2007, also reported reduced mitochondrial activity in RIP140 overexpressing transgenic mice, concluding that RIP140 and the PGC-1 co-regulators "serve mutually antagonistic functions" regarding mitochondrial activity.

Nuclear receptor co-repressor 1 (NCoR1) is a highly conserved repressor of PPARβ/δ, ERRs and MEF2; knockouts of NCoR1 in mice show increases in oxidative capacity and lipid oxidation (Yamamoto et al., 2011). Forkhead box class-O protein (FoxOI) is an additional transcription factor, which promotes the expression of PGC-1α. FoxOI is phosphorylated and deactivated by AKT in response to insulin signalling, reducing the transcription of PGC-1α (Fernandez-Marcos and Auwerx, 2011). Glucagon signalling has also been shown to activate PKA, and subsequently activate CREB, to induce PGC-1α transcription (Fernandez-Marcos and Auwerx, 2011). The complex web of transcriptional control of PGC-1α transcription is summarised in Fig 1.3.

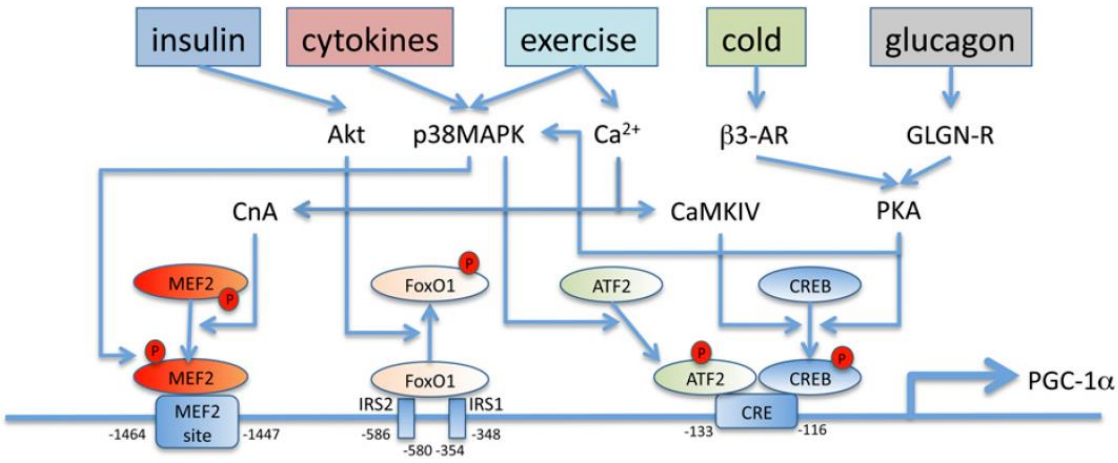

Fig 1.3. *Regulation of peroxisome proliferator-activated receptor coactivator 1a (PGC-1α) transcription*. At the PGC-1a promoter, there are binding sites for transcription factors myocyte enhancer factor 2 (MEF2), forkhead box class-O (FoxO1), activating transcription factor 2 (ATF2), and cAMP response element–binding protein (CREB), all of which enhance PGC-1a transcription. Additionally: insulin activates AKT, which leads to cytoplasmic sequestration and inhibition of FoxO1; cytokines and exercise activate p38 mitogen-activated protein kinase (p38MAPK), which phosporylates and activates MEF2 and ATF2; exercise also stimulates Ca2+ signalling, which leads to MEF2-mediated PGC-1a transcription. Cold activates ß3-adrenergic receptors (ß3- AR) lead to CREB activation. (Fernandez-Marcos and Auwerx, 2011)

Post-translational Control of PGC-1α

Post-translational activity suppression is primarily controlled through acetylation by GCN5 at a large number of lysine sites throughout the structure of PGC-1α (Lerin et al., 2006, Fernandez-Marcos and Auwerx, 2011). GCN5 was shown to sequester PGC-1α to nuclear foci in hepatocytes and significantly reduce its transcriptional activity (Ploumi et al., 2017). This repressor is under the control of the transcription factor SRC-3 (Scarpulla et al., 2012), a sensor of caloric excess. Conversely, caloric restriction is a well-documented inducer of MB (Jornayvaz and Shulman, 2010, Komen and Thorburn, 2014), which also serves to increase the lifespan of a variety of laboratory animals (Weindruch and Sohal, 1997). GCN5 utilises acetyl groups from ATP-citrate lyase. The concentration of these groups is dependent on high levels of ATP, and on the availability of acetyl-CoA as a provider of acetyl groups and is thereby closely linked to high nutrient availability (Jeninga et al., 2010, Fernandez-Marcos and Auwerx, 2011).

Oxidative stress has been shown to activate GSK3β which in turn phosphorylates PGC-1α at Thr295 – initiating the signalling cascade necessary for PGC-1α degradation (Fernandez-Marcos and Auwerx, 2011).

Post-translational activation of PGC-1α is largely regulated by sirtuin-1 (SIRT1), an NAD^+ dependent protein deacetylase (Fernandez-Marcos and Auwerx, 2011, Cerutti et al., 2014). SIRT1 is a sensor of the NAD^+:NADH ratio, which becomes active with high levels of NAD^+ relative to NADH. NAD^+ levels increase with exercise and fasting *in vivo* (Rodgers et al., 2005, Cantó and Auwerx, 2009), therefore, SIRT1 acts as a monitor for the respiratory and glycolytic activity of a cell. As a sensor of NAD^+, SIRT1 further monitors and mitigates against oxidative stress. An increase in SIRT1 activity leads to the downstream expression of anti-oxidant enzymes such as SOD1, SOD2, catalase and glutathione peroxidase (Dong et al., 2008), through the action of PGC-1α on NRF2 (Fernandez-Marcos and Auwerx, 2011). PGC-1α is activated by SIRT1 through deacetylation, at the GNC5 acetylation sites in PGC-1α (Fernandez-Marcos and Auwerx, 2011).

As well as playing key roles in PGC-1α expression, p38MAPK has been shown to phosphorylate PGC-1α at Thr263, S266 and Thr299 increasing its co-transcriptional activity (Fernandez-Marcos and Auwerx, 2011).

AMPK is a sensor of AMP levels (in the form of AMP:ATP ratio), which is activated with high AMP levels. This occurs during periods of caloric restriction and chronic exercise, (Röckl et al., 2008). AMPK has been shown to phosphorylate PGC-1α at Thr177 and Ser538 leading to PGC-1α inducing its own transcription (St-Pierre et al., 2006). AMPK also acts on PGC-1α indirectly through the downstream upregulation of NAD^+ levels. This is caused by an increase in fatty acid oxidation, due to AMPK signalling cascades, and an elevation in the rate of synthesis of NAD^+ - which serves to activate SIRT1 and increase PGC-1α activity (Fernandez-Marcos and Auwerx, 2011).

Necdin has been identified as a potential stabiliser of PGC-1α. Necdin/PGC-1α complexes inhibit the ubiquitin-dependent degradation of PGC-1α (Hasegawa et al., 2016). Knockdowns of necdin have been shown to reduce the expression of PGC-1α induced genes. The overexpression of necdin in primary cortical neurons elicited a neuroprotective effect upon insults with oligomycin, and also prevented neurodegeneration in experimental models of Parkinson's disease (Hasegawa et al., 2016).

1.5.2 Import of Nuclear Encoded Proteins into Mitochondria

Mitochondria contain approximately 1,100 proteins, of which only 13 are encoded by mtDNA; the remainder are imported from the cytosol (Calvo et al., 2016, Craven et al., 2017, Rath et al., 2021). Efficient protein import from the cytosol is vital to ensure mitochondria remain functional, and to facilitate effective mitochondrial biogenesis. To date five protein import pathways have been described, all of which rely on the Translocase of the Outer Membrane (TOM) complex and the maintenance of the proton motive force and mitochondrial membrane potential (Wiedemann and Pfanner, 2017).

Targeting Pre-Sequence Containing Proteins

Targeting pre-sequences on the N-termini are found on proteins destined for import into the mitochondrial matrix, or for insertion into the inner boundary membrane or crista membrane. Subunit TOM20 of the import complex forms a receptor groove into which the alpha-helical import sequences dock, through predominantly hydrophobic interactions (Abe et al., 2000). The presence of cations in the pre-sequence is essential for import as the MOM spanning channel formed by TOM40 shows cationic selectivity (Ahting et al., 2001). Once a pre-sequence is recognised, the protein is passively drawn towards the IMS through TOM40 and shuttled to the Translocase of the Inner Membrane (TIM) complex. At this point, a protein is sorted into one of two sites: the matrix, or the inner mitochondrial membrane. In the case of the matrix, TIM50 recognises the pre-sequence and shuttles the protein through a pore in the MIM formed by TIM23, this process is driven by both active and passive processes. Heat Shock Protein 70 (Hsp70), bound to TIM44, interacts with the protein in transit – its kinase activity results in a ratcheting effect allowing further Hsp70 proteins to bind to the imported protein (Kang et al., 1990, Craig, 2018). This active process is complemented by the relative negative charge of the matrix passively drawing the cationic pre-sequence through the pore, (Martin et al., 1991).

Once in the matrix, the targeting pre-sequence is cleaved from the protein by Mitochondrial Processing Peptide (MMP). Protein folding is often facilitated by Hsp60 and Hsp10 giving the final matrix protein (Ostermann et al., 1999). In the case of inner membrane proteins, work carried out in yeast found that TIM23 acts in concert with Mgr2, human homolog being ROMO1 (Norton et al., 2014), to release proteins with very hydrophobic targeting sequences into the inner membrane itself – forgoing pre-

sequence cleaving (Wiedemann and Pfanner, 2017). Another pathway combining these two processes has been described – conservative sorting (Hartl et al., 1986, Rojo et al., 1995). In Oxidase Assembly (OXA) protein sorting, proteins are shuttled through TIM23 and pre-sequences are cleaved in the matrix, as previously described, but C-termini are inserted into the MIM via OXA1L (Wiedemann and Pfanner, 2017). OXA1L also facilitates the insertion of mitochondrially encoded proteins into the MIM, to combine with nuclear encoded proteins to form respiratory chain complexes (Wiedemann and Pfanner, 2017).

The Carrier Pathway

The carrier pathway, so named as it specifically imports metabolite carriers into the MIM, requires the chaperone Hsp70 to bind the protein for import in the cytosol, which interacts with TOM70 before the protein is passed through the MOM via TOM40 (Wiedemann and Pfanner, 2017). The N-terminus of TOM40 recruits a hexameric complex formed of three TIM9 and three TIM10 subunits, which acts as a chaperone through the IMS (Wiedemann and Pfanner, 2017). The imported protein is passed, mid-section first, to the IMS chaperone (Wiedemann et al., 2001). Once in the IMS, interactions between TIM54 and the IMS chaperone result in the imported protein being passed to TIM22, which in the presence of a membrane potential, transports the imported protein laterally into the MIM (Rehling et al., 2003).

Import of Cysteine Rich Proteins

Cysteine rich precursors, destined for the IMS, are maintained in a reduced state in the cytosol and translocated across the MOM by TOM40 (Wiedemann and Pfanner, 2017). Once in the IMS, the proteins are oxidised by MIA40, which is in turn indirectly reduced by Cytochrome C Oxidase (via Erv1 and Cytochrome C) (Mesecke et al., 2005). The oxidation of the sulphide containing residues forms disulphide bridges, forming the proteins' tertiary structure (Wiedemann and Pfanner, 2017).

Import of Mitochondrial Beta-Barrel Proteins

Beta-barrel precursors to be inserted into the MOM first cross the membrane through TOM40, to be further chaperoned by the TIM9/10 IMS chaperone complex to the Sorting and Assembly Machinery (SAM) complex in the MOM, for protein folding and insertion into the MOM (Klein et al., 2012, Wiedemann and Pfanner, 2017).

Import of Mitochondrial Alpha-Helical Proteins

The fifth known import pathway acts upon alpha-helical proteins to be inserted directly into the MOM. The mitochondrial import complex recognises N-terminal signal anchor sequences to facilitate their insertion. This is distinct from the previously discussed mitochondrial import pre-sequence, because anchor sequences are not cleaved from the protein, and are instead used to hold the protein in place in the MOM (Wiedemann and Pfanner, 2017). Proteins of this nature with IMS domains are translocated to the IMS, where the TIM50 receptor protein of TIM facilities the transfer of the protein to the MOM (Wiedemann and Pfanner, 2017).

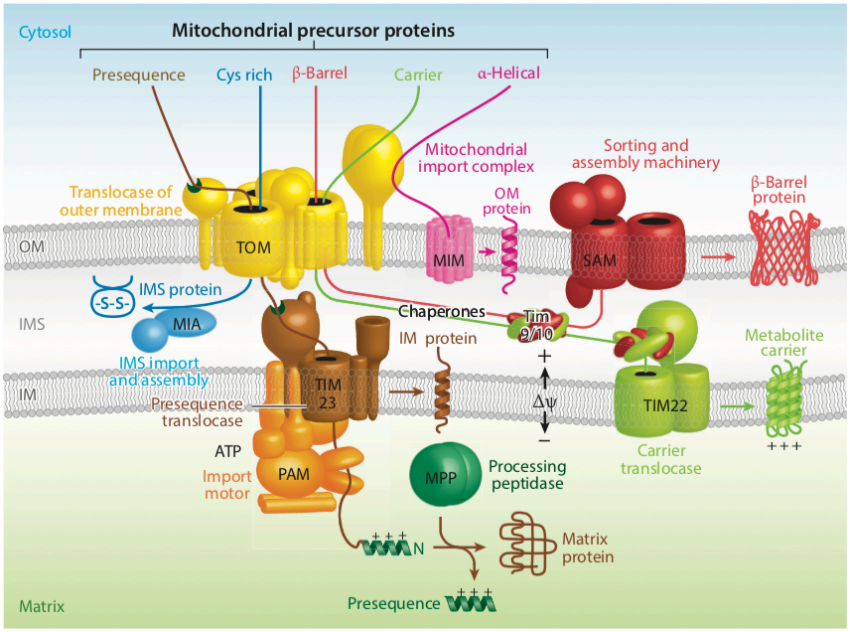

Fig 1.4. *A schematic of the five major mitochondrial protein import pathways (Wiedemann and Pfanner, 2017).*

1.5.3 Mitophagy

Degradation of whole mitochondria is achieved through mitochondrial-specific autophagy (mitophagy). Mitophagy is invoked to control the health of the mitochondrial population or adjust the metabolism of the cell to suit the environment (Palikaras et al., 2018). Effective mitophagy is dependent on mitochondrial fission, the two processes are tightly interlinked (Twig and Shirihai, 2011). Mitochondrial material needs to be of an appropriate size to be engulfed by an autophagosome; mitochondrial fission plays a key role in separating damaged mitochondrial material for destruction from an otherwise healthy and functional mitochondrial network (Shirihai et al., 2015).

PINK1/Parkin

Under basal conditions and in the presence of a well-maintained membrane potential, the PINK1 kinase is imported into the MIM where is it proteolytically cleaved (Sekine and Youle, 2018). Once cleaved, PINK1 is unable to trigger mitophagy. If a significant membrane potential is lacking in a mitochondrion, a common marker of mitochondrial dysfunction, PINK1 is not imported and is instead stabilised in the MOM (Harper et al., 2018). PINK1 autophosphorylation recruits the ubiquitin ligase, Parkin, to the MOM (Harper et al., 2018, Sekine and Youle, 2018). PINK1 subsequently phosphorylates Parkin, activating its ubiquitin (Ub) ligase activity (Harper et al., 2018). Due to Parkin activity, MOM proteins become poly-ubiquitinated. Poly-Ub chains are substrates for phosphorylation by PINK1 (Ordureau et al., 2014). Poly-phospho-Ub chains are poor targets for deubiquitinases, relative to poly-Ub chains, creating a stable marker for mitophagic degradation (Palikaras et al., 2018).

PINK1 further indirectly triggers Drp1 activity, which leads to mitochondrial fission, in preparation for autophagosome encapsulation of the dysfunctional mitochondrion (Palikaras et al., 2018). Parkin has also been shown to inhibit the function of mitofusin proteins, preventing the re-incorporation of dysfunctional mitochondria into the remaining healthy mitochondrial network (Gong et al., 2015).

The presence of poly-phospho-Ub chains leads to autophagosome engulfment of the dysfunctional mitochondrion through indirect recruitment of autophagosomal light chain 3 (LC3) (Palikaras et al., 2018).

Mitophagy Receptors

Several proteins have been shown to localise to the MOM, which directly interact with LC3II to recruit autophagosomes to mitochondria (Palikaras et al., 2018). LC3II plays an important role in binding to cargo for degradation in autophagy, (Gatica et al., 2018). Autophagy is dependent on the conversion of inactive LC3 to active LC3II through the conjugation of phosphatidylethanolamine to the protein, through the action of ATG7 and ATG3 (Tanida et al., 2004, Tanida et al., 2008). Mitophagy receptor proteins are briefly outlined below.

BNIP3

As well as directly interacting with LC3II, BCL2 interacting protein 3 (BNIP3) serves to stabilise PINK1 by inhibiting its degradation (Zhang et al., 2016), promoting mitophagy via the PINK1/Parkin pathway. BNIP3 has further been shown to disassemble OPA1, while recruiting Drp1 to the MOM, to both reduce the rate of mitochondrial fusion and increase that of fission (Palikaras et al., 2018). BNIP3 can also be ubiquitinated by Parkin to enhance LC3II interaction and thereby autophagosome recruitment (Palikaras et al., 2018). Under hypoxic conditions mitochondrial Complex IV (CIV) cannot reduce molecular oxygen to water as effectively as in normoxia, leading to increased ROS production. Hypoxia inducible factor 1 (HIF-1α) upregulates BNIP3 expression under hypoxic conditions, increasing the rate of mitophagy to mitigate against ROS production (Palikaras et al., 2018).

NIX

NIP3-like protein X (NIX) deficient cells have been shown to develop abnormally large populations of mitochondria resulting in a higher rate of apoptosis (Esteban-Martinez et al., 2017). The absence of NIX also impairs metabolic shifts required for cellular differentiation of retinal ganglion cells and the development of erythrocytes (Sandoval et al., 2008, Esteban-Martinez et al., 2017). NIX can also be modified by Parkin to increase the efficiency of autophagosome recruitment and, like BNIP3, the expression of NIX is upregulated in the presence of active HIF-1α (Palikaras et al., 2018).

FUNDC1

FUN14 domain-containing protein 1 (FUNDC1) provides a Parkin independent mechanism to promote mitophagy specifically during hypoxic stress (Liu et al., 2012); under normal conditions FUNDC1 recruitment of LC3 is inhibited as a result of phosphorylation of FUND1 by Sc and CK2 kinases (Chen et al., 2014). FUNDC1 has been shown to migrate to ER/mitochondrial contact sites and play a role in the recruitment of Drp1 to mitochondrial fission sites, further linking mitophagy processes to mitochondrial fragmentation (Palikaras et al., 2018).

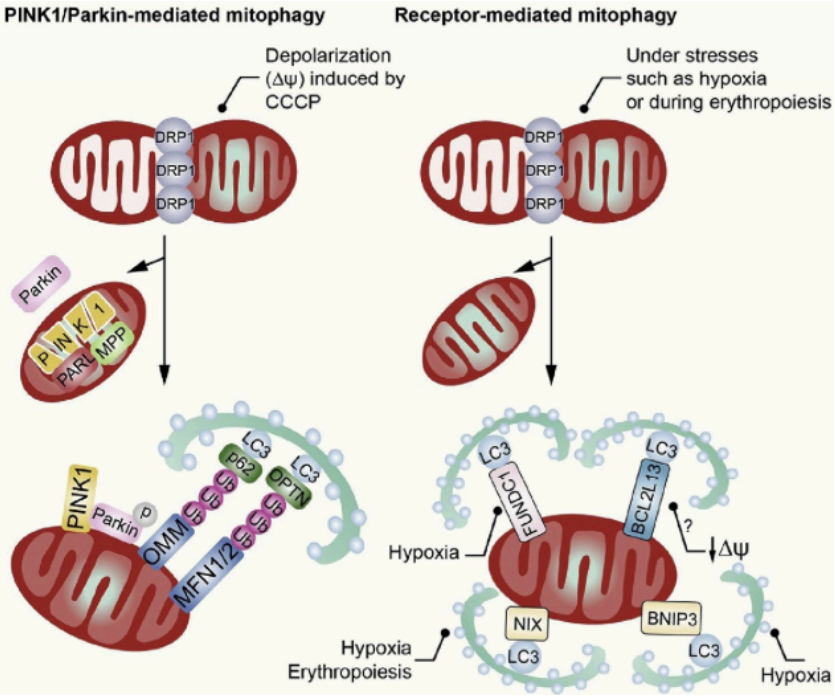

Fig 1.5. *A schematic of two different mechanistic pathways of mitophagy (Liu et al., 2020)*

1.5.4 Degradation of Aberrant Mitochondrial Proteins

The biogenesis of mitochondrial electron transport chain complexes requires the co-ordinated expression of multiple genes from nuclear and mitochondria DNA. Subunits must localise both spatially and temporally for complex assembly to be successful. Subunits that do not assemble into complexes pose a threat of potential pathogenic protein aggregation (Tatsuta and Langer, 2009). This is mitigated by the presence of four nuclear-encoded mitochondrial proteases which specifically target and degrade aberrant proteins: iAAAprotease, mAAAprotease and LonP and CPLX/P.

The i (intermembrane space facing) and m (matrix facing) AAAproteases are both localised to the MIM, which are responsible for the degradation of unincorporated respiratory subunits in the MIM in an ATP dependent manner (Leonhard et al., 1996). The mitochondrial i and mAAAproteases have been shown to play an additional role in the processing of imported OPA1 (Tatsuta and Langer, 2009), which performs a critical structural role in the stability of cristae junctions; mAAAprotease deficient mice have been shown to exhibit abnormal swollen mitochondrial morphology (Martinelli et al., 2009). mAAAprotease has been further shown to be vital to mitoribosome biogenesis, through its role in the maturation of MRPS32 by removing its mitochondrial targeting sequence (Tatsuta and Langer, 2009).

LonP and CPLX/P fulfil the role of matrix localised mitochondrial proteases (Haynes et al., 2007, Quiros et al., 2014). Further to degrading aberrant proteins, an important role of LonP is to degrade mitochondrially imported ATFS-1. ATFS-1 serves as a sensor of mitochondrial health: its import to mitochondrial is proportional to the membrane potential, the loss of which (due to mitochondrial stress) allows ATFS-1 to localise to the nucleus to bring about cellular responses to mitochondrial stress (Naresh and Haynes, 2019). CLPX/P has been shown to play a role in mitochondrial chaperone induction and modulates heat shock protein expression, acting as a sensor of mitochondrial impairment as a result of increases in temperature (Haynes et al., 2007).

1.6 Mitochondrial Function

Mitochondria are central to a wide array of cellular functions. These include metabolism, calcium homeostasis, reactive oxygen species (ROS) signalling, steroid synthesis, iron-sulphur (FeS) cluster synthesis and apoptotic regulation. All mitochondrial functions are directly linked to the mitochondrial membrane potential.

1.6.1 Metabolism and The Complexes of the Electron Transport Chain

Mitochondria play a critical role in the generation of ATP from ADP and inorganic phosphate, in the process of oxidative phosphorylation carried out by the F_0F_1 ATP synthase (Complex V, CV). Various metabolic pathways are used to generate the reduced electron carriers NADH and $FADH_2$, which are oxidised by the respiratory chain to pump resulting protons across the MIM to be utilised by CV.

Glycolysis

While not a mitochondrial process, glycolysis provides key substrates utilised by mitochondria. It describes a series of enzymatic reactions in the cytosol which facilitate the breakdown of glucose. The oxidation of one molecule of glucose generates two molecules of NADH, two of ATP and two of pyruvate:

$$\text{Glucose} + 2NAD^+ + 2ADP + 2P_i \rightarrow 2\ \text{Pyruvate} + 2NADH + 2ATP + 2H_2O + 2H^+$$

The Tricarboxylic Acid Cycle

Pyruvate is imported into the mitochondrial matrix to act as a substrate for the Tricarboxylic Acid (TCA) Cycle. Before entering the cycle, pyruvate is oxidatively decarboxylated, by the pyruvate dehydrogenase complex in the MIM, and combined with Coenzyme A (CoA) to produce acetyl-Coenzyme-A (Ac-CoA) and NADH:

$$\text{Pyruvate} + CoA + NAD^+ \rightarrow AcCoA + NADH + CO_2 + H^+$$

The TCA cycle itself consists of a combination of redox, isomerase and de-carboxylase enzyme mediated reactions. One complete cycle can be summarised as below:

$$\text{Ac-CoA} + 3NAD^+ + FAD + ADP + GDP + 2P_i + 2H_2O \rightarrow CoA + 3NADH + FADH_2 + ATP + GTP + 2CO_2 + 2H^+$$

Therefore, before the action of the respiratory chain and OXPHOS, one molecule of glucose results in the production of 4ATP and 2GTP, as well as 10NADH and 2$FADH_2$ to be used by the respiratory chain.

The Respiratory Chain

Mitochondrial complexes I-IV (CI, II, III and IV) form the respiratory chain, which utilises all proteins encoded by mtDNA. This system is responsible for electron transport, which releases energy to facilitate the movement of protons, by CI, III and IV, across the MIM from the matrix to help establish and maintain the pH gradient of the mitochondrial membrane potential.

Complex I

NADH:Ubiquinone Oxidoreductase (CI) is a 1MDa, 45 subunit protein complex. Fourteen of these are central to the function of CI and are conserved throughout evolution (Wirth et al., 2016). The remaining subunits have integral roles in CI assembly. All seven mtDNA encoded subunits of CI, MTND1-MTND6 and MTND6L, are highly hydrophobic and are all part of the functionally essential core (Wirth et al., 2016). The structure of mammalian CI has been resolved by cryo-electron microscopy to a resolution of 3.3 angstroms (Agip et al., 2018). NADH molecules are reduced in the matrix-facing N module of CI, by flavin mononucleotide (Rao et al., 1963). Electrons from this reaction are passed through eight FeS clusters to the Q module to reduce the electron carrier ubiquinone (Q).

Q is an 863Da organic small molecule comprising a paraquinone ring with an additional two hydroxymethyl groups, at positions 2 and 3, and a methyl group at position 6 – an isoprene tail of 10 units, in humans, extends from ring position 5 (Ernster and Dallner, 1995), giving the full IUPAC name of Decamethyltetraconta-5,6-dimethoxy-3-methylcyclohexa-2,5-diene-1,4-dione. The biosynthesis pathway of Q, conserved from yeast to humans, stems from aromatic amino acids, tyrosine or phenylalanine, forming the paraquinone ring, and from acetyl-CoA to build the isoprene chain (Ernster and Dallner, 1995). The pathway relies on numerous enzymes to synthesise Q, including dehydrogenases, aminotransferases reductases and kinases (Ernster and Dallner, 1995, Stefely and Pagliarini, 2017).

Reduction of Q produces ubiquinol (QH_2), after progressing through a series of single electron reduction reactions transitioning through ubisemiquinone (Ohnishi, 1998, Hirst, 2013, Gnandt et al., 2016).

Ubiquinol is released into the MIM to be utilised later in the respiratory chain. The electron transport process through CI, and the resultant reduction of ubiquinone, leads to a conformational change allowing the movement of four protons from the matrix to the IMS (Wirth et al., 2016). CI activity can be summarised as below:

$$NADH + Q + 5H^+_{Matrix} \rightarrow NAD^+ + QH_2 + 4H_{IMS}$$

Complex II

Succinate ubiquinone oxidoreductase (CII) is a 128kDa heterotetramer formed from SDHA, B, C and D, all of which are encoded by the nucleus (Kluckova et al., 2013, Anderson et al., 2014). CII is critical to the completion of the TCA cycle. It oxidises succinate to fumarate and thereby reducing CII bound FAD to $FADH_2$ (Anderson et al., 2014). CII contains three FeS clusters that transfer electrons and protons from $FADH_2$ to Q, reducing it to QH_2, though no protons are transferred from the matrix to the IMS as a result of CII activity (Cecchini, 2003). CII activity can be summarised as below:

$$Succinate + Q \rightarrow Fumarate + QH_2$$

Complex III

Ubiquinol: cytochrome c oxidoreductase (CIII) is formed from 11 subunits, only one being encoded by mtDNA, with a total mass of 500kDA (Solmaz and Hunte, 2008). The central catalytic units of CIII required for its electron transfer are cytochrome b (which contains a Reiske Fe-S cluster), cytochrome c1 and two haem groups: b1 and b2 (Xia et al., 1997). These groups are required for the Q cycle, which sees two protons translocating to the IMS from the matrix upon the oxidation of QH_2. The Q cycle can be broken into several stages. First sees the association of one QH_2 to quinone binding site 0 (Q_0). This process leads to QH_2 oxidation, liberating two electrons and two protons, producing Q, which is released. One electron is transferred to the Reiske FeS cluster, which is subsequently passed to cytochrome c1 and used to reduce the second mobile electron carrier, cytochrome c (CytC) (Cramer et al., 2011).

CytC is a 12kDa protein encoded by the nuclear gene CYCS that contains a haem binding domain. A haem b group is bound to the protein with two thioether bonds,

which link Cys34 and Cys37, to one vinyl group each, of the haem structure (Sanders et al., 2010). Histidine residues serve to further secure the haem group by coordinating the iron ion held in the haem structure, allowing the stereo-specificity of haem binding in CytC to be universally conserved (Bowman and Bren, 2008). The iron ion at the centre of the haem group is essential for the redox activity of CytC, being reduced from Fe^{3+} to Fe^{2+} by CIII to be oxidised later in the respiratory chain, to Fe^{3+}, by CIV. After the oxidation of one CytC, the second electron released from QH_2 reduces cytochrome b before being transported, by two haem groups in CIII, to a Q molecule in the Q_1 site, producing ubisemiquinone. The Q_0 binds a second QH_2, once again liberating two electrons and two protons. The described cycle repeats, though oxidation at the Q_1 results in the conversion of ubisemiquinone to QH_2 (Cramer et al., 2011). One complete Q cycle sees the complete oxidation of two QH_2 molecules at the Q_0 site, with the subsequent reduction of two CytC and one Q molecule, to QH_2. Therefore, CIII activity can be summarised as below:

$$QH_2 + 2CytC_{Ox} + 2H^+_{Matrix} \rightarrow Q + 2CytC_{Red} + 4H^+_{IMS}$$

Complex IV

Cytochrome C Oxidase (CIV) is a 200kDa protein complex, formed of thirteen subunits, of which three are encoded by mtDNA. CIV reduces molecular oxygen to water using electrons from cytochrome C and protons from the IMS. The activity of CIV is dependent on two catalytic copper ions, Cu_A and Cu_B, held in MTCOI and II respectively (Faxen et al., 2005). MTCOI further houses two haem groups, also essential for CIV activity (Tsukihara et al., 1996). Cytochrome C oxidation results in the transfer of two electrons in a two-step process to Cu_A – reducing it. One electron is subsequently passed to Cu_B, the second to haem group A3, via haem A (Faxen et al., 2005). These reduced groups act as a binding site for molecular oxygen, resulting in the formation of a peroxide bridge (Faxen et al., 2005). Oxidation of another Cytochrome C molecule, again in a two-step process, sees a further two electrons combine with two protons (of matrix origin) at the peroxide bridge site, resulting in the production of two hydroxide groups – one bound to each copper atom. An additional two protons react with the hydroxide groups forming two molecules of water and, using the energy released from the reaction, allowing the translocation of four protons from the matrix to the IMS (Faxen et al., 2005).

$$4CytoC_{Red} + O_2 + 8H^+_{Matrix} \rightarrow 4CytoC_{Ox} + 2H_2O + 4H^+_{IMS}$$

Complex V and Oxidative Phosphorylation

Oxidative phosphorylation (OXPHOS) is a chemical reaction that is catalysed by ATP Synthase (CV). CV comprises 15 different subunits split between two domains. The relative rotation of these domains, driven by the proton gradient established by the afore mentioned complexes, produces adenosine triphosphate (ATP) from adenosine diphosphate (ADP) and inorganic phosphate (P_i).

One domain (F_0) is housed within the MIM, the second (F_1) extends into the mitochondrial matrix (Okuno et al., 2011). Structurally, the F_0 domain comprises of a ring of eight c subunits forming a proton conducting channel, shown to be subject to rotation upon the passage of protons (Jonckheere et al., 2012b). The F_1 domain is formed from two sections: a stationary hexameric ring of α and β subunits in a 1:1 ratio and a central rotating stalk of γ, δ and ε subunits. A further peripheral stalk extends from the c-ring, the function of which is to support the rotating domains as ATP synthesis proceeds (Okuno et al., 2011, Jonckheere et al., 2012b).

The rotation of the mobile units of CV is driven by the translocation of protons through the F_0 domain, which protonate arginine residues on c-ring subunits (Ballmoos et al., 2009). Subsequent de-protonation releases protons to the matrix. This process leads to the rotation of the γ, δ and ε subunits of the F_1 domain. As a result, conformational changes of β subunits allow the binding of ADP and P_i, continued rotation forces further conformational changes facilitating the conversion of ADP to ATP followed by its release (Jonckheere et al., 2012b). A full rotation results in the synthesis of three molecules of ATP, with each molecule requiring the movement of, on average, 2.7 protons from the IMS into the matrix (Watt et al., 2010).

Further to its biochemical role, CV also fulfils a critical morphological role in maintaining the structure of cristae membranes through the formation of CV dimers at the tips of the evaginations, thus the majority of CV is localised to the cristae membranes (Rampelt H et al., 2017).

Super-complexes

Complexes I, III and IV have been shown to organise into higher order complexes, termed respiratory super-complexes (Dudkina et al., 2010). Supporting evidence for the formation of super-complexes includes the identification of bands indicative of super-complex masses, found to hold respiratory activity, in BN-PAGE experiments (Schagger and Pfeiffer, 2000), and the visualisation of super complexes in EM experiments (Schafer et al., 2006, Dudkina et al., 2010).

The largest super complex, the respirasome, formed from two copies of CI and one each of III and CIV: CIII forms a homodimeric complex ($CIII_2$) while CI and IV bind to this central structure as monomers (Dudkina et al., 2010). Tight protein-protein interactions have been shown to binding the respirasome together. Interactions between NDUFA11/UQCRB and UQCRQ/UQCRH in the MIM and NDUFB4/UQCRC1 in the matrix bind CI to CIII; interactions between COX7A and UQCR1/UQCR11 bind CIV and CII; while CI is bound with CIV through ND5-COX7C interactions (Letts and Sazanov, 2017).

The presence of CIII and CIV has been shown as a requirement for the complete assembly of CI in mammalian mitochondria (Perez et al., 2004, Diaz et al., 2006). As well as aiding the assembly of individual complexes, and stabilising them, super complex formation has been proposed to convey functional benefits through the reduction in substrate diffusion distances between complexes, in comparison to a purely fluidic model of proteins the MIM, and lowering ROS production (Letts and Sazanov, 2017).

Complex V also forms super-complex structures, in the form of oligomeric homodimers that retain functional independence, which act to define the curvature of cristae (Dudkina et al., 2008, Hahn et al., 2016, Rampelt H et al., 2017, Spikes et al., 2020).

1.6.2 Iron-Sulphur Cluster Biosynthesis

Iron-Sulphur (FeS) cluster biosynthesis is the only conserved function of mitochondria across all eukarya (Wang et al., 2011b, Lill and Freibert, 2020). FeS clusters play vital roles in ETC activity, amino acid biosynthesis, tRNA modification and DNA repair (Rocha and Dancis, 2015, Fuss et al., 2015). The generation of FeS clusters in the mitochondrion is dependent on protein import, and thereby on the maintenance of the

mitochondrial membrane potential (Lill and Freibert, 2020). Rho0 cells, lacking mtDNA, and thereby functional OXPHOS machinery, have been shown to actively transport protons from the matrix to the IMS to maintain the proton motive force and membrane potential - to facilitate FeS cluster biosynthesis (Buchet and Godinot, 1998).

Within the mitochondrion, imported iron binds to the ISCU2 scaffold protein in the mitochondrial matrix, to which sulphur is donated from cystine - a process catalysed by cysteine desulphurase within the frataxin complex (Lill and Freibert, 2020). Electrons from NADPH, transported via ferredoxin, are required to finalise *de novo* 2Fe-2S cluster synthesis. 2Fe-2S clusters are chaperoned to monothiol glutaredoxin (GLRX5), by a dedicated complex (comprising of HSPA9, HSC20 and GRPE1), which inserts the cluster into target proteins in a glutathione-dependent manner (Lill and Freibert, 2020). In the case of 4Fe-4S clusters, two molecules of GLRX5 pass two 2Fe-2S clusters to an iron containing ISC complex (ISCA1, 2 and IBA57). The clusters are fused through reductive coupling, facilitated by ferredoxin and NADPH oxidation, and inserted into target proteins (Lill and Freibert, 2020). Iron-Sulphur clusters synthesised in the mitochondrion can be exported to the cytosol by ABCB7 complexes, to be utilised by a total of 11 cytosolic iron-sulphur protein assembly proteins; these facilitate the formation of complete holoenzymes from their apo forms through FeS cluster insertion (Lill and Freibert, 2020).

1.6.3 Steroid Hormone Synthesis

The endoplasmic reticulum (ER) and mitochondria both contribute to vital stages in steroid biosynthesis. These hormones play critical roles in the regulation of the body and include: cortisol, progesterone, testosterone and oestrogen (Miller, 1988). Mitochondria harbour P450scc, an essential enzyme for the synthesis of steroid hormones, on the matrix facing side of the MIM (Miller, 1988, Issop et al., 2013). P450scc is responsible for completing the rate-limiting chemical reaction in the synthesis of all steroid hormone synthesis: the conversion of cholesterol to pregnenolone (Miller, 1988, Sanderson, 2006). This reaction requires electrons from NADPH, oxidising it to $NADP^+$. Therefore, maintaining the activities of the TCA cycle, converting NAD^+ to $NADP^+$, and the pentose phosphate pathway (required to reduce $NADP^+$), are key to maintaining the availability of reduced electron carriers for steroid biosynthesis (Frederiks et al., 2007).

Enzymes from the ER heavily contribute to steroid biosynthesis pathways; intermediate products are transported to the mitochondrion to be processed by mitochondrially localised enzymes (Miller, 1988). Mitochondrial-ER contact sites are vital for the transport of both cholesterol, for initial P450scc processing, and pathway intermediates (Issop et al., 2013). A loss of optimal mitochondrial morphology, achieved through MFN2 knockout (Naon et al., 2016), disrupts ER-mitochondrial contact sites and has been shown to significantly reduce the rate of steroid biosynthesis (Duarte et al., 2012).

1.6.4 Generation of Reactive Oxygen Species

Reactive oxygen species (ROS) such as superoxide ($O_2^{\cdot -}$) and hydrogen peroxide (H_2O_2) are required for a variety of cellular signalling processes; a deficiency in ROS can result in cellular dysfunction (Thannickal and Fanburg, 2000). An excess of ROS, however, can lead to the unregulated oxidation of biomolecules such as DNA, proteins and lipids, which impairs their function. The primary means of mitochondrial electron leakage and thereby superoxide formation is via the partial reduction of molecular oxygen by flavin mononucleotide (Lambert and Brand, 2009). CI becomes a prominent source of superoxide under dysfunctional conditions, such as CI activity impairment through disease or via small-molecule inhibition (Zorov et al., 2014). Molecular oxygen can also interact with nicotinamide adenine dinucleotide phosphate (NADPH) to produce superoxide, shown in the equation below.

$$2O_2 + NADPH \rightarrow 2O_2^{\cdot -} + NADP^+ + H^+$$

The superoxide anion is highly reactive and capable of generating singlet oxygen, which can disrupt pathways through the indiscriminate oxidation of biomolecules. To mitigate against oxidative stress caused by excess superoxide, enzymes from the superoxide dismutase (SOD) family rapidly convert $O_2^{\cdot -}$ to H_2O_2, reaction shown below (Nimse and Pal, 2015).

$$2O_2^{\cdot -} + 2H^+ \rightarrow H_2O_2 + O_2$$

The SOD family contains three members: SOD1 and 2 are intracellular and under the transcriptional control of NRF2, which is then also influenced by PGC-1 α (Dong et al., 2008, Fernandez-Marcos and Auwerx, 2011). SOD1, containing copper and zinc cofactors, is found in the cytosol and mitochondrial IMS (Cao et al., 2008), while SOD2 contains manganese and is found in the mitochondrial matrix (Borgstahl et al., 1996). SOD3, also known as ecSOD, is extracellular and contains zinc and copper cations in a similar manner to SOD1 (Antonyuk et al., 2009). In all cases, the metal ions are vital

to the functionality of the enzyme due to their redox roles in the active sites. Hydrogen peroxide, produced by the dismutation of superoxide (above), is also a potent oxidant. It can interact with iron, through the Fenton reaction, which results in the reduction of H_2O_2 to the hydroxyl radical ($\cdot OH$) – an additional form of ROS. The Haber-Weiss reaction can also occur between $O_2^{\cdot -}$ and H_2O_2 to produce hydroxyl radicals. Equations 1 and 2 show the Fenton and Haber-Weiss reactions, respectively (Kostic et al., 2013, Nimse and Pal, 2015).

1) $H_2O_2 + Fe^{2+} \rightarrow \cdot OH + OH^- + Fe^{3+}$ 2) $O_2^{\cdot -} + H_2O_2 \rightarrow \cdot OH + OH^- + O_2$

To lower the rate of spontaneous and unregulated formation of hydroxyl radicals, cells contain multiple pathways to reduce H_2O_2 in a controlled manner. Catalase catabolises H_2O_2 to form water and oxygen, while the glutathione/glutathione peroxidase (GPX) cycle fulfils this role in the extracellular environment. Both catalase and GPX are under the transcriptional control of NRF2 (Dong et al., 2008). Glutathione (GSH) is an antioxidant tripeptide (comprising of cysteine, glutamic acid and glycine) that dimerises upon oxidation (and subsequent reduction of the target oxidant) to form GSSG. This reaction is reversed by GPX: GSH functionality is restored by the reduction of GSSG through the oxidation of NADPH. An additional antioxidant, Peroxiredoxin, also converts hydrogen peroxide to water via a redox cycle, which is completed through the thioredoxin system. The thioredoxin system also requires NADPH, to provide electrons and protons for the reduction of hydrogen peroxide (Collet and Messens, 2010, Zhang and Martin, 2014, Nimse and Pal, 2015).

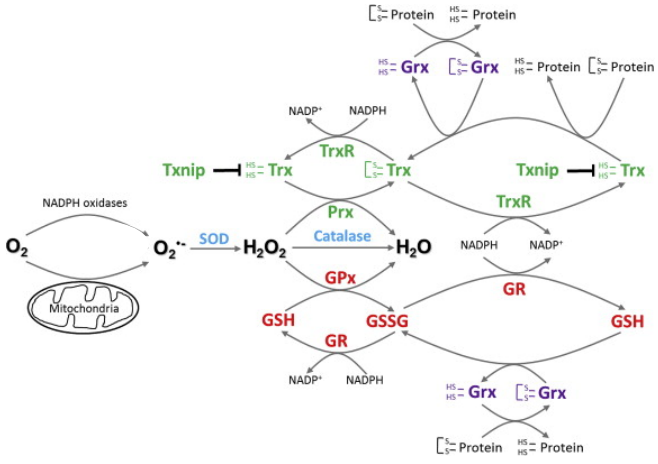

Fig 1.6. *Homeostatic antioxidant pathways.* ROS are generated as a result of metabolism in mitochondria and via the action of NADPH oxidases. Detoxification of ROS is achieved by a number of antioxidant enzymes. Acronyms: SOD, superoxide dismutase; GPx, glutathione peroxidase; Prx, peroxiredoxin; GSH, reduced glutathione; GSSG oxidised glutathione; Trx, thioredoxin; TrxR, thioredoxin reductase; GR, glutathione reductase; Grx, glutarredoxin; Txnip, thioredoxin-interacting protein NADPH, nicotinamide adenine dinucleotide phosphate. 'HS' represents the reduced form of a protein; 'S' denotes an oxidised form (Zhang Y and Martin S, 2014).

1.6.5 Calcium Handling

The endoplasmic reticulum (ER) serves as the primary means of calcium ion (Ca^{2+}) storage in cells, though the mitochondria serve as a vital secondary means of mediating intracellular calcium concentrations (Marchi et al., 2018). Calcium serves as a ubiquitous and versatile means of transmitting secondary signals within cells that mediate many physiological functions such as muscle contraction, synaptic excitation and neurotransmitter release, cell motility and apoptosis (Giorgi et al., 2018). Calcium concentrations in the extracellular matrix *in vivo* has been approximated at 1mM and has been measured to be 100-200nM in the cytoplasm, while concentrations in mitochondria are 10-20 fold higher than the cytoplasm, the ER exhibits much higher concentrations of greater than 300μM (Giorgi et al., 2018). This elevated ER Ca^{2+} concentration is achieved through active Ca^{2+} pumps using the energy released from ATP hydrolysis.

The MOM is found to be in close proximity to the ER in numerous locations across the cell – termed mitochondria-associated membranes (MAMs) (Marchi et al., 2018, Giorgi et al., 2018). These contact sites are maintained by the ERMES complex in mammalian cells (Hirabayashi et al., 2017). Further interactions between PTPIP51 (MOM) and VAPB (ER) contribute to MAM site integrity (De Vos et al., 2012), with knockdowns of any of the afore mentioned MAM site proteins resulting in decreases in the number of MAMs and mitochondrial calcium concentrations (Stoica et al., 2014, Paillusson et al., 2017). Mitochondrial calcium uptake is driven by the electrochemical gradient of the mitochondrial membrane potential – the net negative charge of the matrix electrostatically attracts positive calcium ions (Giorgi et al., 2018). Depletion of the mitochondrial membrane potential using small molecules (such as FCCP) eliminates the movement of calcium to the mitochondrial matrix (Babcock et al., 1997). Upon stimulation of Ca^{2+} release from the ER via $Ins(1,4,5)P_3$ receptors, Ca^{2+} concentrations at the MAM reach ten-fold of that of the cytoplasm (Giacomello et al., 2010). The high local concentration of calcium ions near MAMs, coupled with the mitochondrial membrane potential, facilitates the rapid movement of calcium to the mitochondrial IMS via VDAC channels (Shimizu et al., 2015). The Mitochondrial Ca^{2+} Uniporter (MCU) forms a pore in the MIM that regulates the movement of calcium ions from the IMS to the matrix, the activity of which is dependent on the association of the essential MCU regulator (ERME), which facilitates calcium sensing in the IMS (Sancak et al., 2013).

Calcium is removed from the mitochondrial matrix, allowing signalling cascades dependent on the secondary messenger to proceed, by two MIM proteins: mitochondrial Na^+/Ca^{2+} exchangers (mNCXs) and H^+/Ca^{2+} exchangers (mHCXs) (Giorgi et al., 2018). mNCX activity exchanges three or four sodium ions (Na^+) for one calcium ion; while mHCX activity is isoelectric, exchanging two protons for one calcium ion (Giorgi et al., 2018). The efflux of calcium, coupled with its uptake from specific locations in proximity to the ER, allows mitochondria to modulate localised calcium-dependent signalling cascades and buffer the cytoplasm against waves of calcium release from the ER (Giorgi et al., 2018).

Calcium and Metabolism

While mitochondria have been shown to play an important role in the modulation of cell-wide calcium signalling pathways, calcium has also been demonstrated to have a significant impact on the efficacy of ATP generation. Three enzymes central to the activity of the TCA cycle have been shown to exhibit increased activities in the presence of calcium: pyruvate dehydrogenase, NAD^+-isocitrate dehydrogenase and 2-oxoglutarate dehydrogenase (Denton and McCormack, 1986). The increased activity of these enzymes, as a result of increased calcium concentration, has been shown to lead to increases in ATP production at the F_0F_1ATPase, as well as increases in both NADH levels and respiratory complex activity (Territo et al., 2000, Maack and O'Rourke, 2007, Glancy et al., 2013). The absence of mitochondrial calcium, achieved through the inhibition of I3P receptors, has been shown to lead to the phosphorylation and subsequent deactivation of pyruvate dehydrogenase (Cardenas et al., 2010). Despite defects in calcium handling being associated with neurodegenerative diseases and some cancers, and calcium having a role in the maintenance of basal metabolism, the exact mechanism of action of the effect of calcium on mitochondrial activity remains unknown (Rossi et al., 2019).

1.6.6 Apoptosis

Mitochondria are central to the induction of apoptosis. Multiple triggers of apoptosis have been well documented; excess of reactive oxygen species, calcium ion overload, ATP deficiency and subsequent loss of active processes, and depletion of the mitochondrial membrane potential (Liberthal et al., 1998, Ly et al., 2003, Yu, 2003, Giorgi et al., 2012, Redza-Dutordoir and Averill-Bates, 2016). The opening of the mitochondrial permeability transition pore (mPTP) is a common factor in a cells' commitment to apoptosis (Hirsch et al., 1997).

While the exact identity of the mPTP remains unknown, recent research is beginning to uncover putative candidate proteins with suggestions of the involvement of the F_0F_1 ATP synthase complex at the MIM and pore-forming Bax oligomers, translocating from the cytosol to the MOM and oligomerising with Bak proteins at the MOM (Kwong and Molkentin, 2016, Jonas et al., 2017, Zhang et al., 2017a, Carraro et al., 2020).

A key step in the induction of mitochondrially mediated apoptosis is the release of Cytochrome C (CytC) from the mitochondria into the cytosol, where it triggers the caspase inflammatory pathways which lead to signalling cascades resulting in apoptosis (Li et al., 1997). CytC, as a key player in the electron transport chain, is localised to the cristae membrane. Thus, CytC must migrate from the cristae membranes to the IMS to be released via mPTP. The disruption of cristae morphology is a hallmark of apoptotic cells (Wang and Youle, 2016). OPA1 contributes to the morphology of cristae, in conjunction with the MICOS complex, which acts to tighten IMS/intra-cristae space junctions, preventing the unregulated release of CytC (Scorrano et al., 2002, Frezza et al., 2006, Varanita et al., 2015). Upon the induction of apoptotic pathways, the proteases OMA1 and PARL have been shown to disrupt the arrangement of OPA1 at these junction sites, perturbing cristae structure, thereby allowing the passage of CytC to the IMS (Frezza et al., 2006, Cipolat et al., 2006, Abate et al., 2020). Under basal conditions, BCL-2 inhibits the formation of the mPTP by preventing the oligermisation of Bax, however, apoptotic stimuli result in the inhibition of this arm of BCL-2 activity by BH3 proteins (Willis et al., 2007). These actions combined result in the realise of CytC to the cytoplasm and, subsequently, apoptosis.

1.7 Mitochondrial Disease and Dysfunction

Mitochondrial diseases can arise from either a mutation in mtDNA or nuclear genes coding for proteins associated with mitochondria. Symptoms, and their severity, are highly variable but centre around tissues with the greatest energy demand such as skeletal muscle, the CNS, cardiac tissue and the gastrointestinal tract. Typical symptoms of mitochondrial disease include, but are not limited to: ophthalmoplegia, cerebellar ataxia, seizures, stroke-like episodes, exercise intolerance, cardiomyopathy, optic atrophy, ptosis, deafness and diabetes mellitus, as well as myalgia, fatigue and gastrointestinal dysfunction (Schaefer et al., 2008, Ng et al., 2021).

Clinical presentations can emerge in patients at any age, having either life-changing or life-limiting impacts on the affected individual. Symptoms which develop later in life are more likely to negatively affect the quality of a patient's life, rather than drastically reducing lifespan, while symptoms that present in paediatric cases a likely to be severely life-limiting (McFarland and Turnbull, 2009).

The overall prevalence of genetic mutations relevant to mitochondrial disease in the general populous is approximately 1 in 5,000 healthy individuals (Gorman et al., 2015).

1.7.1 Primary Mitochondrial Diseases

Point Mutations

Point mutations in mtDNA and nuclear DNA can at first, be thought to cause mitochondrial diseases in a similar manner. A point mutation that invokes no change in the amino acid encoded, due to codon degeneracy, will result in the synthesis of a fully functional protein – otherwise known as a silent mutation. While a mutation that does change the encoded amino acid may not result in a dysfunctional protein due to similarity in the chemistry of encoded residues. For example, a residue substitution of Asp (GAC) to Glu (GAA) may not reduce protein functional activity, due to both containing carboxyl functional groups in their variable chains. Meanwhile, the same mutation at a different position in the protein may result in a reduction in protein function, due to the longer variable chain in Glu relative to Asp.

Similar principles apply to mutations in gene encoding rRNAs or tRNAs, however, the biochemical diversity of these molecules is limited to comparison to proteins. This is due to a lack of coding degeneracy, and the fact that the molecules pull components from a pool of only four nucleotides as opposed to twenty amino acids – which are further subject to highly selective Watson and Crick base pairing in some cases. As such, the tolerance for mutations in RNA structure is limited.

In addition to these genetic factors mentioned above, mtDNA mutations are subject to an additional layer of complexity that directly impacts whether a phenotype will be present; and how severe a single patients' symptoms may be.

Heteroplasmy and the Threshold Effect

Due to the polyploidy of mtDNA in the mitochondrial network in any single cell, mtDNA mutations can coexist with wild type (WT) mtDNA in a cell. This phenomenon is termed heteroplasmy. Should a cell possess a mutant mtDNA to WT mtDNA ratio of 1:3, the heteroplasmy level is said to be 25%, just as a ratio of 3:1 is 75%. Cells containing only one mtDNA species are homoplasmic, be it homoplasmic for WT mtDNA or homoplasmic for mutant mtDNA.

Mitochondrial diseases often require a particular level of heteroplasmy to be exceeded for a phenotype to present, termed the heteroplasmy threshold (Holt et al., 1990). This value is dependent on the gene affected and the severity of the mutation, but also the nuclear background of individual patients (Rossignol et al., 2003, Nissanka and Moraes, 2020). Additional factors such as age and skeletal muscle mtDNA copy number as well as heteroplasmy level have been found to correlate with disease severity. For example, a consistent progression of disease burden with increasing age is observed in patients suffering from Mitochondrial Encephalopathy, Lactic acidosis, and Stroke-like episodes (MELAS) (Grady et al., 2018).

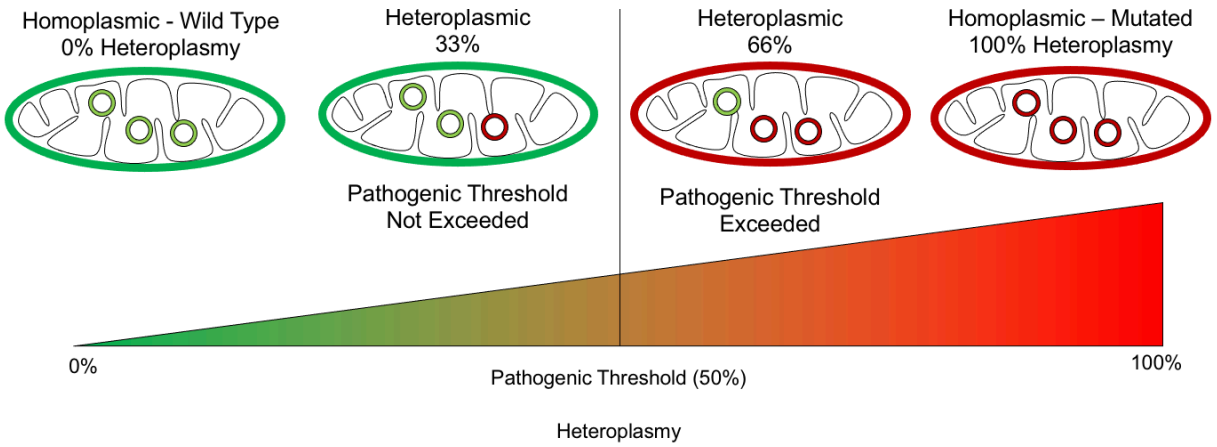

Fig 1.7. *A schematic demonstrating heteroplasmy and the threshold effect of mitochondrial DNA mutation load.* Mitochondria highlighted in green are not subject to a disease phenotype, while those in red exhibit mitochondrial dysfunction. Mitochondrial DNA in green do not contain a pathogenic mutation, those in red carry a pathogenic mutation. Clinical heteroplasmy thresholds vary greatly, numbers presented in this figure are for illustrative purposes only.

Genetics and Transmission of Primary Mitochondrial Diseases

Mitochondrial DNA is transmitted exclusively through the maternal line in humans (Giles et al., 1980, Wei and Chinnery, 2020). The first evidence for a genetic bottleneck for mtDNA was observed in 1982 in Holstein cows; offspring heteroplasmy, from a cow with 35% heteroplasmy ranged from 20% to 80% (Hauswirth and Laipis, 1982, Ashley et al., 1989). This effect can be explained through the fact that individual primordial follicles produce primary oocytes through miosis, during which a subpopulation of primordial follicle mtDNA is replicated to form the mtDNA populations of primary oocytes. Further, a significant decrease in mtDNA copy number per cell in the early stages of mammalian embryo development can act to alter the mtDNA heteroplasmy of an embryo (Wai et al., 2008, Cree et al., 2008). A high level of heteroplasmy in the remaining population will be conferred to offspring, which will present with systemically high heteroplasmy; whereas if predominantly WT mtDNA is selected, heteroplasmy can fall across generations. The exact mechanisms of this selection of mtDNA for replication in early embryos remain unknown (Wei and Chinnery, 2020).

A further contributor of heteroplasmy variability within an organism stems from stochastic segregation of mitochondria during cell division (Mishra and Chan, 2014). Cells are highly mitotic during embryo development. The random nature of mitochondrial segregation in cell division means that different tissues can present with differing levels of heteroplasmy, dependent on the differentiation fate and heteroplasmy of cells within the blastocyst. This may further alter the clinical presentation (if any) of offspring compared to the mother.

Clonal Expansions

Clonal expansion is the process by which any low-level mtDNA haplotype or mutation becomes the dominant mtDNA species in a post-mitotic cell, for example, a muscle fibre changing from low to high heteroplasmy, such that it exhibits reparatory chain defects. This process proceeds despite impairments to OXPHOS activity and mitochondrial membrane potential.

A key characteristic of age-related clonal expansion of random mtDNA mutations is a low overall level of mutant mtDNA concentrated in a small number of cells (Elson et al., 2001). Dysfunction of post-mitotic tissues, for example, neurons of the CNS, is brought about when key cells in a tissue become metabolically impaired as a result of clonally expanded mtDNA mutations. Clonally expanded mtDNA deletions (mtDNA molecules with large sections absent) have been linked to ageing and Parkinson's disease (Bender et al., 2006). Clonal expansion also is clinically relevant to inherited disorders involving mtDNA maintenance defects, as these increase the mutation rate of mtDNA compared to healthy controls, allowing more future clonal expansion events to occur (Tyynismaa et al., 2005, Vermulst et al., 2008).

The process of clonal expansion of mtDNA mutations is slow, requiring the majority of an organism's lifespan for a phenotype to develop. As such mtDNA mutations generated early in life can clonally expand, resulting in a single mutation predominating throughout a cell; rather than multiple as would be expected should age-related mtDNA mutations originate from decreased respiratory efficacy and increased ROS production (Elson et al., 2001).

Syndromes Associated with Mitochondrial Disease

Mitochondrial diseases are highly heterogeneous, exhibiting a wide range of clinical presentations and severities, even within one clinical diagnosis, between different patients. The diagnosis of mitochondrial disease is dependent on genetic sequencing. Several mutations in the mitochondrial genome have been linked to mitochondrial diseases. Presented below are the predominant examples of mutations in mt-tRNAs, mtDNA protein products and an outline of nuclear associated mitochondrial disease.

Mutations in mt-tRNA's

MELAS - m.3243A>G mt-tRNA$^{Leu(UUR)}$

Mitochondrial myopathy, encephalopathy, lactic acidosis and stroke-like episodes (MELAS) is most commonly caused by an m.3243A>G mutation in mt-tRNA$^{Leu(UUR)}$. This mutation accounts for 80% of MELAS cases, requiring a heteroplasmy threshold of approximately 85% (Goto et al., 1990). Lower levels of heteroplasmy of m.3243A>G (approximately 45%) have been associated with Maternally Inherited Diabetes and Deafness (MIDD) (Kadowaki et al., 1994). The discrepancy of phenotypes presented, rather than simply a milder case of MELAS in patients with a lower heteroplasmy, can be partially explained by differing cellular responses to heteroplasmy (McMillan et al., 2019), as well as different nuclear backgrounds between patients. In a cohort of mitochondrial disease patients in the North East of England, m.3243A>G derived MELAS alone accounts for 36% of all mitochondrial disease cases; it is the single most common pathogenic mtDNA mutation (Gorman et al., 2015) - approximately 24/10,000 individuals carry the mutation (Manwaring et al., 2007).

Clinically, patients with MELAS can be characterised by recurrent stroke-like episodes, muscle weakness, developmental hindrances, migraines, visual loss, nausea and vomiting (Chinnery et al., 1997, Zhang et al., 2015a, Ng et al., 2021).

Biochemically, MELAS manifests as deficiencies in complexes I and IV, resulting in a severe respiratory chain defect and significant neurological damage (Lax et al., 2016, Alston et al., 2017). The m.3243A>G mutation prevents complete mt-tRNA$^{Leu(UUR)}$ maturation by precluding a 5'-taurinomethyluridine modification, Fig 1.8, thereby disrupting UUG codon recognition of the mt-tRNA$^{Leu(UUR)}$. This has the effect of reducing the rate of translation of mt-mRNA's, with severe effects on MT-ND6 synthesis due to its mt-mRNAs' high UUG codon count (Kirino et al., 2004).

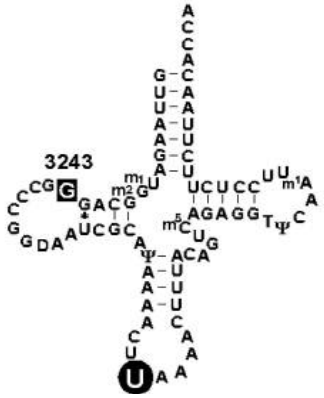

Fig 1.8. *A schematic diagram of mt-tRNALeu$^{(UUR)}$ highlighting the m.3243A>G mutation at the base of the D-Loop*. The subsequently unmodified Uridine base is highlighted at the codon wobble position – in the absence of the mutation the Uridine would be subject to a 5'-taurinomethyluridine modification. The absence of this modification has been shown to reduce the rate of translation of mitoribosomes (Kirino et al., 2004).

MERRF – m.8344A>G mt-tRNA^{Lys}

Myoclonus epilepsy and ragged-red fibres (MERRF) is commonly associated with the m.8344A>G mutation in the mt-tRNA^{Lys} gene, accounting for 80-90% of all MERRF cases (Shoffner et al., 1990, Shoffner and Wallace, 1992). MERRF, specifically the m.8344A>G mutation, has a prevalence of approximately 0.7/100,000 individuals (Gorman et al., 2015). Heteroplasmy levels of the m.8344A>G mutation varies widely between individual patients, even within families, with observed values ranging between 44-88%, as such the establishment of a distinct threshold for heteroplasmy for m.8344A>G has proved elusive (Altmann et al., 2016, Jeppesen et al., 2017).

Clinically, patients suffering from MERRF present with hearing impairments, muscle weakness, epileptic seizures, fatigue and exercise intolerance as well as muscular atrophy (Altmann et al., 2016, Ng et al., 2021). MERRF affected muscle fibres often exhibit a characteristic abnormality of subsarcolemmal mitochondrial accumulation – giving the muscle a distinct “Ragged-Red” appearance (Blakely et al., 2014, Altmann et al., 2016).

Biochemically, the m.8344A>G mutation prevents the taurine modification of a uridine base present in the wobble position of the tRNA (Yasukawa et al., 2001), Fig. 1.9. Investigations using cybrid cell lines have found significant impairments in oxygen consumption rate and OXPHOS activity - thought to be as a result of a reduction in the rates of protein synthesis - due to poor codon recognition and ribosome frameshifting (Masucci et al., 1995).

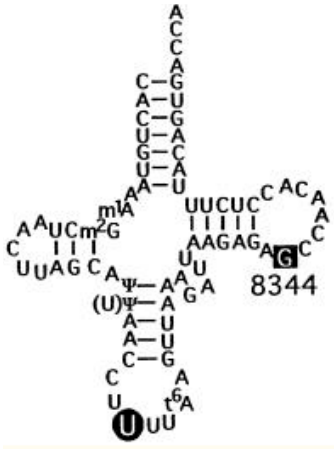

Fig 1.9. *A schematic diagram of mt-tRNA^{Lys} highlighting the m.8344A>G mutation at the TΨC-Loop*. The subsequently unmodified Uridine base is highlighted at the codon wobble position – in the absence of the mutation the Uridine would be subject to a taurinouridine modification. The absence of this modification has been shown to reduce the rate of translation of mitoribosomes (Yasukawa et al., 2001).

Mutations in Mitochondrially Encoded Proteins

LHON

Over 90% of Leber's hereditary optic neuropathy (LHON) cases can be attributed to one of three mtDNA point mutations: m.3460G>A, m.11778G>A, and m.14484T>C; affecting the genes MT-ND1 (p.T52A), MT-ND4 (pR340H) and MT-ND6 (p.M64V) respectively (Man et al., 2011, Lott et al., 2013), all of which reside in highly conserved areas of each respective protein's structures (Wallace et al., 1988, Howell et al., 1991, Johns et al., 1992). The heteroplasmy threshold required for biochemical defect and a LHON phenotype is approximately 60% (Chinnery et al., 2001, Man et al., 2011). LHON affects approximately 1 in 31,000 individuals, with a marked bias towards males; of those carrying a LHON associated mutation, 50% of males experience visual loss compared to 10% of females (Man et al., 2011).

Clinically, LHON is characterised by visual loss, which first manifests as a loss of a small area of central vision. The phenotype rapidly progresses (within 6 weeks) to optic atrophy and blindness (Man et al., 2011, Cruz-Bermudez et al., 2016). Additional symptoms of LHON can include cardiac arrhythmias, dystonia and peripheral neuropathy (Man et al., 2011, Ng et al., 2021).

Biochemically, LHON affected cells exhibit significant respiratory defects *in vitro*, exhibiting up to an 80% reduction in CI activity and up to a 50% reduction in respiration rate (Man et al., 2011). Further *in vitro* investigations have shown significant increases in lactate levels and ROS production, but no CI assembly defect, in cybrid cells harbouring LHON mutations; including patient-derived cells containing all three common LHON mutations discussed above (Cruz-Bermudez et al., 2016). Intriguingly, no synergistic effect between LHON mutations, biochemical nor clinical, is apparent in this patient (Cruz-Bermudez et al., 2016).

mtDNA Associated Leigh Syndrome

Approximately 50% of mtDNA associated Leigh Syndrome cases can be attributed to mutations in MT-ATP6, specifically m.8993T>G or m.8993T>C (Thorburn et al., 2003, Ogawa et al., 2017). The remaining 50% of cases comprise of a wide variety of mutations in mitochondrially encoded genes; those of CI are the most common - MT-ND3, MT-ND5 and MT-ND6 (Thorburn et al., 2003, Lake et al., 2016). Mutations in MT-ATP6 result in the phenotypes of Neurogenic Muscle Weakness, Ataxia, and Retinitis Pigmentosa (NARP) or Leigh Syndrome, dependent on heteroplasmy level. Cases exhibiting a heteroplasmy level below 60% are often asymptomatic, levels between 70-90% result in a NARP phenotype, while a heteroplasmy in excess of 90% results in Leigh Syndrome (Thorburn et al., 2003, Claeys et al., 2016). Leigh Syndrome is estimated to affect approximately 1/40,000 individuals (Rahman et al., 1996).

Clinically both NARP and Leigh Syndrome present very early in life; generally within a patient's first two years (Sofou et al., 2014). NARP is characterised by a loss of peripheral vision, ataxia, muscle weakness, learning difficulty and seizures. Additional symptoms can include sensory loss, deafness and anxiety. Patients with NARP are often stable for long periods, experiencing occasional lapses in their condition (Thorburn et al., 2003). Patients with Leigh Syndrome commonly present with seizures, respiratory defects (for example hyperventilation), dystonia, cerebellar ataxia and thermoregulation dysfunction – though the symptoms and their severity are highly heterogeneous (Thorburn et al., 2003, Rahman et al., 2017, Ng et al., 2021). Leigh Syndrome is often fatal before the age of three years, due to cardiac or respiratory failure (Thorburn et al., 2003).

Biochemically, the m.8993T>G or m.8993T>C mutations result in an amino acid substitution at a highly conserved site in MT-ATP6; p.L156R and p.L156P respectively, the former being more common and resulting in more severe disease (Thorburn et al., 2003). m.8993T>G specifically has been shown to reduce the ability of the *c* ring of CV to rotate, thus reducing the rate of OXPHOS by 70% in NARP patients (Sgarbi et al., 2006). Deficiencies of mitochondrial complexes I and IV are common causative factors of Leigh Syndrome, in cases where mutations in MT-ATP6 are not found, as a result of both mitochondrial and nuclear DNA mutations (Thorburn et al., 2003, Baldo and Vilarinho, 2020).

1.7.2 Mutations in Nuclear Encoded Mitochondrial Proteins

The majority of mitochondrial proteins are encoded in the nucleus, synthesised in the cytosol and imported into the mitochondrion. It reasons that nuclear DNA mutations present as a significant cause of mitochondrial disease. Mutations in nuclear-encoded mitochondrial genes are subject to Mendelian inheritance and are not subject to any further factors, as mtDNA mutations are subject to heteroplasmy.

Respiratory Chain Proteins

Mutations in structural and functional subunits of respiratory complexes are often associated with mitochondrial disease phenotypes. Despite an association with CI I, II, IV and V deficiency, cases of CI and CIV deficiency are the most common causes of Leigh Syndrome. These are as a result of mutations in CI subunits NDUFS1, 2, 3, 4, 7 and 8 as well as CIV subunits COX10 and 15; to highlight but a few of over 75 genes (Lake et al., 2016). Mutations in respiratory complex assembly factors have also been widely reported, alongside proteins playing key roles in FeS cluster synthesis, ubiquinone and heme group biosynthesis (Ghezzi and Zeviani, 2018).

Maintenance and Replication of mtDNA

Nuclear encoded genes such as POLγ and Twinkle are vital for the maintenance and replication of mtDNA. Pathogenic mutations in POLγ subunit POLG1 are common causes of mitochondrial disease, while mutations in POLG2 are rare (Hikmat et al., 2019). Mutations in POLγ and Twinkle present with similar phenotypes, owing to their shared function in maintaining mtDNA. Associated diseases include Alpers Syndrome, mitochondrial spinocerebellar ataxia and epilepsy (MSCAE) and ataxia neuropathy spectrum syndrome (ANS) (Alpers, 1931, Tzoulis et al., 2010, Hikmat et al., 2019, Hikmat et al., 2020). Pathogenic POLγ mutations are predicted to affect approximately 1 in 30,000 individuals (Gorman et al., 2015). A set of common mutations are known to give rise to the majority of POLγ associated disease cases: p.A467T, p.W784S, p.G848S and p.Y955C; of these p.A467T accounts for over a third of all POLγ associated mitochondrial disease (Chan and Copeland, 2009, Hikmat et al., 2019).

Clinically, patients with pathogenic POLγ mutations present with a variety of symptoms, largely dependent on the age of disease onset. Symptoms common to all age groups include seizures, neuropathy, muscle weakness, migraines and liver dysfunction or failure. In addition to the above, early onset in disease is further associated with liver failure, hypotonia and seizures. Adolescents and young adults present with ataxia and peripheral neuropathy, whereas those over the age of 40 years exhibit milder, but still significant, symptoms of ptosis, progressive external ophthalmoplegia and ataxia (Hikmat et al., 2020, Ng et al., 2021). Similar to many other mitochondrial diseases, the prognosis of a patient is often worse in case of earlier onset of symptoms; while the presence of epileptic seizures has a similar negative effect on prognosis (Hikmat et al., 2020).

Biochemically, dysfunctions in mtDNA maintenance result in mtDNA depletions, deletions and multiple mtDNA mutations, leading to a variety of metabolic defects and respiratory enzyme deficiencies (Hikmat et al., 2017, Vincent et al., 2018).

1.7.3 Mitochondrial Dysfunction in Neurological and Age-Related Diseases

Ageing can be described as the time-dependent degradation of cellular functionality, resulting in an increased vulnerability to chronic diseases and eventual death (Lopez-Otin et al., 2013). The accumulation of somatic nuclear mutations plays a significant role in this process. It is hypothesised that the addition of accumulated mtDNA mutations, and subsequent mitochondrial dysfunction, exacerbates and accelerates the ageing process; as opposed to directly causing or acting simply as a consequence of it (Kujoth et al., 2005, Srivastava, 2017).

The clonal expansion of somatic mtDNA mutations acquired early in life has been demonstrated, with an *in-silico* investigation, to accumulate in post-mitotic cells. These clonally expand in key cells, such as neurones or muscle fibres, to bring about dysfunction in tissue, despite overall heteroplasmy levels at a tissue or organ level remaining low (Elson et al., 2001). Dysfunctions in both mitochondrial biogenesis and mitophagy combined with mtDNA mutations lead to increases in oxidative stress, and in the rate of apoptosis, to contribute to age-related disease (Kujoth et al., 2005, Lopez-Otin et al., 2013, Chistiakov et al., 2014).

Beyond the ageing process itself, mitochondrial dysfunction has been strongly associated with Parkinson's disease (PD), which is characterised by the loss of dopaminergic neurons in the presence of Lewy Bodies formed from α-synuclein (Lane et al., 2015). CI dysfunction is the most common mitochondrial defect observed in PD patients (Schon and Manfredi, 2003). Rotenone inhibition of CI *in vitro* triggers increases in α-synuclein aggregate formation, concomitant with a reduction in ATP levels (Lee et al., 2002). Quadruple immunofluorescent analysis of PD neurones has identified TFAM and mtDNA copy number deficiencies, in conjunction with CI defects (Grunewald et al., 2016). Mitochondrial dysfunction has since been confirmed as a key component of PD pathogenesis, however, the exact nature of its role remains elusive (Chen et al., 2019a).

Increased ROS production in microglia, resulting in CNS neurone demyelination from subsequent oligodendrocyte apoptosis, is a hallmark of multiple sclerosis (Andrews et al., 2005, Mirshafiey and Mohsenzadegan, 2008). It is hypothesised that increased neuroinflammation, marked by elevated levels of inflammatory cytokines such as TNFα and IL-1β, are present in a patient in the pre-clinical stage before a multiple sclerosis

phenotype presents (Friese et al., 2014). Resultant cellular stress responses in glial cells lead to increased ROS production, which induces secondary damage to mtDNA and mitochondrial proteins in surrounding cells (Campbell et al., 2011, Kozin et al., 2018). This effect contributes to oligodendrocyte apoptosis and subsequent mass demyelination of CNS neurones. Additionally, a reduction in the expression of PGC-1α has also been associated with MS, confirmed by an *in vitro* model of the condition (Witte et al., 2013). Failure to meet the energy needs of a neurone results in further ROS production, which further accelerates neurodegeneration (Mahad et al., 2015, Peixoto de Barcelos et al., 2019).

The role of mitochondrial dysfunction in type two *Diabetes mellitus* has also been explored, in which excessive free radical generation from dysfunctional mitochondria is implicated in the development of the disease (Yaribeygi et al., 2018). Early work saw the generation of cybrid cells using mitochondria from patients with type two *Diabetes mellitus* (Anderson, 1999). The resultant cells exhibited increased ROS production and decreased ATP synthesis – not observed in cybrid cells formed using type one *Diabetes mellitus* derived mitochondria (Anderson, 1999). Endocrine dysfunction is commonly observed in primary mitochondrial disease patients, of which *Diabetes mellitus* is the most common (Schaefer et al., 2013); the archetypal example presenting in the form of Maternally Inherited Diabetes and Deafness (MIDD), as a result of the m.3243A>G mutation (Kadowaki et al., 1994). Despite clear associations between mitochondrial dysfunction and type two *Diabetes mellitus*, no causative or commonly associated genes have been identified in patients presenting with type two *Diabetes mellitus*.

Dysfunctional mitochondria are also highly relevant to the most prevalent condition affecting human health today: obesity. In obese rats, MFN2 expression was significantly reduced relative to controls; this effect was accompanied by reduced oxygen consumption and fragmented mitochondrial networks in skeletal muscle (Bach et al., 2003). A lack of fusion activity associated with obesity has also been shown to increase ROS production and proton leak in muscle tissue (Liesa and Shirihai, 2013). A reduction in the levels of PGC-1α and TFAM were found in hepatocytes from obese mice, accompanied by a reduction in CI activity (Holmstrom et al., 2012). Adipocytes sampled from obese human volunteers exhibited reduced oxygen consumption rates and citrate synthase activities, in a manner independent of adipocyte size, though

mtDNA content per cell did not vary relative to controls (Yin et al., 2014). These findings support the notion that mitochondrial efficiency per unit of mitochondrial mass is reduced in obese subjects, as opposed to a reduction in total mitochondrial mass per adipocyte. Reductions in mitochondrial mass have been noted, however, in hepatocytes and skeletal muscle fibres from obese subjects (Haas De Mello et al., 2018). Dysfunctional mitochondria have been proposed to perpetuate obesity through the early onset of fatigue and muscular pain in obese patients, due to a lack of efficient energy utilisation (Rogge, 2009). This produces a negative feedback loop based on a reduction in physical activity. As discussed in 1.5.1, exercise is a potent stimulator of transcription factors associated with mitochondrial biogenesis. Increases in free fatty acids and ROS induce inflammatory responses in macrophages, resulting in decreases in lipolysis in adipocytes, while increases in de-novo lipogenesis in hepatocytes further raise disease burden in obese subjects (Rogge, 2009).

Mitochondrial dysfunction has further been implicated in the risk of developing cancer, which increases exponentially with increasing age. Mitochondrial dysfunction has become one of the key markers of the disease, alongside the metabolic phenomenon known as the Warburg effect (Wallace, 2012, Pavlova and Thompson, 2016, Potter et al., 2016).

1.7.4 Quantifying Phenotypic Burden in Mitochondrial Disease Patients

The high disease heterogeneity in mitochondrial disease patients results in great difficulty in establishing a single, reliable method of quantifying the severity of disease phenotypes among patient groups. Clinicians at the NHS Rare Mitochondrial Disorders Service in Newcastle Upon Tyne developed the Newcastle Mitochondrial Disease Scale for Adults (NMDAS), to act as a semi-quantitative scale for mitochondrial disease burden to measure progression in patients and to assess the efficacy of clinical, and future potential pharmaceutical, interventions (Schaefer et al., 2006).

The NMDAS assessment covers overall physical functionality, symptom specific issues (such as difficulty swallowing) and a detailed clinical assessment. The NMDAS score is now commonly employed across a variety of mitochondrial diseases as a measure of disease severity, for instance, patients harbouring the m.3243A>G mutation at pathogenic levels were assessed to exhibit severe phenotypes concerning physical function, fatigue and mental cognition (Verhaak et al., 2016).

Improvements in NMDAS score through the course of a clinical trial can be interpreted as improvements to disease phenotype, as experienced by the patient. This data can be combined with other clinical (for example exercise capacity testing) and biochemical parameters, for instance, mtDNA heteroplasmy and blood lactate levels or imaging and histochemical analyses of patient tissue. As a result, trials targeting mitochondrial diseases can assess both quantitative and subjective readouts of disease burden with a wide variety of techniques, to best investigate the efficacy of the treatment (Steele et al., 2017).

A wide variety of other performance measures are also used to assess and monitor the severity or clinical progress of phenotypes and measure outcomes for clinical trials. These methods include the nine-hole peg test (assesses co-ordination and fine motor skills), the six-minute walk test (walking efficiency), a Timed Up and Go (TUG – mobility) and the Five Times Sit to Stand test (mobility) as well as a low-contrast letter acuity test (assesses vision) (Lynch et al., 2005, Newman et al., 2015).

1.7.5. Current Methods of Mitochondrial Disease Diagnosis

Chronically suffering mitochondrial disease patients engage in consultations with, on average, eight clinical professionals before receiving a final diagnosis of their condition (Grier et al., 2018). Approximately 70% undergo invasive muscle biopsy procedures and more than half receive an incorrect non-mitochondrial diagnosis, before a correct diagnosis of mitochondrial disease (Grier et al., 2018). The time taken to receive this diagnosis results in a loss of opportunity to increase the quality of life of a patient using symptom ameliorating treatments. More severe cases of mitochondrial disease, which emerge in early childhood, are more simply correctly identified; requiring on average 1.5 years (from symptom onset) for a diagnosis to be achieved (Eom et al., 2017). Despite a comparatively rapid diagnosis period in children, the increased disease severity and current lack of disease-modifying therapeutics results in an insignificant improvement to a patient's prognosis, following a diagnosis, in these cases (Eom et al., 2017, Rahman, 2020).

The methods used in the diagnosis of mitochondrial disease have greatly evolved with the emergence of next-generation sequencing technologies. Whole Genome Sequence (WGS) is rapidly becoming the dominant method of diagnosis. Once a mutation has been identified, further investigations are employed to establish the presence of a biochemical defect, which is the cause of the suspected mitochondrial disease. Once a validating defect is identified, a diagnosis can be made.

Genetic Sequencing

Efforts to identify pathogenic mutations associated with mitochondrial diseases are complicated by the dual origin of the mitochondrial proteome. Over 300 mutations in nuclear genes have been linked with mitochondrial disease pathologies (Abicht et al., 2018), though the majority of mitochondrial disease cases arise as a result of mutations in mtDNA (Gorman et al., 2015).

The advent of next-generation genetic sequencing has revolutionised the diagnosis workflow for mitochondrial diseases, with whole-genome sequencing (WGS) being projected to become the first port of call for suspected cases of mitochondrial disease (Schon et al., 2020). WGS is capable of identifying pathogenic mutations in both nuclear and mitochondrial genomes, from a single blood sample, using an unbiased shotgun approach (Wei et al., 2019, Schon et al., 2020). While prospects are promising as WGS technology advances, current applications of the method are limited by the financial cost and reliance on both bioinformatic and clinical expertise (Wright et al., 2018, Schon et al., 2020).

The unbiased nature of WGS can additionally identify novel pathogenic mutations, to further expand the scientific knowledge surrounding mitochondrial disease. This aspect must be supported by further biochemical investigations, which are currently limited in both assay completion rate and scope (Schon et al., 2020).

Secondary Confirmatory Assays Used in Mitochondrial Disease Diagnosis

Immunological and histochemical assays are most commonly employed on muscle tissue sections, however, they are not diagnostic of mitochondrial disease alone as the presence of a mitochondrial defect in tissue is not exclusive of the condition (Alston et al., 2017). As a result, these methods are often used to support the results obtained from genetic diagnoses, by confirming that pathogenic mutations result in a biochemical deficiency. Additionally, immunological and histochemical methods are currently key to the confirmation of pathogenicity of novel disease mutations.

The acquisition of a muscle biopsy is a highly invasive procedure in which a section of muscle is surgically removed from a patient. Once acquired, the very limited quantity of available tissue is snap-frozen to be analysed for respiratory chain defects. Biochemical activity of CIV can be assessed through COX/SDH staining using 3,3'-diaminobenzidine, which polymerises in the presence of COX activity giving a brown

product (Ross, 2011). COX staining is followed by nitro-blue tetrazolium (NBT) staining, which forms a blue product in the presence of SDH activity (Ross, 2011). As a result, COX positive fibres appear brown, while COX-negative fibres appear blue. The biochemical deficiency is quantified by counting the number of CIV negative versus CIV positive fibres in a given muscle section, giving a semi-quantitative result.

Immunological staining is also readily employed against muscle sections. Targeted proteins include sub-units of mitochondrial complexes; for example, NDUFB8 (CI) and MTCOI (CIV). These proteins are co-stained with porin, as a marker of the outer mitochondrial membrane, and laminin, as a marker of muscle fibre boundaries, to facilitate automated identification of areas of interest and quantification of staining intensities (Rocha et al., 2015, Ahmed et al., 2018). Fibres are classed as CI or CIV positive or negative, dependent on fold change (and significance of changes) of staining intensities from control tissue. Immunological staining provides further insights into mitochondrial disease pathologies when applied to post-mortem brain samples, though with significant limitations to therapeutic and diagnostic applications due to the nature of the samples (Alston et al., 2017).

Current muscle section staining methodologies (outlined above) analyse two of the four mitochondrial complexes that incorporate mtDNA products. Analysing additional proteins of interest within a single assay, using these methods, is not possible due to the requirement of laminin and porin staining. While complexes I and IV are the most commonly affected in mitochondrial disease, biochemical defects in complexes III and V, while rarer, are present in the patient cohort (Barel et al., 2008, Bénit et al., 2009, Jonckheere et al., 2012a, Fernández-Vizarra and Zeviani, 2015, Imai et al., 2016, Jackson et al., 2017). The methods are also precluded from related applications, such as phenotypic small molecule library screening, due to poor experimental throughput and the low availability and unscalable nature of the test tissue.

Gel Electrophoresis and Immunoblotting

Primary fibroblast cultures from patients are routinely used for gel-based methodologies to give additional insight into the state of proteins in diseased cells, complementing genetic sequencing and immunological and histochemical analysis (Tuppen et al., 2010, Leary, 2012, Newell et al., 2019). Sodium dodecyl sulphate (SDS) or blue native (BN) polyacrylamide gel electrophoresis (PAGE) techniques are readily employed against patient-derived cells to detect deficiencies in specific proteins of interest, or in the levels of mitochondrial complex assembly, respectively. These methodologies have long been a standard and well-validated means of quantifying protein levels and complex formation in cell lysates. Recent developments in in-gel activity assays have further increased the yield of information from gel-based methods. These are particularly useful in cases in which individual point mutations can be detrimental to complex activity, without negatively impacting protein expression or complex assembly (Newell et al., 2019). Despite being reliable laboratory methods, in a manner similar to muscle section analysis, low sample throughput and time-consuming protocols preclude gel-based methods from screening applications.

1.8 Therapeutic Discovery for Mitochondrial Diseases

1.8.1 Models of Mitochondrial Diseases for Therapeutic Research

Cellular

The introduction of mutations in nuclear encoded mitochondrial components into stable human cell lines, to create *in vitro* models for experimentation, can be achieved through CRISPR/Cas9 techniques (Oliveira et al., 2019). However, genetic manipulation of mtDNA in this manner remains an elusive prospect, due to the inability to import the guide RNA (gRNA) strands into the mitochondrial network, which is critical for CRISPR/Cas9 functionality (Gammage et al., 2018). The formation of transmitochondrial cybrid cell lines has become a prominent technique for laboratories investigating the effects of mutations in the mitochondrial genome *in vitro*. This method enables the study of a variety of mtDNA mutations in the presence of a defined nuclear background, through the fusion of cytoplasts derived from patient cells with Rho0 cells devoid of mitochondrial DNA (Wilkins et al., 2014). The resulting cybrid cells exhibit the nuclear DNA of the Rho0 line, but the mtDNA of the cytoplast, giving researchers the tools to directly compare patient mutations across a common nuclear background.

However, the range of mutations available for study in cybrid cells lines is limited to those present in an available patient cohort, often precluding those mutations responsible for the most severe phenotypes causing early death. Cybrid formation also invokes the issue of heteroplasmy; researchers must ensure that the heteroplasmy of cytoplasts used in cybrid formation reflects the heteroplasmy level of the original patient tissue/cell line.

Carrying out experiments directly on immortalised patient cells presents as the most accurate solution for researching mitochondrial disease cell lines. Though in the absence of an archetypal patient for each condition, due to disease heterogeneity, identifying a representative patient from which to base treatment efforts is an impossible task. Putative therapeutics discovered through screening in patient cell lines will need to demonstrate efficacy amongst numerous mitochondrial disease genotypes, which generate similar clinical phenotypes, to form an effective treatment option.

Animal

The transition from *in vitro* validation to *in vivo* trials is a significant hurdle for putative drug candidates; approximately 70% of drug discovery projects fail at this stage (Takebe et al., 2018) due to issues covering drug absorption, distribution, metabolism, excretion and toxicity (ADMETox). While the use of appropriate cellular models is key for identifying effective lead compounds, animal models are indispensable in pre-clinical research before human clinical trials commence. It is therefore vital that *in vivo* models of the targeted diseases are as accurate to patient phenotypes as possible. Unfortunately, as in cellular models of mitochondrial disease, current genetic manipulation technology is ineffective in introducing specific mutations to the mitochondrial genome *in vivo*. Despite this, mouse models carrying mutations in nuclear-encoded mitochondrial proteins, including those associated with mtDNA maintenance, have been produced using current genetic manipulation and breeding methods. For example, mice subject to an NDUFS4 knockout exhibit lower body weight, reduced life span and significantly impaired CI assembly, relative to control litter mates, to serve as a model of CI deficiency (Silva-Pinheiro et al., 2020). Mice carrying a TWINKLE helicase mutation show severe mitochondrial impairments as measured by reduced mtDNA copy number, the presence of mtDNA deletions and biochemical defects in skeletal muscle, to serve as a model of mtDNA deletions (Tyynismaa et al., 2005).

In the absence of targeted mutagenesis in the mitochondrial genome, the induction of sporadic point mutations serves as a means of investigating their deleterious effects. The “Mutator Mouse” model, in which mice express POLγA lacking its native proof-reading activity, serves as a model of POLγ mutations and has also been proposed to mimic accelerated ageing due to a correlation of phenotypes between the mitochondrial disease and the aged state: reduced subcutaneous fat, weight and hair loss, anaemia, osteoporosis and curvature of the spine (Trifunovic et al., 2004). Biochemically, Mutator Mice exhibit respiratory chain defects in the brain, cardiac tissue and skeletal muscle fibres as a result of multiple clonally expanded, sporadic mtDNA mutations (Trifunovic et al., 2004). While this mouse model has many applications in the investigation of the role of somatic mitochondrial mutations in ageing and general metabolic dysfunction, the unregulated nature of the resultant mtDNA mutations precludes its application to drug discovery projects that are focused on specific syndromes and diseases.

1.8.2 Preventing the Transmission of Mitochondrial Disease

The optimal method to reduce suffering generated by a disease is to prevent it from occurring, rather than treating it when it arises. At present, there are no curative methods, nor treatments to ameliorate the phenotypes associated with mitochondrial diseases beyond symptom management and pain reduction. Stopping or slowing the transmission of pathogenic mtDNA mutations presents an important tool for reducing the prevalence of mitochondrial diseases in the population.

The genetic bottleneck effect on mtDNA through oocyte maturation serves as a complicating factor in calculating the risk of a mother passing on pathogenic levels of mutant mtDNA. Thus, even mothers with low heteroplasmy levels can be considered at risk of passing on high levels of mutant mtDNA to their child. A variety of reproductive options are available for women carrying mitochondrial mutations, presenting personal choices to prospective parents looking to minimise the risks of disease transmission to their offspring. These options are briefly outlined below.

Oocyte Donation

The *in vitro* fertilisation of a mitochondrially healthy donor oocyte with the father's sperm presents as a simple solution, though resultant offspring are not genetically related to the mitochondrial disease patient. However, the woman who carries and births the child is legally recognised as the mother. To mitigate the risk of unintentional transmission of pathogenic mtDNA, an oocyte from an unrelated woman must be used. Should closely related relatives of the patient be carrying an mtDNA mutation at lower heteroplasmy, and their oocytes donated, a significant risk of disease transmission is present due to the mtDNA bottleneck in oocyte maturation (Smeets et al., 2015).

Prenatal Diagnosis

Prenatal DNA diagnosis uses the natural fertilisation of a mother's oocyte, with subsequent genetic diagnosis of the embryo early in the pregnancy. This technique uses either a chorionic villus biopsy or amniotic fluid sampling for DNA sequencing. Critically, both of these sampling techniques are representative of whole body heteroplasmy of the offspring post-birth (Craven et al., 2017).

In the case of nuclear DNA-associated mitochondrial disease, sequencing efforts commonly yield simple results due to the well-understood mendelian inheritance of

nuclear DNA. For mtDNA-associated disorders, the compounding effect of heteroplasmy threshold complicates data interpretation (Smeets et al., 2015). This is due in part to the change in the nuclear background relative to the mother, which means that accurately predicting the disease burden of a child from heteroplasmy level alone is a difficult task, even if the disease is well characterised. Genetic counselling is key to help prospective parents make their own choices regarding whether to terminate or continue a pregnancy to full term, should potentially pathogenic levels of mtDNA mutations be detected.

Preimplantation Genetic Diagnosis

Suitable for both nuclear and mtDNA-associated mitochondrial disease patients, preimplantation genetic diagnosis begins with the *in vitro* fertilisation of patient oocytes with the intended father's sperm. The resulting embryos are assessed for heteroplasmy levels using one or two blastomeres from the eight-cell stage of development, or a small sample of trophectoderm cells from blastocyst stage embryos (Craven et al., 2017). Both methods of sampling have been shown to reliably generate cell samples that reflect the heteroplasmy of the remaining embryo and have resulted in the births of healthy offspring (Monnot et al., 2011, Sallevelt et al., 2013, Heindryckx et al., 2014). A suggested heteroplasmy threshold of below 18% has been proposed to select embryos for implantation, though this value will vary with each mutated gene, location in the gene and the severity of mutation (Hellebrekers et al., 2012). Embryos with heteroplasmy levels below the critical threshold are selected for implantation into the mother. This technique requires a low level of heteroplasmy in the mother to maximise the probability of a low heteroplasmy oocyte being identified through the *in vitro* fertilisation and preimplantation diagnostic processes (Craven et al., 2017). This is due to the mtDNA genetic bottleneck resulting in female mitochondrial disease patients, with even low to moderate heteroplasmy levels, potentially producing high heteroplasmy oocytes.

Mitochondrial Donation

Mitochondrial donation has recently emerged as a new tool to minimise the risk of mitochondrial disease inheritance. The technique requires a patient's oocyte (intended mother) to be enucleated *in vitro*; the nucleus of the mother's oocyte is then transferred to an enucleated donor oocyte with healthy mtDNA (Craven et al., 2017). Similar to oocyte donation, it is vital that the donor is not a closely related family member of the patient, to minimise the risk of unknowingly using an oocyte from an unaffected mitochondrial disease carrier. The mitochondrially sound donor oocyte containing the intended mother's nucleus is then fertilised *in vitro* and implanted into the mother.

Mitochondrial donation can be achieved using one of three methods: polar body transfer, maternal spindle transfer or pronuclear transfer. Both polar body and maternal spindle transfer involve the movement of maternal genetic material before fertilisation. Whereas pronuclear transfer requires the *in vitro* fertilisation of both patient and donor oocytes, enucleation of resultant pronucleate zygotes and transfer of pronuclear material from patient-derived zygote to donor zygote cytoplasm (Craven et al., 2017). The resultant embryo contains nuclear DNA from both intended parents but the mtDNA of the donor oocyte, regardless of the mitochondrial donation method used. Pronuclear transfer inevitably includes a small amount of cytoplasmic material – often including patient mitochondria. Progress in the pronuclear transfer methodology has minimised the carry-over of mutant mtDNA to the resultant zygote to 2% (Craven et al., 2010). Prenatal diagnosis is also carried out on the developing embryo, post-implantation, to verify low mutant mtDNA transmission (Craven et al., 2017).

The United Kingdom became the first country to approve mitochondrial donation using pronuclear transfer for the prevention of mitochondrial disease transmission in 2015, after decades of research and legislative work accompanied by clinical and ethical challenges (Craven et al., 2016, Craven et al., 2020). Treatment is subject to intense, careful planning and approved only on a case-by-case basis (Gorman et al., 2018).

1.8.3 Current Methods for Mitochondrial Disease Treatment

Exercise

Exercise training has long been known to induce the strengthening of muscle tissue and to increase mitochondrial mass. Common symptoms of mitochondrial disease often include impairments to skeletal muscle function and exercise therapy has been proven to be safe to undertake in those patients capable of doing so (Ahmed et al., 2018). Exercise therapy using gradual progressive overload, through either aerobic or resistance-based training, in the presence of trained professional guidance and supervision, has been explored as an intervention for mitochondrial disease patients with numerous beneficial readouts, regarding both clinical and biochemical parameters (Taivassalo et al., 2001, Jeppesen et al., 2006, Bates et al., 2013). The objective of exercise therapy is to ensure that current functionality is maintained, with the goal of reducing physical deconditioning, through maximising strength and delaying reductions in patient endurance, to increase the day-to-day quality of life of a patient (Parikh et al., 2013, Muraresku et al., 2018).

Symptom Management

Symptoms of mitochondrial disease are wide-ranging both in the symptom presented and in severity, but often centre around tissues with the greatest energy demand such as skeletal muscle, the CNS, the gastrointestinal tract and cardiac tissue (Schaefer et al., 2008). General management of mitochondrial disease patients includes nutritional management, sleep scheduling and taking steps to minimise acute viral or bacterial infections (Muraresku et al., 2018). Skeletal muscle weakness is managed through a reduction in unsupervised physical activity (Steele et al., 2017) and exercise therapy, see above. Interventions targeting CNS symptoms, such as anti-convulsant and anti-epileptic medication, must be carefully explored (Finsterer and Scorza, 2017), though Phenytoin is commonly used to control seizures associated with MELAS (Ng and Turnbull, 2016). Pseudo-obstruction of the gastrointestinal tract, as a result of reduced gut motility, can be treated with the use of laxatives (Ng and Turnbull, 2016). Continued monitoring of a patient's heart is vital in those exhibiting cardiomyopathies, though treatment is reactive rather than preventative. Management of additional symptoms such as ptosis, *Diabetes mellitus* and deafness are similar to the general population, which can be addressed using corrective surgery, insulin treatment and the employment of hearing aids or cochlear implants, respectively (Ng and Turnbull, 2016).

Supplementation

Supplementation of key compounds in specific disease cases has yielded some positive outcomes in mitochondrial disease patients. These efforts have been aimed at slowing disease progression and ameliorating symptoms, as opposed to directly correcting or compensating for a biochemical defect (Avula et al., 2014). A variety of vitamins and metabolic supplements are suggested: riboflavin, α-lipoic acid or folinic acid for patients with neurological symptoms and L-carnitine or CoQ10 for those with specific deficiencies of these compounds (Muraresku et al., 2018).

Cocktails of compounds targeted at improving mitochondrial function have also been employed in individual cases, for example, thiamine, CoQ, vitamin E and C and carnitine supplementation was used in one Leigh Syndrome case and found to improve obstructive sleep apnoea (Mermigkis et al., 2013). Specifically, supplementation with arginine and citrulline have shown beneficial effects on stroke-like episodes and nitric oxide production in MELAS patients (Koga et al., 2005, Hattab et al., 2012).

Despite the growing use of supplements, such as those outlined above, rigorous clinical trial data regarding the efficacy and safety of supplementation with vitamins or metabolic intermediates in mitochondrial disease patients remains sparse (Camp et al., 2016, Garone and Viscomi 2018). Only one exemption currently exists; the FDA and EMA-approved drug, Idebenone (a derivative of CoQ), for treatment of visual loss in LHON syndrome patients (Rudolph et al., 2013, Garone and Viscomi 2018, Russell et al., 2020) – discussed in section 1.8.5.

Organ Transplants

Solid organ transplants are tolerated in mitochondrial disease patients to a similar degree as patients without a mitochondrial disorder, however, with the notable exception of those with POLγ associated disease (Parikh et al., 2016, Weiner et al., 2020). Thus, in instances in which one organ is predominately affected by a mitochondrial defect, the application of organ transplantation as a reactive, rather than preventative, treatment for mitochondrial disease can be pursued.

The most commonly transplanted organs in mitochondrial disease patients are the heart, liver and kidneys (Parikh et al., 2016). Patients exhibiting cardiomyopathy, hepatopathy or renal failure have been successfully treated using organ transplantation (Bonnet et al., 2001, Faraci et al., 2007, Grabhorn et al., 2014, Sasaki et al., 2017, Ducharlet et al., 2018, Weiner et al., 2020), though these procedures do not affect systemic symptoms of mitochondrial diseases, such as neurodegradation, seizures, ataxia or myopathy of skeletal muscle.

1.8.4 Hypotheses for the Treatment of Mitochondrial Diseases

The current lack of approved small molecule therapeutics for mitochondrial diseases represents a vast unmet clinical need. This vacuum has resulted in the generation of multiple hypotheses, which are currently being explored by the scientific community. The general approaches being employed across multiple laboratory groups are outlined below.

Antioxidants

Reactive oxygen species (ROS) can be produced in mitochondria as a result of the unregulated reduction of molecular oxygen, primarily through complexes I and III (Murphy, 2008). ROS have important roles in cellular signalling, severe reductions in cellular ROS levels can result in severe cellular dysfunction (Thannickal and Fanburg, 2000), however, elevated ROS levels are capable of inducing sporadic oxidative damage to biomolecules.

Dysfunctional mitochondria are more prone to producing ROS, strongly implicating ROS in the pathology of mitochondrial disease (Esposito et al., 1999, Wallace et al., 2010, Hayashi and Cortopassi, 2015). This is a result of an impairment of electron flow in the electron transport chain complexes leading to the potential reversal of the F_0F_1 ATPase to maintain membrane potential (Mailloux, 2020). Elevated ROS can negatively impact mitochondrial function, through lipid peroxidation and oxidative damage to mitochondrial proteins, furthering increasing ROS production to create a positive feedback loop for ROS production.

Lowering excessive ROS levels with exogeneous small molecule antioxidants presents as a viable method for interrupting the destructive cycle of mitochondrial dysfunction and biomolecule damage, though it does not address the underlying cause of mitochondrial diseases.

Gene Therapy

The expression of mitochondrially targeted wild-type copies of mutant mitochondrial genes from the nuclear genome, allotopic expression - achieved using recombinant adeno-associated virus (rAAV)-mediated gene therapy, provides a promising lead for a curative therapy of mitochondrial diseases (Ellouze et al., 2008). However, clinical investigations into the allotopic expression of ND4 in human LHON patients have yielded inconsistent and often negative results (Yang et al., 2016, Guy et al., 2017, Fightaging, 2019). While an rAAV therapy for LHON requires further research to prove efficacy in humans, promising data from the use rAAVs as a means of delivering NDUFS4 have been obtained in rodent models of Leigh Syndrome (Silva-Pinheiro et al., 2020). While not fitting the definition of allotopic expression, this work provides proof of principle in the correction of nuclear associated mitochondrial diseases with rAAV methods.

Direct removal of mutated mtDNA molecules in mitochondria, using targeted degradation, presents as an ideal solution to primary mitochondrial disease. This is because treatment would hypothetically not only ameliorate a patient's symptoms but also eliminate pathogenetic mtDNA molecules, lowering heteroplasmy levels and thereby reducing the risk of disease transmission to offspring. Two methods of mutant mtDNA genome degradation are currently being researched in a pre-clinical setting.

Mitochondrially localising Zinc Finger Nucleases (mtZFNs), formed in part from two Fok1 nuclease domains - each with specific mtDNA binding domains tailored to flank sites of mutated mtDNA, have been optimised to selectively induce double-strand breaks in some mutant mtDNA molecules (Minczuk et al., 2008). To ensure mitochondrial localisation, mtZFNs are linked to mitochondrial targeting sequences and nuclear export sequences, to mitigate off-target effects in the nucleus (Minczuk et al., 2006, Minczuk et al., 2008). mtZFNs have been shown to effectively reduce heteroplasmy of m.8993T>G and 'common deletion' (m.8483_13459del4977, present in 30% of mtDNA deletion patients (Schon et al., 1989)) mtDNA mutant cell lines *in vitro,* resulting in a recovery of OXPHOS parameters (Gammage et al., 2014).

Mitochondrially localising Transcription Activator-Like Effector Nucleases (mtTALENs), which require dimerization facilitated by DNA binding domains, tailored to bind in a sequence-specific manner in regions flanking the mutation, have similarly been investigated to reduce heteroplasmy. TALENs have been employed against the 'common deletion' mtDNA genotype and an m.14459G>A point mutation, with resultant shifts of heteroplasmy towards wild-type mtDNA (Bacman et al., 2013).

The recent discovery of a double-stranded DNA cytidine deaminase (DddA) facilitated the development of putative mtDNA modifying constructs, in which specific cytidine bases (targeted using TALEs) can be deaminated to uracil and subsequently repaired by mtDNA replication; causing C-G to T-A mutations (Mok et al., 2020). This is the first instance of CRISPR-free DNA base editing, CRISPR methods being precluded from development as a result of the inability to import gRNA into mitochondria. When fully optimised, DddA-derived cytosine base editors (DdCBEs), and other similar tools, could pioneer a field of mtDNA correction and targeted editing. These methods would enable researchers to create *in vitro* and *in vivo* models which accurately recapitulate human patients' phenotypes, thereby accelerating the development of mitochondrial disease therapeutics.

While a promising prospect, gene or protein delivery therapies, such as rAAVs, mtZFNs, TALENs and CRISPR-free DNA editing techniques, are unlikely to be widely adopted as therapeutic methods, as they require tailoring to each individual pathogenic genotype. This process is very high in both cost and scientific labour and would likely require validation, through clinical trials, for each targeted mutation. This work is also dependent on the easing of the restrictions on the *in vivo* use of genetic techniques in humans.

Selective Mitophagy

Pharmacological induction of selective mitophagic degradation of dysfunctional mitochondria presents as a conventional pharmaceutical intervention to achieve reductions in heteroplasmy, relative to gene or protein therapies; given the barriers to human genetic modification. The triggering of native cellular pathways, as discussed in 1.5.2, using small molecules has been proposed as a viable method of mtDNA modulation, provided appropriate advancements in knowledge to identify suitable protein targets (Paz et al., 2016). Mitophagy induction using rapamycin or carbonyl cyanide m-chlorophenylhydrazone (CCCP: a small molecule capable of mitochondrial membrane depolarisation) has been attempted in mitochondrial disease cell lines with mixed results (Sharma et al., 2019, Lin et al., 2019).

Selective mitophagy is a promising prospect for the treatment of primary mitochondrial diseases, which are not homoplasmic. Selective mitophagy is not viable, however, in cases where the entire mitochondrial network is deleteriously affected by a mutation (homoplasmic primary mitochondrial diseases and diseases originating from a nuclear mutation – see sections 1.7.1 and 1.7.2 respectively), due to the lack of opportunity to reduce heteroplasmy.

Currently, deferiprone presents as the only small-molecule inducer of mitophagy (McWilliams et al., 2016a). Deferiprone is, however, unsuitable for therapeutic use in mitochondrial disease patients as the mitophagy processes induced, which are PINK1/Parkin independent, are not specific to dysfunctional mitochondria (Ivatt and Whitworth, 2014). Furthermore, deferiprone is an approved drug for the treatment of Thalassaemia (excessive free iron), exhibiting strong iron chelation activity and could trigger adverse side effects in mitochondrial patients who present without excessive levels of free iron - (Balfour and Foster, 1999, Cohen et al., 2000).

Mitochondrial Biogenesis

Increasing the overall quantity of mitochondrial material, through the expansion of the mitochondrial network, is hypothesised to increase the overall oxidative capacity of a cell, despite not treating any underlying molecular dysfunction. Should a pathogenic mutation result in a patient's muscle fibre exhibiting a 50% reduction in mitochondrial capacity, inducing a doubling of the mitochondrial network is proposed to return a patient's capacity to wild type levels (note this is an extreme example). Concerns regarding excessive ROS generation through the proliferation of dysfunctional mitochondria can be resolved through the expression of antioxidant enzymes such as SOD2, which is indirectly under the transcriptional control of PGC-1α (Tufekci et al., 2011, Patel et al., 2014, Besse-Patin et al., 2017).

As discussed in section 1.8.3, exercise therapy is one of the most commonly employed interventions for mitochondrial disease, however, progress is often limited by a patient's ability to engage in sufficient exercise. Major pathways which activate PGC-1α expression and activity are themselves activated by physical exercise (Fernandez-Marcos and Auwerx, 2011). Thus, the identification of a small molecule agent capable of activating PGC-1α, directly or otherwise, is paramount to an exercise mimetic; which could be of significant value to mitochondrial disease patients and the general population alike (Ruegsegger and Booth, 2018).

Complex Bypass

Inactivity of any single complex in the respiratory chain creates a blockage for the flow of electrons through the chain. For example, dysfunction in CI would lower levels of QH_2, which imposes impairments across the remainder of the respiratory chain. In this case, providing substrates to CII, in the form of succinate, or to CIII, as ubiquinol mimetics, is hypothesised to ameliorate the resultant phenotype (Avula et al., 2014). In contrast, dysfunctions in CIII or CIV results in an accumulation in QH_2 or CoQ_{Red} respectively. Therefore, therapeutic options in these situations are limited to agents capable of oxidising these key electron carriers to allow CI to continue proton translocation (Hirano et al., 2018). Investigations are exploring alternative oxidases in mammalian cell lines and in *Drosophila* to achieve this effect (Dassa et al., 2009, Fernandez-Ayala et al., 2009).

Promising outcomes have been observed in LHON patients with CI dysfunction or deficiency. In this context, complex bypass was employed using the delivery of electron carriers to CIII, most prominently the ubiquinol mimetic Idebenone (Rudolph et al., 2013, Garone and Viscomi 2018, Russell et al., 2020).

1.8.5 Therapeutic Prospects in Literature and Ongoing Clinical Trials

Rapamycin

One of the first reported exogenous influencers of the metabolic signalling pathways was rapamycin (Vézina et al., 1975, Swindells et al., 1978). This natural product, produced by *Streptomyces hygroscopicus,* binds to the mammalian Target of Rapamycin (mTOR), a serine/threonine kinase, and acts to inhibit its complex formation with one of its mutually competing binding partners. Complex formation between mTOR and regulatory associated protein of mTOR (Raptor) forming mTORC1, is inhibited by rapamycin, while complex formation with the rapamycin-insensitive companion of mTOR (Rictor), giving mTORC2, is not (Schieke et al., 2006, Cunningham et al., 2007, Foster and Fingar, 2010).

Decades of research into rapamycin and mTOR have yielded little information regarding precise mechanisms of action of the downstream effects of mTOR binding by rapamycin. However, mTORC1 has been identified as a key regulator of the mitochondrial stress response in mitochondrial diseases (Khan et al., 2017). Inhibition of mTORC1 with rapamycin in the “Deletor” mouse model addressed imbalances in one-carbon metabolism and serine synthesis while suppressing mitochondrial stress (Khan et al., 2017). In addition to these effects, rapamycin has also been shown to both delay the onset of symptoms and extend life span in mouse models of Leigh Syndrome; an NDUFS4 knockout (Johnson et al., 2013). Mice harbouring a COX15 mutation, resulting in a CIV assembly defect, exhibited an increase in autophagic turnover and lysosome biogenesis when treated with rapamycin, indicating mitophagic degradation of dysfunctional material, leading to a reduction in phenotype severity (Civiletto et al., 2018).

Rapamycin presents as a promising pre-clinical candidate for mitochondrial myopathies, however, as a repurposed drug (originally an immunosuppressant) it exhibits an array of side-effects with chronic dosing: stomatitis, thrombocytopenia, elevated cholesterol, and impairment of wound healing (Kaeberlein, 2013). These side effects, including its originally intended immunosuppressant activity, severely limits the application of rapamycin to mitochondrial disease patients as a therapeutic agent.

Resveratrol

Resveratrol (first isolated from the skins of red grapes) is one of the most well characterised putative means of inducing mitochondrial biogenesis (Lagouge et al., 2006, Feige and Auwerx, 2007). A mechanism for resveratrol was proposed in which resveratrol binds to an allosteric site of SIRT1 to improve substrate binding (Borra et al., 2005). More recently a further study showed that resveratrol, among other putative SIRT1 activators, does not interact with SIRT1 directly, but instead resveratrol interacts with a fluorophore present on a substrate molecule to increase target binding (Pacholec et al., 2010).

The pharmacokinetics of resveratrol have been investigated and reviewed (Cottart et al., 2010), in which it was cited as a promising compound, however, later reviews of resveratrol clinical trials concluded that due to the high bioactivity, but low bioavailability, derivatives of the compound would be likely to yield improved outcomes in clinical trials (Tomé-Carneiro et al., 2013). It has also been proposed that resveratrol leads to the translocation of tyrosyl tRNA synthetase to the nucleus, at which point it complexes with PARP1 to alter NAD^+ signalling, with a downstream positive effect on the activity of SIRT1 (Sajish and Schimmel, 2015). It is perhaps unsurprising that a molecule as small as resveratrol, with no obvious means of specific protein targeting, has been proposed to act through such a wide variety of mechanisms.

A clinical trial investigating the effects of various polyphenols on mitochondrial respiration in the elderly is due to publish results soon (NCT02123121); a second clinical trial, investigating the effects of resveratrol in twenty patients of mitochondrial myopathies is currently underway (NCT0378777).

Epicatechin

Epicatechin has been shown to induce resistance to fatigue in mice, accompanied by increases in the levels of proteins associated with the electron transport chain, as well as TFAM, indicative of mitochondrial biogenesis (Nogueira et al., 2011). Increases in the levels of porin, citrate synthase and TFAM were also noted upon the administration of epicatechin - and various derivatives - to *in vitro* cultures of bovine coronary artery endothelial cells (Moreno-Ulloa et al., 2013). Epicatechin was recently discovered to act as an agonist for pregnane X receptor (PXR) in skeletal muscle, resulting in increased myogenin expression and myoblast differentiation (Ortiz-Flores et al., 2020). Recent investigations into the effects of epicatechin in healthy human volunteers have produced markedly contrasting data to pre-clinical earlier studies, reporting that epicatechin dosing blunted increases in mitochondrial activity and markers of mitochondrial mass, which were conversely observed to increase in the placebo group (Schwarz et al., 2018). A phase II clinical trial regarding the efficacy and safety of epicatechin use for the treatment of Friedreich's ataxia over 24 weeks has been completed, with no significant change noted between start and end point measures of disease severity (clinicaltrials.gov: NCT02660112). No further trials are underway, or currently recruiting, for epicatechin use in primary mitochondrial diseases.

Omaveloxolone

Omaveloxolone has been shown to increase levels of glutathione and trigger mitochondrial biogenesis in ALS mouse models (Neymotin et al., 2011). When applied topically, omaveloxolone has also been shown to activate NRF-2 in rats, a key regulator of mitochondrial biogenesis downstream of PGC-1α (Reisman et al., 2014, Rai et al., 2015). Omaveloxolone has been investigated in a phase II clinical trial involving patients with mitochondrial myopathies (genetic diagnosis and biochemical defect in at least one mitochondrial complex - various clinical diagnoses) in a dose-escalating manner, to assess both its safety and its efficacy in treating the diseases (NCT02255422). Resultant data has shown activation of NRF-2 related pathways with improvements to lactate levels and heart rate during submaximal exercise (Madsen et al., 2020). Suggestions of the potential benefit to patients with Friedreich's ataxia have been made (Lynch et al., 2019); a clinical trial investigating these prospects is currently underway, which is expected to conclude in 2022 (NCT02255435).

Quercetin

Quercetin is a polyphenolic organic compound, which has been shown to increase parameters associated with mitochondrial biogenesis in rodents, such as PGC-1α and SIRT1 mRNA levels, through activation of the NRF-2 pathway, with evidence building for over a decade (Davis et al., 2009, Rayamajhi et al., 2013, Kim et al., 2015, Li et al., 2016, Lee and Kim, 2018, Davinelli et al., 2020).

Quercetin presents as a potential agent for complete mitochondrial turnover, activating both biogenesis and mitophagic pathways, such as PINK1/Parkin and HIF-1α (Wang et al., 2011a, Yu et al., 2016, Liu et al., 2018, Davinelli et al., 2020). Quercetin has also been cited as an antioxidant capable of scavenging superoxide ions, further increasing its scope for potential use in mitochondrial disease patients (Nimse and Pal, 2015, Koopman et al., 2016). However, despite encouraging claims to its effects, both *in vitro* and *in vivo* (Davis et al., 2009, Ay et al., 2017), studies in healthy humans have shown no statistically significant increases in mRNA expression levels of PGC-1α, SIRT1, CytC or citrate synthase; despite trends to increases (Nieman et al., 2010).

The effects of quercetin have been assessed in clinical trials in multiple unrelated diseases and conditions, (Ferry et al., 1996, Okamoto, 2005, Zahedi et al., 2013, Amirchaghmaghi et al., 2015, Kooshyar et al., 2017, Hezaveh et al., 2019) with many more planned or underway in various diseases and conditions including cancer, COPD, *Diabetes mellitus,* Alzheimer's disease and COVID-19 (clinicaltrials.gov: NCT01912820, NCT03989271, NCT00065676, NCT04063124 and NCT04377789 respectively). Despite the wide extent of interest in quercetin, no clinical investigations are yet to take place in mitochondrial disease patients.

Pyrroloquinoline Quinone

Pyrroloquinoline Quinone (PQQ) acts to cycle NADH with NAD+, with the equilibrium of this reaction in favour of NAD^+. Increases in NAD^+ levels have been shown to activate SIRT1 when PQQ is used at micromolar (10-30 μM) concentrations *in vitro* (Zhang et al., 2015b). PQQ has further been shown to exhibit antioxidant capabilities in healthy human volunteers (Harris et al., 2013). PQQ has also been shown to modulate CREB pathways *in vitro*, to increase PGC-1α expression and lead to the induction of mitochondrial biogenesis at 30μM (Chowanadisai et al., 2010). It is noted that SIRT1 activation of PQQ via its redox cycling is not mutually exclusive of its action on CREB.

The injection of mg quantities per kg body weight of PQQ has also been shown to induce MB, via the AMPK axis, in rotenone induced mouse models of Parkinson's disease; resulting in a partial phenotypic improvement over 21 days (Cheng et al., 2021). Results from a trial in untrained human males, supplemented with PQQ while exercising, showed that the oral administration of 20mg/day PQQ resulted in the increased expression of PGC-1α, as measured by ELISA of muscle biopsy homogenate (Hwang et al., 2019). However, no differences were observed in peak oxygen consumption and no ergogenic effects were noted. It is important to note increases in PGC-1α expression does not necessarily result in increased mitochondrial mass or enhanced aerobic performance, due to tight post-transcriptional control of PGC-1α activity.

One *in vitro* study by Saihara *et al*., 2017, claimed PQQ efficacy at nanomolar concentrations, as well as physiological relevance, however, this study's experiments were dependant on serum starvation of cells *in vitro* prior to and during PQQ exposure (Saihara et al., 2017). Serum starvation was likely employed to circumvent the well-documented reactions of PQQ with free amino acids, forming the redox inactive major products oxazolopyrroloquinoline and imidazolopyrroloquinoline in an equilibrium reaction heavily favouring the redox inactive products (Mitchell et al., 1999, Zhang et al., 2015b). The work of Saihara *et al.*, 2017, provides a proof of concept of PQQ stimulated mitochondrial biogenesis at nanomolar levels. Derivatives of PQQ which do not undergo reactions with free amino acids, but retain their redox cycling capabilities, may yet prove to be interesting lines of inquiry for the induction of mitochondrial biogenesis.

Bezafibrate

Bezafibrate, a pan-PPAR agonist and putative inducer of mitochondrial biogenesis, has been explored for potential applications in remedying mitochondrial dysfunction (Tenenbaum et al., 2005, Yatsuga and Suomalainen, 2011).

Yatsuga and Suomalainen, 2011, showed that bezafibrate dampened the cumulative onset of mtDNA deletions and the progressive development of cytochrome c oxidase-negative muscle fibres in mouse models of late-onset mitochondrial myopathy (Yatsuga and Suomalainen, 2011). However, the mice presented multiple detrimental side effects, including (but not limited to) hepatomegaly and severe weight loss, indicating drug toxicity (Komen and Thorburn, 2014). Bezafibrate has also been shown to be ineffective and even detrimental in some rodent models of mitochondrial disease (Viscomi et al., 2011). However, these side effects have previously not been reported in humans (Goldenberg et al., 2008), thus clinical trials investigating the use of bezafibrate in patients with mitochondrial diseases have continued - www.clinicaltrialsregister.eu: 2012-002692-34 (ongoing), 2015-001382-10 (ongoing), 2011-001205-27 (ongoing).

One trial has been completed, in which six patients with m3243A>G associated MELAS (www.clinicaltrialsregister.eu: 2015-000508-24) were given oral doses of 200-400mg bezafibrate, at six-week internals for twelve weeks. The trial showed a 12% increase in CII activity over the twelve-week period, but no changes to any other mitochondrial complex activities, mtDNA copy number or in levels of PGC-1α: and no statistically significant reduction in NMDAS score.

AICAR

AMPK influences both the transcription and activity of PGC-1α. Thus, the efficacy of a synthetic selective AMPK agonist, 5-aminoimidazole-4-carboxamide-1-β-d-ribofuranoside (AICAR), has been explored in the context of mitochondrial biogenesis.

AICAR, a pro-drug metabolised in cell cytoplasm to the active drug ZMP, has been shown to increase physical endurance, reduce exercise intolerance, mimic caloric restriction and rescue mitochondrial dysfunction in mouse models of cytochrome c oxidase deficiency (Viscomi et al., 2011). AICAR has also been associated with increases in PGC-1α and SIRT1 activity, resulting in significant increases in mitochondrial biogenesis in rodents (Gurd et al., 2009, Gurd et al., 2011). Therapeutic relevance for this compound has also been cited regarding liver steatosis, kidney diseases and *Diabetes mellitus* in obese mice (Borgeson et al., 2016).

Despite growing pre-clinical evidence, this compound is yet to be assessed for a therapeutic effect in mitochondrial disease patients in a clinical setting (El-Hattab et al., 2014, Russell et al., 2020).

NAD$^+$ Precursor Supplementation

An impairment to mitochondrial activity can result in the accumulation of NADH, and the subsequent lowering of the levels of NAD$^+$, which also prevents the redox cycling of the NAD$^+$/NADH system. This can lead to dysfunctions in an array of mitochondrial functions and trigger knock-on effects on pathways reliant on NAD$^+$. Therefore, compounds that increase the levels of NAD$^+$ in cells are of potential therapeutic interest. This is not only due to the correction of the NAD$^+$/NADH ratio, but also because of the impact on the NAD$^+$ dependent deacetylase SIRT1, and thereby on PGC-1α activity and mitochondrial biogenesis.

Nicotinamide riboside (NR - a direct precursor of NAD$^+$) and polyADP-ribose polymerase (PARP – a major consumer of NAD$^+$ in the nucleus) inhibitors have been shown to increase endogenous NAD+ levels, thereby raising the activity of SIRT1 (Russell et al., 2020). This approach has seen various levels of success within *in vitro* studies and *in vivo* models (Gorman et al., 2016). NR has been shown to increase the activity of PGC-1α and lead to the upregulation of mitochondrial biogenesis in the "Deletor" mouse model (Khan et al., 2014). NR and PARP inhibition has also demonstrated a recovery of OXPHOS associated gene expression in *Sco*^{KOKI} mice (Cerutti et al., 2014). Administration of nicotinamide mononucleotide (NMR), an additional NAD$^+$ precursor downstream of NR in the synthesis pathway of NAD$^+$, to mouse models of Leigh Syndrome (NDUFS4 knockout) ameliorated lactic acidosis and increased lifespan (Lee et al., 2019).

Another NAD$^+$ precursor, the vitamin B3 derivative niacin, has been shown in a clinical trial in patients with mitochondrial myopathy (NCT03973203) to return NAD$^+$ levels to that of controls and increase both muscle strength and mitochondrial biogenesis, without altering mtDNA deletion levels or intra-mitochondrial structure (Pirinen et al., 2020). The study conducted by Pirinen *et al.*, 2020, not only advances efforts to produce a treatment for mitochondrial myopathies but also acts as a proof of principle for the beneficial effects of mitochondrial biogenesis; despite not addressing or correcting the underlying mtDNA defect (Pirinen et al., 2020). Clinical investigations into vitamin B3 derivatives continue: acipimox is planned to undergo clinical investigation in m.3243A>G and large-scale mtDNA deletion patients; the trial (AIMM) is currently recruiting.

Idebenone

Idebenone is a synthetic analogue of CoQ capable of donating electrons to CIII of the mitochondrial respiratory chain. This allows the bypass of CI to restore activity to CIII and thereby CIV via the reduction of cytochrome C. Idebenone is also hypothesised to act as a membrane localised antioxidant to suppress lipid peroxidation (Russell et al., 2020).

A phase II clinical trial, in 85 patients with genetically confirmed LHON conducted over three years, has shown improvement in visual acuity (Klopstock et al., 2011, Klopstock et al., 2013), resulting in Idebenone subsequently being approved for use in these patients (Rudolph et al., 2013, Garone and Viscomi 2018, Russell et al., 2020). Follow-up clinical studies are planned (NCT02774005) and currently recruiting (NCT02771379).

Elamipretide

Elamipretide is a modified cationic cell-permeable tetrapeptide, which localises to mitochondria and has been demonstrated to bind cardiolipin (Birk et al., 2013). This effect has been shown to aid the formation of super-complexes and thereby increase respiratory efficiency (Chatfield et al., 2019). Elamipretide also restores cristae structure and connectivity through aggregating and stabilising cardiolipin, as measured by serial block-face scanning electron microscopy, in ischemic rat hearts, which also resulted in the recovery of respiratory function (Allen et al., 2020).

Clinically, elamipretide has been under investigation in the MMPOWER trial series (NCT02367014). The phase II trial (MMPOWER-II), conducted over four weeks, resulted in patients exhibiting approximately a 5% improvement in distance covered in a six-minute walk test (Cohen et al., 2018). Although this failed to achieve statistical significance, a trend was noted and a phase III clinical trial (MMPOWER-III, NCT03323749) was initiated (Cohen et al., 2018). MMPOWER-III published results in 2019, showing that the primary endpoints of improvements in the six-minute walk test and the Primary Mitochondrial Myopathy Symptom Assessment (PPMSA) total fatigue score were not met; the trial has since been terminated (Prnewswire, 2019).

KH176

KH176 is a derivative of vitamin E, shown to be an orally bioavailable potent antioxidant in mitochondria, capable of permeating the blood-brain-barrier (Koopman et al., 2016). Pre-clinical investigations using NDUFS4 knockout mice showed that KH176 normalised lipid peroxidation and improved motor performance; as measured by a rotor-rod test (De Haas et al., 2017). A phase II clinical trial, assessing the effects of KH176 in twenty m.3243A>G associated MELAS patients (KHENERGY - NCT02909400) was completed in 2017. The trial observed no significant improvements in the primary outcome measure of gait parameters, though improvements to mood and alertness were apparent (Janssen et al., 2018). As a result, a follow-up study (KHENERGIZE - NCT04165239) to confirm these beneficial effects is currently recruiting MELAS patients.

Bromo-Domain Protein Inhibitors

A high throughput CRISPR screen spanning the entire human genome, in complex I deficient cybrid cells (m.14459G>A) screening for an improvement to cell survival in galactose media, has identified a competitive repressor of some PCG-1α promoter/enhancer sites: BRD4 (Barrow et al., 2016). A subsequent screen of a small molecule library, screening for the same outcome, uncovered I-BET-525762A; a potent small-molecule inhibitor of BRD4, currently used in the treatments of various cancers (Barrow et al., 2016). While CRISPR knockout, or IBET treatment, did not resolve complex I deficiency itself, metabolic reprogramming was evident. A bypass of complex I was observed in treated cells, demonstrated by increases in levels of the CII substrate $FADH_2$, due to a shift to glutamine becoming a significant substrate of the tricarboxylic acid cycle. Functionally, IBET treatment increased CII and CIV derived oxygen consumption and allowed ND6 mutation harbouring cybrid cells to survive acute exposure to galactose media (Barrow et al., 2016). Non-specific BRD inhibition using I-BET-151, targeting BRD2/3/4, is highly damaging to the ultrastructure of cardiomyocyte mitochondria in rodents; leading to reductions in respiration rate and mitochondrial mass (Piquereau et al., 2019). Therefore, the pharmaceutical development of I-BET compounds required for their re-application to mitochondrial diseases must be undertaken with a high degree of caution to maintain target specificity to BRD4.

Table 1.1. *Summary of putative small molecule therapeutics under investigation for the treatment of mitochondrial diseases.*

.

Putative Therapeutic	Proposed Mechanism	Development/Clinical Trial Stage
Rapamycin	Metabolic reprogramming	Pre-clinical
Resveratrol	MB – SIRT1 Activation	Phase II
Epicatechin	MB – PXR Activation	Phase II – Failed Primary Endpoints
Omaveloxolone	MB – NRF2 Activation	Phase II
Quercetin	MB – NRF2 Activation	Phase II (excl. mito. dis.)
PQQ	MB – Indirect SIR1 Activation	Pre-clinical
Bezafibrate	MB – Pan-PPAR Agonist	Phase II
AICAR	MB – AMPK Agonist	Pre-clinical
NR	MB – SIRT1 Activation	Pre-clinical
Niacin	MB – SIRT1 Activation	Phase II
Acipimox	MB – SIRT1 Activation	Phase II (Recruiting)
Idebenone	Complex Bypass – CIII	Approved for use in LHON Patients
Elamipretide	Cardiolipin Binding	Phase III – Failed Primary Endpoints
KH176	Small Molecule Antioxidant	Phase II
I-BET-525762A	Bromo-Domain Inhibitor	Pre-clinical

1.9. An Overview of Drug Discovery Methods

The panel of putative treatment options for mitochondrial disease under investigation, section 1.8.5, demonstrates the need for the continual discovery of new lead compounds; several initially promising compounds have failed to meet primary trial endpoints. Drug discovery projects can proceed along one of two routes, targeted directed design or phenotypic screening. While, if successful, both arrive at the identification of a lead compound, they are rooted in opposing principles.

1.9.1 Target Directed Drug Design

Target directed drug design relies on the identification of a suitable protein target, to allow specificity of targeting. This requires in-depth knowledge of the pathological mechanisms underlying the targeted disease to allow for the identification and assessment of putative target proteins (Anderson, 2003). A target is chosen through *in vitro* methods, for example, genetic knock-down/knock-out investigations, screening for an improvement in the disease state of *in vitro* cellular models, or through the use of positive control suitable for *in vitro* use in cell lines - but not clinically approved for patient use. Specific targeting of a key protein in disease pathology further requires not only absolute knowledge of the disease state but also homogeneity among the patient population to ensure that any resultant drug will be of significant therapeutic value.

Near atomic-resolution structural information of the final targeted protein is required to guide the synthesis of putative therapeutic compounds. Compounds are purposely designed to bind to a target site and interact with key residues within (Anderson, 2003). This is achieved through a variety of chemical interactions including Van der Waals forces, pi stacking, polar interactions and hydrogen bonding and often sees the employment of *in silico* modelling of drug/target interactions. A lead compound is selected once efficacy is proven and taken forward for lead optimisation through structural activity relationship (SAR) experiments.

While target directed drug design projects can ensure the development of a potent ligand to a protein target of interest, the biological implications of such an agent often remain unknown until the *in vitro* validation of lead compounds. Degenerate systems are common in biology: the inhibition or activation of a biomolecule in the cell can result in the activation of compensatory mechanisms to enforce the pre-intervention status quo. This results in target directed drug design presenting as a high risk, high reward strategy, which can see extensive financial and labour investments on lead candidates

which never progress beyond the pre-clinical laboratory setting (Morgan et al., 2011, Hingorani et al., 2019).

1.9.2 Phenotypic Screening

Phenotypic screening is reliant on the rapid assessment of large libraries of samples, be they individual, characterised compounds or natural product extracts containing complex mixtures of biomolecules. It is a powerful tool when knowledge of possible protein targets is incomplete, but when distinct differences between diseased and healthy cell populations are easily recorded. Thus, phenotypic screening projects are dependent on the generation of repeatable and reproducible assays, yielding consistent responses to positive controls, when available. In lew of a positive control for phenotypic improvement, the state of wild-type control cells serves as a surrogate, however, this increases assay complexity due to the requirement of an additional cell type.

Once a hit sample is identified, mechanistic elucidation can commence, often in the form of protein pull-down experiments to identify binding partners of the compound. When a target protein has been identified, experiments can commence to optimise the lead compound in a manner analogous to target directed drug design. However, SAR analysis-like experiments can also be completed, through the random exploration of chemical space around the lead compound, guided by phenotypic results using investigative experiments analogous to the initial screen.

Projects employing libraries of natural product extracts must follow the intermediate step of sample purification, prior to lead optimisation, to identify the active component(s) of the sample. This process uses chromatographic techniques, to separate samples into component parts, followed by the screening of resultant fractions in a manner similar to the initial screen.

Phenotypic screening often includes a lengthy assay development and optimisation period. Screens of large chemical libraries are both time-consuming and expensive, thus it is favourable to expend significant effort to produce a reliable assay to ensure multiple replicate screens are not required. Despite this, a significant advantage of phenotypic screening in novel fields for drug discovery is that it allows the assessment of previously undescribed molecular pathways. This aspect opens a new avenue for therapeutic development, regardless of whether a final optimised therapeutic is

discovered, as the identification of novel pathways facilitates target directed drug design approaches.

The Z' Score in Phenotypic Screening Assays

The Z' score is used to assess the viability of screening methods by calculating the relationships between means and standard deviations of positive and negative controls. Z' scores range from 0 to 1, with a Z' score of 1 indicating complete separation of negative and positive control data. A Z' score of $0.5 < Z' < 1.0$ is indicative of a workable screening assay with sufficient separation between positive and negative control, minimising the risk of identifying false positives or false negatives. A result of $Z' < 0.5$ indicates that the assay is unsuitable for screening - as the method cannot reliably distinguish between positive and negative results. The Z' score is calculated as follows:

$$\mathbf{Z' = 1 - 3(\sigma_p + \sigma_n)/|\mu_p - \mu_n|}$$

$\sigma_{p/n}$: Standard Deviation of positive or negative control data.

$\mu_{p/n}$: Mean of positive or negative control data

1.10.3 Phenotypic Screening with Target Based Lead Optimisation

Despite the above two drug discovery methods outlined above being rooted in contrasting principles, their use is complimentary. Projects commence with phenotypic assays, screening for a desired effect, and culminate in lead optimisation of hit compounds once a target protein is identified. Drug discovery projects such as the Drp-1 inhibitor, MDivi-1, and POLRMT inhibitor, IMT1B, exemplify the real-world applications of phenotypic and target directed drug discovery (Cassidy-Stone et al., 2008, Bonekamp et al., 2020).

1.10 Project Aims

1.10.1 High Throughput Screening for Mitochondrial Proliferators

Evidence for the beneficial effect of mitochondrial biogenesis in models of mitochondrial disease has been mounting over the previous decade. Despite numerous candidate compounds being presented in the literature for many years, with notable *in vitro* and pre-clinical *in vivo* improvements to various mitochondrial disease associated phenotypes, only one class of compound (vitamin B derivatives) have shown promise as a putative treatment of mitochondrial diseases via mitochondrial biogenesis.

Due to the highly unpredictable nature of drug development and clinical trials, the current project seeks to identify further lead compounds for mitochondrial biogenesis, using the high-throughput phenotypic screening of natural products in conjunction with an industrial collaborator (Nanna Therapeutics).

The employment of phenotypic screening was selected for drug discovery purposes in this project. This decision was made due to the large number of complex and interconnecting pathways implicated in mitochondrial health, as shown by the numerous mechanisms of action of putative treatments in section 1.8.5. The targeting of a single pathway, for drug design efforts, significantly reduces the scope for the identification of novel therapeutics, in a field with no fully characterised positive control to guide a target directed project.

1.10.2 Investigation of the Effects of Agents Capable of Increasing Mitochondrial Mass on the rate of Mitophagy

The current project aims to further the knowledge surrounding any hit bacterial extracts, as a result of aim 1.11.1, to aid in their progress in the drug discovery pipeline. As part of the mechanism of action investigation plans for mitochondrial biogenesis hits identified as per aim 1.11.1, the assessment of the effects of hit bacterial extracts on the rate of mitophagy will be employed, using MitoQC analysis. Mechanistic insights can be gained by establishing whether mitophagy rates are reduced in cells exposed to mitochondrial biogenesis inducing hit bacterial extracts.

1.10.3 Development of Novel Methods for the Characterisation of Disease Burden in Cell Line Models of Mitochondrial Diseases

The heterogeneity of mitochondrial diseases, and the biochemical defects therein, have hampered therapeutic development due to a lack of simple and reliable *in vitro* phenotypic screens. The most common biochemical defects in mitochondrial diseases are deficiencies in either complex I, complex IV, or both (Swalwell et al., 2011, Nouws et al., 2012, Lake et al., 2016, Alston et al., 2017, Lax et al., 2016).

The development of a high-throughput technique for the quantification of the levels of complexes I and IV has the potential to enable generalised phenotypic screening and accelerate patient diagnosis. Current methods for the quantification of protein complex levels in patient cells rely on low-throughput gel-based techniques, such as Western Blotting, Blue Native–PAGE analysis and muscle biopsy analysis (Ng et al., 2021).

The current project aims to develop and validate a multi-well-plate assay to facilitate the high-throughput quantification of phenotypic burden represented by the levels of mitochondrial complexes I and IV.

Chapter 2:

Methods

2.1 Materials

Index of equipment, consumables and reagents.

2.1.1 Equipment

Applied Biosystems StepOnePlus Real-Time PCR System (4376600)

BD Biosciences FACS Symphony

BD Biosciences High Throughput System

Cellometer Auto 1000 Cell Counter (Nexcelom Biosciences)

ChemiDoc System (Bio-rad)

Eppendorf Thermomixer C (5382000015)

IncuCyte Live Cell Analysis System (Essen Biosciences)

Seahorse XF96 Analyser (Agilent)

Tecan D300e Digital Dispenser

Tecan HydroSpeed Plate Washer

Thermo Multidrop Combi Reagent Dispenser

Trans-Blot Turbo System (Bio-rad)

Zeiss Cell Discoverer 7

2.1.2 Consumables

384 well glass-bottomed imaging plate (PerkinElmer CellCarrier384 Ultra – 6057300)

96 well glass-bottomed imaging plate (PerkinElmer CellCarrier96 Ultra - 6055300)

96 well U-bottomed plates (Greiner Bio-One CellStar - 650185)

96-well Flat-Bottomed Plates (Greiner Bio-One CellStar - 655160)

96-well Flat-Bottomed Plates (TPP - 92096)

96-well PCR plate (Applied Biosystems MicroAmp Fast Optical 96-Well Reaction Plate – 4346906)

ADP (Sigma Life Science, 01905-1G-F)

Antimycin A (Sigma Life Science, A8674-25MG)

Bradford Reagent (Bio-rad)

Cellometer Disposable Cell Counting Chambers (Nexcelom Biosciences, PD100)

Cryotubes (CryoPure Röhren, 72.380)

Dialysed Foetal Bovine Serum (dFBS, Sigma Life Science – F0392)

Dimethyl Sulfoxide (DMSO, Sigma Life Science – D2660-100ML)

Dulbecco's Modified Eagles Medium – Glucose Free (GluFree-DMEM, Sigma Life Science – 11966025)

Dulbecco's Modified Eagles Medium (DMEM, Sigma Life Science D5796-500ML)

Dulbecco's Phosphate Buffered Saline (DPBS, Thermo Fisher - 14190-094)

Foetal bovine serum (FBS, Sigma Life Science - F0926)

G418 antibiotic (Sigma Life Sciences – A1720-5G)

Iscove's Modified Dulbecco's Media (IMDM, Gibco Life Technologies 31980-022)

Magnesium Chloride Solution 50mM (Bioline - BIO-37026)

Mini-PROTEAN TGX 12% precast gels (Bio-rad)

Non-Essential Amino Acid Solution (Sigma Life Science – M7145)

Normal Goat Serum (NGS – Sigma Aldrich; G9023)

Paraformaldehyde Solution 4% in PBS (ChemCruz – sc-281692)

Penstrep (Gibco Life Technologies – 15140-122)

Proteinase K (Invitrogen – 1777172)

Reservoirs (StarLab, E2310-1010)

Rotenone (Sigma Life Science, R8875-1G)

Seahorse XF Plasma Membrane Permeabilizer (PMP, Agilent - 102504-100)

Seahorse XFe96 Cell Culture Microplates (Agilent, 101085-004)

Seahorse XFe96 Sensor Cartridges (Agilent, FluxPack Mini, 102601-100)

Sodium Pyruvate Solution (100mM, Sigma Life Science – S8636)

Sodium Succinate (Sigma Life Science S2378-100G)

StarSeal Advanced Polyolefin Film (E2796- 9795)

StarSeal Sealing Tape – Aluminium Foil (E2796-1100)

TAQMAN master mix (Thermo Fisher Scientific - Applied Biosystems, 4440038)

Trypan Blue (Invitrogen - T10282)

TrypLE Solution (Gibco Life Technologies – 12605-010)

Universal Tissue Culture Tubes (Griener Bio-One, 201172)

Uridine (Sigma Life Science – U3003)

Vented T300 Adherent Cell Flasks (VWR, 10062-884)

Vented T75 Adherent Cell Flasks (Sarstedt – 83.3911.302)

Vented T75 Suspension Cell Flasks (Sarstedt – 83.3911.502)

2.1.3 Buffers and Solutions

Laemmli Sample Buffer – 2x. (4ml Glycercol, 4ml 20% SDS, 0.02g Bromophenol blue, 2ml dH_2O)

PBS (0.137M NaCl, 0.0027M KCl, 0.01M Na_2HPO_4, 0.0018M K_2HPO_4 – pH 7.4)

qPCR Lysis buffer (10% v/v 0.5M TrisHCl – pH 8.5 - 1% Tween20 in PBS, 39% deionised water and 1% Proteinase K)

RIPA Lysis Buffer (50mM Tris-HCl, 150mM NaCl, 0.1% Sodium Dodecyl Sulphate, 0.5% Sodium deoxycholate, 1% IPEAGAL, Protease Inhibitor Cocktail - 1 Tablet, 10ml dH_2O)

TBST (0.014M NaCl, 0.002M Tris base 0.1% Tween20 – pH 7.6)

Tris-glycine running buffer – 5x. (144g glycine, 30g Trizma Base, 10g SDS, 2l dH_2O – pH. 8.8).

Western Blot Blocking Buffer (5g Powered Milk, Marvel, 100ml TBST)

2.1.4 Antibodies and Target Binding Small Molecules

Table 2.1. *Index of primary and secondary antibodies employed throughout the project.*

Primary Antibodies				
Host Species	**Isotype**	**Protein Target**	**Stock Concentration (mg/ml)**	**Source & Reference Number**
Rabbit	IgG	TOM20	0.235	Abcam: ab186734
Mouse	IgG1	NDUFB8	1.0	Abcam: ab110242
Mouse	IgG1	NDUFS3	1.0	Abcam: ab110246
Mouse	IgG1	SDHA	1.0	Abcam: ab14715
Mouse	IgG2a	MTCOI	1.0	Abcam: ab14705
Mouse	IgG2b	TFAM	1.0	Abcam: ab119684
Mouse	IgG2b	NDUFA13	1.0	Abcam: ab110240
Secondary Antibodies				
Host Species	**Target Species & Isotype**	**Conjugated Fluorophore**	**Stock Concentration (mg/ml)**	**Source & Reference Number**
Goat	Rabbit IgG	Alexa-Fluor-405	2.0	Invitrogen: A31556
Goat	Rabbit IgG	Alexa-Fluor-488	2.0	Invitrogen: A11008
Goat	Mouse IgG1	Alexa-Fluor-488	2.0	Invitrogen: A21121
Goat	Mouse IgG1	Alexa-Fluor-546	2.0	Invitrogen: A21123
Goat	Mouse IgG1	Alexa-Fluor-647	2.0	Invitrogen: A21240
Goat	Mouse IgG2a	Alexa-Fluor-546	2.0	Invitrogen: A21133
Goat	Mouse IgG2a	Alexa-Fluor-647	2.0	Invitrogen: A21241
Goat	Mouse IgG2b	Alexa-Fluor-546	2.0	Invitrogen: A21143
Goat	Mouse IgG2b	Alexa-Fluor-647	2.0	Invitrogen: A21242

Table 2.2 *Small molecules used in fluorescent microscopy to label cellular structures.*

Target Binding Small Molecules				
Molecule	**Target**	**Conjugated Fluorophore/Intrinsic fluorescence**	**Source & Reference Number**	**Solvent/Stock Concentration**
Phalloidin	F-Actin	Alexa-Fluor-568	Invitrogen: A12380	Methanol/6.6μM
DAPI	dsDNA	350/460nm	Thermo Fisher: D21490	dH_2O/36mM

2.1.5 DNA Oligomers for qPCR Reactions

Table 2.3. *DNA oligomers purchased from Eurofin Genomics for use in qPCR reactions*

DNA Oligomer	**Sequence**
MT-ND1 Probe	VIC-5′-CCATCACCCTCTACATCACCGCCC-3′-MGB
B2M Probe	6-FAM-5’ATGTGTCTGGGTTTCATCCATCCGACA-3’MGB
MT-ND1 forward primer	5′CCCTAAAACCCGCCACATCT-3′
MT-ND1 reverse primer	5′- GAGCGATGGTGAGAGCTAAGGT-3′
B2M forward primer	5’- CCAGCAGAGAATGGAAAGTCAA-3’
B2M reverse primer	5’-TCTCTCTCCATTCTTCAGTAAGTCAACT-3’

2.2 Cell Culture Methods

2.2.1 Mammalian Cell Culture

All cultured cell lines were routinely incubated at 37°C in a humidified atmosphere containing 5% CO_2.

K562 cells were cultured in T75 suspension flasks in IMDM supplemented with 10% (v/v) foetal calf serum (FCS) and 1% (v/v) penstrep, forming complete IMDM. A line of K562 cells has previously been transfected to constitutively express GFP fused to a COXVIII mitochondrial import sequence (K562-m-GFP). The transfection also conveyed G418 resistance to the cells to facilitate selection. K562-m-GFP cells were routinely cultured in complete IMDM treated with 300µg/ml G418.

HeLa cells were cultured in T75 flasks in DMEM supplemented with 10% (v/v) foetal bovine serum and 1% (v/v) penstrep, forming complete DMEM. Immortalised fibroblast cells, derived from human mitochondrial disease patients (NDUFS2 mutant) and healthy controls, were cultured in T75 or T300 flasks in complete DMEM further supplemented with 1% (v/v) non-essential amino acid solution and 50ng/ml uridine, forming glucose fibroblast media. As experiments required, to force the presentation of the OXPHOS defect, NDUFS2 mutant fibroblasts were also cultured in galactose fibroblast media: GluFree-DMEM supplemented with 10mM galactose, 10% (v/v) dFBS, 1% (v/v) Penstrep, 1% (v/v) non-essential amino acid solution, 50ng/ml uridine, 1% sodium pyruvate solution.

2.2.2 Cell Passaging

All adherent cells were passaged, once at 80% confluence, by trypsinisation. Cells were washed once with DPBS and treated with 2ml or 5ml TrypLE trypsin solution, for T75 or T300 flasks respectively. Trypsin was quenched using 8ml or 20ml of appropriate complete media, for T75 or T300 flasks respectively, and subsequently transferred to universal tissue culture tubes followed by centrifugation at 160g for four minutes. The supernatant was aspirated from the universal tubes and resultant cell pellets were resuspended in appropriate media for reseeding or plating at desired confluences. Suspension cell lines were passaged by the removal and replacement of half of the culture media.

2.2.3 Cryogenic Preservation of Cell Lines

Adherent cells were prepared for cryo-preservation through trypsinisation and pelleting as described above, with resultant pellets resuspended in 1ml or 4ml FBS with 10% (v/v) DMSO, per T75 or T300 flask respectively. Suspension cell lines were prepared for cryo-preservation by centrifugation and aspiration of supernatant followed by resuspension in 1ml FBS with 10% (v/v) DMSO per T75 flask equivalent area (i.e., 4ml FBS/DMSO for a cell pellet originating from one T300 flask). 1ml aliquots of cell suspension were transferred to individual cryotubes, which were frozen at -80^{o}C for 24 hours and subsequently transferred to liquid nitrogen storage vessels.

2.2.4 Cell Counting

Cell counts were obtained by staining 10µl cell suspension with Trypan blue (1:1 v/v). 10µl of the resultant mixture was transferred to a disposable cell counting chamber for use in a Nexcelom Cellometer Auto 1000. Three replicate counts were acquired per cell line to facilitate the calculation of an accurate mean cell density (cells/ml). This value was used in cell plating for all assays carried out in multi-well plates, described in the following subsections.

2.3 Methods Utilised in the Development of an Assay Pipeline for the Identification of Agents Capable of Inducing Mitochondrial Biogenesis

Methods Used by Nanna Therapeutics Collaborators

2.3.1 Bacterial Library Formation and Primary Screening

The following information in section 3.3.1 has been provided by a senior member of staff at Nanna Therapeutics, which has been interpreted by the author. The experimental methodologies briefly outlined in section 3.3.1 were carried out by staff at Nanna Therapeutics; the author makes no claims of ownership regarding any aspect of the work in this specific section.

Library Formation

Bacterial libraries were formed using over 100,000 unique bacterial species from a variety of ecological niches, but largely from soil-dwelling bacteria. Bacteria were subject to random transposon mutagenesis, using transposons containing promoters of five different expression strengths. Due to the random nature of transposon insertion into the bacterial genomes, limited to one insertion event per cell through the stoichiometric use of reagents and transposon vector, in excess of $1x10^9$ unique clones can be produced per species. The transposon insertion events can give rise to a number of possible outcomes for the randomly targeted gene: overexpression, truncation or knockout. This results in the production of approximately 20-50 unique metabolites per clone, due to the change in the expression level of the transposon effected gene. The process is outlined in Fig 2.1.

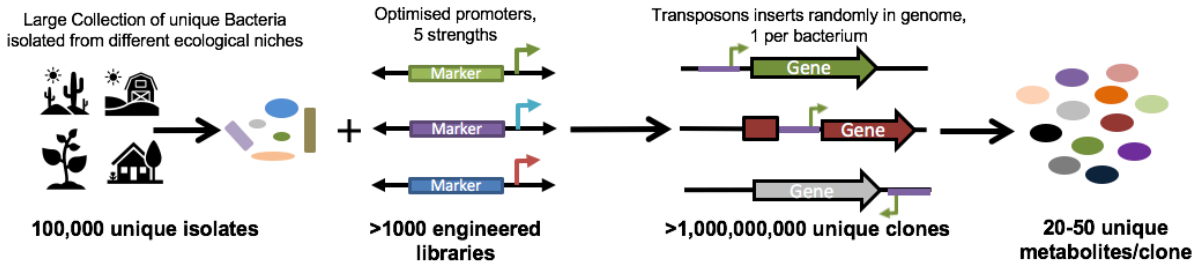

Fig 2.1. A representation of the steps taken to produce natural product extract libraries at Nanna Therapeutics. Sequencing of libraries showed that the transposons were distributed around the genome, except within essential genes.

Primary Screening

Individual bacterial clones, single cells, from the Nanna Therapeutics natural products library were encapsulated alongside mammalian cells in 0.5nl vesicles of silicone or flurous based oils with 'Nanna-Surfactants' (precise formula withheld on request by Nanna Therapeutics). Co-cultures were created by diluting bacteria to approximately 250,000 colony-forming units/ml of media, either RPMI or Freestyle293T, containing mammalian cells: Jurkat, HEK293T or HepG2s (all acquired from ATCC) at 0.2-1x10^6 cells/ml. The microdroplets were formed using modified flow-focusing devices (Dolomite, UK or Micronit, NL) whereby the aqueous liquid mix of bacterial and mammalian cells was fed into the device under pressure and mixed with the oil at the junction, Fig 2.2.

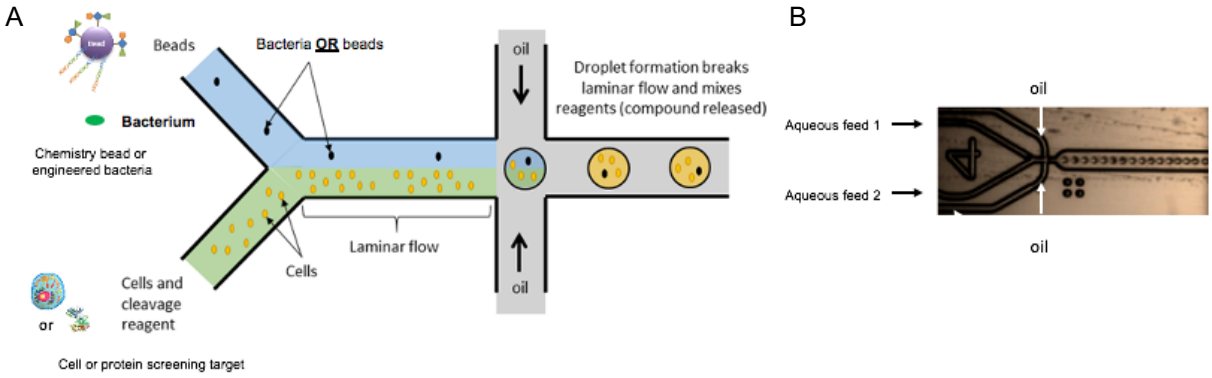

Fig 2.2. *Representations of a Nanna Therapeutics microfluidic chip used in microdroplet production*. A. Schematic of a microfluidic chip. B. Light microscope image of a microfluidic chip in use.

Flow rates used were routinely 100-200 µl/minute of aqueous cell mixtures and 300-400µl/minute of oil. The flow rate was determined empirically for each mixture by generating vesicles and ensuring the droplet size was 100µm in diameter, as measured by light microscopy. Modifications to the flow rates were made to consistently generate microdroplets of this size.

The generation of microdroplets proceeded for 2-3 hours to generate 30-50ml of aqueous microdroplets in a total volume of >100ml. Excess oil was gently decanted from the product mixture and the vesicles were incubated for 120 hours at 37°C + 5% CO_2 in standard tissue culture flasks. This allowed time for bacterial clones to grow and produce metabolites and for the mammalian cells to respond.

Microdroplets were subsequently separated from suspension media, using a 125μm mesh particle strainer above a 40μm mesh particle strainer (Fisher, UK), to remove any large particles and bacteria outside the vesicles. The cells within the vesicles were then stained by addition of 5nM TMRM (Fisher, UK) for 1h, incubated at 37°C in an atmosphere containing 5% CO_2, in standard tissue culture flasks. Thereafter the cells were further stained using 20nM Hoechst (Fisher UK - 33342) for thirty minutes.

Sorts were performed on custom, modified MoFloXDP cell sorters using a 200μm nozzle. Excitation of Hoechst was achieved using a 100mW, 405nm laser. Emission from Hoechst staining was detected via a filter set for 480+/- 30nm. TMRM was excited from a 488nm, 100mW, laser - detection was achieved using a 590nm +/- 25nm filter set. Hoechst and TMRM signals were detected on a logarithmic and linear scale respectively. Single-way sorts were performed on microdroplets showing a relative increase of TMRM of greater than 25% of the mean these vesicles were collected and then burst to free bacteria within. These hit-producing bacteria were plated onto agar, containing antibiotics to select for the transposons within, and allowed to grow until colonies appeared.

Once colonies appeared, they were isolated by streaking onto fresh agar. Stocks of hit-producing bacteria were formed through cryo-preservation of bacterial cultures.

2.3.2 Putative Hit Sample Preparation

Putative hit bacteria were thawed in Freestyle media at room temperature, from cryopreserved stocks, and streaked onto agar in 10cm petri dishes and incubated at 37°C overnight. Single colonies were subsequently picked and used to inoculate 100ml Freestyle media in T75 suspension flasks and incubated at 37°C for five days to allow for the conditioning of the growth medium with bacterial metabolites.

After the incubation period, bacterial cultures were centrifuged to clarity. The resultant supernatant was filtered through a 0.22µm PVDF filter, to remove bacterial cells and other contaminants. Filtered supernatant samples were lyophilised by rotary evaporation to complete dryness and frozen at -20°C. Putative hit samples were transferred to containers suitable for transport to the Wellcome Centre for Mitochondrial Research (WCMR); U bottomed 96 well plates, deep well 96 well plates or Eppendorf tubes, dependent on the amount of sample to be transported.

Once received at WCMR, samples were reconstituted in sterile-filtered dH_2O to the pre-lyophilised volume, or one-tenth of the pre-lyophilised volume, dependent on experimental requirements.

Methods Used in Mitochondrial Proliferator Screening at WCMR

A high throughput screening approach was employed to assess samples for mitochondrial biogenesis effects on human cell lines. To fulfil this requirement a variety of stages were used, which can be summarised in the figure below.

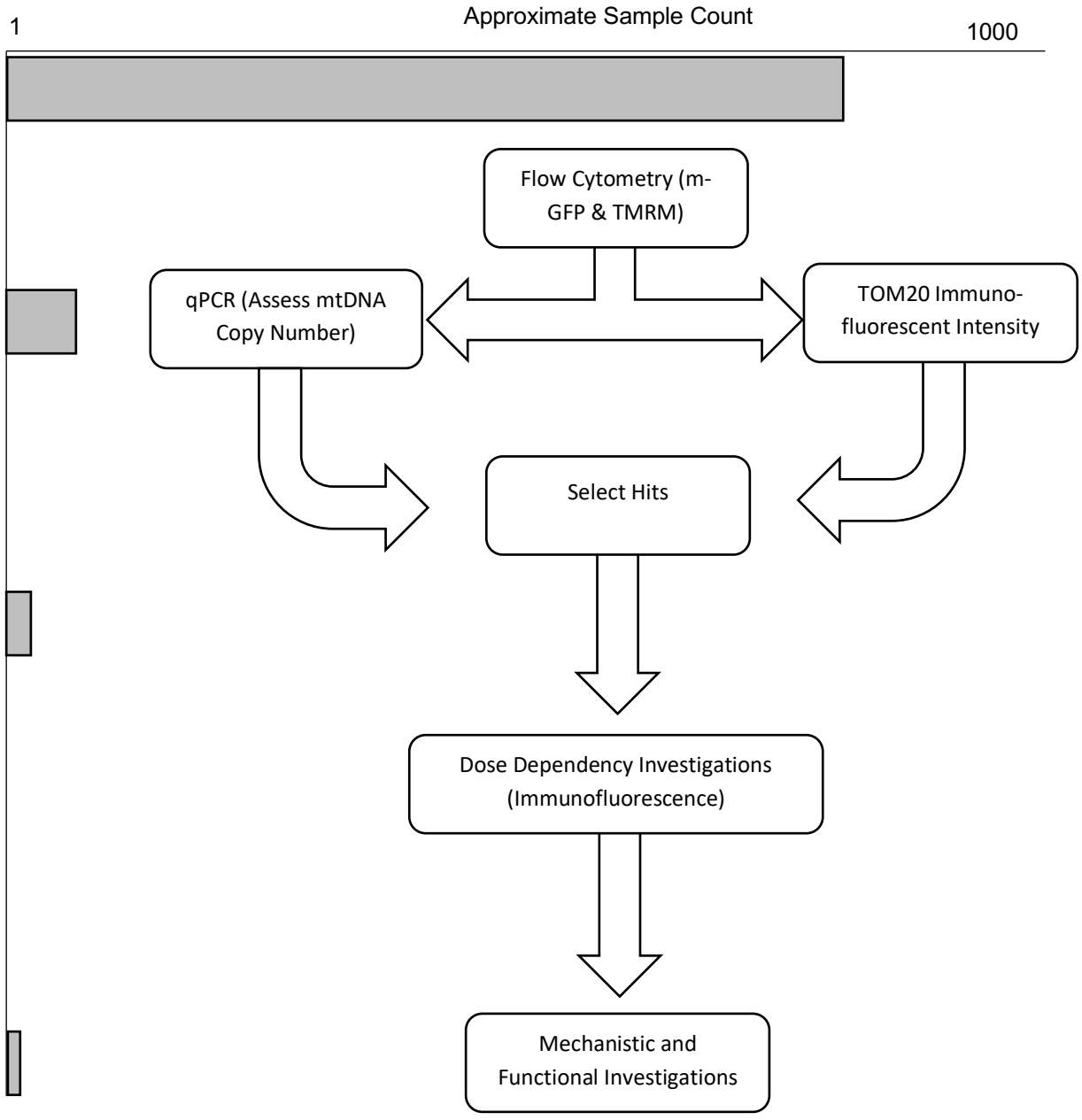

Fig 2.3. *A flow diagram illustrating the planned high throughput screening approach, which was applied to efforts to identify mitochondrial proliferating agents.*

2.3.3 Flow Cytometry

Cell Incubation and Sample Preparation

During a previous project, a K562 lymphoblastoma cell line was transfected to constitutively express COXVIII-N-terminal mitochondrial targeting sequence-green fluorescent protein (m-GFP). This current project employed these K652-mGFP cells, which were plated into 96 well U-bottomed plates at a density of 10,000 cells, in 50µl complete IMDM, per well. Putative hit bacterial extracts were added to wells at a 1:1 volume ratio with IMDM. Cells were then incubated at 37^{o}C in a humidified atmosphere containing 5% CO_2 for 48 hours. Before data collection, cells were subject to staining with 5nM tetramethylrhodamine methyl ester (TMRM) for thirty minutes.

Flow Cytometry Methodology

All flow cytometry screening at WCMR was carried out using a BD Biosciences FACS Symphony instrument, coupled with a High Throughput System (HTS) attachment to allow for efficient sampling from 96 well plates. Lasers to stimulate GFP and TMRM fluorescence were selected: 488nm and 561nm respectively, emission intensities were detected at 530nm and 586nm for GFP and TMRM respectively. Prior to flow analysis, the contents of each well were briefly mixed using a multi-channel pipette, set at 75µl, to minimise cell clumping. Wells were subjected to a further four mixing cycles of 50µl each using the BD Biosciences HTS at a mixing rate of 200µl/second. Sampling from the HTS to the FACS Symphony consisted of 10µl cell suspension from each well in succession, at a flow rate of 3µl/second.

Data Processing and Analysis

Data were processed using FCS Express 6 Flow Research Edition software (DeNovo Software FCS Express 6.05.0028) to calculate mean and standard deviation values of m-GFP and TMRM signals for all samples. These data were exported in Microsoft Excel CSV files to allow import into R Studio for further processing with a ggplot2 package (R Core Team, 2017, R: A language and environment for statistical computing: https://www.R-project.org/). This method allowed for data normalisation to untreated controls, the automatic identification of samples present in the top five percentiles in each measured parameter and the creation of scatterplots for data visualisation. The computational code for flow cytometry data processing can be found in section 7.1: Appendix A.

2.3.4 qPCR

Cell Incubation and Sample Preparation

HeLa cells were plated in 96-well flat-bottomed plates at a density of 5000 cells, in 50µl complete DMEM, per well. To allow for cell adherence to the well surface, the plates were incubated for 24 hours at 37^{o}C in a humidified atmosphere containing 5% CO_2. The cells were treated with samples of interest at a 1:1 dilution in culture media and further incubated for 48 hours. To extract lysates for qPCR analysis, cells were subsequently incubated with 100µl lysis buffer per well at 37^{o}C for thirty minutes, mixed at 300rpm while being heated to 55^{o}C in a thermomixer for two hours, followed by 10 minutes at 95^{o}C without mixing. All samples were then immediately frozen at -20^{o}C.

qPCR Methodology

The qPCR reaction utilised TAQMAN master mix in an Applied Biosystems StepOnePlus Real-Time PCR to calculate the relative levels of an *MT-ND1* amplicon as a measure of mtDNA copy number normalised against an amplicon of the beta-2-macroglobulin single-copy nuclear gene (*B2M*) (Rygiel et al., 2015). An index of DNA oligomers used can be found under section 2.1.5. All probes were made up to 5µM stocks in autoclaved dH_2O, all primers were made up as 10µM stocks in autoclaved dH_2O. Appropriate volumes of complete master mixes were calculated for the production of *MT-ND1* and *B2M* amplicons (1.5ml per 96 well plate of samples) and were prepared as shown in table 2.4.

Table 2.4. *Composition of complete MasterMix used in qPCR reactions to determine mtDNA copy number per cell.*

MT-ND1	
Component	**Ratio Value**
TAQMAN Master Mix	5
ND1 Probe	0.2
ND1 Forward Primer	0.3
ND1 Reverse Primer	0.3
Autoclaved dH_2O	1.7
B2M	
Component	**Ratio Value**
TAQMAN Master Mix	5
B2M Probe	0.2
B2M Forward Primer	0.3
B2M Reverse Primer	0.3
$MgCl_2$	0.6
Autoclaved dH_2O	1.9

A tenfold serial dilution of a recombinant plasmid (originally pcDNA3.1) containing *MT-ND1* and *B2M* targets was prepared in dH_2O, for use as an internal calibration curve (log_{10}([amplicon]) vs *dd*CT) to facilitate the calculation of the concentration of *MT-ND1* and *B2M* genes in unknown samples, by linear interpolation of the standard curve. Cell lysates (6x5µl) were transferred to wells of a 96-well PCR plate, to allow for triplicates for both *MT-ND1* and *B2M* reactions. Each dilution of the internal calibration curve was also added in triplicate to separate wells. 15µl of the appropriate complete master mix was added to each of the triplicates. Plates were sealed using Star Seal Advanced Polyolefin Film, pulse vortexed five times and centrifuged at 300rpm for ten seconds. Sealed plates were loaded into an Applied Biosystems StepOnePlus Real-Time PCR System and subjected to the following reaction conditions: 2 minutes at 50°C, 10 minutes at 95°C and 40 cycles of 15 seconds at 95°C and 1 minute at 60°C. The resulting *dd*CT data for each amplicon in unknown samples were processed by linear interpolation of internal calibration curves to generate *MT-ND1* and *B2M* amplicon concentrations for each sample, from which a ratio of *MT-ND1*:*B2M* concentrations was taken as a measure of the average number of mtDNA molecules per cell.

2.3.5 Immunofluorescent Imaging

Cell Incubation and Sample Preparation

HeLa cells were seeded per well in a 96 well glass-bottomed imaging plate at a density of 5,000 in 50µl of complete media. For further confirmatory work investigating dose-dependency of hit samples, 384 well glass-bottomed imaging plates were also employed, into which 750 fibroblasts were seeded per well in 25µl of glucose culture media.

To allow for cell adherence to the well surface, the plates were incubated for 24 hours at 37^{o}C in a humidified atmosphere containing 5% CO_2. The cells were subsequently subject to treatment with samples of interest.

Sample Dosing – Screening

Samples (50µl) were dosed onto cells at a 1:1 dilution of extract to culture media, unless otherwise stated. Such a dilution was denoted as 50% relative concentration. Experiments were conducted in biological triplicate across three plates – one replicate per plate.

Sample Dosing – Dose Dependency Investigation

Hit extracts were reconstituted in autoclaved, sterile filtered dH_2O at one-tenth of the pre-lyophilised volume, to facilitate cell viable doses of relative concentrations of 100% in culture media. Samples were dosed at a maximum relative concentration of 100% (1:10 dilution of 10x concentrated extract) and subject to a two-fold serial dilution descending down the 96 well plates, leaving the bottom row for negative controls to which was added 50µl culture media alone. Experiments were conducted in biological triplicate using three 96 well plates. Replicate experiments were also carried out in 384 well plates, in which two rows and two columns formed the samples for each concentration, providing an internal biological quadruplicate per plate.

Preparation for Immunofluorescent Imaging

All volumes reported below are for a 96 well plate experiment protocol, volumes used for 384 well plates are a quarter of those for 96 well plates.

After a 48-hour incubation period, the cells were washed twice with 200µl per well PBS. Cells were then fixed using 100µl per well 4% paraformaldehyde in PBS and incubated at room temperature for 15 minutes. All wells were washed with 100µl PBS and permeabilised with 50µl of 5% Normal Goat Serum, in TBST, per well and gently rocked for one hour at room temperature. The cells were then treated with primary antibodies: anti-TOM20 antibody and anti-TFAM antibody (as required), at a 0.03% (v/v) dilution in 5% (v/v) NGS in TBST. The cells were incubated with the primary antibody solution overnight at 4^{o}C, with gentle rocking. All wells were then washed three times with 100µl TBST prior to incubation with secondary antibody solution: 0.2% (v/v) secondary antibody in 30% (v/v) NGS in TBST. DAPI (10mg/ml in dH_2O) and phalloidin-Alexa-fluor-568, were both diluted at 0.1% (v/v) into the secondary antibody solution. The subsequent staining cocktail was added to the plate at 50µl per well and incubated, covered and sealed using StarSeal Sealing Tape – Aluminium Foil, at room temperature for one hour, with gentle rocking. All cells were washed twice with 100µl 0.02% (w/v) sodium azide in PBS and stored at 4^{o}C, covered and sealed with StarSeal Sealing Tape – Aluminium Foil, for later imaging.

Data Acquisition and Processing

Samples were imaged using a Zeiss Cell Discoverer 7 high throughput widefield microscope at 25x magnification, 50x water immersion objective with a 0.5x optovar, acquiring four images per well as technical replicates. Z stacks were obtained at 1µm intervals at each position, consisting of five images centred on the focal plane, to ensure full capture of mitochondrial morphology. Images were processed using Zen Blue software. Orthogonal projections of Z stacks were obtained, and resultant images were imported to PerkinElmer Columbus Software for analysis.

Data analysis pipelines were created, using the data processing package Columbus, to identify cells as areas of interest based on nuclear and cytosolic markers. Mean staining intensity and object areas were calculated for TOM20 and TFAM signals and ratios between areas were then taken as required, i.e., TOM20 area per unit cell area, as required. An example pipeline is presented in section 7.2: Appendix B. Data was exported from Columbus and imported to TIBCO Spotfire software for visualisation.

2.4 Methods Utilised to Assess the Therapeutic Prospects of Mitochondrial Turnover

2.4.1 Mito-QC Analysis

Cell Seeding and Sample Treatment

MitoQC expressing fibroblasts were seeded at 2,500 cells per well in 96 well glass-bottomed imaging plates in glucose media. Cells were left to adhere to the well base over 24 hours. Cells were subsequently treated with bacterial extracts at the same relative concentration used in secondary flow cytometry screening, 50%, section 2.3.5. After a 48-hour incubation period, the cells were washed twice with 200µl per well PBS. Cells were then fixed using 100µl per well 4% paraformaldehyde in PBS; incubated at room temperature for 15 minutes. The plates were washed as before, sealed using StarSeal Sealing Tape – Aluminium Foil and stored at 4^{o}C for later imaging.

Imaging

MitoQC analysis images were captured for further analysis using a Zeiss Cell Discoverer Series 7 HT widefield microscope, as per section 2.3.5.

Data Processing

Analysis of mitoQC data was kindly performed by Dr. S. Bell. The protocol employed for data analysis was established by Dr. S. Bell, (Bell, 2020), but can be briefly summarised as follows. PerkinElmer Columbus Software facilitated the identification of mCherry spots, denoting punctate mitochondrial mass, regardless of mitophagy status. The mGFP signal intensity was calculated within each mCherry spot. The ratio of mCherry/GFP signal intensity was subsequently calculated, such that a low mGFP signal with high mCherry intensity (i.e. a high ratio) denotes a mitophagy positive mCherry spot. In order to exclude punctate, mitophagy negative, mitochondria from the analysis, i.e., those with above-average GFP fluorescence, a minimum threshold of $\mu_{untreated}+1\sigma_{untreated}$ was used to identify mitophagy positive mCherry spots. This same threshold ratio was also applied to treated cells. The number of mitophagy positive spots, those above the threshold mCherry/GFP ratio, was taken as a percentage of the total mCherry spot count, to give a % mitophagy reading for sample comparison.

2.5 Methods Used in the Development of an Immunofluorescent Method for Mitochondrial Defect Quantification and Phenotypic High Throughput Screening

2.5.1 NDUFS2 Mutation in Patient Derived Fibroblasts as a Cell Line Model of Complex I Deficiency

A patient presented at 8 months of age with a Leigh Syndrome phenotype, suffering from repeated vomiting, failure to thrive and developmental delay – patient 3 (Tuppen et al., 2010). Plasma and cerebral spinal fluid lactate levels were found to be elevated (11.66mmol/l and 5.56mmol/l respectively, versus normal readings of 0.5-1mmol/l and 1-2mmol/l) and cranial MRI scans revealed abnormal development of the cerebral peduncles, dorsal pons and upper medulla (Tuppen et al., 2010). Two heterozygous pathogenic mutations were identified (c.353G>A and c.875T>C) in the NDUFS2 gene, which resulted in two single amino-acid substitutions: p.Arg118Gln and p.Met292Thr (Tuppen et al., 2010).

Phenotypically, the mutation manifested as a severe complex I assembly and activity defect. Muscle homogenate from the patient exhibited 20% residual CI activity. BN-PAGE analysis revealed trace levels of fully assembled complex I, in gel-activity assays from fibroblasts showed an absence of activity. Deficiencies in NDUFB8 and NDUFA9 complex I subunits, determined by SDS-PAGE, were also demonstrated (Tuppen et al., 2010). The combination of this genetic and biochemical data resulted in a diagnosis of Leigh Syndrome.

Biochemically, NDUFS2 binds with NDUFS3, 7 and 8 to form the first major intermediate of CI assembly pathway (Mckenzie and Ryan, 2010, Guerreo-Castillo et al., 2017), detailed in section 5.1.2. This hydrogenase intermediate binds FeS clusters and NDUFA9 to combine with the MIM bound ND1 containing intermediate, with the influence of NDUFAF3 and 4 assembly factors (Vogel et al., 2007, Mckenzie and Ryan, 2010, Guerreo-Castillo et al., 2017). It is hypothesised that the pathogenic mutations in NDUFS2 severely limit the rate of formation of the hydrogenase intermediate, and thereby significantly inhibit the rate of CI assembly.

These mutations are predicted to be damaging to the function of NDUFS2 by the online prediction tool PolyPhen-2 (Adzhubei et al., 2010), showing that both reside in highly conserved regions of the protein – result displayed in Fig 2.4.

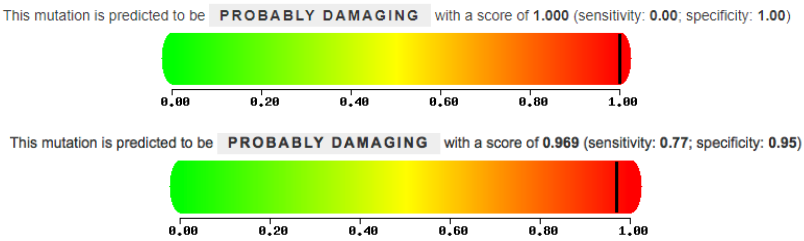

Fig. 2.4. Prediction of the severity of the p.Arg118Gln (top) and the p.Met292Thr (bottom) mutation in the NDUFS2 gene of CI deficient fibroblasts from a Leigh Syndrome Patient used as a model of CI deficiency. Prediction made using the online tool: PolyPhen-2 (Adzhubei et al., 2010). Both mutations were found to reside in a highly conserved area and was predicted to be damaging.

The region surrounding position 118 has been shown to directly interact with NDUFS3 and FeS clusters vital to CI catalytic function (Jaokar et al., 2013). It can therefore be hypothesised that the p.Arg118Gln mutation reduces the rate of Q module assembly by lowering the stability of the NDUFS2-NDUFS3 interaction, (Guerreo-Castillo et al., 2017). Met292 forms a key component of the interior, the p.Met292Thr mutation introduces an additional protein kinase C phosphorylation site, which may impact protein structure (Pagniez-Mammeri et al., 2011).

Other clinical presentations of NDUFS2 mutations have shown varying defects. Of note is Asp446Asn, which caused severe CI biochemical defects, but no CI deficiency (Ngu et al., 2012). NDUFS2 mutations more commonly result in CI deficiency and subsequent CI activity defects: Glu148Lys, Arg228Gln, Pro229Gln, Arg333Gln, Arg408Cys, Ser413Pro, Asp446Asn (Tuppen et al., 2010, Ngu et al., 2012). Mutations in NDUFS3 (Thr145Ile and Arg199Trp) result in similar clinical phenotypes and biochemical dysfunctions as the afore mentioned NDUFS2 mutations, in the form of CI deficiency (Bénit et al., 2004).

Immobilised fibroblasts derived from patient 3, (Tuppen et al., 2010), produced using the protocol described in 2.5.4, are referred to as NDUFS2 mutant fibroblasts.

2.5.2 NDUFS6 Mutation in Patient Primary Fibroblasts as an Additional Model of CI Deficiency

A paediatric male was found to harbour a homozygous mutation in the NDUFS6 gene: c.316_319delGAAA. The mutation manifested as a p.Glu106Glnfs*41 mutation in the NDUFS6 protein; a frameshift resulting in a substitution of Glu106 to Gln and the generation of a stop codon 41 base pairs downstream of the substitution. The length of wild-type NDUFS6 is 124 residues, this mutation creates a polypeptide of 120 residues, including the aforementioned residue substitution. Muscle homogenate from the patient was found to present with 5% residual CI activity and exhibited an NDUFB8 deficiency, as measured by quadruple immunofluorescent analysis of muscle biopsy sections – patient 6 (Ahmed et al., 2017).

Biochemically, NDUFS6 is a component of the N module, vital for the catalytic activity of CI (Mimaki et al., 2012). The N module, required for the binding and oxidation of NADH, is assembled in the mitochondrial matrix and binds to the Q module after Q/P intermediate assembly (Mckenzie and Ryan, 2010, Guerreo-Castillo et al., 2017). This final assembly step leads to the release of all associated assembly factors, NDUFAF1 2, 3 and 4 and ECSIT, to leave mature CI in the MIM (Guerreo-Castillo et al., 2017). This pathogenic mutation is hypothesised to reduce the binding affinity of NDUFS6 for zinc, a step shown to be critical to the assembly of mature CI in yeast (Kmita et al., 2015). The loss of any one of three conserved cysteine residues in human NDUFS6, between positions 115-124, is fatal (Rouzier et al., 2019). The frameshift and subsequent stop codon after c.316_319delGAAA, in this patient, eliminates this conserved region.

2.5.3 SURF1 Mutation in Patient Derived Fibroblasts as a Cell Line Model of Complex IV Deficiency

A paediatric female, presenting with a Leigh Syndrome like phenotype, was found to harbour a c312_320del10insAT mutation in SURF1. The mutation manifested as a premature stop codon in the gene transcript, resulting in the truncation of the translated protein at Leu105 (p.Leu105X), from its wild type length of 300 residues.

This pathogenic mutation renders SURF1 unable to aid in the assembly of CIV: SURF1 is essential to facilitate the binding of the MTCOI and MTCOII assembly intermediates of CIV, potentially through heme group delivery (Signes and Fernandez-Vizarra, 2018). Cells harbouring this mutation have been found to exhibit significantly reduced COX levels (Wedatilake et al., 2013).

2.5.4 Immortalisation of Mitochondrial Disease Patient Derived Fibroblasts

Primary fibroblast cell lines were immortalised using a retroviral construct, carrying the E6E7 gene region of human papillomavirus type 16, and were a kind gift from Dr. Kyle Thompson.

2.5.5 Galactose Growth Assay

Fibroblasts harbouring the NDUFS2 mutation were seeded at a density of 2,500 cells per well in 96-well Flat-Bottomed Plates (TPP - 92096), in glucose media (see section 2.2.1 for media recipe). Cells were allowed to adhere to the base of the wells over 24 hours before undergoing a media change to galactose media (see section 2.2.1 for media recipe). Media changes consisted of the removal of glucose media, 1x wash with PBS and the careful addition of 100µl of galactose media. During the media change, wells requiring application of MOA2 were dosed to yield a final drug concentration of 3µM, unless otherwise stated.

After the media change, cell plates were inserted into an IncuCyte Live Cell Analysis System (Essen Biosciences), which uses phase-contrast imaging to capture images of cells in multi-well plates every 3 hours for a set duration of time. Computational analysis using Incucyte Zoom software was used to calculate the mean confluence of cells, per condition (e.g., treated versus un-treated cells), at each time point, to facilitate the generation of cellular growth curves.

2.5.6 Immunofluorescent Imaging

Immunofluorescent methodologies underwent extensive optimisation during the project. An index of antibodies and small molecules employed can be found under section 2.1.4, table 2.1 and 2.2. The protocol below details the final optimised procedure in PerkinElmer Cell Carrier Ultra glass-bottomed 384-well imaging plates.

Cell Seeding and Compound Incubation

Fibroblasts harbouring the mitochondrial disease mutations (various), as well as wild-type control fibroblasts, were seeded in PerkinElmer Cell Carrier Ultra glass-bottomed 384-well imaging plates at 1000 cells per well in glucose media. To allow for cell adherence to the well surface, the plates were incubated for 24 hours at 37^{o}C in a humidified atmosphere containing 5% CO_2. The cells were subsequently subject to a media change to galactose media, as described in 2.5.5 but to a final volume of 25µl and dosed with 3µM MOA2 as required. Cells were subject to re-application of 3µM MOA2 after 96 hours had elapsed from the initial dose. Cells were incubated for a further 96 hours.

Sample Preparation

After an eight-day incubation period, cells were washed once with PBS using a Tecan HydroSpeed Plate Washer. All subsequent plate washes were also carried out using a Tecan HydroSpeed Plate Washer. Cells were then fixed by the addition of 20µl of 4% paraformaldehyde in PBS to dry wells. Plates were incubated at room temperature for 10 minutes. All wells were then washed once with PBS, after which 20µl PBS-1%(v/v) BSA was added to dry wells using a Thermo Multidrop Combi Reagent Dispenser. Plates were incubated for 30 minutes at room temperature with gentle rocking. All wells were washed again with PBS and 20µl methanol was added to dry wells using a Thermo Multidrop Combi Reagent Dispenser. Plates were incubated for 30 minutes at room temperature with gentle rocking. Plates were subsequently washed three times with PBS, leaving 10µl PBS remaining in all wells, to which 10µl of primary antibody cocktail was added. The cocktail was formed using PBS containing 2% w/v BSA and 0.2% (v/v) TritionX100 (PBS-BSA-TritonX100), to which antibody stocks were added to produce 0.5% v/v (5µg/ml) anti-NDUFA13, anti-NDUFS3 and 0.066% v/v (0.16µg/ml) anti-TOM20. Other antibodies also employed included anti-NDUFB8, anti-MTCOI, anti-SDHA as experimentally appropriate. The cells were incubated overnight at 4^{o}C, with gentle rocking. All wells were then washed three times with PBS, leaving

10µl PBS remaining in all wells, prior to incubation with secondary antibody solution. Appropriate secondary antibodies were added to PBS-BSA-TritonX100 solution, as previously described, to form a final working stock concentration of 0.2% v/v (4µg/ml). When experimentally required for quadruple immunofluorescent experiments, a working stock concentration of 0.4% v/v (8µg/ml) Goat-Anti-Rabbit-AF405 secondary was used. When appropriate, nuclear staining was achieved using DAPI (10mg/ml in dH_2O) at 0.1% (v/v) in the secondary antibody cocktail. The secondary antibody cocktail was added to the washed plates at 10µl per well, which were incubated, covered and sealed using StarSeal Sealing Tape – Aluminium Foil, at room temperature for one hour with gentle rocking. Plates were subsequently washed three times in PBS containing Penstrep (Gibco Life Technologies – 15140-122) 1% (v/v), leaving 10µl remaining in all wells. Plates were analysed immediately, after which they were stored at 4^{o}C.

Data Acquisition and Processing

Samples were imaged using a Zeiss Cell Discoverer 7 high throughput widefield microscope at 25x magnification, using a Plan-APROCHROMAT 50x water-immersion objective lens with a 0.5x optovar. Z stacks were obtained at 1µm intervals at each position consisting of five images centred on the focal plane, as determined by maximal TOM20 immunofluorescent intensity, to ensure full capture of mitochondrial morphology. Images were processed using Zen Blue software: orthogonal projections of Z stacks were obtained, and resultant images were imported to PerkinElmer Columbus Software for analysis. Columbus pipelines were created to identify mitochondrial areas using TOM20 immunostaining. The intensities of immunofluorescent signals from stained proteins, within mitochondrial areas, were then quantified and totalled. Data processing was also incorporated into Columbus pipelines, in the form of total immunofluorescent intensity, in individual channels of interest, normalised per unit mitochondrial area. An example pipeline is presented in Appendix D. Data was exported from Columbus was imported to TIBCO Spotfire software for visualisation, at which stage custom plate mapping tables were applied and figures were produced.

2.5.7 SDS-PAGE and Western Blotting

Cell Culture and Protein Extraction

Cells for protein expression analysis were seeded in 6 well plates at 125,000 per well, in glucose cell culture media, and allowed to proliferate to approximately 90% confluence.

Protein extraction consisted of washing cells once in ice-cold PBS, followed by scraping with cell scrapers (Santa Cruz), in 2ml PBS. The resultant suspension was transferred to 2ml laboratory tubes and centrifuged at 500g at 4^{o}C for 10 minutes. Next, the liquid was removed from the tube and disposed of. 20µl RIPA lysis buffer was added to the cell pellet and vortexed for 30s. The vortexed tubes were placed on ice for 10 minutes and then centrifuged at 2400g for 2 minutes at 4^{o}C. The supernatant was subsequently transferred to clean sample tubes and frozen at -20^{o}C for storage.

Bradford Assay

A standard Bradford assay was employed to determine protein concentration in protein extracts, before gel loading. A standard curve of BSA was prepared in dH_2O (to form standards of 2.5ng/ml, 6.25ng/ml, 12.5ng/ml, 18.75ng/ml and 25ng/ml) to a total volume of 800µl per standard. Samples for analysis (1µl of total lysate) were added to 799µl dH_2O. Bradford reagent (Biorad), 200µl, was added to all standard curve tubes and samples and vortexed vigorously. The standard curve and samples were added, in duplicates of 200µl each, to wells in an optical bottomed 96 well plate. A SpectraMax M3 plate reader was used to record the absorbance of 595nm light in all wells. Concentrations of protein in analysis samples were determined through linear interpolation of the standard curve.

SDS-PAGE and Protein Transfer

Samples for SDS-PAGE were prepared by combining appropriate volumes of sample to give 20µg protein (as determined by Bradford assay) in 1x Laemmli sample buffer, with 10% v/v DTT, to make up 20µl of a sample. Samples were heated to 95^{o}C for 10 minutes and subsequently centrifuged for a further 10 minutes, at approx. 65,000g. Mini-PROTEAN TGX 12% precast gels (Bio-rad) were loaded into an electrode assembly and lowered into a buffer tank, filled with 1x tris-glycine running buffer. Samples were loaded into the precast gel, along with a molecular protein ladder - 20µl. The gel was run at 120V for one hour, after which time the gel was removed from the assembly and place on a pre-wetted PDVF membrane between two ion reservoir stacks (Bio-rad). This assembly was loaded into a cassette for a Trans-Blot Turbo System (Bio-rad) to facilitate the transfer of proteins to the membrane over three minutes at 25V/2.5A.

Western Blotting and Image Acquisition

The protein-containing PDVF membrane was placed into western blotting blocking buffer for one hour, at room temperature with gentle rocking. Primary antibodies were diluted into blocking buffer and added to the membrane, which was incubated overnight at 4^{o}C with gentle rocking. The membrane was subsequently washed three times, 10 minutes each, in TBST. HRP-secondary antibodies were diluted in blocking buffer and added to the membrane, which was incubated for one hour at room temperature with gentle rocking. The membrane was again subjected to three washes of TBST, 10 minutes each. The membrane was developed using an Amersham ECL Prime kit, as per the manufacturer’s instructions. Resultant bands were imaged using a Biorad ChemiDoc system.

Chapter 3:

Development of an Assay Pipeline for the Identification of Agents Capable of Inducing Mitochondrial Biogenesis

3.1 Introduction

Mitochondrial diseases present as a significant area of unmet need, with no cure and limited treatment options available. The single therapeutic approved for use in mitochondrial disease patients is Idebenone, used for the treatment of visual loss associated with LHON (Klopstock et al., 2011, Klopstock et al., 2013). Despite several putative therapeutic compounds present in the literature, both in pre-clinical and clinical trials (section 1.8.5), the low success rate of drug discovery projects demands that more lead compounds are continually put forward for development.

As a result of the high degree of genetic and biochemical heterogeneity in mitochondrial diseases, current treatments, such as Idebenone, are beneficial to a minimal fraction of the patient population. This is especially relevant to newly developing methods of mtDNA editing, such as ZFNs, TALENs or DdCBEs, which require targeting to individual mtDNA genotypes (Minczuk et al., 2008, Bacman et al., 2013, Gammage et al., 2014, Gammage et al., 2018, Mok et al., 2020). The identification of novel treatments, which can improve total mitochondrial function irrespective of disease aetiology, presents as an extremally valuable prospect for mitochondrial disease patients.

Global increases in mitochondrial oxidative capacity could also have implications for the wider population. Metabolic dysfunction is a hallmark present in a variety of age-associated and neurodegenerative diseases. Cancers, Parkinson's disease, dementia, Alzheimer's disease, multiple sclerosis, obesity and *Diabetes mellitus*, as well as the ageing process itself, all have links to mitochondrial dysfunction. The induction of mitochondrial proliferation, with the view of increasing oxidative capacity, presents as a novel line of investigation for the treatment of common age-associated diseases and metabolic dysfunction.

Despite the apparent simplicity of the phenotypic rescue by the MB hypothesis, concerns regarding the implication of indiscriminate mitochondrial biogenesis can be raised. Activation of mitochondrial biogenesis is hypothesised to act uniformly across the entire mitochondrial population. In the case of primary mitochondrial diseases this would preclude heteroplasmy shifts, increasing the total amount of mutated mtDNA as well as wild type mtDNA. This has implications for the generation of ROS from dysfunctional components of the electron transport chain, increasing the number of these components is thought to result in a concomitant increase in ROS production (Cui et al., 2012, Murphy, 2013, Guo et al., 2014, Pichaud et al., 2019). ROS have been shown to cause indiscriminate oxidative damage to biomolecules, most notably to disulphide bridges in protein structure and to DNA molecules – with particular relevance to mitochondrial DNA in close proximity to the ETC (Zorov et al., 2014). However, it is hypothesised that this theoretical increase in ROS could be mitigated against as a result of an increased expression of the antioxidant enzymes: SOD1 and 2, catalase and glutathione peroxidase are under the transcriptional control of NRF-2 (Dong et al., 2008). The activity of NRF2 is predicted to be elevated in the event of mitochondrial biogenesis, as a result of increased activity of PGC-1α: the widely accepted master regulator of mitochondrial biogenesis (Wallace et al., 2010, Komen and Thorburn, 2014, Lightowlers et al., 2015, Ploumi et al., 2017).

3.2 Aim

Mitochondria comprise a wide variety of nuclear and mitochondrially encoded proteins, as well as an array of lipids, phospholipids and biomolecules involved in the various pathways of mitochondrial function. This results in many parameters that could potentially be used as readouts for the assessment of mitochondrial mass. These include: mtDNA content, mitochondrial membrane potential, mitochondrial membrane area/total envelope volume, mitochondrial protein content, enzymatic activity assays, oxygen consumption rate assays as well as protein or mRNA quantification and post-transcriptional state of key proteins involved in mitochondrial biogenesis pathways; for example, PGC-1α.

Given the number of potential parameters for available for assessment, research projects assessing mitochondrial mass must ensure an adequate variety of experimental readouts to ensure project efficacy. For instance, increases in the protein expression of PGC-1α will not necessarily result in the increased expression of mitochondrial genes, due to the tight and complex post-transcriptional control of PGC-1α activity. Just as an increase in mtDNA copy number does not necessarily indicate increases in mtDNA expression, nor does an increase in mitochondrial protein expression result in increases in fully assembled mitochondrial complexes. In the screening process, several methods are precluded from available experiments due to the requirements of high throughput work. Oxygen consumption rate and enzymatic activity analyses, as examples, require hours of active laboratory time to complete a single assay of one multi-well plate and both methods require an array of costly consumables, as well as a large number of cells to be cultured for each experiment. These methods are inferior to immunofluorescent imaging for example, which does require potentially lengthy staining/set up protocols but can be passively analysed by automated microscopes and data set analysis pipelines to facilitate the screening of large libraries of samples.

This project concluded that the measurement of mitochondrial mass, for the purposes of phenotypic screening, centres on high throughout, primarily fluorescence-based, techniques. Mitochondrial mass can be measured through mitochondrially localising fluorescent markers and TOM20 immunostaining. Mitochondrial activity can be approximated with the assessment of mitochondrial membrane potential, while mitochondrial mtDNA expression can be approximated through TFAM immunostaining.

This project aims to establish a set of assays to form a reliable pipeline for the assessment of mitochondrial mass *in vitro*, using stable cell lines. It was planned to commence with the ultra-high-throughput assessment of cells exposed to natural product extracts, from bacterial transposon libraries, by flow cytometry using TMRM staining – conducted by an industrial partner: Nanna Therapeutics. Hit extracts from this initial screen were then be passed to The Wellcome Centre for Mitochondrial Research (WCMR) for further assessment.

A secondary assay high throughput flow cytometry assay utilising mitochondrially localising green fluorescent protein (m-GFP, accumulating in the mitochondrial matrix) and TMRM (localising on both outer and inner surfaces of the MIM, fluorescence in proportion to the mitochondrial membrane potential once localised) was then used to assess putative primary screen hits. Immunofluorescent imaging techniques for a marker of mitochondrial mass (TOM20, a key component of the TOM complex) and qPCR for mtDNA content were employed against hit extracts from the secondary flow cytometry screen to select final lead extracts. The pipeline was planned to culminate in the demonstration of dose-dependency in lead extracts by immunofluorescent imaging, assessing the mitochondrial area and TFAM (mitochondrial transcription factor A, coating mtDNA) immunofluorescent spot count. Combined, it was envisaged that these assays would allow for the assessment of mitochondrial membrane potential (TMRM), mitochondria mass per cell (m-GFP, flow cytometry and TOM20, immunofluorescent imaging) and mtDNA copy number (qPCR), as well as an indicator of mtDNA transcription (TFAM, immunofluorescent imaging).

3.3 Results

3.3.1 Primary Screening

Nanna Therapeutics screened in excess of $1.6x10^7$ unique bacterial clones, in individual co-cultures with HEK-293T cells, through a modified flow cytometry instrument capable of analysing micro-droplets, using the protocol outlined in 3.3.1. Briefly, staining with TMRM was used in HEK-bacteria co-cultures to determine whether unique metabolites generated from individual clones, from the transposon insertional library of bacteria, were able to promote mitochondrial biogenesis in HEK-293T cells.

Encapsulation of both bacterial and mammalian cells, separately and in co-culture, was confirmed using flow cytometry and visual inspection by optical microscopy, Fig 3.1.

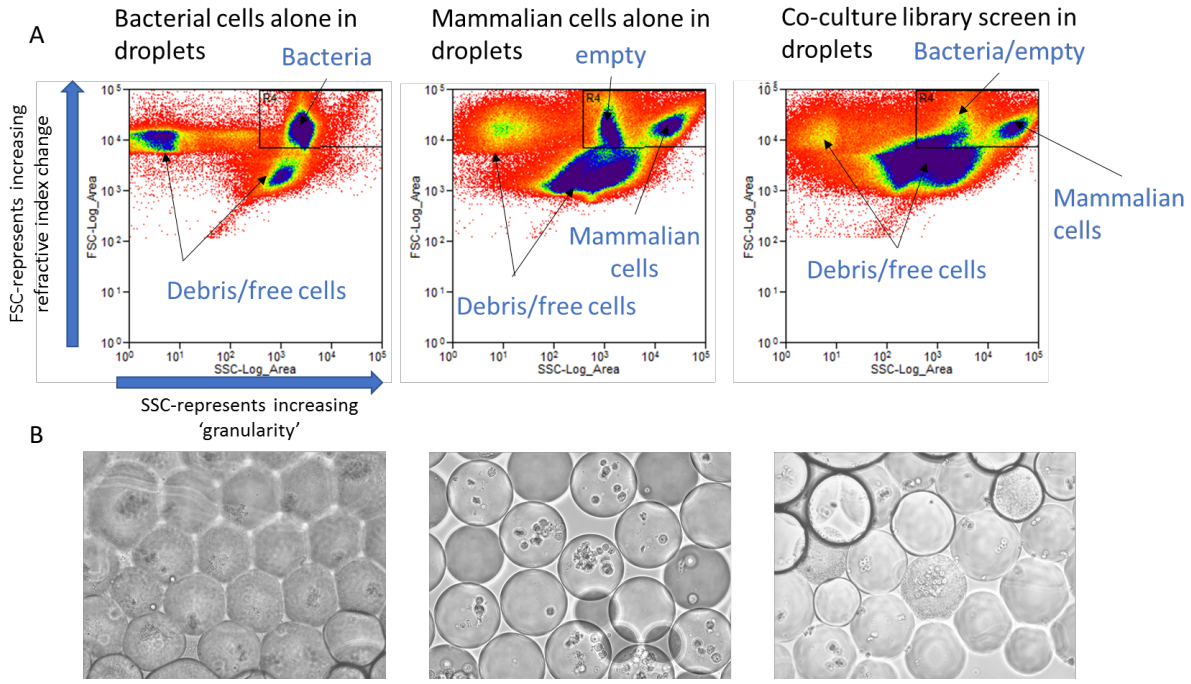

Fig 3.1. *Confirmation of bacteria/HEK-293T co-culture in Nanna Therapeutics microdroplets.* A. Selection of Nanna Therapeutics microdroplets containing bacterial cells, mammalian cells and co-cultures. B. Visual confirmation of the presence of separate bacterial and mammalian cultures and co-culture in Nanna Therapeutics microdroplets by optical microscopy

The three sets of droplets were subject to TMRM and DAPI staining: bacteria and HEK-293T cells alone and then in co-culture. Results in Fig 3.2 show minimal TMRM fluorescence and low DAPI staining, relative to selected threshold fluorescent intensities for both (denoted as gate R7), in microdroplets containing bacterial cells alone. Higher intensities are noted in both fluorescent channels in microdroplets containing mammalian cells, however, the population above the threshold intensity of TMRM remains low relative to the optimised threshold, R7. Co-culture of bacterial and mammalian cells significantly enriches the number of microdroplets exhibiting TMRM fluorescent intensities that exceed the hit selection threshold, R7.

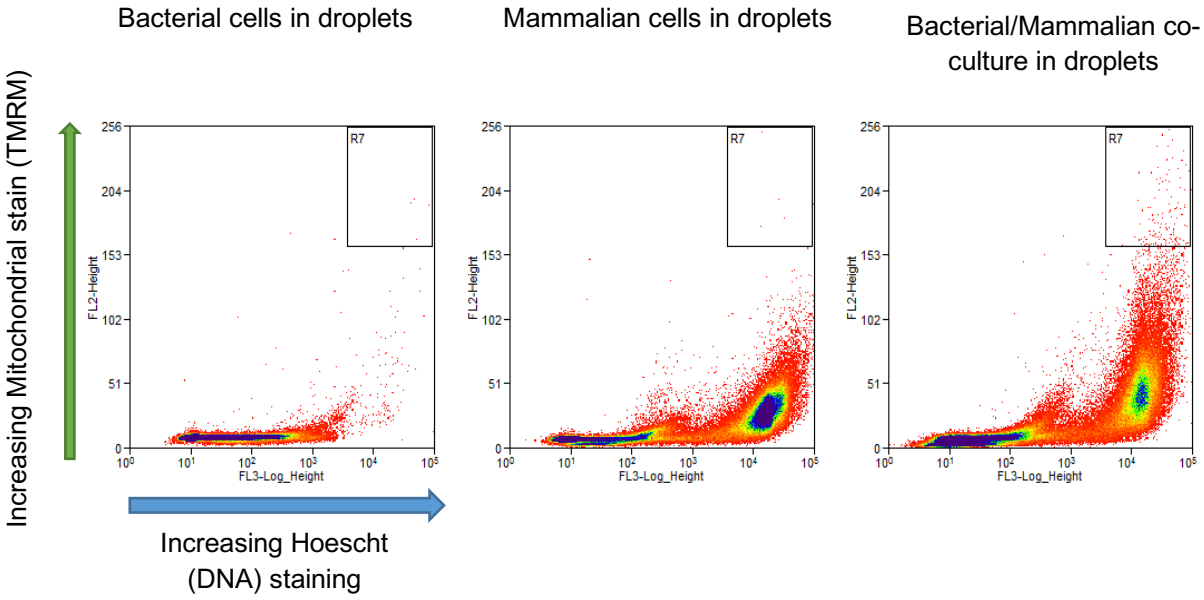

Fig 3.2. *Primary screen results provided by Nanna Therapeutics* A. Heat maps from a single library screen showing fluorescent intensities of A, bacterial cells, B, mammalian cells and C, co-cultured bacterial and mammalian cells, encapsulated in Nanna Therapeutics microdroplets, stained with TMRM and DAPI. The gated area "R7" denotes samples of interest. Each library screen was performed in triplicate, samples present within gate R7 in all three replicates were selected as primary screen hits.

The screen was performed in triplicate, with those samples that satisfied the constraints of gate R7, in all three replicate screens, being identified as primary screen hits. Approximately 1.6×10^7 unique clones were analysed in total. This screening gave rise to 744 primary screen hits. Primary screen hit microdroplets were sorted and retrieved. Bacteria contained within were cultured, and resultant bacterial supernatant was processed and lyophilised, as described in section 3.3.1. Lyophilised primary hit extracts were transported to WCMR in 96 well plates, 93 extracts per plate, alongside three replicates of blank media to serve as internal untreated controls.

3.3.2 Secondary Screening – Flow Cytometry

Secondary screening at WCMR commenced with flow cytometry experiments in K562-m-GFP cells, stained with TMRM as described in section 2.3.3. This methodology both replicated the work of Nanna Therapeutics (staining with TMRM, binding the inner and outer faces of the MIM) and introduced a second measure of mitochondrial mass (m-GFP, localising to the mitochondrial matrix). Prior to the start of secondary screening, the WCMR assay underwent experimental validation.

Assay Validation

As shown in Fig. 3.3, A in the absence of both fluorescent probes (fluorescence null) cells exhibited negligible levels of fluorescence: 10^2 arbitrary units. The experiment also included m-GFP expressing, TMRM stained, K562 cells (fluorescence positive cells). Fluorescent signals increased by two orders of magnitude, in fluorescence positive cells relative to fluorescence null cells (wild type K562 cells, not expressing m-GFP, not subjected to TMRM staining), to 10^4 arbitrary units: a 270-fold increase in m-GFP signal, and 450-fold increase in TMRM, Fig. 3.3. B.

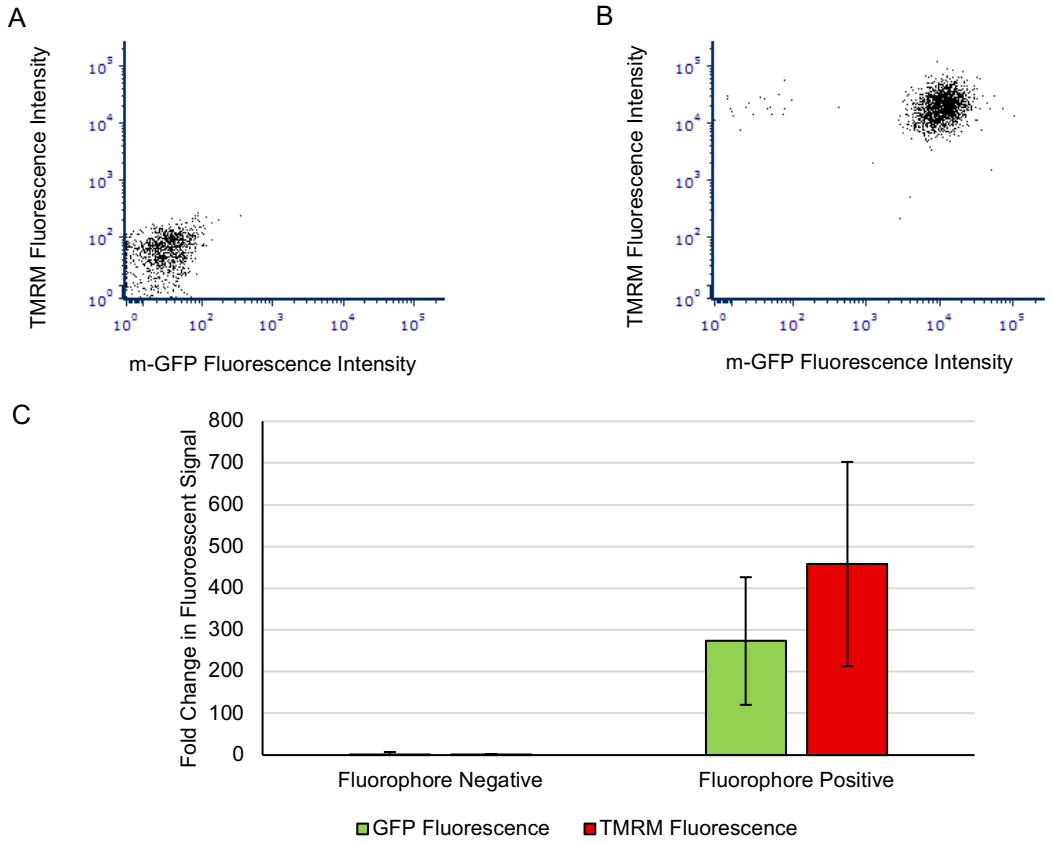

Fig 3.3. Flow cytometry analysis K562 cells with and without fluorescent markers. Representative dot plots for A) data for fluorescence null cells. B) data fluorescence positive cells. Data processed from fluorophore investigations showing negligible signals in fluorophore negative cells (C).

This result confirmed the specificity of the fluorescence as a result of the probes and showed that background readings were negligible in comparison to the true signals.

To eliminate the possibility of intrinsic fluorescence in samples giving rise to false-positive readings, Nanna Therapeutics samples were investigated using a spectrophotometer (Molecular Devices SpectraMax M3). Nanna therapeutics sample plates, prepared as per 3.3.2, were assessed using 488nm and 561nm wavelengths – the excitation wavelengths of m-GFP and TMRM molecules. Emitted light was recorded within the ranges 510-650nm and 580-700nm to capture specific data from m-GFP and TMRM respectively, Fig 3.6.

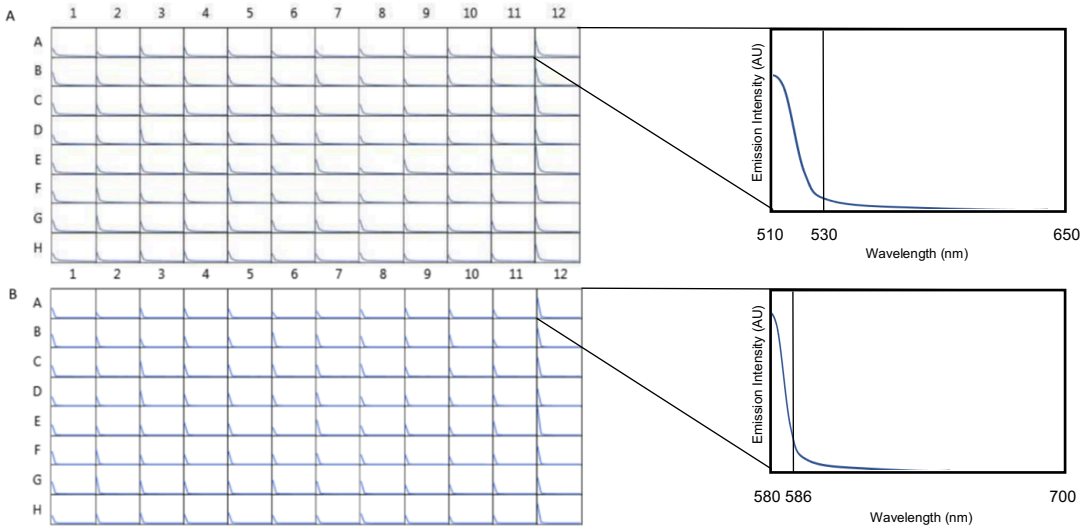

Fig 3.4. *Representative data from a single Nanna Therapeutics sample plate showing emission spectra within plate layouts.* Grids are representative of a 96 well sample plate. Each well forms x and y axes, denoting relative scales for wavelength of light and signal intensity, respectively, as shown by the expanded views of well A12 for each wavelength investigated. A) m-GFP (excitation: 488nm, recorded emission 510-650nm, vertical black line in the expanded view shows the m-GFP emission peak) and B) TMRM (excitation: 561nm, recorded emission: 580-700, vertical black line in the expanded view shows the TMRM emission peak).

None of the assessed Nanna Therapeutics samples exhibited significant intrinsic fluorescence properties at the emission peak wavelengths of interest (marked by vertical black lines in the expanded views in Fig. 3.4). This result, in combination with the absence of fluorescent signals in fluorescent null K562 cells (Fig 3.5), supports the conclusion that any increases in fluorescence intensities noted in this assay are due to changes in mitochondrial marker signals, m-GFP and TMRM, as a result of sample effects on the cells.

Dose-Dependent Response of a Mitochondrial Biogenesis Positive Control – OR-1

A natural product extract of unknown composition was identified as an agent capable of inducing mitochondrial biogenesis, in mammalian cells, by Dr. O. Russell, in an independent screening project at WCMR (Russell, 2013). The extract is herein termed OR-1. Having been previously validated for activity, OR-1 was used as a positive control for mitochondrial biogenesis in the current flow cytometry assay.

To confirm that this method can detect increases in mitochondrial mass, fluorescence positive K562 cells were incubated with OR-1, as outlined in section 2.3.3, in a two-fold serial dilution ranging from 10% (v/v) to 0.313% (v/v) in quadruplicate. Resultant data were processed in R Studio, using the analysis code shown in Section 7.1 Appendix A. A dose-dependent response was observed, with an increase of 1.55-fold in mean TMRM fluorescent signal and an increase of 1.36-fold in mean m-GFP fluorescent signal, in cells dosed with 10% (v/v) extract. The processed data is shown in Fig. 3.5.

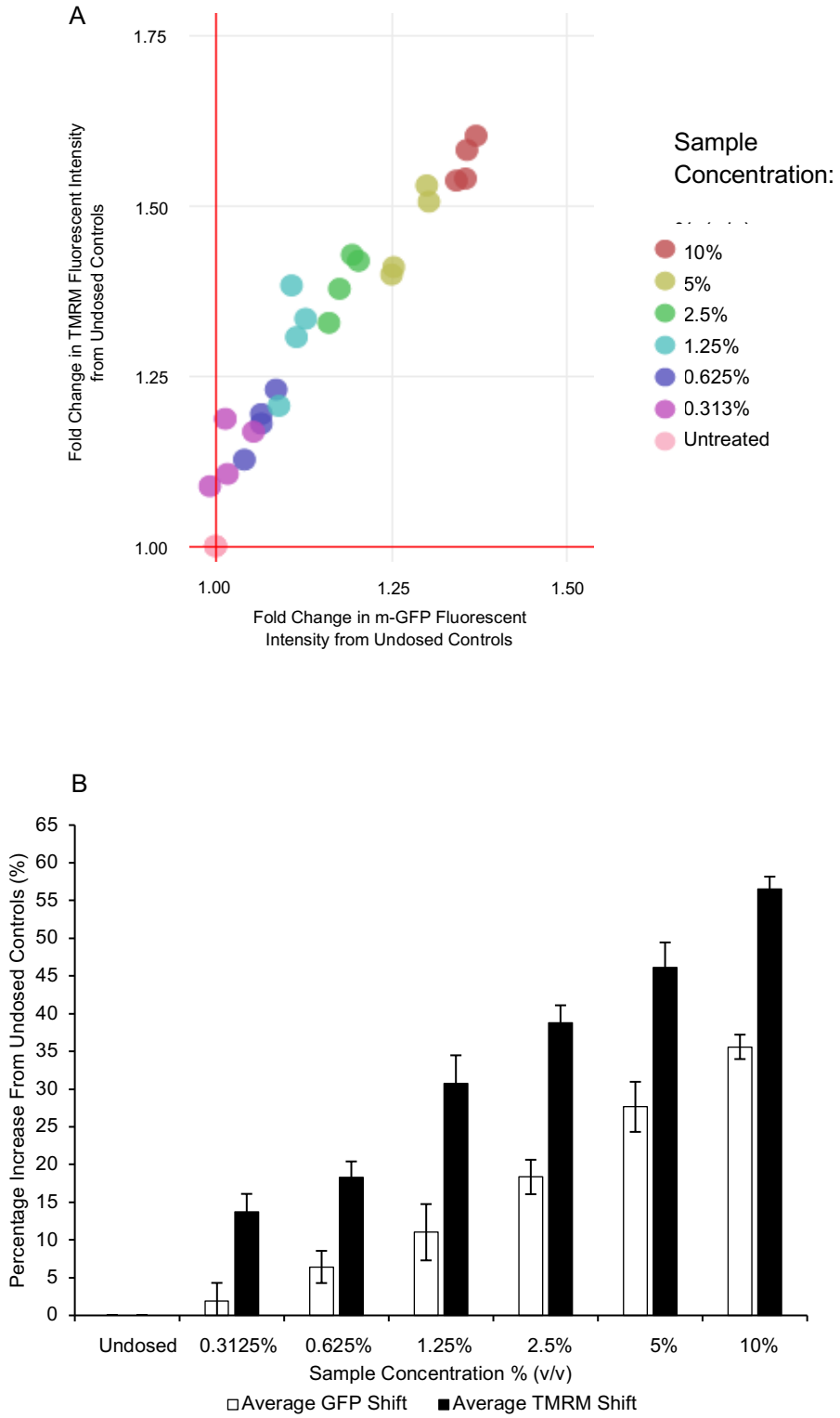

Fig. 3.5. *Average percentage shift in markers for mitochondrial mass and membrane potential for a serial dilution of a natural product extract, identified by Dr. O. Russell, acting as a positive control for mitochondrial biogenesis – herein termed OR-1.* A) Scatterplot generated as per data processing protocols outlined in section 3.3.3. Colours denote differences in sample concentration, n=4, each point of the same colour represents an average reading from approximately 10,000 events from one well of a 96-well plate of a quadruplicate. B) Data processed as a bar chart to show average shifts in m-GFP and TMRM fluorescence.

The stepwise increases noted in TMRM and m-GFP fluorescent intensities, with increasing concentration of OR-1, demonstrates the ability of the assay to quantify increases in mitochondrial mass.

The Z' score (see 1.9.2) of this flow cytometry assay was determined to be approximately 0.65, using data from no dose control cells and cells incubated in OR-1, 5% (v/v) in culture media, for 48 hours. While data generated from the use of 10% (v/v) of the positive control yielded a better Z' score, the amount of OR-1 available for use was limited. As such, 5% (v/v) OR-1 was selected for use as an internal positive control in screening plates.

Employment of Secondary Flow Cytometry Screening

To establish whether putative hits from the primary screen could be supported by more detailed analysis, the samples received (prepared as per 3.3.2) were subjected to WMCR flow cytometry screening, as validated above.

The first two plates received from Nanna Therapeutics were denoted as set 1 (1.1 and 1.2), which contained lyophilised media only. Set 1 was used solely for the purposes of screening protocol familiarisation (data not shown). Subsequent putative hit samples for secondary screening were received in batches of four plates, denoted set 2 (2.1-2.4) and set 3 (3.1-3.4). Plates from set 2 and set 3 were subjected to the WCMR flow cytometry screen on arrival. Sample identification codes were completed with the inclusion of well number (by row). For example, well A11 of set 2, plate 3, was assigned the sample ID: 2.3.11, while well E11 of set 3, plate 3, was assigned the ID: 3.3.59.

All sample plates were analysed in biological triplicate, with one media blank sample per plate being spiked with 5% (v/v) OR-1. Scatterplots showing all data acquired from the screen are shown in Fig. 3.6. A wide range of responses were observed, ranging from reductions in m-GFP (0.9-fold reduction) and TMRM fluorescent intensity (maximum 0.5-fold reduction), to upwards of 1.5-fold increases in both parameters, depending on the sample analysed.

Data processing within R Studio was employed to automatically identify samples present in the upper five percentiles of either parameter, in each sample plate. The analysis code used can be found in Section 7.1 Appendix A. Extracts that satisfied the afore mentioned rule were designated as putative secondary hits and were taken forward for further analysis.

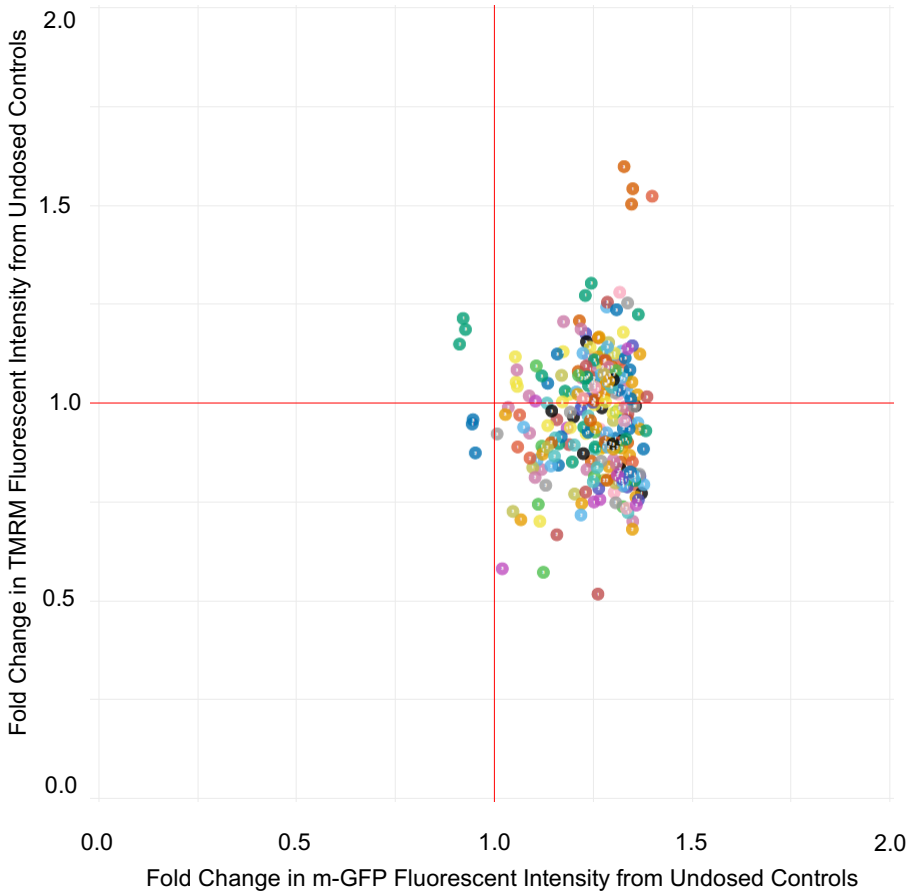

Fig. 3.6. Average fold change in markers for mitochondrial mass and membrane potential for a single sample plate of putative hit bacterial extracts received from Nanna Therapeutics. Wells containing TMRM stained, m-GFP expressing, K652 cells treated with individual extracts were prepared and subjected to flow cytometry analysis, as described in section 3.4.1. Colours denote different samples within each plot, each point represents an average reading from approximately 10,000 events, from one well of a 96-well plate in biological triplicate. Data presented for sample plate 2.1 only, additional plots for the remaining plates (2.2 – 3.4) can be found in Appendix B.

3.3.3 Hit Confirmation from Secondary Screening

To confirm hits from the WCMR flow cytometry screening assay and assess the reproducibility of the assay, all putative hits were subjected to blinded re-analysis. Bacterial strains responsible for the production of hit extracts, identified in the WCMR flow cytometry screen, were cultured from cryopreserved aliquots at the Nanna Therapeutics site. A sample plate containing these extracts was produced as before, section 3.3.2. The positions of putative hit samples within the plate were blinded for the duration of this confirmatory replicate analysis. Multiple replicates of extracts were included from independent cultures of bacteria. This confirmation plate also contained extracts from untransformed, transposon null, bacteria as well as lyophilised media alone (no bacteria controls) in randomly selected positions. Data was not compared to the first round of screening, due to the samples being produced from independent cultures of bacterial library members. Predictions were made regarding the presence or absence of transposon positive bacterial extract: samples that exhibited a combination of readings of below 1.20-fold increase for TMRM readout and below a 1.9-fold increase of m-GFP readout were identified as transposon null (wild type control or media only). Any samples exceeding these thresholds were designated as transposon positive (a putative hit from the previous screen), Fig. 3.7.

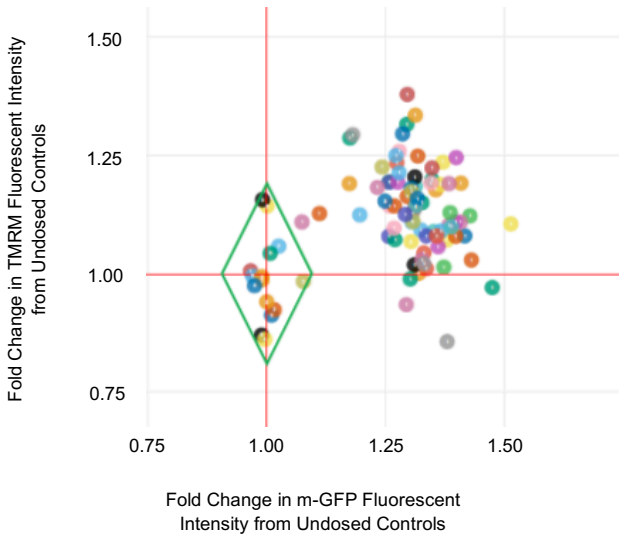

Fig. 3.7. Average percentage shift in markers for mitochondrial mass and membrane potential for bacterial extracts received from Nanna Therapeutics, present in the upper five percentiles, by rank, in the initial flow cytometry screen - alongside transposon null bacterial extracts. Data represented in scatterplot format generated as per data processing protocols outlined in section 3.3.3. Colours denote different samples, each point of the same colour represents an average reading from approximately 10,000 events, from one well of a 96-well plate. Predictions were made regarding the presence or absence of transposon positive bacterial extract: Samples which exhibited a combination of readings of below 20% for TMRM readout and below 10% of m-GFP readout were identified as transposon null. This region is highlighted using a green rhombus.

The identities of bacterial extracts were unblinded after data acquisition and analysis, Fig. 3.8.

A

	1	2	3	4	5	6	7	8	9	10	11	12
A	2.1.08	2.2.49	2.3.05	2.3.61	2.4.09	2.4.90	3.1.05	3.2.06	3.3.20	3.4.10	Media	Media
B	2.1.08	2.2.49	2.3.05	2.3.61	2.4.09	2.4.90	3.1.05	3.2.06	3.3.20	3.4.10	Media	Media
C	2.1.49	2.2.85	2.3.08	2.3.84	2.4.09	3.1.01	3.1.09	3.2.12	3.3.24	3.4.11	Media	Media
D	2.1.49	2.2.85	2.3.08	2.3.84	2.4.09	3.1.01	3.1.10	3.2.13	3.3.25	3.4.12	XNAA5	XNAA5
E	2.1.85	2.3.01	2.3.11	2.4.06	2.4.24	3.1.02	3.1.49	3.2.60	3.3.59	3.4.12	DCBB1	DCBB1
F	2.1.85	2.3.01	2.3.11	2.4.06	2.4.24	3.1.02	3.1.49	3.2.60	3.3.59	3.4.12	DABE3	DABE3
G	2.1.92	2.3.02	2.3.47	Media	2.4.25	3.1.04	3.2.01	3.3.10	3.4.01	3.4.91	WCEC9	WCEC9
H	2.1.92	2.3.02	2.3.47	Media	2.4.25	3.1.04	3.2.01	3.3.10	3.4.01	3.4.91	TFTH1	TFTH1

Key: Correctly Identified as Media Only or Transposon Null Bacterial Extract

Correctly Identified as Transposon Positive Secondary Hit Extract

Incorrectly Identified as Transposon Positive Secondary Hit Extract

Incorrectly Identified as Media Only or Transposon Null Bacterial Extract

Sampling Error

B

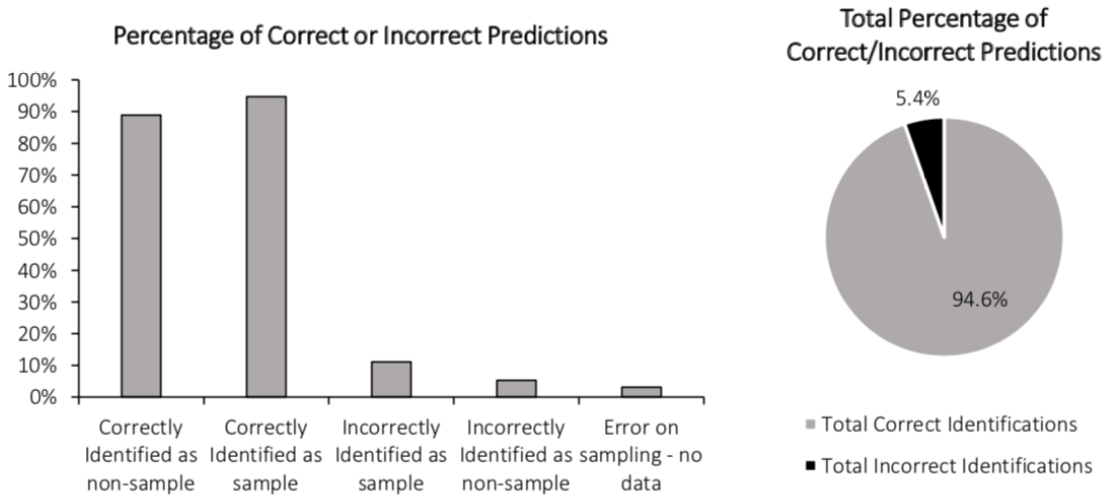

Fig. 3.8. Results from blinded analysis of flow cytometry putative hits, once sample identifiers were obtained. A) Plate layout for the hit confirmation plate containing blinded, randomly positioned extracts from bacterial culture media alone, transposon null or transposon transformed bacterial cultures. Extracts have been colour-coded, revealing the outcome of predictions generated by the flow cytometry screening assay. B) Graphical representations of the outcome of predictions generated by the flow cytometry screening assay.

This hit confirmation step showed reproducible activity, as measured by increases in m-GFP and TMRM fluorescence intensities, in re-cultures of previously identified hit extracts. Cells treated with extracts from re-cultured secondary hits were successfully distinguished from cells treated with wild-type extracts and untreated controls in 94.6% of cases, supporting the reliable identification of mitochondrial biogenesis inducing samples by this assay, while controlling for conformation bias. The assay also confirmed the reproducible nature of active extracts using Nanna Therapeutics novel transposon mutagenesis methods.

All secondary hit bacterial extracts (n=38), denoted by fold changes in m-GFP or TMRM fluorescence in the upper five percentiles in each sample plate of the secondary screen (Fig 3.8), proceeded to tertiary assays.

Intriguingly, duplicate extracts from media conditioned with transposon null bacteria, “XNAA5” were incorrectly identified as hit extracts. Given that transposon positive strains of XNAA5 were present in the secondary hit plate, but the untransformed strain had not been assessed before, further investigations into untransformed XNAA5 were undertaken. Samples from media pre-conditioned by untransformed XNAA5 were prepared and analysed, alongside transposon positive secondary hits from XNAA5, and analysed using the WCMR flow cytometry assay, Fig. 3.9.

Significant elevations in m-GFP fluorescent intensity are observed in K562-m-GFP cells incubated with an extract of media conditioned by XNAA5 transposon null bacteria ($P<0.0001$). No significant effects on TMRM fluorescent intensities were recorded in cells treated with transposon positive or negative bacterial extracts from XNAA5 ($P>0.05$). Extracts from transposon positive XNAA5 strains exhibited a wide range of activities with respect to m-GFP fluorescent intensity, indicating that the production of the active agent(s) by XNAA5 bacteria can either be suppressed or further enhanced by single transposon insertion events.

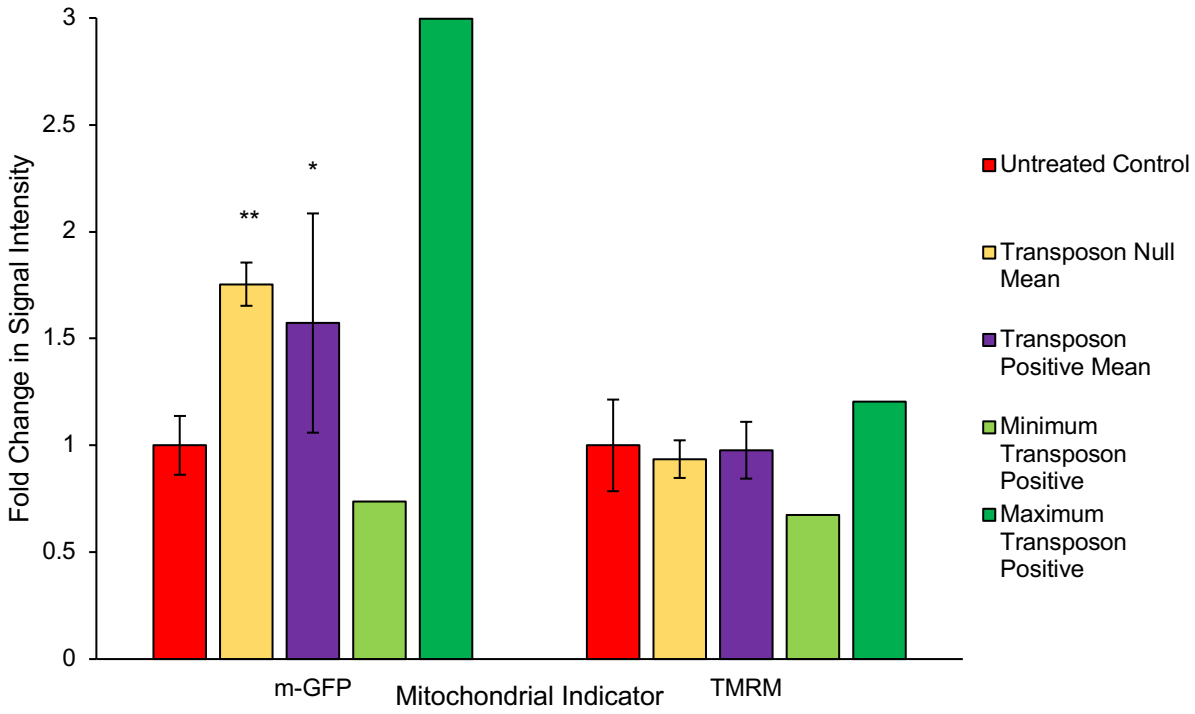

Fig. 3.9. *Graphical representations of flow cytometry data collected from cells incubated in extracts from XNAA5 transposon null and positive bacteria*. Samples investigated included media only samples (red), samples from transposon null XNAA5 (yellow) and transposon positive secondary hits originating from XNAA5 (purple – mean, pale green – minimum, dark green - maximum). * = P<0.05 **P<0.0001

3.3.4 Tertiary Assays – qPCR

Secondary hit extracts (n=38) were investigated using qPCR methods in HeLa cells, as detailed in section 2.3.4, to quantify the average mtDNA nucleoid count per cell. Increases in mtDNA count would be further indicative of increased mitochondrial mass.

Primers against the nuclear gene encoding beta-2 microglobulin (B2M) and the mtDNA encoded gene for NADH:Ubiquinone Oxidoreductase Core Subunit 1 (ND1) were used in the analysis. An internal calibration curve, formed by a serial dilution of a recombinant plasmid containing both amplicons, was used to calculate the quantities of each present in a per well of cells. The ratio of ND1:B2M copy numbers was then taken to obtain the number of mtDNA nucleoids per cell, Fig. 3.10.

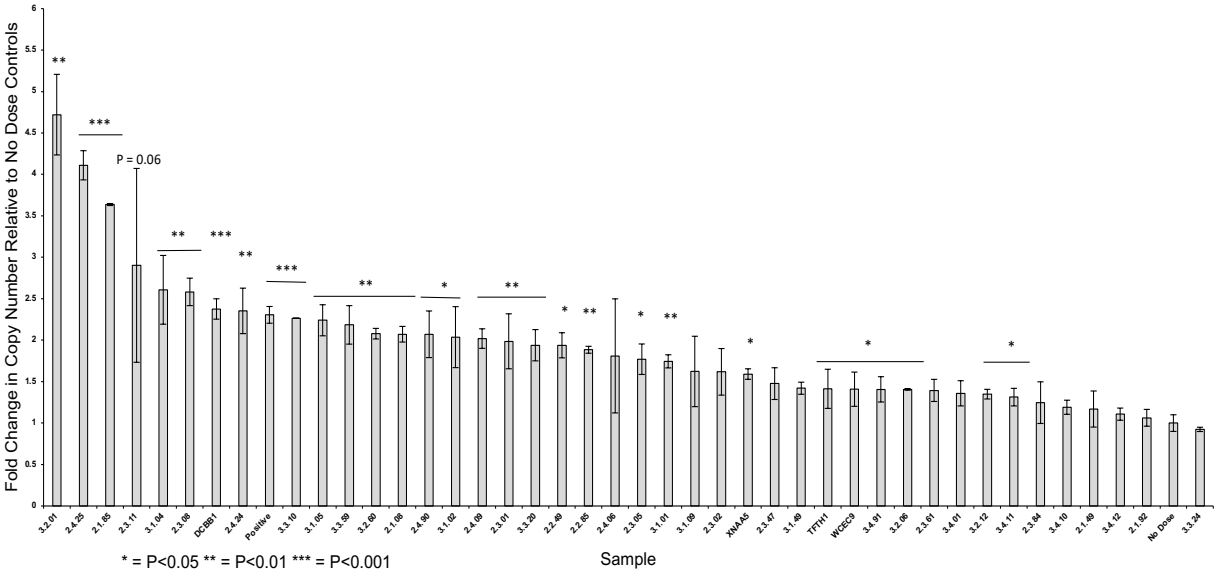

Fig. 3.10. *Graphical representation of qPCR data showing fold change in mtDNA copy number per cell in cells incubated in secondary hit relative, to no dose controls*. Total DNA was isolated HeLa cells and subject to qPCR analysis for mtDNA copy number, as per 2.3.4. Fold change of mtDNA copy number is presented per extract analysed. N=3.

The majority of secondary hit extracts resulted in an increase in mtDNA copy number per cell, relative to untreated cells. The maximum mean increase observed was a 4.72-fold increase, while the median increase caused by the extracts was a doubling in mtDNA content per cell. A single putative hit extract, 3.3.24, resulted in a non-statistically significant reduction in mtDNA copy number, a 0.9-fold change. Transposon negative bacterial extracts TFTH1, WCEC9, XNAA5 and DCBB1 gave 1.4, 1.5, 1.6 and 2.30-fold increases in mtDNA count respectively.

3.3.5 Tertiary Assays – Immunofluorescent Imaging

In order to investigate potential increases in the quantity of mitochondrial material, secondary hit extracts were investigated using immunofluorescent staining for TOM20 and subsequent imaging in HeLa cells, carried out as detailed in section 3.3.5. Columbus imaging quantification software was employed to calculate the mean immunofluorescent staining intensity of TOM20 in TOM20 positive areas (mitochondria), Fig. 3.11.

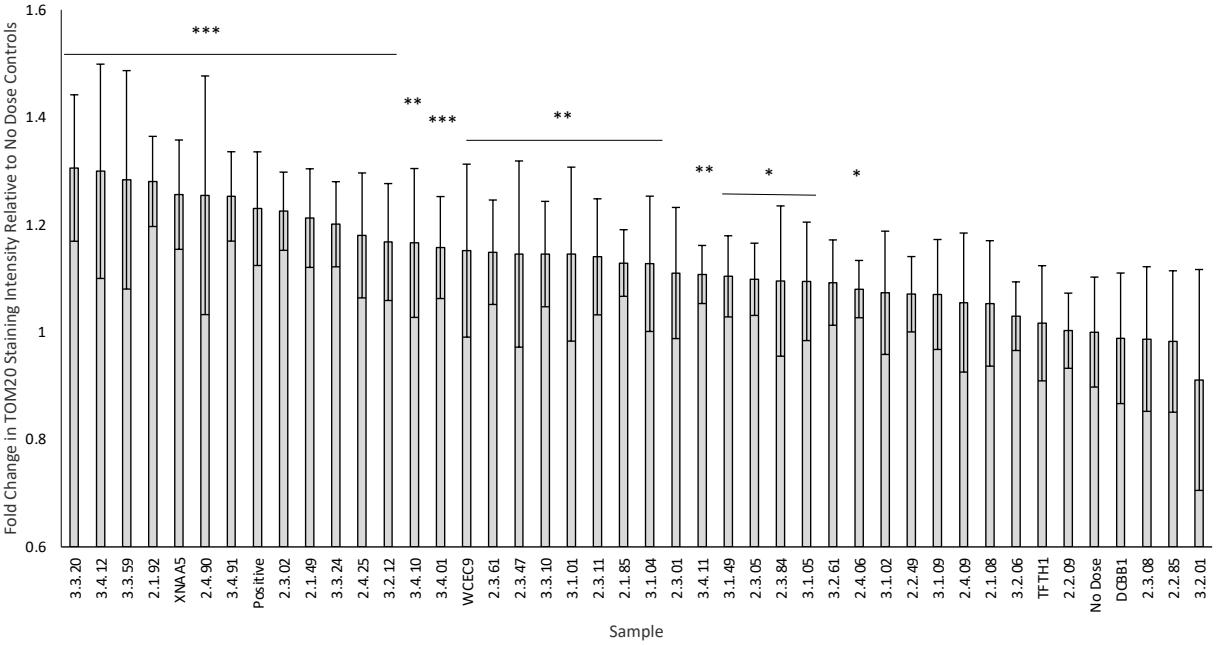

Fig. 3.11. *Graphical representation of immunofluorescent imaging data showing fold change in TOM20 immunofluorescent staining intensity in cells incubated in secondary hit relative to no dose controls.*

The majority of samples increased the mean TOM20 immunofluorescent stained intensity, relative to untreated cells. The maximum mean increase observed was 1.3-fold over untreated cells, while the median increase as a result of samples incubation was a 1.2-fold increase in TOM20 immunofluorescent stained intensity. Four tested extracts resulted in non-statistically significant reductions in TOM20 immunofluorescent stained intensity in the HeLa cells: DCBB1 (an untransformed control), 2.3.08, 2.2.85 and 3.2.01: giving 0.988, 0.987, 0.982 and 0.911- fold changes respectively. Untransformed WCEC9, XNAA5 resulted in statistically significant 1.18 and 1.25-fold increases in TOM20 immunofluorescent stained intensity. Untransformed TFTH1 and DCBB1 bacterial extracts did not induce statistically significant responses.

3.3.6 Combining Tertiary Assays to Select Final Hits

Due to the multi-factor nature of mitochondrial biogenesis, data from sections 3.3.4 and 3.3.5 were correlated to each other, to allow for the prioritisation of hits accounting for increases in both TOM20 immunofluorescent and mtDNA copy number parameters. The following selection rules were applied to secondary hits: samples must result in a TOM20 immunostaining intensity reading greater than OR-1 or be present in the top 50%, by rank, in both TOM20 immunostaining intensity and mtDNA copy number parameters, Fig. 3.12.

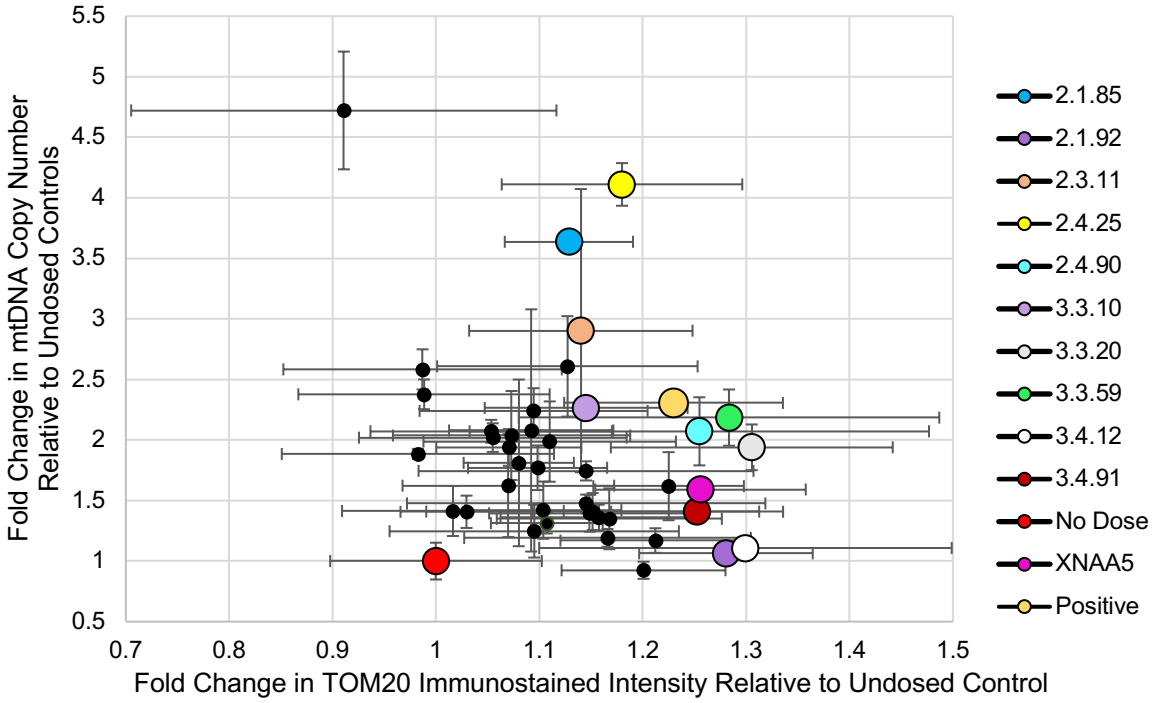

Fig. 3.12. *Graphical representation of data correlating immunofluorescent imaging (x) and mtDNA copy number data (y) in cells incubated in secondary hit relative to no dose controls.* All data has been normalised to readings for no dose controls (red). Hits were assigned (coloured and enlarged) as per the following selection rules; TOM20 immunostaining intensity reading greater than the OR-1, or sample present in the top 50%, by rank, in both TOM20 immunostaining intensity and mtDNA copy number parameters.

Application of these selection rules resulted in the following transposon positive extracts being identified as hits: 2.1.85, 2.1.92, 2.3.11, 2.4.25, 2.4.90, 3.3.10, 3.3.20, 3.3.59, 3.4.12, 3.4.91. These extracts proceeded to dose-dependent investigations. The XNAA5 extract met the above criteria, however, it was discounted from further WCMR work due to its transposon null status, which was predicted to increase the variability of subsequent re-cultures. Nanna Therapeutics proceeded with further investigations into XNAA5 extracts.

3.3.7 Confirmation of Selected Hits Using Dose Response Curves

Hit bacterial extracts, identified in section 3.3.6, were further investigated for dose-dependent mitochondrial biogenesis effects on fibroblasts using immunofluorescent imaging. The employment of fibroblasts, as opposed to HeLa cells, allowed for the quantification of mitochondrial morphology, for example area, due to the more planar nature of fibroblasts.

Upon receipt of newly produced lyophilised extracts, samples were reconstituted to one-tenth of their original pre-lyophilised volumes to allow for investigation of higher relative concentrations. The greatest cell-viable dilution of extracts into culture media was found to be 1:1, used in previous screens and assays. Cells were not viable when cultured in extract exclusively, due to a lack of FBS. The concentration of extracts to 10x, followed by a 1:10 dilution in culture media formed the same concentrations of extract compounds within media as found in extracts (100% relative concentration) while retaining cell viable levels of culture media nutrients. A two-fold serial dilution allowed the investigation of 50% (equivalent to the original 1:1 dilution of extracts used in WCMR flow cytometry screening), 25% (1:3) 12.5% (1:7) and 6.25% (1:15) relative concentrations.

Mitochondrial density (mitochondrial area normalised to total cell area), mean mitochondrial mass per cell, mean mitochondrial length and TFAM immunofluorescent spot count per cell were calculated from immunofluorescent images of fibroblasts subjected to a 2-fold serial dilution of hit extract, incubated and analysed as detailed in section 3.3.5 (Fig 3.15-17).

Samples 2.1.82, 2.1.92, 2.3.11, 2.4.25, 2.4.90, 3.3.10, 3.3.20 and 3.3.59 exhibited a non-linear type dose-dependency for mitochondrial density in the concentration range investigated. As a trend for these samples, mean mitochondrial density increased from near DMEM control levels at a relative concentration of 6.25%, to a maximum (approx. 1.3-fold increase) at 25% to 50% relative concentration dependent on sample. Mean mitochondrial density was observed to universally decrease with extract dosing at a relative concentration of 100%, from levels observed at 50%. No dose dependency was observed in samples 3.4.12 or 3.4.91, showing approximately a 10% increase in mitochondrial density at all investigated relative concentrations.

Mean mitochondrial mass per cell increased linearly for cells subject to incubation with extracts 2.1.85, 2.1.92, 2.3.11, 2.4.25, 2.4.90, 3.3.10 and 3.4.12, with the trend continuing in cells incubated in samples at 100% relative concentration. Extract 3.3.20 showed between a 1.33-fold and 1.48-fold increase in mitochondrial mass per cell throughout relative concentrations of 6.25-50%, with a further increase to 1.87-fold increase over DMEM controls at a relative concentration of 100%. A similar trend was noted with data collected from cells incubated in extracts 3.3.59 and 3.4.91.

Increasing relative concentrations of extracts 2.1.85, 2.1.92, 2.3.11, 2.4.25, 2.4.90, 3.3.10 and 3.4.12 resulted in linear increases in TFAM immunofluorescent stained spot count per cell. Extracts 3.3.20 and 3.3.59 showed no dose-dependent effects in this parameter, giving rise to approximately a two-fold increase at all assessed relative concentrations. A non-linear negative trend is noted in cells dosed with extract 3.4.91. TFAM immunofluorescent stained spot count per cell increases to 1.82-fold and 2.34-fold over DMEM control levels at 50% and 100% relative concentrations respectively, reaching statistical significance in the latter only.

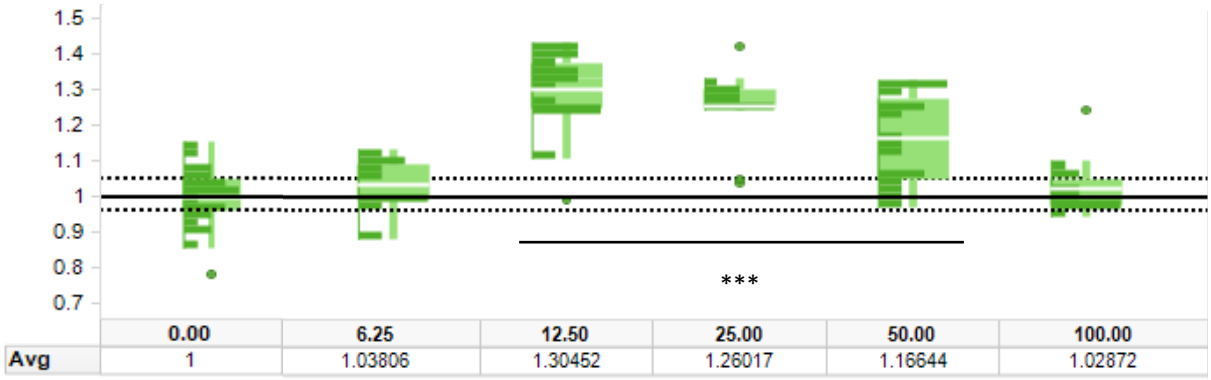

	0.00	6.25	12.50	25.00	50.00	100.00
Avg	1	1.03806	1.30452	1.26017	1.16644	1.02872

Fig. 3.13. *Graphical representation of mean mitochondrial mass per unit cell area (mitochondrial density) in cells incubated in hit extract 3.3.20, relative to no dose controls, n=16 images per condition.* Each box within the plot contains a histogram (dark bars) showing the distribution values from individual images. A solid black line indicates the mean reading from no dose controls (DMEM only), dotted lines indicate the interquartile range of readings from no dose controls. All data has been normalised to the mean of no dose control cells and presented as a fold change. Plots for all hit extracts can be found in appendix C. P<0.001: ***

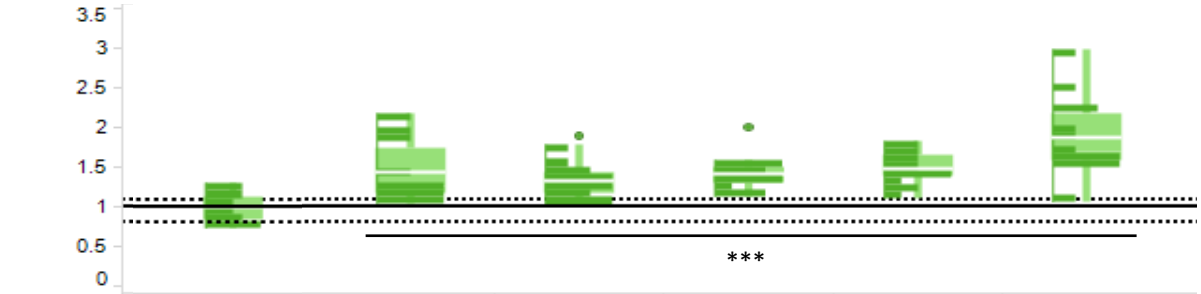

	0.00	6.25	12.50	25.00	50.00	100.00
Avg	1	1.44078	1.33164	1.40489	1.48302	1.86587

Fig. 3.14. *Graphical representation of mean mitochondrial mass per cell in cells incubated in hit extract 3.3.20, relative to no dose controls, n=16 images per condition.* Each box within the plot panels contains a histogram (dark bars) showing the distribution values from individual images. A solid black line indicates the mean reading from no dose controls (DMEM only), dotted lines indicate the interquartile range of readings from no dose controls. All data has been normalised to the mean of no dose control cells and presented as a fold change. Plots for all hit extracts can be found in appendix C. P<0.001: ***

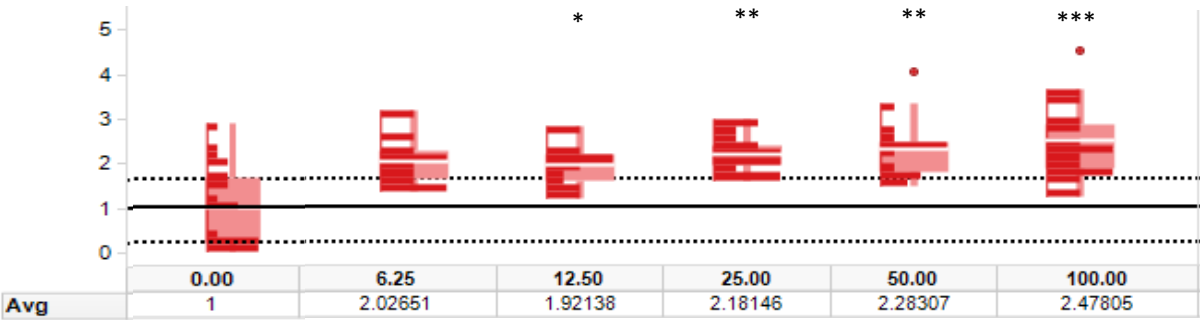

	0.00	6.25	12.50	25.00	50.00	100.00
Avg	1	2.02651	1.92138	2.18146	2.28307	2.47805

Fig. 3.15. *Graphical representation of TFAM immunofluorescent stained area per cell in cells incubated in hit extract 3.3.20, relative to no dose controls, n=16 images per condition.* Each box within the plot panels contains a histogram (dark bars) showing the distribution values from individual images. A solid black line indicates the mean reading from no dose controls (DMEM only), dotted lines indicate the interquartile range of readings from no dose controls. All data has been normalised to the mean of no dose control cells and presented as a fold change. Plots for all hit extracts can be found in appendix C. P<0.05: *, P<0.01: **, P<0.001: ***

Commonly, the greatest increases in mitochondrial density were observed in cells exposed to 25-50% relative concentration of extract in culture media. Using mitochondrial density as the primary readout, the optimum concentration of each extract was identified (maximum fold increase). Various parameters associated with mitochondrial biogenesis were also measured in cells: mitochondria area per cell, TOM20 immunofluorescent staining intensity, TFAM spot count per cell and mean mitochondrial length, Table 3.2 and Fig 3.18. Representative images for each extract at optimal concentrations are shown in Fig 3.19.

When analysed at their optimal concentrations, all extracts (except 3.4.12 and 3.4.91), resulted in greater than 1.2-fold increases in mitochondrial density. Extracts 2.1.85, 2.1.92, 2.3.11 and 3.3.20 resulted in greater than 1.3-fold increases. In all cases, increases in mitochondrial density were accompanied by increases in mitochondrial mass per cell. All extracts yielded highly significant ($P<0.001$) increases in TOM20 immunostaining intensity.

Table 3.1. *Fold changes in mitochondrial parameters in cells treated with hit mitochondrial biogenesis inducing samples, at optimal relative concentrations, as determined by maximal fold increases in mitochondrial densities.*

Extract	Relative Concentration (%)	Fold Increase Relative to No Dose Controls				
		Mitochondrial Density	Mitochondrial Mass per Cell	TOM20 Fluorescent Intensity	TFAM Spot Count per Cell	Mean Mitochondrial Length
2.1.85	50.0	1.30	1.49	1.78	1.88	1.16
2.1.92	25.0	1.35	1.28	1.77	1.76	1.12
2.3.11	25.0	1.33	1.33	1.71	1.91	1.12
2.4.25	50.0	1.28	1.48	1.76	1.94	1.15
2.4.90	12.5	1.28	1.25	1.81	1.76	1.16
3.3.10	12.5	1.24	1.26	1.84	1.69	1.12
3.3.20	12.5	1.30	1.28	1.73	1.92	1.08
3.3.59	12.5	1.26	1.32	1.64	1.82	1.08
3.4.12	25.0	1.12	1.21	1.73	1.61	1.00
3.4.91	25.0	1.12	1.18	1.62	1.58	1.04

To prioritise extracts from which to first isolate active compound(s), data from table 3.2 was normalised to relative concentration for each extract, to give a figure of the efficiency of each extract dose in inducing mitochondrial biogenesis. Extracts were sorted for maximum fold increase for each mitochondrial parameter, relative to the concentration required, and issued a score from 10 to 1 according to their rank order. Rank scores were summed and taken as a percentage of the available score of 50 (10 per measured parameter), table 3.3.

Table 3.2. *Rank scoring of hit mitochondrial biogenesis extracts to facilitate sample prioritisation for further work.* Extracts presented in rank order, from most to least effective when normalised to concentration required for maximal fold increase in mitochondrial density.

Extract	3.3.20	2.4.90	3.3.10	3.3.59	2.1.92	2.3.11	3.4.12	3.4.91	2.1.85	2.4.25
Rank Score (%)	90	86	82	82	56	52	40	32	18	12

While all extracts yielded significant increases in mitochondrial density, mitochondrial mass per cell and TOM20 immunofluorescent stained intensity, samples 2.4.90, 3.3.10, 3.3.20 and 3.3.59 gave rise to the greatest increases in these parameters when the relative concentration of extract required was controlled for. These extracts were prioritised for further investigations.

This increased efficacy of these extracts, when compared to other confirmed mitochondrial biogenesis hit extracts, could be due to two factors. The concentration of an active compound is increased within these particular extracts relative to others, or these extracts contain one, or multiple, unique compound(s) not present in others. The identities of any compounds within these extracts responsible for inducing mitochondrial biogenesis remain unknown as further work is carried out by Nanna Therapeutics.

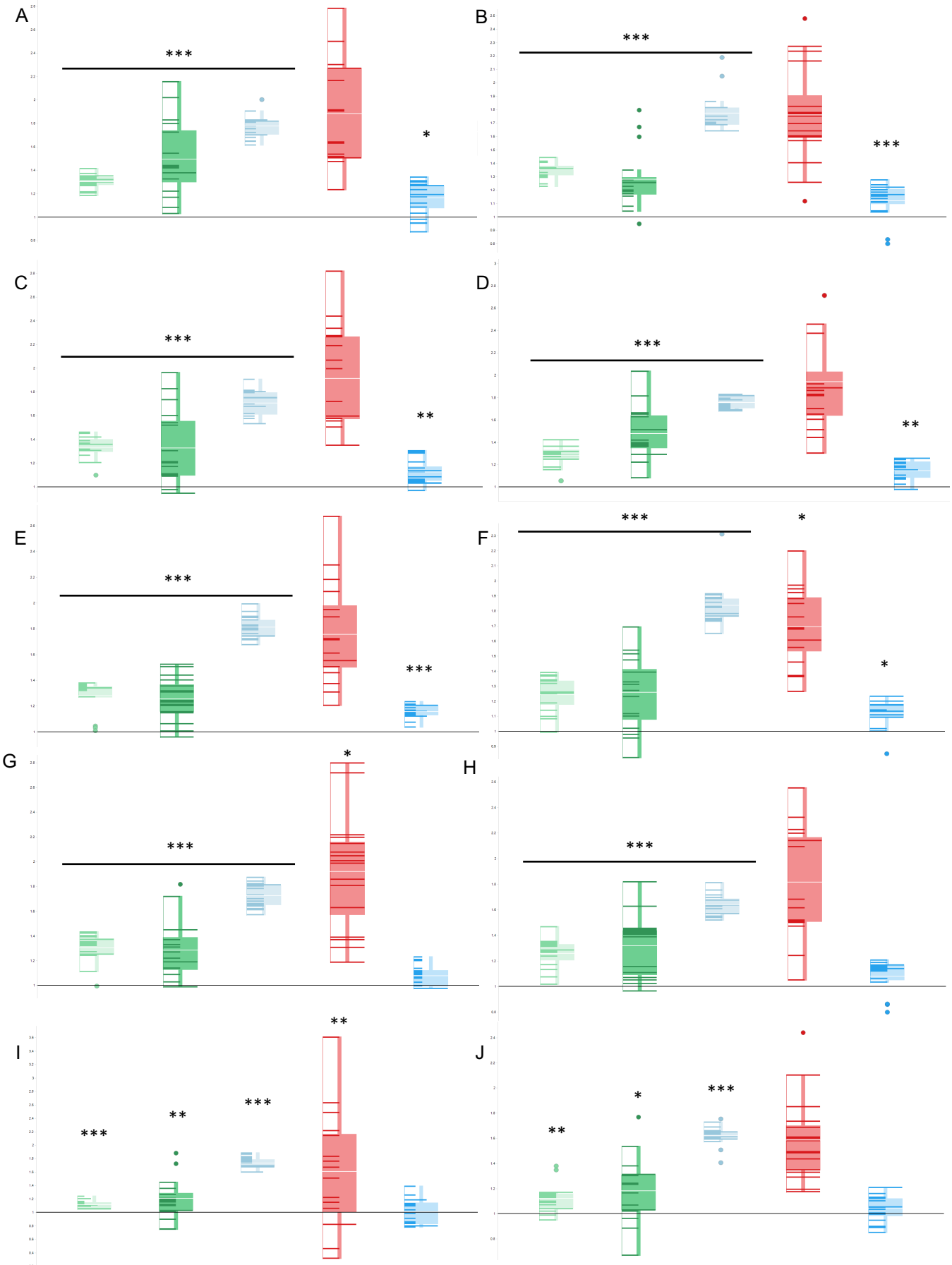

Fig. 3.16. *Graphical representations for mitochondrial density (pale green), mitochondria area per cell (dark green), TOM20 immunofluorescent intensity (grey), TFAM spots per cell (red) and mean mitochondrial length (blue) in cells dosed with sample at optimum relative concentrations of each extract.* All data are presented as a fold change from cells culture in DMEM culture media only (no dose controls), the mean of which is represented by a horizontal black line at y=1. A) 2.1.85, 50%. B) 2.1.92, 25%. C) 2.3.11, 25%. D) 2.4.25, 50%. E) 2.4.90, 12.5%. F) 3.3.10, 12.5%. G) 3.3.20, 12.5%. H) 3.3.59, 12.5%. I) 3.4.12, 25%. J) 3.4.91, 25%. P<0.05: *, P<0.01: **, P<0.001: ***

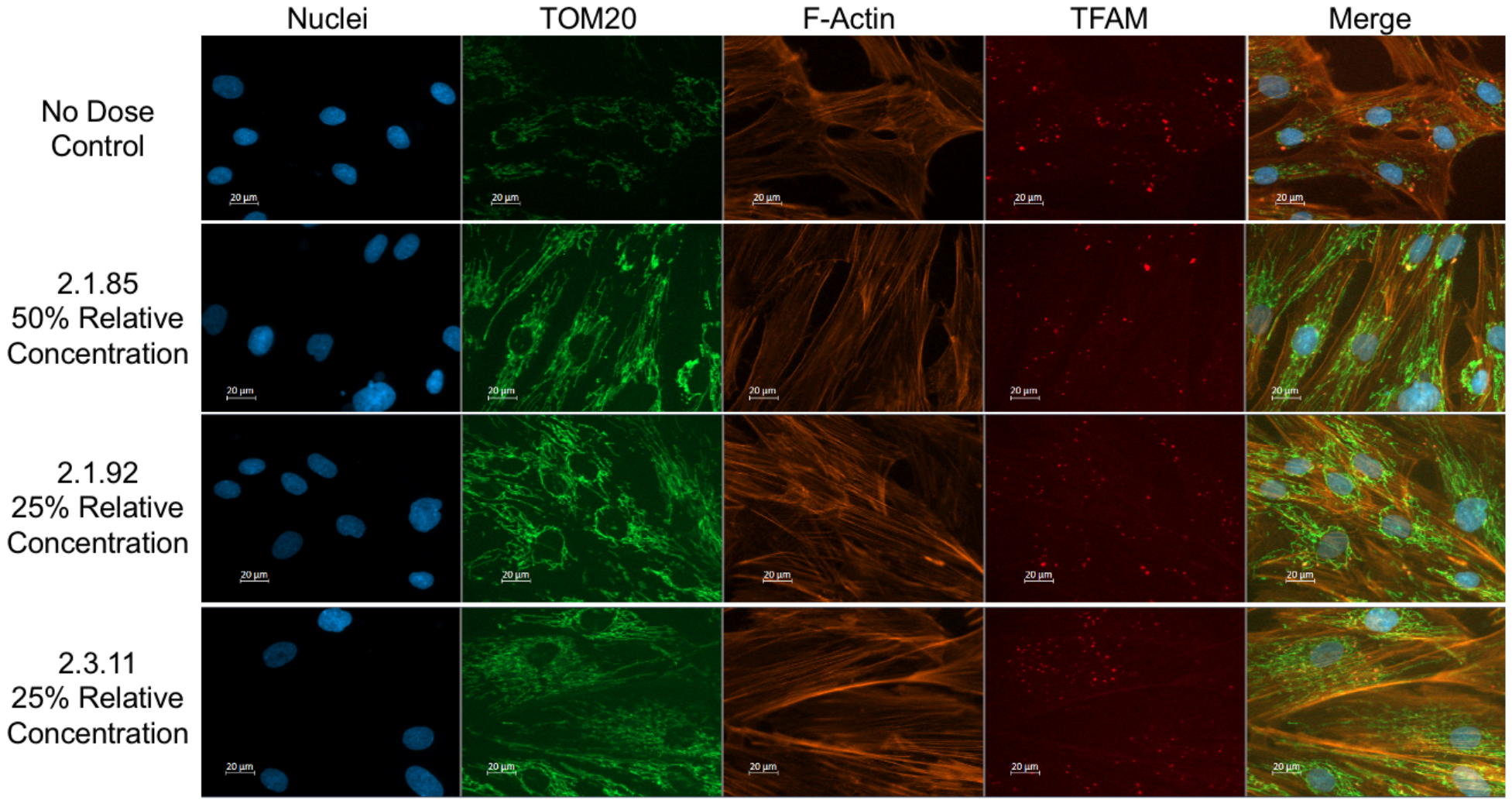

Fig. 3.17. *Representative images for mitochondrial biogenesis hit extracts, at their optimum relative concentrations as indicated.* Nuclei (blue), TOM20 (green), F-Actin (orange) and TFAM (red). Image display settings optimised for extract 2.1.85 and applied universally across all images – including DMEM controls. Image display settings were not optimised to untreated controls as doing so gave rise to over saturation of the TOM20 channel in images of extract dosed cells. Scale bar = 20µm.

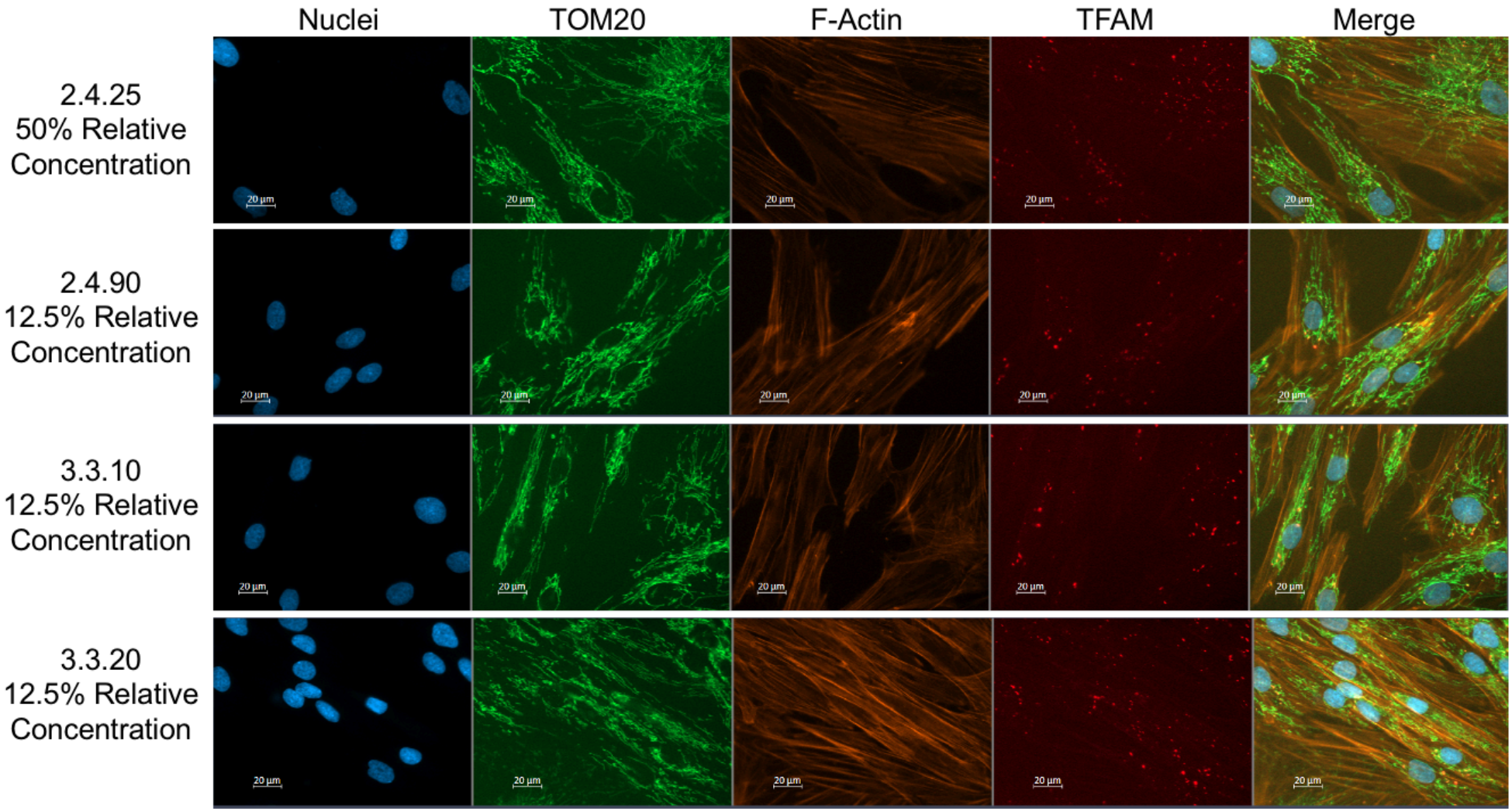

Fig. 3.17, continuned. *Representative images for mitochondrial biogenesis hit extracts, at their optimum relative concentrations as indicated.* Nuclei (blue), TOM20 (green), F-Actin (orange) and TFAM (red).

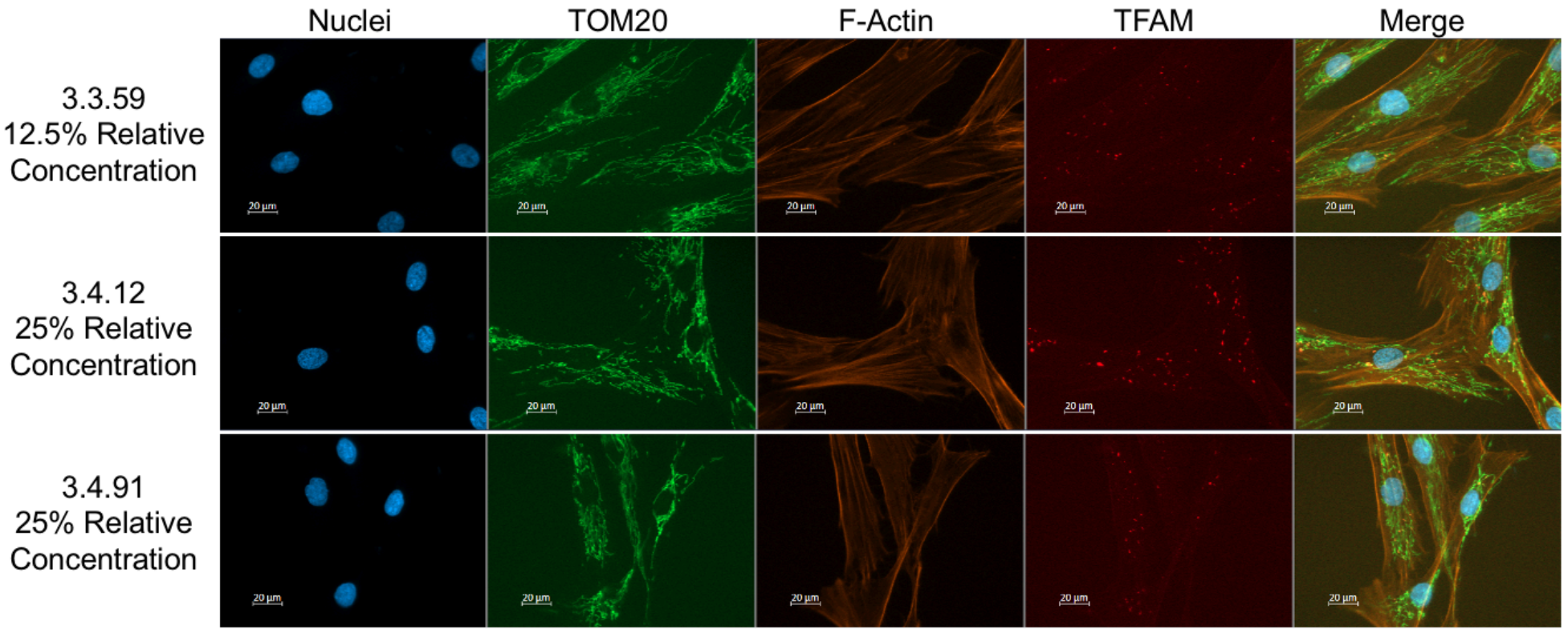

Fig. 3.17, continued. *Representative images for mitochondrial biogenesis hit extracts, at their optimum relative concentrations as indicated.* Nuclei (blue), TOM20 (green), F-Actin (orange) and TFAM (red).

3.4 Discussion

3.4.1 Development of an Assay Pipeline for the Assessment of Mitochondrial Biogenesis

The term mitochondrial biogenesis is yet to be appointed a clear definition and constitutes multiple factors; hence it was necessary to quantify as many associated parameters as practically possible. Due to the variety of parameters associated with mitochondrial biogenesis, the use of a single assay or screen is not viable. Hence the aim of the project was to design a series of experiments, beginning with HTS compatible work, to successively triage active samples as they progressed along the assay pipeline.

Primary screening assessed membrane potential (TMRM) and subsequent secondary screening corroborated these results, by measuring mitochondrial mass through the use of m-GFP. While not suitable for HTS, qPCR has been employed as a multi-well plate compatible measure of mtDNA copy number. Increases in mitochondrial DNA (mtDNA) copy number per cell are indicative of increases in mitochondrial mass within the cell. This can be as a result of increases in mtDNA content per unit mitochondrial mass or increases in mitochondrial mass, while the density of mtDNA within mitochondria remains constant. Both situations necessitate mtDNA replication.

Increases in mtDNA are widely used in the literature to make claims of mitochondrial biogenesis (Lin et al., 2002, Wu et al., 2002, Nisoli et al., 2005, Nisoli et al., 2003, Schreiber et al., 2004, Davis et al., 2009, Dillon et al., 2012, Zhao and Pu, 2019). Elevated mtDNA copy number does not, however, necessitate increases in mtDNA transcription or overall mitochondrial activity. Increases in mtDNA transcription indicate an increased demand for mitochondrial complex biogenesis, itself a vital component of complete mitochondrial biogenesis. Quantification of transcription rate is an appealing prospect in mitochondrial biogenesis assays; however, no rapid multi-well plate assay currently exists for the assessment of mtDNA transcription rate. The cost of current transcriptomic analysis techniques precludes their use in the assessment of large numbers of samples.

Increases in mean TOM20 immunofluorescent staining intensity can also be considered indicative of mitochondrial biogenesis, due to the implication of increased protein import into the mitochondria from the cytosol. The majority of mitochondrially targeted subunits in the cytosol are rapidly imported into the mitochondria via the pre-

sequence pathway through the TOM complex (Nickel et al., 2019). Increases in mitochondrial pre-sequence protein import rate have been linked with mitochondrial biogenesis (Takahashi et al., 1998). If the basal import capacity is exceeded, as a result of increases in the expression of mitochondrially targeted proteins, it is plausible that cells may increase the expression of mitochondrial import machinery complexes. This satisfies the higher demand for mitochondria subunits, which occurs during mitochondrial biogenesis.

It is noted that fold increases of TOM20 immunofluorescent staining intensity were lower than those noted in qPCR experiments, exhibiting a maximum increase of 1.31-fold compared to a maximum observed 4.72-fold increase in mtDNA levels (note different samples gave rise to these two maxima). This difference can be explained by the fact that, once replication is initiated, a new daughter strand of mtDNA can be fully synthesised within ninety minutes (Forslund et al., 2018). The quantity of fully assembled TOM complexes (synthesis and subsequent import and insertion of the mitochondrial membrane) has been found to significantly increase 1.4-fold *in vitro* in skeletal muscle only after 7 days of continual contractile stimulation (Joseph and Hood, 2012). In both qPCR and TOM20 immunofluorescent staining experiments the cells were exposed to extracts for the same period of time (48 hours), therefore the increased rate of mtDNA synthesis, over TOM complex biogenesis, would be expected to yield a larger fold increase from untreated controls.

The application of selection criteria drawing from both qPCR and immunofluorescent tertiary assays resulted in the selection of the following extracts as hits: 2.1.85, 2.1.92, 2.3.11, 2.4.25, 2.4.90, 3.3.10, 3.3.20, 3.3.59, 3.4.12, 3.4.91 and XNAA5. Despite meeting the selection criteria, XNAA5 was dropped from the line of investigation, see section 3.4.2.

Further immunofluorescent investigations showed the co-localisation of increases in mitochondrial density, area per cell, mean mitochondrial length, TOM20 immunostaining intensity, TFAM spot count in the above putative hits, selected for previously demonstrating increases in m-GFP and TMRM fluorescent signals. The combination of increases in all of these parameters presents a well-rounded case for the induction of mitochondrial biogenesis.

3.4.2 Activity in Untransformed Strains

Despite extracts from transposon null XNAA5 meeting the stated selection criteria, it was not further perused with more in-depth immunofluorescent analysis. This is because the lack of an inserted transposon renders the production of active metabolites unreliable, due to the largely conditional expression of bacterial genes. Furthermore, the lack of a transposon complicates the process of identifying an active molecule; genome sequencing and subsequent transposon identification allows for the discovery of the affected gene – which in turn provides information as to the potential nature of an active compound. XNAA5 remains, however, of interest as a potential natural producer of (a) compound(s) capable of influencing mitochondrial biology in mammalian cells.

The identification of effects on mammalian mitochondrial status in several untransformed bacterial strains at first seems highly unlikely: TFTH1, DCBB1, WCEC9 and XNAA5 increased mtDNA count, the latter two also increased TOM20 immunofluorescent stained intensity. However, these strains have only been investigated because their transformed clones resulted in mitochondrial biogenesis activity. A species must possess relevant genes in order for them to be affected by transposon insertion; the transposons serve only to alter the expression of wild-type genes to reduce the conditionality of compound production. Thus, the presence of activity in extracts from these particular untransformed strains is not surprising.

The above observations highlight the multi-factor nature of mitochondrial biogenesis. Samples from species that induce mtDNA count increases, may not necessarily induce increases in other mitochondrial parameters (DCBB1 for example). It is therefore key when screening for mitochondrial biogenesis inducers, to assess multiple means of measuring increases in mitochondrial mass. This ensures that potential leads are not missed, and sub-optimal leads (or even false positives) are not unduly pursued.

3.4.3 Maximum Mitochondrial Capacity

It is noted that that mean increases in mitochondrial density, in the current project, tend to plateau at approximately 1.3-fold increase and do not increase beyond 1.35-fold at 1:1 dilution of extract culture media. Further increasing extract concentrations in cell media caused a decrease in mitochondrial density relative to 1:1 dilution in all analysed extracts, and instead raised mitochondrial area per cell, indicating an increase in cell size (section 3.3.7, Fig 3.15-3.16). It is possible that this response was forced, in order to accommodate the expanding mitochondrial network. This apparent constraint on mitochondrial density could have arisen due to a limit on the volume fraction mitochondria can occupy in a cell, before causing deleterious effects. This theoretical limit hypothesised to be set at 40% of a cell's volume, though actual volumes vary with species and cell type (Vazquez, 2018). Mitochondria occupy 35% of human cardiomyocyte volume under basal conditions (Anastacio et al., 2014), cardiac tissue being one of the most energetically demanding, a near-maximal cellular volume fraction of mitochondria would be expected in cardiomyocytes.

PGC-1α overexpression has been shown to result in cardiac failure (Lehman et al., 2000, Russell et al., 2004), hypothesised to be due to the physical limitation of available space for additional mitochondria in the cell (Riehle and Abel, 2012). This observation could pose a significant obstacle for the development of mitochondrial biogenesis-based treatments; however, it is worthy of note that genetic expression of key regulatory transcription factors is not comparable to pharmaceutical intervention, instead genetic overexpression methods embody an extreme situation. Drug target, compound efficacy and dose can all be adjusted during pre-clinical investigations to minimise off-target effects and detrimental outcomes when employing small molecules as a therapeutic intervention.

3.5 Future Work

3.5.1 Active Compound Purification

Having identified ten bacterial extracts capable of increasing mitochondrial mass in mammalian cells, the purification of hit extracts is next required to allow further progress into lead optimisation stages of a drug discovery pipeline.

Chromatographic techniques will be used to facilitate the separation of hit extract components into individual fractions, followed by their phenotypic characterisation. Due to extracts containing a wide variety of compounds, ranging from inorganic salts to large biomolecules, and the unknown character of these compounds, the optimisation of separation techniques to specific molecules is not viable. There is a low probability that salts and small biomolecules, such as simple sugars, are the active components. Therefore, the dialysis of large volumes of each extract, through small molecular weight exclusive semi-permeable membranes, is recommended to reduce analyte load on chromatography columns. Size exclusion chromatography presents as a means of separating analyte species regardless of chemical properties, and thereby minimises permanent binding of an analyte to the stationary phase. All fractions from such columns should be collected, to avoid unknowingly discarding active fractions. This method, therefore, yields a large number of fractions that essentially form an additional library requiring further phenotypic screening.

Once purified methods to quantify mitochondrial activity, such as Seahorse extracellular flux analysis, will be used. These methods were specifically reserved for the latter stages of drug development due to their high cost, high variability and incompatibility with high throughput work.

3.5.2 Identification of Active Compounds

All fractions obtained by separation techniques, suggested in 3.5.1, will be subject to high throughput analysis of their effects on mitochondrial mass. This screening effort is analogous to the work detailed in this chapter, using purified compounds from hit extracts as opposed to bacterial extracts, thus each extract forms its own library. This process can then be repeated, using hit fractions as chromatography analytes, until a pure compound is obtained. It is proposed that hit compounds will be identified and their structures elucidated using a combination of mass spectrometry and H^1/C^{13} nuclear magnetic resonance spectroscopy.

3.5.3 Mechanistic Elucidation

Mechanistic elucidation of hit compounds requires the identification of a binding target in the cell for the hit compound. This can be achieved through two methods:

Knockdown and Knockout Library Techniques

Genetic screening using siRNA or CRISPR methodologies relies on the significant reduction (knockdown), or removal (knockout) respectively, of potential target proteins from the cell by genetic means. Negative screening methods can then be applied with the goal of identifying a gene that is required for a compound to elicit its function; denoted by a loss of mitochondrial biogenesis upon extract dosing in cells, which do not express the required protein targets. While this is a comprehensive method, which is scalable to cover the entire genome, should a compounds' mechanism of action implicate any proteins which are essential for cell viability, a loss of function would be conflated with cell death and not detected. The ability to generate hypotheses regarding potential targets can significantly lower the financial cost and the amount of time spent on such work. For example, if the molecular structure of a lead compound resembles a known drug, for example a kinase inhibitor, carrying out a siRNA screen of the kinome is a feasible means of beginning mechanistic investigations into the novel lead compound.

Protein Pulldown

Protein pulldown experiments are reliant on both high drug-target specificity and high drug-target affinity, as well as a completely characterised chemical structure of the lead compound in question. The latter is required to identify a suitable site to which a highly specific ligand can be attached – for example a biotin group – without inhibiting the ligand-target interactions to maintain activity. Once such a derivative is identified, cells can be incubated with a biotinylated derivative, to facilitate drug-targeting binding of the lead compound. Cell lysate from these cells can then be incubated with stationary phase–streptavidin immobilised on a membrane in the case of a biotin ligand. Several washes of the station phase with solvent removes non-specific binding, such that only the biotinylated compound and its direct binding partners are retained. Protein mass spectrometry can then be employed to identify the bound protein(s). The protein hits can then be confirmed as essential for compound activity through the use of siRNA knockdown or applying a highly potent and specific known inhibitor (if available), in a negative assay seeking to identify a loss of compound activity.

3.6 Conclusion

The identification of ten bacterial culture extracts capable of inducing dose-dependent increases in multiple parameters associated with mitochondrial biogenesis, marks the beginning of wider investigations into the prospects of using mitochondrial biogenesis as a treatment for mitochondrial disease.

Functional investigations are yet to be carried out on cells dosed with the identified hit extracts. In the future it is suggested at extracts are investigated using models of nuclear mitochondrial diseases in the form of cell types implicated with the common symptoms of mitochondrial disease – for instance iPSC derived patient neurones or primary patient myoblasts differentiated to myotubes. Therapeutic molecules which can penetrate the blood-brain barrier are envisaged to be of greater therapeutic value compared to those that cannot, however, without an identified lead from the afore mentioned bacterial extracts, hypothesises cannot be formed regarding chemical properties. Regardless, due to the vast unmet clinical need associated with mitochondrial disease patients, the amelioration of non-neurological symptoms would still significantly enhance the quality of life of these patients.

In lew of functional data and compound identity, conclusions as to the potential therapeutic viability of the active compounds within the aforementioned bacterial extracts cannot be made. The collaboration between WCMR and Nanna Therapeutics has since concluded.

Chapter 4:

Therapeutic Prospects of Mitochondrial Turnover

4.1 Introduction

Two prominent novel hypotheses for the treatment of mitochondrial disease are centred on expanding the mitochondrial network through mitochondrial biogenesis (Komen and Thorburn, 2014, Lightowlers et al., 2015, Ploumi et al., 2017) or selective mitophagy (Paz et al., 2016, Sharma et al., 2019, Lin et al., 2019). Both are introduced in section 1.9.4.

As outlined in section 3.1.1, the use of mitochondrial biogenesis as a treatment is dependent on the assumption that the residual activity of mitochondrial complexes, affected by pathogenic mutations, is sufficient to meet cellular needs after mitochondrial biogenesis induction. The absence of negative side effects, as a result of increasing the amount of dysfunctional mitochondrial material in cells, is also an important assumption. A significant concern is one of excess ROS accumulation as a result of dysfunctional electron transport. The master regulator of mitochondrial biogenesis (PGC-1α) indirectly upregulates the transcription of genes for multiple antioxidant enzymes: SOD1, 2, catalase and glutathione peroxidase, which is hypothesised to mitigate against increases in ROS (Dong et al., 2008, Wallace et al., 2010).

Similarly, the use of mitophagy stimulation as a treatment is dependent on the assumption that a means of targeting mitophagy to dysfunctional mitochondria will be pharmacologically viable. The exploitation of the membrane potential dependent PINK1/Parkin mitophagy pathway is one option (outlined in section 1.5.2). In contrast to mitochondrial biogenesis, mitophagy is limited as a treatment for heteroplasmic primary mitochondrial disease cases (see section 1.8.1). The degradation of mitochondria in heteroplasmic primary disease cases gives the opportunity to target dysfunctional mitochondria, and thereby those areas associated with mutant mtDNA. The degradation of mitochondrial material in the case of nuclear mitochondrial gene pathologies, or homoplasmic mtDNA mutations, would not result in phenotypic improvement as the dysfunction is present ubiquitously across all mitochondria.

To date, no small molecule has been generally accepted to cause mitochondrial proliferation. Deferiprone, however, is a positive control for the induction of mitophagy, though its action results in the indiscriminate degradation of mitochondria, regardless of the presence or absence of dysfunction (Ivatt and Whitworth, 2014, McWilliams et al., 2016b). Multiple pathways for the induction of mitophagy are known, summarised in 1.5.2, which provide possible targets for future drug development projects.

Mitophagy can be quantified through the fluorescent imaging of cells expressing the recently developed mito-QC probe, which consists of an mCherry-GFP fusion protein, linked to the MOM targeting sequence of FIS1 (residues 101-152) (McWilliams et al., 2016b). The tandem fluorescence of mCherry and GFP produces merged yellow fluorescence in mitochondria. Mitochondria subject to lysosomal degradation (mitophagy) exhibit red fluorescence only in merged channel images, as GFP fluorescence is rapidly quenched due to the acidic environment of the lysosome. As a result, the quantification of mitophagy positive red puncta in fluorescent images is indicative of the amount of mitophagy occurring in a cell (McWilliams et al., 2016b, Bell, 2020).

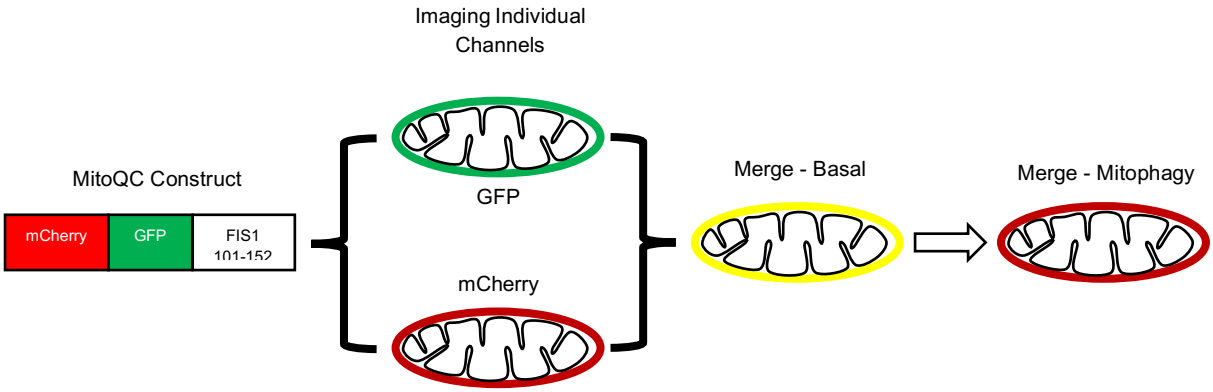

Fig. 4.2. *A representation of the mechanism of mitoQC fluorescent imaging.* The mitoQC construct contains the fluorophores mCherry and GFP, fused to a FIS1 MOM targeting sequence. Fluorescence appears yellow in merged channel images when mitochondria are under basal conditions. When undergoing mitophagy, mitochondria appear read in merged channel images due to the quenching of GFP fluorescence in the acid environment of the lysosome.

The identification of ten bacterial culture extracts capable of increase total mitochondrial mass in mammalian cells, chapter 3, provides a unique opportunity to assess the interplay of the two antagonistic processes that control cellular mitochondrial content. Any remaining samples from biogenesis screening investigations (chapter 3), of sufficient volume, were used for further investigations using Mito-QC analysis: 2.1.85, 2.1.92, 2.3.11, 2.4.25, 2.4.90, 3.3.10 and 3.4.12.

4.2 Aims

This project aims to further investigate the effect of candidate mitochondrial proliferators on mitophagy. Mito-QC analysis of fibroblasts will be used to quantify mitophagy positive puncta, in fibroblasts treated with bacterial extracts capable of inducing net increases in mitochondrial mass, identified in chapter 3.

Readouts from the experiment are indicative of a general mechanism of action of the extracts. Given the nature of the extracts, possible actions include mitophagy inhibitors, mitochondrial biogenesis inducers (indicated by no reduction in mitophagy as measured by this assay) or a combination of the two in which a net gain of cellular mitochondrial mass is achieved.

4.3 Results

To assess the mitophagic effects of bacterial extracts, shown previously to induce increases in net mitochondrial mass in mammalian cells, mitoQC analysis was employed to facilitate the quantification of mitochondrial material within autophagosomes (mitophagy positive spots).

The mitoQC probe results in all mitochondrial material exhibiting red mCherry signal. Mitochondria outside of autophagosomes also exhibit green GFP signal. Due to acidic quenching of GFP fluorescence, GFP signal intensities are significantly lower than mCherry signal intensities within mitochondria activity undergoing mitophagy. A ratio of mCherry/GFP signal was calculated for all mCherry spots (total mitochondrial area). An elevated mCherry/GFP ratio indicates a mitochondrial punctum within an autophagosome; termed mitophagy positive. The classification of "mitophagy positive" was made using a threshold of $\mu_{untreated}+1\sigma_{untreated}$; any mCherry spots exceeding this mCherry/GFP ratio were designated mitophagy positive. This threshold was applied to cells treated with bacterial extracts, Fig. 4.2.

The number of mitophagy positive puncta was taken as a percentage of the total number of puncta to give the final readout of % mitophagy:

$$\% \text{ Mitophagy} = \frac{\text{Number of mitophagy positive mitochondrial spots}}{\text{Total number of mitochondrial spots}} \text{X100}$$

Treatment of mitoQC expressing fibroblasts with bacterial extracts, previously demonstrated to increase mitochondrial mass, triggered decreases in % mitophagy in comparison to untreated cells, Table 4.1. Analysis was conducted as a pilot experiment in a single well per extract due to the limited availability of extracts, at the time of the analysis, as such significances of the changes in % mitophagy cannot be calculated. Table 4.1 further relates the mitoQC data to the mitochondrial density, and mass per cell, changes observed in chapter 3 (3.3.7).

Table 4.1. *The effects of selected mitochondrial biogenesis inducing bacterial extracts on mitochondrial density (section 3.3.7) and % mitophagy in fibroblasts.* Data acquired at a relative concentration of 50% (1:1 dilution of stock extract in culture media) presented as fold change from untreated controls.

Sample	**Mitochondrial Density**	**Mitochondria Mass/Cell**	**% Mitophagy (Fold Change)**
2.1.85	1.30	1.49	0.24
3.3.10	1.18	1.26	0.36
2.4.90	1.22	1.25	0.37
3.4.12	1.08	1.21	0.37
2.3.11	1.32	1.52	0.38
2.4.25	1.28	1.48	0.67
2.1.92	1.35	1.28	0.74
Control	1.00	1.00	1.00

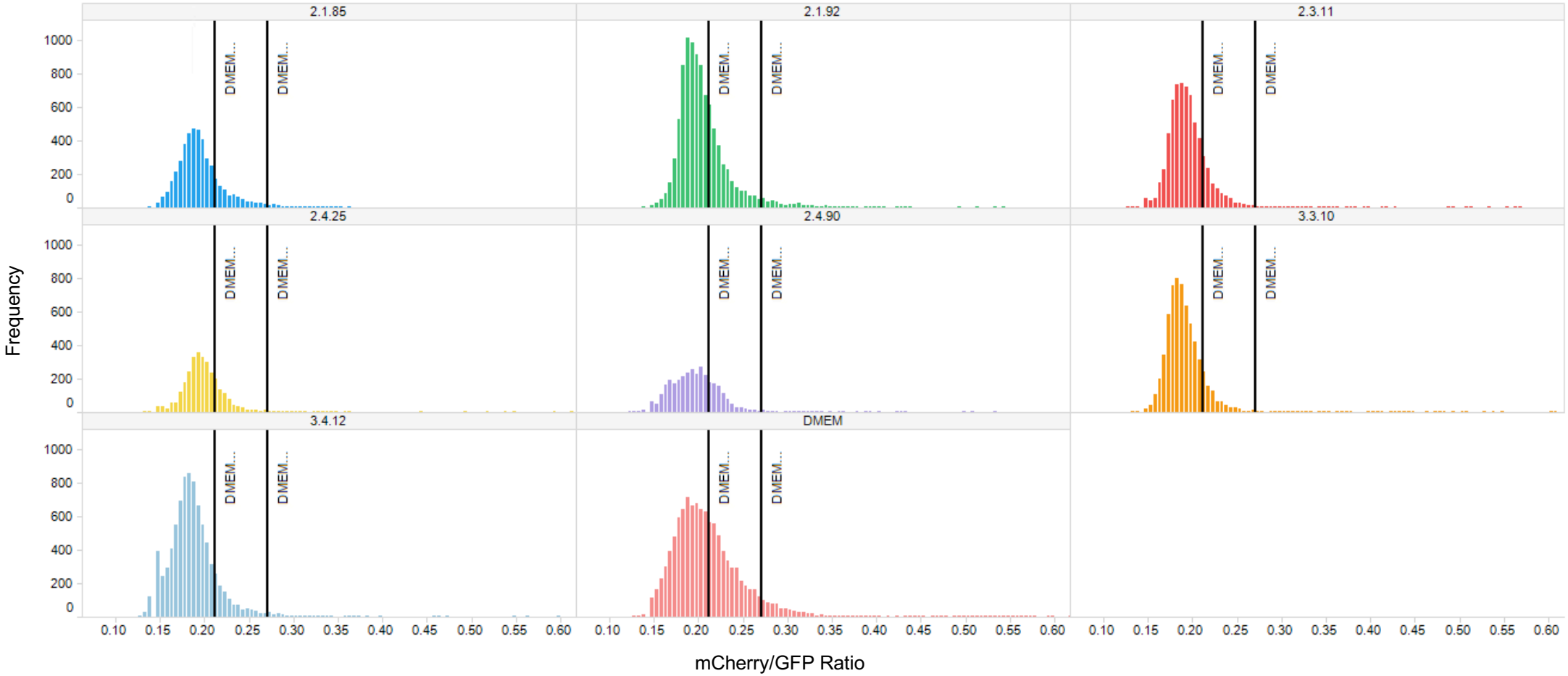

Fig. 4.2. *Graphical representation (frequency histogram) displaying the mCherry/GFP signal ratios of mCherry spots, in MitoQC expressing fibroblasts treated with bacterial extracts capable of increasing net mitochondrial mass.* Vertical black lines in each plot represent untreated (DMEM only) mean ($\mu_{untreated}$) mCherry/GFP ratio, at 0.21 mCherry/GFP ratio, and this mean reading plus 1 standard deviation ($\mu_{untreated}+1\sigma_{untreated}$), at 0.27 mCherry/GFP ratio. Any mCherry spots exhibiting a ratio in excess of the $\mu_{untreated}+1\sigma_{untreated}$ threshold was designated mitophagy positive. A decrease in the number of mCherry spots exhibiting mCherry/GFP ratios in excess of $\mu_{untreated}+1\sigma_{untreated}$ denote a reduction in the levels of mitophagy in response to treatment.

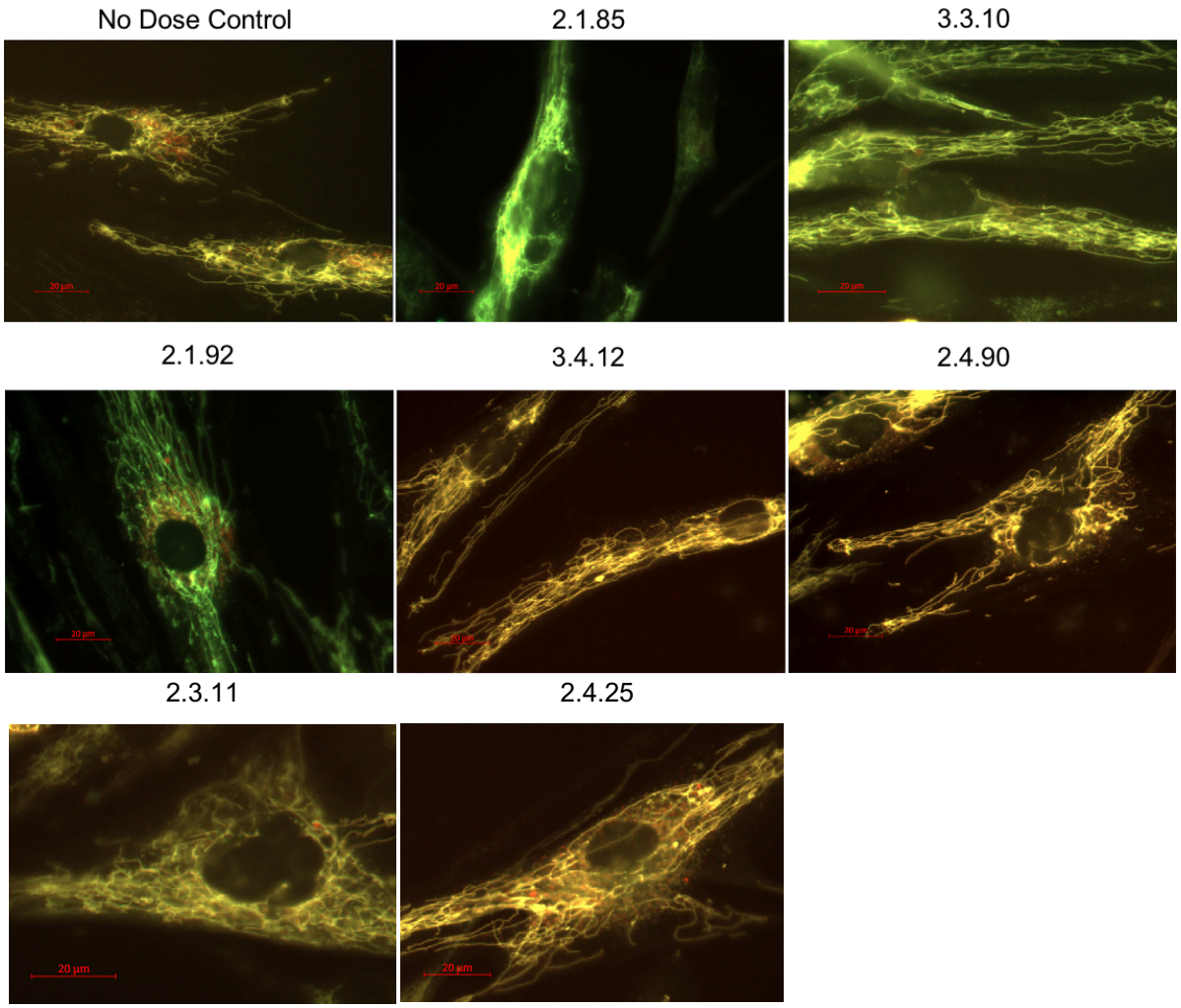

Fig. 4.3. *Representative images of MitoQC expressing fibroblasts treated with bacterial extracts, capable of increasing net mitochondrial mass.* Images presented are merges of mCherry and GFP fluorescent channels, to allow for the visualisation of mitophagy positive spots within cells. Yellow: stable mitochondria. Red: mitochondria undergoing mitophagy. Scale bar = 20µm.

4.4 Discussion

4.4.1 Mechanistic Implications for Mitochondrial Biogenesis Inducing Extracts

Mitochondrial biogenesis and mitophagy are antagonistic processes, used for both the quality control and morphology maintenance of mitochondria, under basal conditions. While the net effect achieved by each of the investigated bacterial extracts was an increase in mitochondrial quantity, this can be achieved through two major pathways: increasing the rate of mitochondrial biogenesis to outpace the basal rate of mitophagy or inhibiting mitophagy such that the basal rate of mitochondrial biogenesis exceeds it. A combination of these two pathways is also theoretically possible. It is important to note that definitive conclusions regarding the mitophagy effects of the analysed bacterial extracts in the pilot experiment presented above cannot be drawn, since this experiment was conducted with a single biological replicate per condition, due to a lack of extract availability. Nevertheless, observations from the analysis are discussed below.

Extracts 2.1.85 and 2.1.92 originate from the same sample plate and both repressed mitophagy, but to different extents. Of the extracts analysed, treatment with 2.1.85 caused fibroblasts to gain 30% and 49% increases in mitochondrial density and mass per cell respectively, section 3.3.7, Fig. 3.13-3.16. From mitoQC analysis, 2.1.85 reduced the rate of mitophagy by 76% relative to untreated controls. It could therefore be hypothesised that 2.1.85 treatment acts to inhibit mitophagy to a greater extent than other extracts, rather than upregulate mitochondrial biogenesis. This conclusion can be drawn because extract 2.1.92 demonstrated similar mitochondrial density increases (+35%); however, it repressed mitophagy by only 26% relative to untreated controls. Similarly, extract 2.4.25 suppressed % mitophagy by 33% relative to untreated controls, but induced 28% increases in mitochondrial density. Therefore, it could be concluded that large reductions in mitophagy rate are not essential for increases in mitochondrial mass but may also contribute to a rise in cellular mitochondrial content. Further, it is plausible to hypothesise that extract 2.1.85 contains one (or more) active compound(s), which act primarily as a mitophagy inhibitor(s) rather than a mitochondrial biogenesis inducer(s). Similarly, extract 2.1.92 can be hypothesised to act primarily as a mitochondrial biogenesis inducer, with lesser suppression effects on mitophagy.

Extracts 2.3.11, 2.4.90, 3.3.10 and 3.4.12 originate from different sample screening plates; however, they share an untransformed wild-type species – TFTH1 – as determined by genetic sequencing carried out at Nanna Therapeutics (data not shown). In the investigations of chapter 3, untransformed TFTH1 extract treatment increased mtDNA count per cell by 1.44-fold in HeLa cells (section 3.3.4) but did not cause statistically significant increases in mean TOM20 immunofluorescent signal cells (section 3.3.5). The analysed TFTH1 transposon positive extracts all exhibited similar reductions in % mitophagy, relative to untreated controls: approximately a 0.37-fold change. While extracts from wild-type TFTH1 were not analysed using mitoQC methods, the consistency of transposon positive extracts in reducing % mitophagy alludes to this characteristic potentially originating from the wild-type strain. The hit bacterial extracts, capable of increasing mitochondrial mass (2.3.11, 2.4.90, 3.3.10 and 3.4.12), from TFTH1 all exhibited increased TOM20 immunofluorescence in section 3.3.7 and (with the exception of 3.4.12) increased mtDNA copy number. It is therefore hypothesised that extracts 2.3.11, 2.4.90 and 3.3.10 retain the assumed mitophagy suppression characteristics of the wild type TFTH1 and, due to the transposon mutagenesis, also produce metabolites associated with the induction of mtDNA replication.

In the presence of extensive mitophagic inhibition only, it may be expected that a cell would act to retain basal levels of mitochondria, with no change in TOM20 or TMRM intensity, by down-regulating mitochondrial biogenesis pathways to maintain mitochondrial homeostasis (Palikaras et al., 2015). A degree of MB induction triggered by drug treatment, as opposed to solely mitophagy inhibition, may be essential to overcome the homeostatic tendencies of a cell. Activation of PGC-1α associated transcription factors, such as NRF-1, 2 and PPAR receptors, would also be required to facilitate increases in TMRM and TOM20 fluorescent intensities as well as the TFAM spot count increases noted in 3.3.3 and 3.3.7, respectively. It can therefore be concluded that the bacterial extracts are not solely acting through the suppression of mitophagy, nor are they completely arresting the process. This data shows that reductions in the rates of mitophagy may contribute to the increases in mitochondrial mass, but large reductions in mitophagic activity are not required for significant increases in mitochondrial mass – as such to view mitochondrial biogenesis and mitophagy as antagonistic is an oversimplification.

4.4.2 Mitochondrial Biogenesis and Mitophagy in Future Therapeutic Developments

Analysis of the above extracts show that an increase in mitochondrial mass can be accompanied by reductions in the rate of mitophagy, though this effect may not be universal due to the limited number of extracts tested and the low replicate number in this analysis. The low replicate count was necessitated due to the limited availability of extracts. While the current project has established a link between increases in mitochondrial mass and reductions in the amount of mitophagy, a causative relationship cannot be proven or precluded. In support of the hypothetical link between MB and suppression of mitophagy with extract treatment is evidence that SIRT1 activation, known to induce mitochondrial biogenesis (section 1.5.1), has been shown to reduce autophagic degradation (Lee et al., 2008). Furthermore, increases in NRF-2 transcriptional activity facilitates the degradation of Drp1 (Sabouny et al., 2017), pushing the mitochondrial network towards a fused state, which is incompatible with mitophagy (Das and Chakraabarti, 2020). In contrast, a second well characterised stimulator of MB, AMPK activation, is implicated with increases in mitophagic activity (Palikaras et al., 2015). A loss of ULK-1, a downstream target of AMPK - activated upon by phosphorylation by AMPK, results in a loss of mitophagic function and accumulation of mitochondria in erythrocytes, which are normally devoid of mitochondria (Egan et al., 2011).

Mitochondrial network fusion is associated with increased network activity (Mitra et al., 2009), while an increase in fission is associated with obesity and elevated ROS production (Gomes et al., 2011, Liesa and Shirihai, 2013). Mitochondrial network hyper-fusion brought about by mDivi-1 treatment, an inhibitor of Drp1 (Cassiday-Stone et al., 2008), reduces mitophagic degradation (Das and Chakraabarti, 2020), but also reduces mitochondrial activity in healthy cells (Qian et al., 2014). mDivi-1 has now been shown to be linked with CI inhibition (Bordt et al., 2017). As such, the hyper-fusion brought about by mDivi-1 treatment does not present as a suitable positive control for treatment development. Further, the mitophagic inhibition induced by liensinine treatment employs the inhibition of lysosomal degradation of mitochondria, rather than preventing engulfment of mitochondrial material (Zhou et al., 2015). As such, if analysed by mitoQC methods, despite no decrease in mitochondrial material in the cell, the method would quantify mitophagy positive puncta as a result of the quenching of mGFP fluorescence in the lysosome. Therefore, liensinine was not used as a positive control for mitophagy inhibition.

The increased mean mitochondrial length brought about by bacterial extract treatment (section 3.3.7), is indicative of increased mitochondrial network fusion. This impact alone could result in a decrease in mitophagy, due to mitochondrial puncta being the only suitable target for mitophagy as a result of their reduced volume. This, however, does not fully explain the wide range of effects on % mitophagy noted in this mitoQC analysis.

The aetiology of primary mitochondrial diseases, those brought about by pathogenic mutations in mtDNA, is closely linked to the level of heteroplasmy, with a threshold beyond which a phenotype presents in each case (section 1.7.1). Cases subject to heteroplasmy contain a population of wild-type mtDNA. Nanoscopy has shown that mtDNA molecules reside in compartments surrounded by cristae, as opposed to being evenly spread throughout the network (Stephan et al., 2019). Despite rapid and dynamic re-modelling of cristae (Kondadi et al., 2020), they remain functionally distinct from their neighbours (Wolf et al., 2019). Mitochondrial dysfunction often results in a reduction in membrane potential, relative to wild-type controls (McKenzie et al., 2007, Szczepanowska et al., 2012). Therefore, it follows that areas of a mitochondrial network containing mutant mtDNA will present with a lower membrane potential, as a result of dysfunction brought about by the expression of pathogenic mtDNA in the locality – due to the close association of mtDNA, mitochondrial RNA granules and mitoribosome assembly and translation (Pearce et al., 2017). Areas of reduced membrane potential are inducers for mitochondrial fission, leading to the loss of affected mitochondrial region from the remaining network, forming mitochondrial puncta that become targets for mitophagic degradation (Wikstrom et al., 2009, Twig and Shirihai, 2011). Imaging in live cells has demonstrated that fissile mitochondria divide to fall within two distinct categories, those which divide towards the periphery of a network or towards the mid-section (Kleele et al., 2021). Peripheral division has been shown to result in the localisation of Parkin and subsequent recruitment of autophagosomes to the smaller ‘daughter’ mitochondrion, while divisions which occur more centrally in ‘parent’ mitochondria do not result in ‘daughters’ that undergo mitophagy (Kleele et al., 2021). Peripheral divisions were further shown to occur to remove sections of mitochondrial material, from the larger network, which display a reduced membrane potential and increased ROS levels (Kleele et al., 2021) – features prominent in mitochondria subject to mtDNA mutations.

It is therefore proposed that retaining a degree of mitophagic activity during treatment that results in a net increase in mitochondrial mass, has the potential to gradually eliminate mutant mtDNA while increasing the total mtDNA pool. The combined actions of MB and mitophagy could potentially induce a heteroplasmy shift towards a lower percentage heteroplasmy value. In certain cases, the shift may only need to be minor to cross a pathogenic threshold to ameliorate a patient's symptoms.

In cases of mutant mtDNA homoplasy, and mutations in nuclear-encoded mitochondrial genes, no such shift is possible. Nevertheless, the total increase in mitochondrial material (and thereby theoretical capacity) still carries significant therapeutic potential (Schon et al., 2010, Komen and Thorburn, 2014, Lightowlers et al., 2015, Ploumi et al., 2017).

4.5 Conclusion

Application of the bacterial extracts, which trigger net increases in mitochondrial mass in mammalian cells, resulted in mitoQC fibroblasts exhibiting suppressed rates of mitophagy, relative to untreated controls. The literature surrounding known MB induction pathways suggests mitophagic modulation is linked to likely targeted pathways. This mitoQC analysis suggests that a correlation between increases in mitochondrial mass and decreases in mitophagy may exist. It does not, however, provide evidence that suppression of mitophagy rate is essential to trigger increases in total mitochondrial mass.

Retaining a degree of mitophagic activity during MB induction, presents as a hypothetical means of inducing a heteroplasmy shift, in heteroplasmic primary mitochondrial disease cases.

Investigations into mitochondrial biogenesis, and its relationship with mitophagy, as a treatment for mitochondrial dysfunction continue at WCMR. The collaboration between Nanna Therapeutics and WCMR was ended shortly after the findings presented in this chapter were made, precluding further investigations of the bacterial extracts at WCMR.

Chapter 5:
Development of an Immunofluorescent Method for Mitochondrial Defect Quantification and Phenotypic High Throughput Screening

5.1 Introduction

5.1.1 Complex I and Complex IV Deficiency in Mitochondrial Disease

Biochemical defects, as a result of mitochondrial disease, are characterised by an impairment in a cell's ability to generate catalytically functional complexes (Fassone and Rahman, 2012). The most common biochemical defect among mitochondrial disease patients is mitochondrial complex I (CI) deficiency, amounting to approximately 25-35% of disease cases (Swalwell et al., 2011, Nouws et al., 2012). Deficiency can arise from either a reduction in the catalytic efficacy of mitochondrial complexes, or in an impairment in complex assembly, or a combination thereof. Biochemical defects in mitochondrial complex IV (CIV) are also common in mitochondrial disease patients, accounting for approximately 15% of Leigh Syndrome cases (Lake et al., 2016). CIV deficiency is most commonly caused by mutations in SURF1, a CIV assembly factor (Wedatilake et al., 2013). Phenotypes combining CI and CIV deficiencies are also commonly observed. The most widely noted aetiology of combined CI and CIV deficiency is $tRNA^{Leu}$ mutation, m.3243A>G, outlined in section 1.7.1, often giving rise to MELAS (Lax et al., 2016, Alston et al., 2017); though combined CI and CIV defects are also noted in cases of Leigh Syndrome (Lake et al., 2016).

Due to their high rate of incidence in mitochondrial diseases, targeting CI or CIV deficiency, or a combination thereof, for high-throughput assay development presents an efficient means of identifying novel therapeutics for mitochondrial diseases.

5.1.2 Mitochondrial Complex I Assembly

Mitochondrial complex I is a 970kDa complex, comprised of 45 subunits, with a dynamic multi-step assembly pathway (Mackenzie and Ryan, 2010, Stroud et al., 2016). Multiple points of entry for intermediate complexes have been identified, however, the complex process can be summarised as follows: NDUFS2, 3, 7 and 8 and NDUFA5 bind in the mitochondrial matrix, forming the Q module. The Q module binds the MIM bound ND1/TIMMDC1 complex, and recruits NDUFA3, 8 and 13, as a result of interactions with assembly factors NDUFAF3 and 4 (Sánchez-Caballero et al., 2016). This results in the anchoring of the Q module to the MIM, leading to an intermediate denoted as Q/P_P-a (Mackenzie and Ryan, 2010, Stroud et al., 2016, Guerrero-Castillo et al., 2017).

Separately, the MCIA complex forms in the MIM from NDUFAF1, ECSIT, ACAD9, TMEM126B, TMEM186 and COA1, into which are inserted MT-ND2 and MT-ND3, MT-ND4L and MT-ND6 proteins (Formosa et al., 2020). The completed intermediate has been designated as P_p-b (Guerreo-Castillo et al., 2017). Simultaneously, the ND4 module assembles independently in the MIM from NDUFB1, 5, 10, 11 and MT-ND4 (P_D-a), as does the ND5 module from NDUFB3, 7, 8, 9 and MT-ND5 (P_D-b) (Sánchez-Caballero et al., 2016, Guerrero-Castillo et al., 2017, Silva-Pinheiro et al., 2020).

The further assembly of the four intermediates, outlined above, into complete CI has been shown to proceed dynamically. Q/P_p-a associates with P_p-b, to give the 736kDa Q/P_p intermediate. P_p-b can bind to P_D-a, and subsequently, P_D-b, either before or after binding to Q/P_p-a to give the 1143kDa Q/P intermediate (Guerrero-Castillo et al., 2017). The N module (NDUFA2, 6, 7, 11 and 12, NDUFS1, 4 and 6 and NDUFV1-3) assembles in the mitochondrial matrix, independently of afore mentioned steps, to bind to the Q module of the Q/P intermediate (Mackenzie and Ryan, 2010, Guerreo-Castillo et al., 2017). The binding of the N module, and release of all associated assembly factors, results in the biogenesis of mature 970kDa CI (Stroud et al., 2016, Guerreo-Castillo et al., 2017).

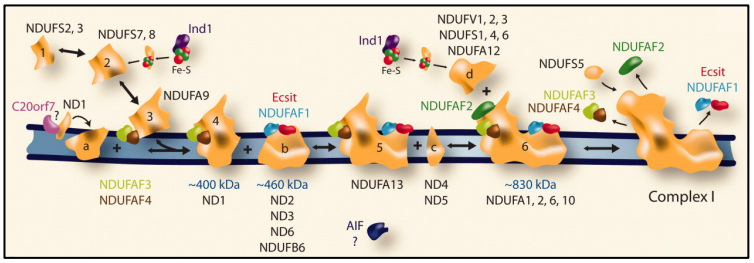

Fig. 5.1. *The assembly pathway of mitochondrial complex I.* (Mckenzie and Ryan, 2010)

5.1.3 Forcing the Presentation of Mitochondrial Disease Phenotypes in vitro

Routinely used cell culture media often contains a high concentration of glucose, 25mM, to ensure sufficient levels of substrate for optimal rates of cell growth. This concentration of glucose is not physiologically relevant, human serum glucose concentrations are approximately 5.5mM (Weil et al., 2009). This excess glucose availability in cell culture gives rise to the Crabtree effect, in which the production of ATP originates largely from glycolysis (Marroquin et al., 2007). HeLa cells in high glucose media almost exclusively rely on glycolysis for ATP production (Melser et al., 2013).

Incubating cells in culture media in which galactose is the primary carbon source forces cells to use OXPHOS. The metabolism of a single molecule of glucose, by glycolysis, results in the net production of 2 ATP molecules. Galactose is slowly converted to glucose-1-phosphate through the Leloir pathway, which is subsequently converted to glucose-6-phosphate for oxidation via glycolysis. This process hydrolyses 2ATP to 2ADP, such that the full glycolytic metabolism of one molecule of galactose leads to no net ATP gain for a cell (Leloir, 1951). Thus, the provision of galactose as the primary carbon source forces the utilisation of the tricarboxylic acid cycle, mitochondrial electron transport chain and OXPHOS to produce ATP (Kase et al., 2013). Under these conditions, wild-type cells have been shown to become more susceptible to mitochondrial toxins (Marroquin et al., 2007), relative to high glucose media, and phenotypes of mitochondrial disease patient-derived cells present themselves more significantly (Rai, 2017). This effect on mitochondrial patient-derived cell lines can be exploited *in vitro* during the development of screening methods.

5.1.4 The Complex I Assembly Defect Rescue – MOA2

A compound, here termed Mechanism of Action 2 (MOA2), was originally identified from a high throughput screen of a small molecule library, provided by the Novartis Institute for Biomedical Research in Basel - Switzerland. A secondary screen, assessing mitochondrial network morphology rate recovery post insult, was performed at The Wellcome Centre for Mitochondrial Research, in which the compound was redesignated as MOA2 (Rai, 2017). MOA2 was further found to increase the complex I dependent oxygen consumption rate (OCR) of NDUFS2 mutant fibroblasts (see section 2.5.1) using seahorse extracellular flux analysis (SEFA) (Rai, 2017). The concentration of MOA2 required for the optimal cellular responses in both phenotypic rescues was found to be 3μM.

Upon the commencement of this project, MOA2 was hypothesised to improve the rate of assembly of CI in NDUFS2 mutant fibroblasts, however, the target and mechanism of action of MOA2 remained unknown.

The structure of the compound has been withheld to preserve the intellectual property surrounding the compound.

5.2 Aims

5.2.1 Development of a novel high-throughput screening method for the detection of Phenotypic Improvement of CI Deficiency

This project will explore the quantification of complex I deficiency in a cell line model of mitochondrial disease. It will focus on two previously established *in vitro* phenotypes of an NDUFS2 mutant cell line: failure to thrive in galactose media and deficiencies in fully assembled mitochondrial complex I. The project aims to develop and optimise a protocol, based on the above phenotypes, for the high throughput screening of compound libraries. The goal of the project is to facilitate the future discovery of novel lead candidates for drug development.

The project also seeks to contribute to the characterisation of the phenotypic improvement of two mitochondrial disease model cells lines, when treated with a lead compound of pharmacological interest – MOA2.

5.2.2 Application of IF Technology and Single Cell Level Microscopy to Mitochondrial Disease Diagnosis

Immunocytochemical analysis has a precedent for use in mitochondrial disease diagnostics in a qualitative manner (Hanson et al., 2002), though the employment of automated data processing has not yet been explored. The current project seeks to apply modern high-throughput imaging and data analysis technology to the phenotypic assessment of mitochondrial disease patient-derived cells lines. It is envisioned that, with additional validation, such a method could circumvent the requirement for muscle biopsies and more easily facilitate the tracking of disease progression; or improvement with yet to be developed therapeutics.

5.3 Results

5.3.1 Galactose Growth Assay

The NDUFS2 mutant fibroblast cell line had previously been shown to fail to thrive in cell culture media with galactose as the carbon source (Rai, 2017). To assess whether this *in vitro* phenotype could be exploited for HTS, NDUFS2 fibroblasts were subjected to growth rate analysis in 96 well plates using an IncuCyte Live system (Essen Biosciences).

Cells were initially seeded in multi-well plates in glucose media and allowed to adhere to the well and proliferate for 48 hours. All media was then refreshed – one-third received standard DMEM cell culture media, one-third received galactose media and the final third received galactose media containing 3μM MOA2. Due to the unknown mechanism of action of MOA2 (in that MOA2 could be acting as a low potency inhibitor), media and treatment were renewed at 72-hour intervals to ensure sufficient availability of substrates and drug.

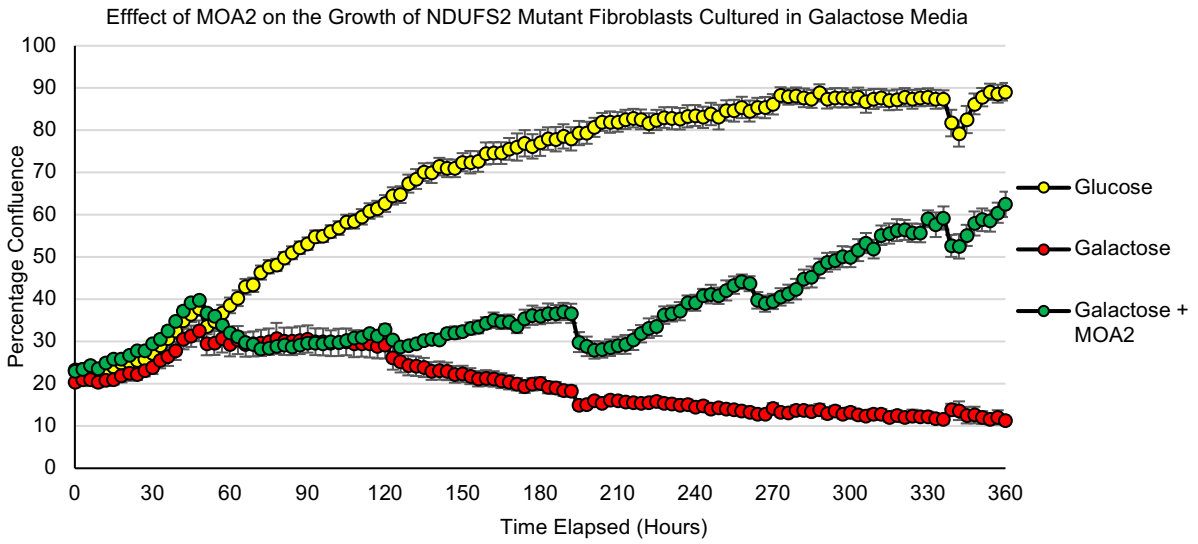

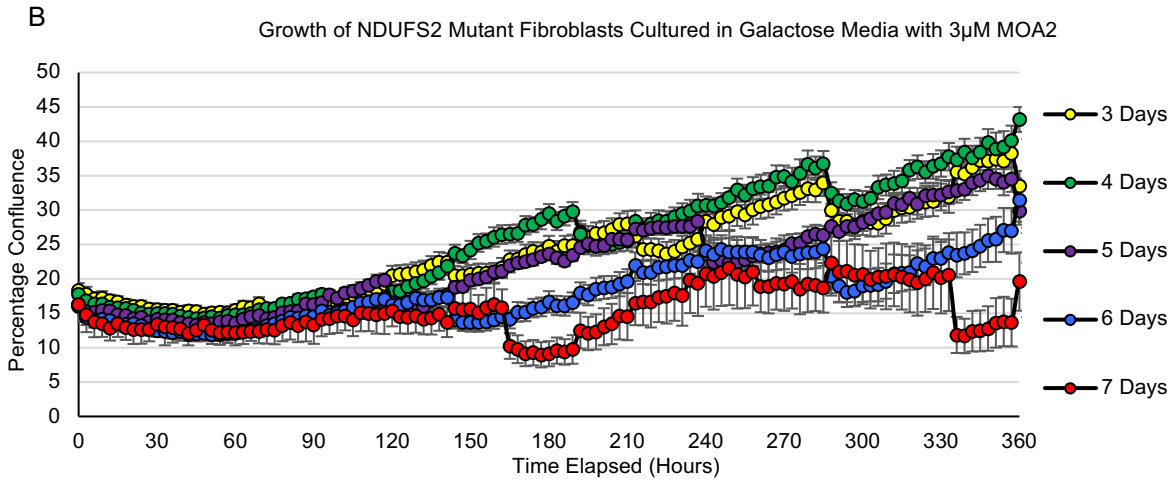

Fig 5.2, Confluences changes of NDUFS2 mutant fibroblasts cultured in galactose media in the presence and absence of MOA2 treatment. A) Confluence of NDUFS2 mutant fibroblasts in glucose media and galactose media - with and without 3μM MOA2 over a 360 hour period. Cells were seeded at 20% confluence in multi-well plates in glucose media and changed to the experimental conditions after 48 hours. Media was subsequently renewed and MOA2 treatment re-applied (where applicable) at 72-hour intervals. NDUFS2 fibroblasts proliferate rapidly in glucose media, while they fail to thrive and proliferate in galactose media. Treatment with 3μM MOA2 facilitates cell survival in galactose media and allows partial restoration of proliferation rate. N=7. B) Growth rate of NDUFS2 mutant fibroblasts in galactose media with 3μM MOA2 in which re-application rates of MOA2 were investigated: 3-, 4-, 5-, 6- and 7-day intervals. Cells were incubated in glucose media for 24h post seeding to allow for well adherence (i.e. t=-24, confluence data not shown), t=0 timepoint is cell exposure to galactose media/MOA2. Optimal growth rates were observed with 3- and 4-day intervals, while a failure to thrive was noted with 7-day re-application intervals. Intervals of 3-6 days: N=12, 7-day interval: N=3, lower replicate number due to cell death.

NDUFS2 mutant fibroblasts grown in glucose media exhibited the expected sigmoidal growth curve, proliferating from 32% confluence at 48 hours (first media change) and plateauing at 90% confluence 222 hours later (Fig. 5.2, A). Cells grown in galactose media failed to proliferate after transitioning to galactose as a carbon source, beginning to drop in confluence after 72 hours in galactose media: confluence dropped to 13%, from 32%, 222 hours post media change. Cells grown in galactose media with 3μM MOA2 also failed to proliferate in the 96 hours post media change, however, after the re-application of 3μM MOA2 a slow rate of growth is noted. Confluence increases from 32% to 40% over the same time in which glucose cultured cells had reached a plateau.

After media change and MOA2 application at 48 hours, MOA2 treated fibroblasts required a further 261 hours to gain a 1.5-fold increase in confluence. Glucose cultured cells required 33 hours to proliferate to the same degree. Culturing and re-dosing the cells for a further 138 hours (13 days post substrate transition) resulted in 3μM MOA2 dosed cells reaching 60% confluence, while untreated controls had dropped to 9% confluence. Visual inspection of untreated galactose cultured cells (t =360h) revealed that cell debris accounted for the 9% confluence reading.

An investigation into the requirement of MOA2 re-application revealed that NDUFS2 mutant fibroblasts required re-treatment with 3μM MOA2 at 6-day intervals, at a minimum, to rescue cellular growth rate in galactose media (Fig. 5.2, B). Optimal growth was observed with 3- and 4-day intervals, growing at a mean rate of 1.20% and 1.68% confluence per day, respectively. Intervals of 5- and 6-days resulted in growth rates of 1.00% and 1.06% confluence per day. Re-treatment at 7-day intervals did not facilitate cell proliferation. Therefore, 4-day re-application intervals were adopted for future experiments.

Long culture periods of NDUFS2 fibroblasts in galactose media with MOA2 (approx. 400 hours), results in a screen viable Z' score difference between treated cells and untreated controls – defined as attaining Z'>0.5, Fig. 5.3. Z' score results are dependent to a greater extent on the standard deviation of positive and negative controls, as opposed to the difference in mean readings between them. As seen in Fig. 5.3, the standard deviation of confluences of MOA2 treated cells is large in comparison to untreated controls. As such Z' scores are inconsistent between consecutive timepoints, despite the fact that that the difference between the two groups was highly significant $P<1x10^{-8}$.

The long period of time required for producing a viable Z' score (approx. 16 days) and high variability of results, is incompatible with high throughput screening.

Time (Hours)	Mean Untreated Control % Confluence	Mean 3μM MOA2 % Confluence	Z' Score
351	10.59	63.88	0.30
354	10.90	64.59	0.35
357	10.81	66.15	0.22
360	10.75	65.35	0.30
363	10.66	66.22	0.39
366	10.77	67.82	0.42
369	10.60	68.55	0.43
372	10.48	68.70	0.51
375	10.30	70.83	0.48
378	10.36	71.05	0.44
381	10.33	70.46	0.48
384	10.26	71.08	0.49
387	10.22	72.43	0.51
390	10.50	71.37	0.43
393	10.23	69.43	0.52
396	10.16	74.16	0.57
399	10.25	74.09	0.53
402	10.37	76.11	0.51

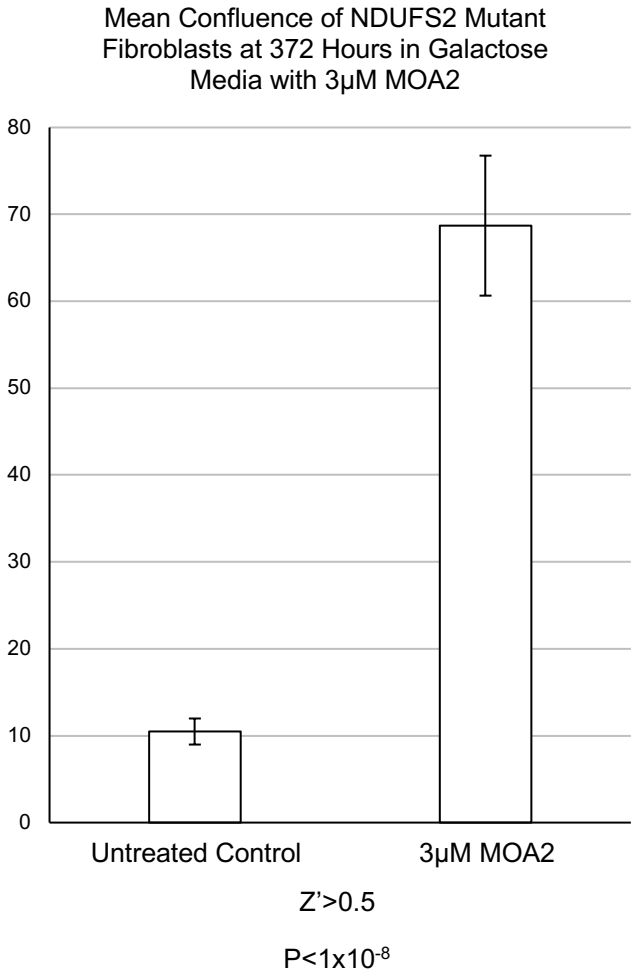

Fig. 5.3, *End point confluence of NDUFS2 mutant fibroblasts cultured in galactose media, in the presence and absence of MOA2 treatment, after approx..400 hours.* A high throughput screen viable Z' Score is obtained after 372 hours in culture. Z' scores exceeding 0.5 are highlighted in green. N = 6.

The requirement of complete media changes in combination with MOA2 re-application for NDUFS2 mutant fibroblast growth in galactose media was also investigated, alongside the effects of a lower concentration of MOA2. To achieve this, cells were seeded in multi-well plates in glucose and allowed to adhere to the wells over 24 hours. Cells were then transitioned to galactose media and treated with MOA2 as experimentally appropriate. At 4-day intervals throughout the 400-hour experiment, media volume in wells was measured and appropriate volumes of MOA2 were added to make up a final in well concentrations of 0.3 and 3μM, data shown in Fig 5.4. The wells at the edges of the multi-well plate were not used, however, they were filled with media to minimise evaporation effects on experimental wells.

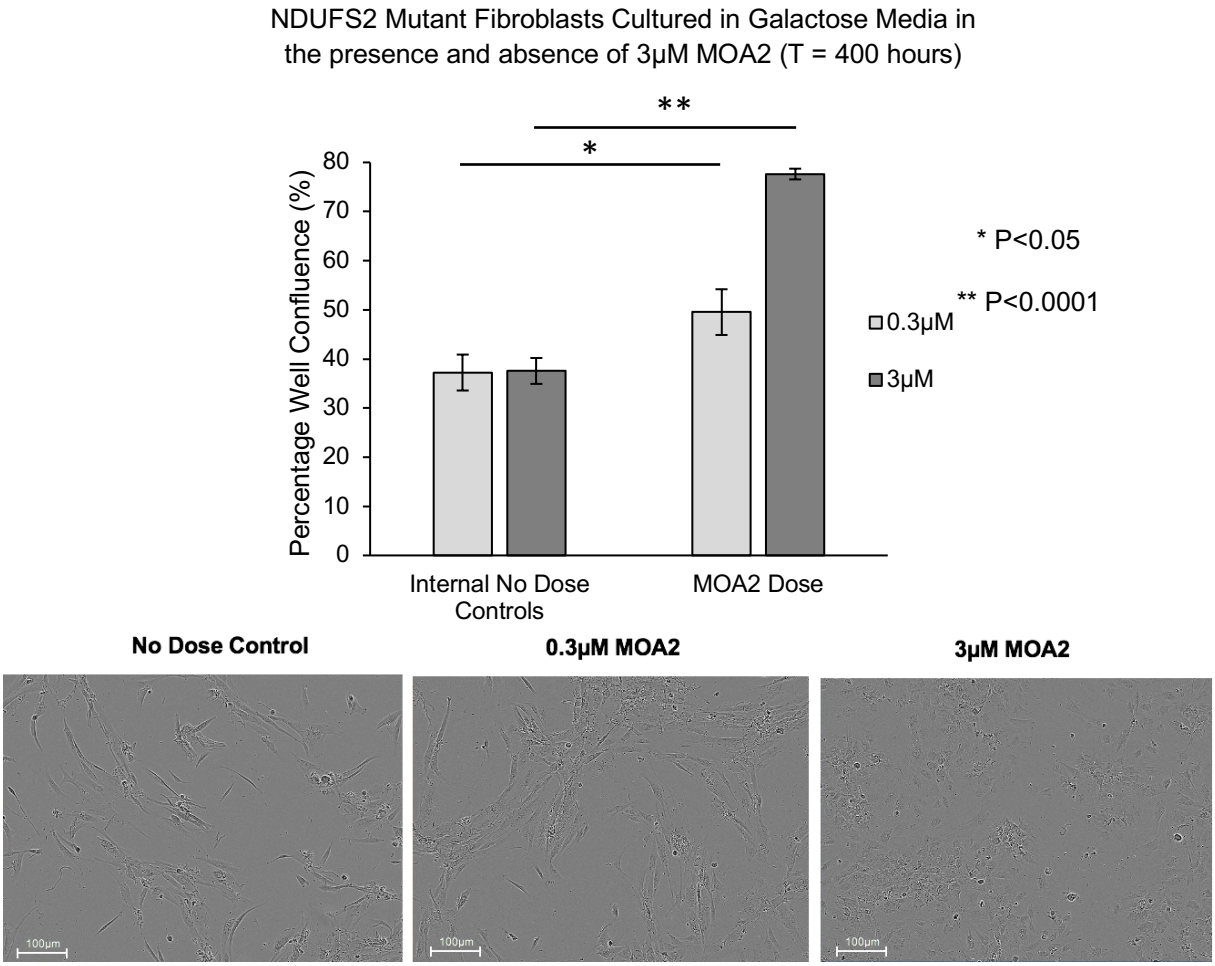

Fig. 5.4*, Confluence of NDUFS2 mutant fibroblasts, cultured in galactose media after 400 hours, with and without 3μM MOA2, avoiding complete media exchanges*. MOA2 was re-applied to remaining well media such that the final concentration was made up to 3μM. N = 5.

This approach led to a less severe decrease in confluence in untreated cells than previously observed and significantly reduced the variability (standard deviation) within each group. A Z'>0.5 was once again achieved, comparing untreated and 3μM MOA2 treated cells. Over the 400-hour period, cells become significantly more confluent with 0.3μM MOA2 relative to untreated controls (49.5% and 37.5% confluence respectively, $P<0.05$), however, the effect was markedly blunted in comparison to 3μM MOA2 treatment (77.6% confluence, $P<0.0001$ versus untreated controls), Fig 5.4.

Despite the detection of the phenotypic rescue in response to the lead compound, MOA2, the galactose growth assay was deemed unsuitable for further use in screen development, due to the low sample throughput, labour intensive re-treatment protocols, and a long experiment duration required to attain a suitable Z' score.

5.3.2 Immunofluorescent Staining Optimisation and Validation for Complex I

Immunofluorescent imaging analysis was explored as means of quantifying levels of CI in the mitochondrial network, with far superior sample throughput compared to gel-based complexomics, such as BN-PAGE. Due to the nature of the Zeiss Cell Discoverer 7 wide-field high throughput microscope available to the project, a total of four fluorescent channels could be employed. Therefore, the nuclear stain DAPI was used as a means of quantifying cell count, while TOM20 immunostaining (assigned to AF488) was used as a reliable means of allowing PerkinElmer Columbus automated data processing to identify the mitochondria as an area of interest. In an attempt to replicate the findings of (Tuppen et al., 2010), in which NDUFS2 mutant fibroblasts were shown to be deficient in CI using anti-NDUFB8 immunoblotting, immunofluorescent optimisation was initiated using an anti-NDUFB8 antibody (2.5µg/ml, as optimised in earlier experiments – data not shown). NDUFB8 is commonly employed as a marker of CI deficiency due to the instability of the isolated P_D-b assembly intermediate, in the presence of CI defects (Stroud et al., 2016), which is subject to continual turnover if not assembled into mature CI (Bogenhagen and Haley, 2020). NDUFA13 was also selected as a potential marker of CI deficiency due to its role in the assembly of the Q/P_P-a CI intermediate and its interactions with both the Q and ND1 modules (Guerreo-Castillo et al., 2017).

Treatment with 3µM MOA2 was included to investigate the mechanism of action of the lead compound, as it was hypothesised to cause increases in CI assembly. The treatment length of 8 days was selected due to the requirement of 140 hours before divergence seen in cell confluences of treated and untreated cells as measured by Incucyte confluence analysis, Fig. 5.2 A section 5.3.1. MOA2 (3µM) was re-applied to culture media at day 4, as determined as the optimal re-application interval in Fig. 5.3, B, section 5.3.1. Cells were fixed, permeabilised and stained as per the protocol detailed in chapter 3, including a methanol gradient step employed for CI protein staining, as used in the anti-NDUFB8 immunofluorescent analysis of muscle sections (Rocha et al., 2015). The effects of cell incubation in glucose and galactose media were also investigated. Data is presented in Fig. 5.5 and 5.6 as box plots containing vertical frequency histograms. The length of horizontal lines within the box indicates the number of wells exhibiting the same fold change (from wild type controls) in the protein of interest staining intensity – rounded to two decimal places. This allows the for assessment of the distribution type of the markers.

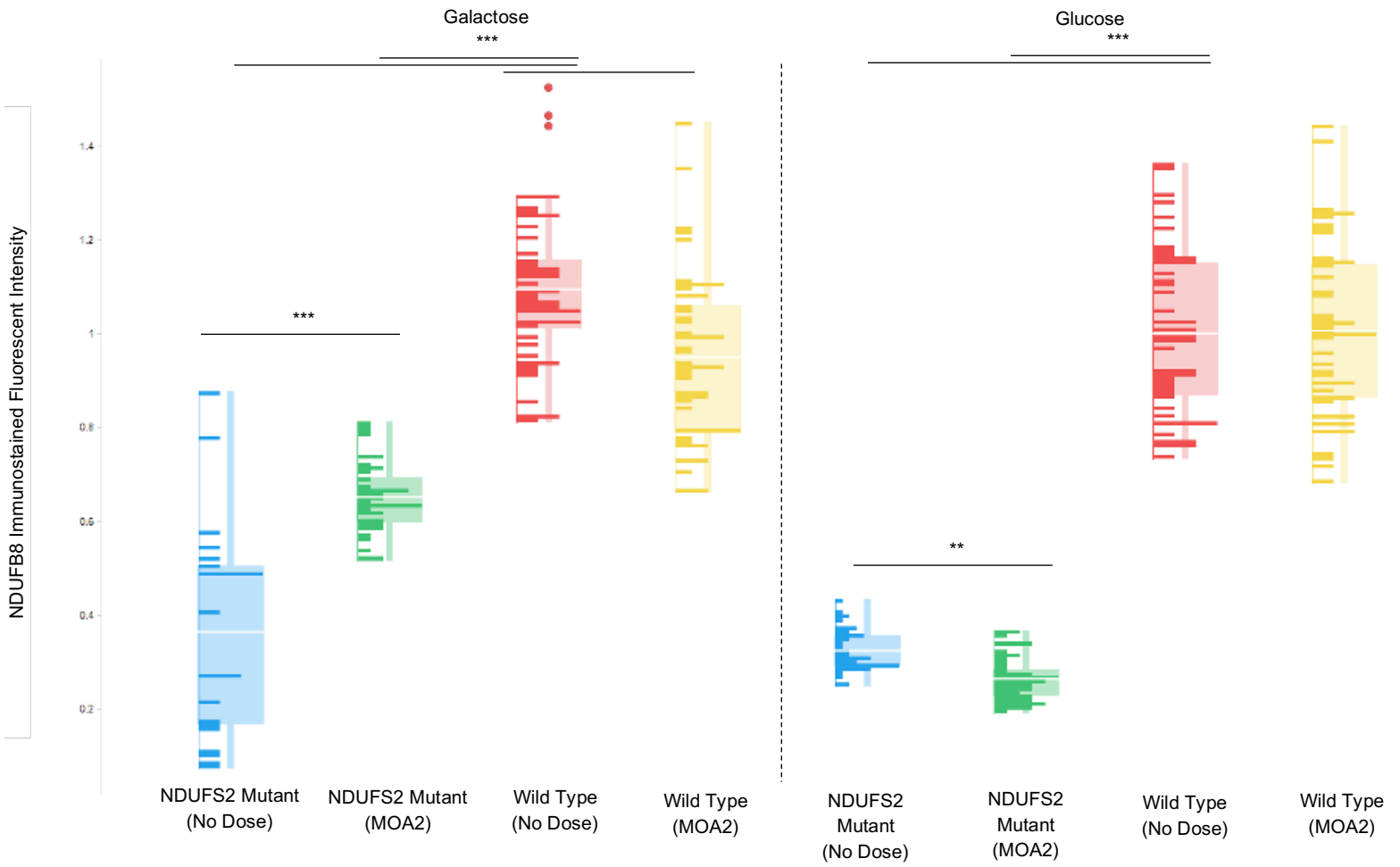

Fig. 5.5. *Box plots representing NDUFB8 immunostained fluorescent Intensity – normalised to cell count – in NDUFS2 mutants and wild type controls cultured in glucose or galactose media* for eight days (left and right of centre respectively), with or without 3μM MOA2. Data presented as fold change from untreated wild type controls cultured in glucose media. Contained within each box is a vertical frequency histogram, the length of horizontal lines within the box indicate the number of wells exhibiting the same fold change in NDUFB8 staining intensity – rounded to two decimal places. This allows the for assessment of the distribution of data. * $P<0.05$, ** $P<0.001$, *** $P<1x10^{-10}$.

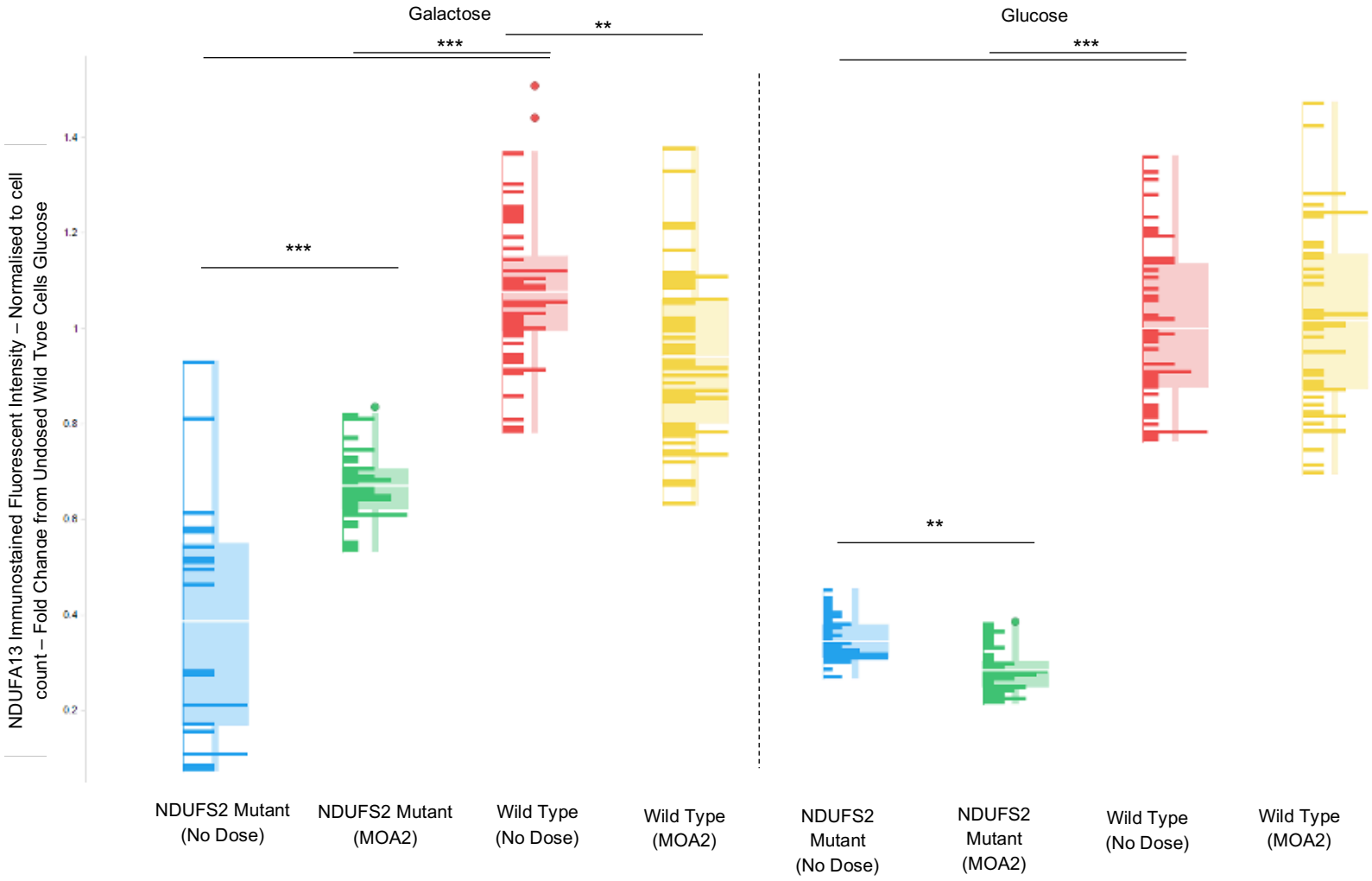

Fig. 5.6. *Box plots representing NDUFA13 immunostained fluorescent Intensity – normalised to cell count – in NDUFS2 mutants and wild type controls cultured in glucose or galactose media for eight days* (left and right of centre respectively), with or without 3μM MOA2. Data presented as fold change from untreated wild type controls cultured in glucose media. Contained within each box is a vertical frequency histogram, the length of horizontal lines within the box indicate the number of wells exhibiting the same fold change in NDUFA13 staining intensity – rounded to two decimal places. This allows the for assessment of the distribution of data. * $P<0.05$, ** $P<0.001$, *** $P<1x10^{-10}$.

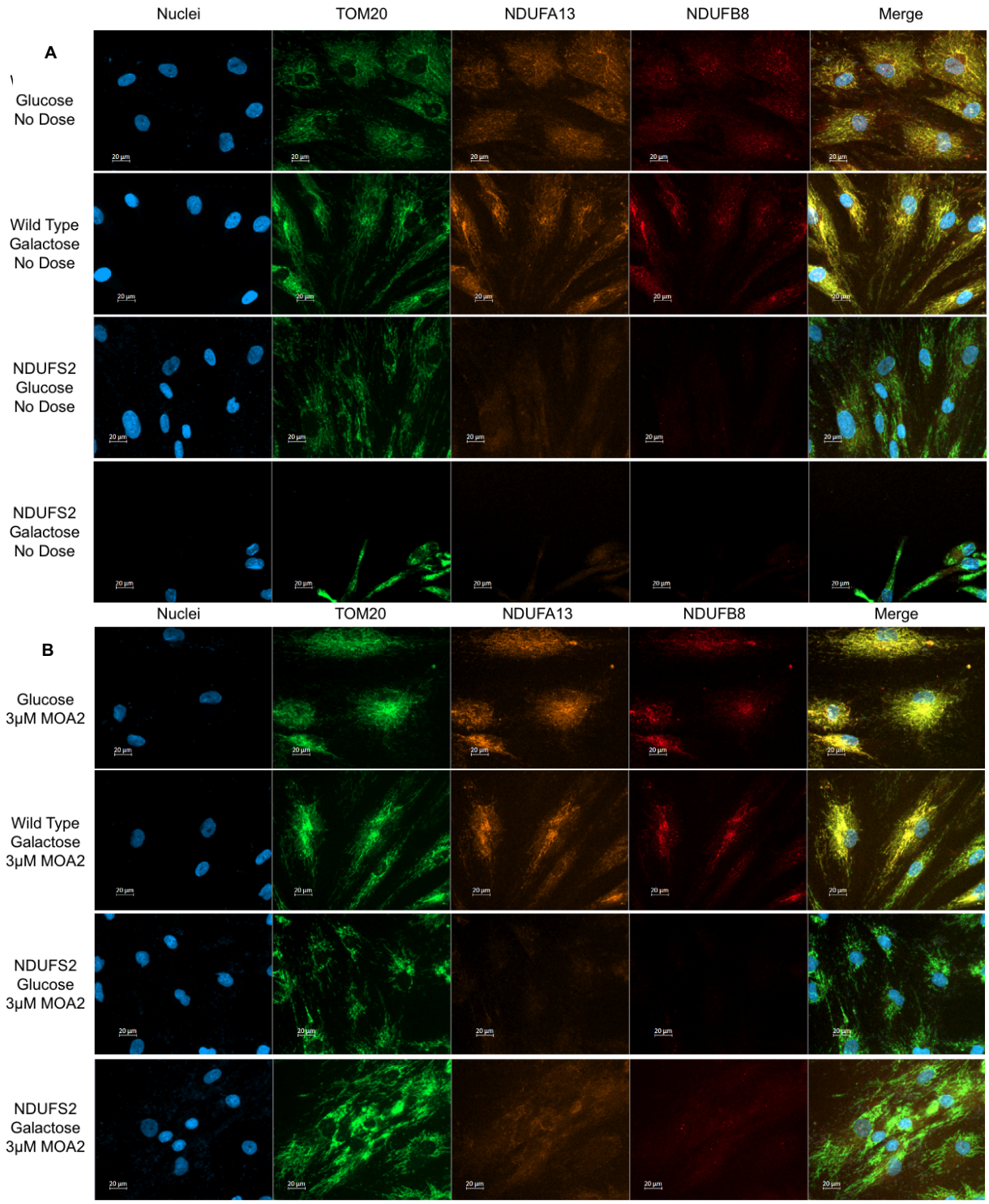

Fig. 5.7. *Representative immunofluorescent images for staining of TOM20, NDUFA13 and NDUFB8 in Wild Type and NDUFS2 mutant fibroblasts*. Cell were cultured in glucose or galactose media, (A) with or (B) without 3μM MOA2. Quantified data displayed in Fig. 5.5 and 5.6, Scale bar – 20μm.

NDUFB8 and NDUFA13 immunostaining colocalised with the mitochondrial network, as marked by TOM20 immunostaining. In glucose media, NDUFS2 mutant fibroblasts were found to exhibit approximately 30% of the staining intensity of NDUFB8 and NDUFA13, within a mitochondrial mask, as compared to wild type fibroblasts. Treatment with 3μM MOA2 did not significantly affect the immunostaining intensity for CI proteins of interest in wild type cells in glucose media, while it appeared to slightly reduce CI protein immunostaining in NDUFS2 mutant fibroblasts in glucose media ($P<0.001$). In galactose media, high variability is noted in untreated NDUFS2 mutant controls. Inspection of images revealed that cells had been washed from the wells during the staining protocol due to poor adherence to well bases. As a result, the low replicate number of NDUFS2 mutant cells grown in galactose, without MOA2, is due to the removal of images with no detected nuclei. Approximately 40% of the staining intensity of NDUFB8 and NDUFA13 was noted in untreated galactose cultured NDUFS2 fibroblasts when compared to wild-type controls ($P<1x10^{-10}$), the occasional high values were attributed to cell debris present in the field of view. Treatment with 3μM MOA2 reduced the CI protein staining profile of wild type controls in galactose media by 10%, however, a marked increase in staining intensity in NDUFS2 mutant fibroblasts is noted, rising from 40% of wild type levels in untreated controls to 65% of wild type levels in 3μM MOA2 treated cells ($P<1x10^{-10}$).

It was noted that NDUFB8 and NDUFA13 immunostaining analysis resulted in the production of very similar data. Both proteins enter the complex I assembly pipeline after Q module formation (Guerreo-Castillo et al., 2017). Staining for NDUFA13 was retained due to its interactions between Q and ND1 modules in CI assembly, NDUFB8 immunostaining was, therefore, surplus to requirements and dropped from the staining panel. The binding partner of NDUFS2 (NDUFS3) was selected to replace NDUFB8 in the panel to probe an additional region of the CI assembly pathway.

Optimisation of NDUFA13 and NDUFS3 co-staining

For the purposes of staining optimisation using anti-NDUFS3 antibodies, wild-type and NDUFS2 mutant cells were seeded in glucose media in a 96 well plate and fixed after 24 hours, without MOA2 treatment. The requirement of a detergent (Tween20) and methanol treatment for the staining was investigated. A two-fold serial dilution of primary antibodies was used when staining, ranging from 1% to 0.25% v/v (10-2.5µg/ml), to establish the optimal concentration of each.

NDUFS3 staining was similar to NDUFA13 staining under all conditions, with the intensity of staining lowering with each reduction in antibody concentration, Fig 5.8, below. Low staining intensity was noted in NDUFS2 mutants, in comparison to wild type cells with methanol treatment, for both NDUFA13 and NDUFS3 under all investigated conditions. The use of methanol in the staining protocol was found to be essential, as wild-type cells without methanol treatment exhibited staining intensities equivalent to NDUFS2 mutant cells, Fig 5.8. The co-staining of NDUFA13 and NDUFS3 was found to be viable at 0.25% v/v (2.5 µg/ml), with a methanol gradient included as part of the sample preparation. Treatment with Tween20 was removed from the protocol, due to a lack of synergistic effect with the methanol gradient.

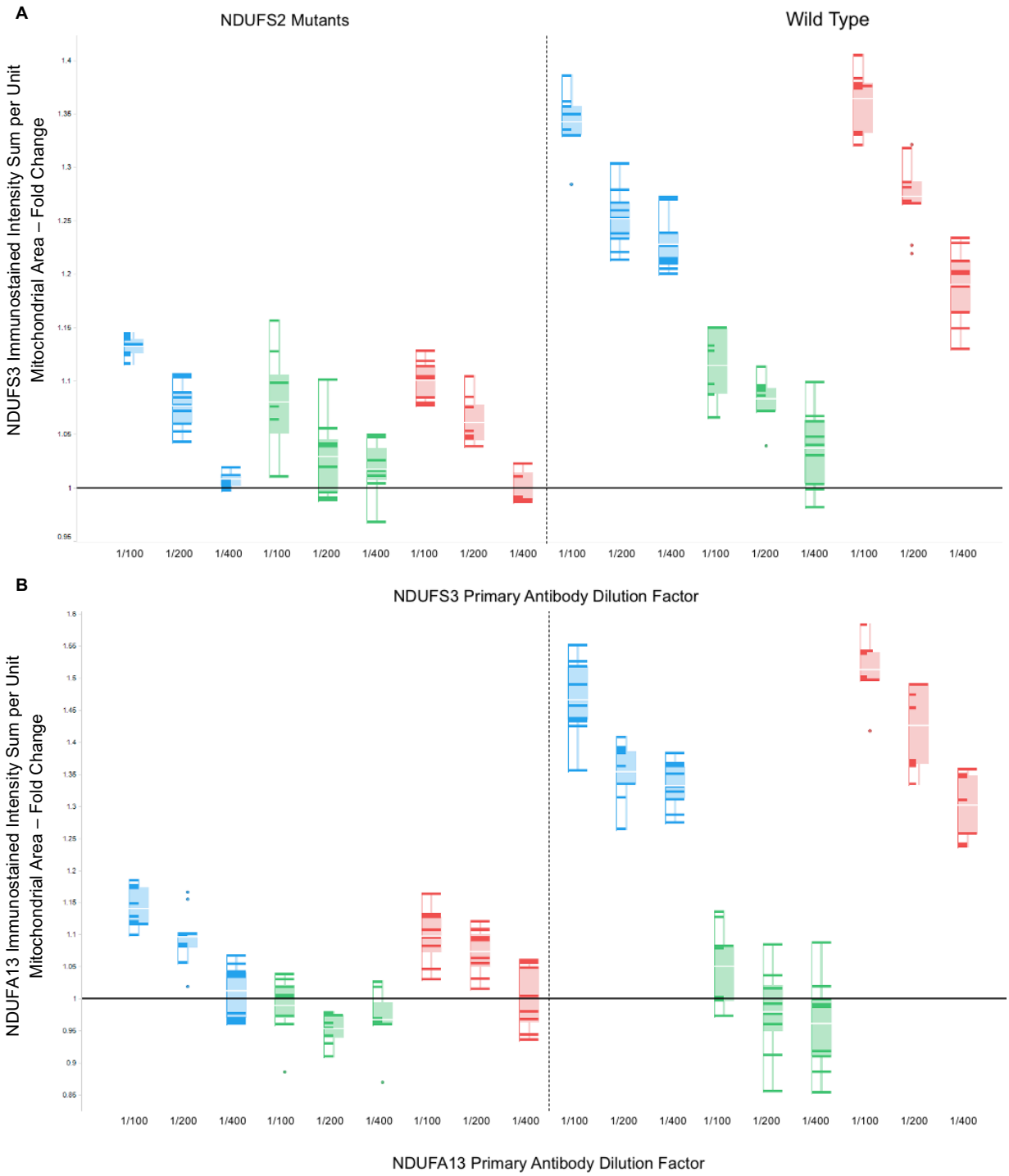

Fig 5.8. *Optimisation of NDUFA13 and NDUFS3 co-staining for high throughput immunofluorescence.* Box plots showing the optimisation of (A) NDUFS3 staining co-stained with (B) NDUFA13. Data presented as a bar chart representing NDUFA13 immunostained fluorescent Intensity – normalised to mitochondrial area – in NDUFS2 mutants and wild type controls. The requirement of tween or methanol treatment for staining in wild type cells was explored. Data presented as fold change from NDUFS2 mutant fibroblasts, stained with 0.25% v/v (2.5µg/ml) CI primary antibodies, subject to Tween20 and methanol gradient treatment. Contained within each box is a vertical frequency histogram, the length of horizontal lines within the box indicate the number of wells exhibiting the same fold change in (A) NDUFA13 and (B) NDUFS3 staining intensity – rounded to two decimal places. Blue: TBS-NGS, Methanol Gradient Green:

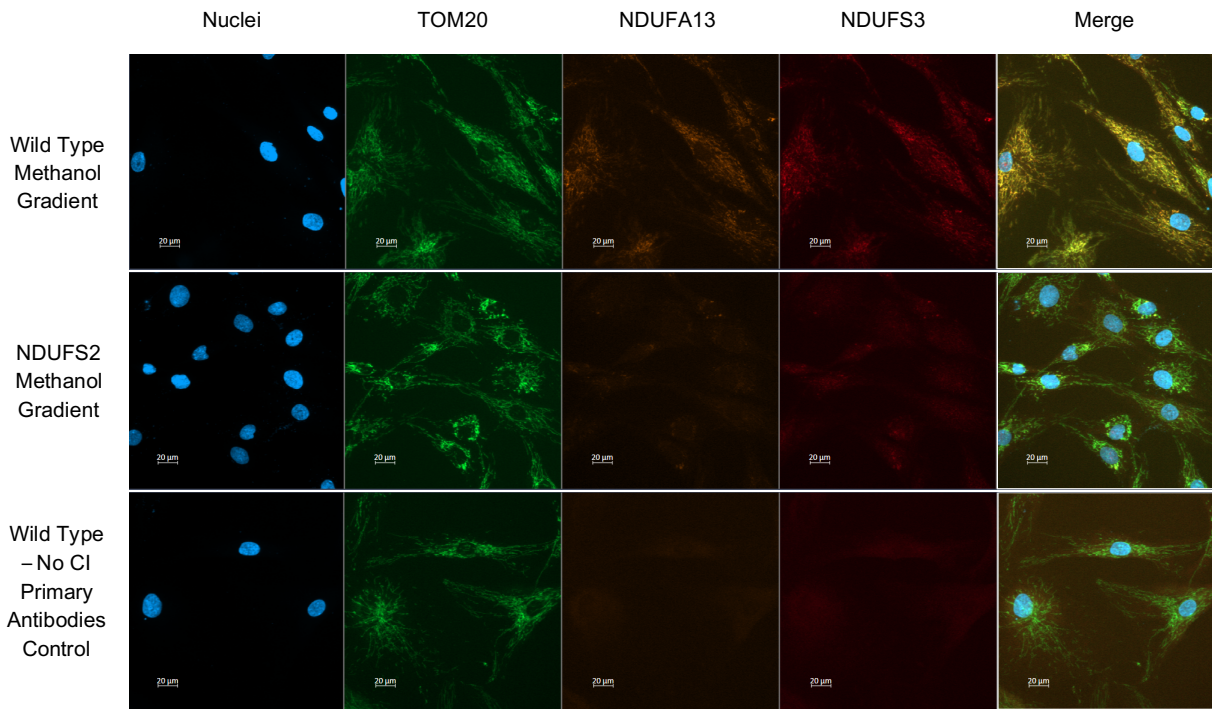

Fig 5.9. *Representative images of experimentally improved staining conditions for NDUFA13 and NDUFS3, in wild type and NDUFS2 mutant fibroblasts*. A no primary antibody control for Complex I proteins of interest is included for comparison. Scale bar = 20nm.

Using the improved protocol above, high replicate count analysis of NDUFS2 mutant fibroblasts was carried out to confirm the requirement of galactose media for complex I assembly rescue. Data were collected from 384 well plates, seeded in glucose media and changed to galactose media after 24 hours. Half of all wells were dosed with 3µM MOA2, incubated for eight days, with MOA2 re-application at day 4. Sample preparation post-fixation consisted of TBS-NGS (30 minutes) followed by a methanol gradient. It is noted in resultant images that the removal of Tween20 treatment has resolved the low cell count/poor cell adherence seen in galactose NDC cells of Fig. 5.6, 5.7 and 5.8. Highly statistically significant ($P<1x10^{-6}$), but minor, increases in NDUFA13 and NDUFS3 staining levels in glucose media were noted after 4 days of MOA2 treatment: +4%, +9% respectively, Fig 5.10. However, NDUFA13 and NDUFS3 levels drop with the application of 3µM MOA2 in glucose media, relative to no dose controls after 8 days: -7%, -10% respectively. A substantial increase in NDUFA13 and NDUFS3 staining was evident after 4 days with 3µM MOA2 treatment in galactose media ($P<1x10^{-6}$): +26% and +29% respectively. Improvements persist after 8 days, exhibiting 34% and 22% increases in NDUFA13 and NDUFS3 staining respectively.

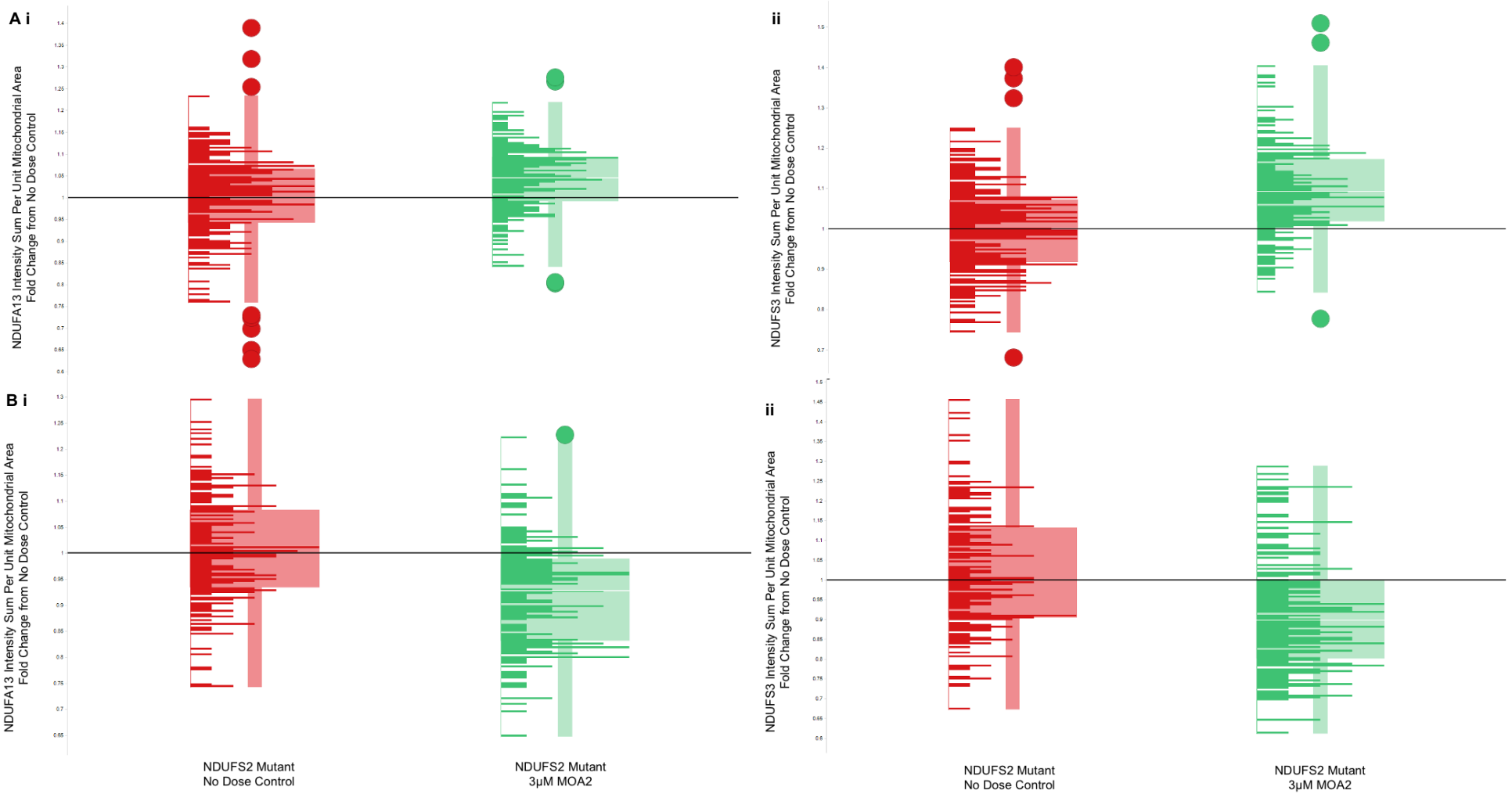

Fig 5.10. *Analysis of MOA2 effects on NDUFS2 mutant fibroblasts in Glucose or Galactose media*. Box plots showing mean intensity of NDUFA13 and NDUFS3 staining in NDUFS2 mutant fibroblasts, in the presence or absence (green and red bars respectively) of 3μM MOA2, in Glucose and Galactose media. In all instances, $P<1x10^{-6}$ as determined by a Students T Test. A) i) NDUFA13 staining in NDUFS2 mutants in glucose media – 4-day timepoint; 4% increase. ii) NDUFS3 staining in NDUFS2 mutants in glucose media – 4-day timepoint; 9% increase. B) i) NDUFA13 staining in NDUFS2 mutants in glucose media – 8-day timepoint; 7% decrease. ii) NDUFS3 staining in NDUFS2 mutants in glucose media – 8-day timepoint; 10% decrease.

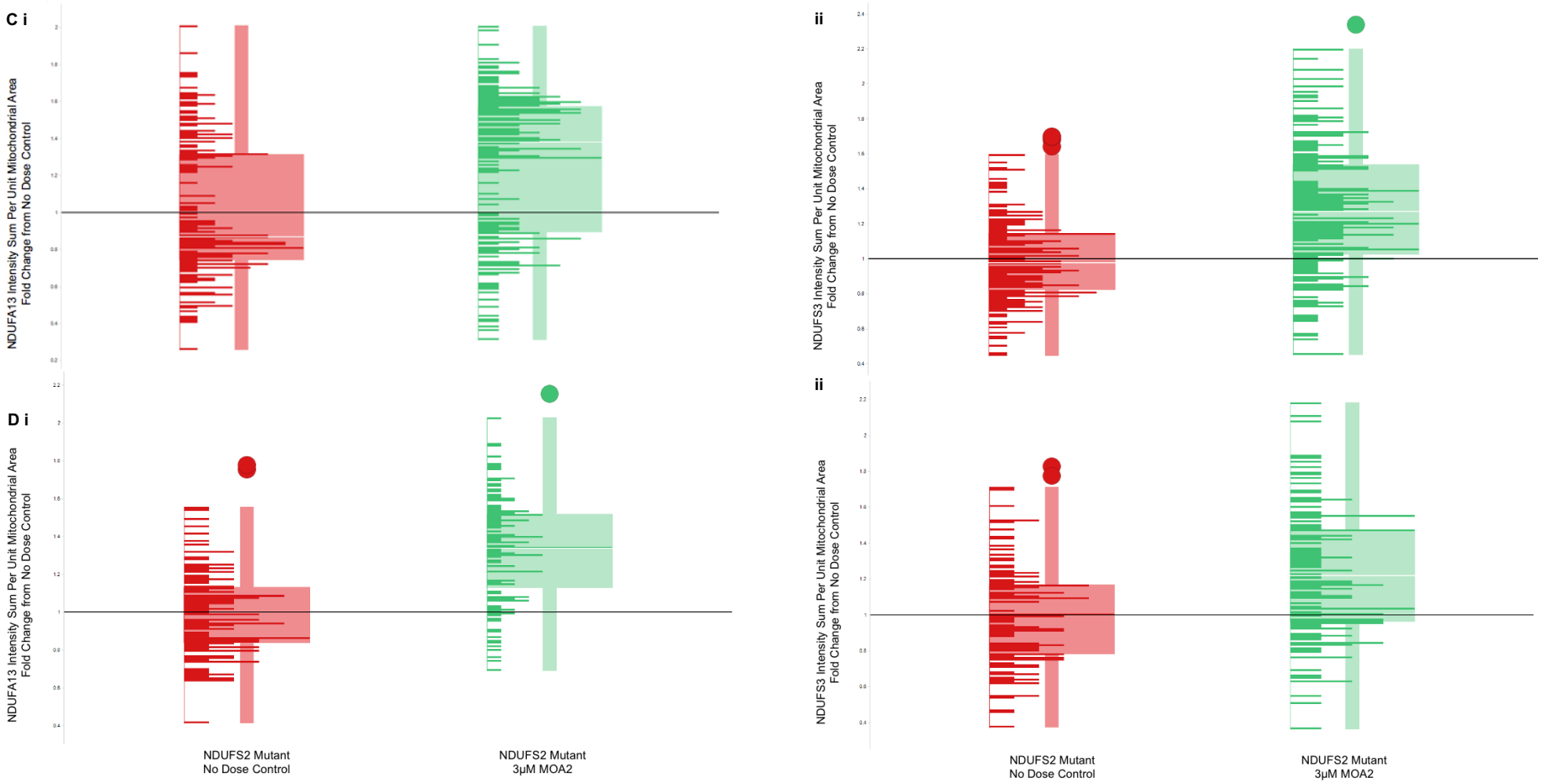

Fig 5.10 – Continued. *Analysis of MOA2 effects on NDUFS2 mutant fibroblasts in Glucose or Galactose media*. Box plots showing mean intensity of NDUFA13 and NDUFS3 staining in NDUFS2 mutant fibroblasts, in the presence or absence (green and red bars respectively) of 3μM MOA2, in Glucose and Galactose media. In all instances, $P<1x10^{-6}$ as determined by a Students T Test. C) i) NDUFA13 staining in NDUFS2 mutants in galactose media – 4-day timepoint; 26% increase. ii) NDUFS3 staining in NDUFS2 mutants in galactose media – 4-day timepoint; 29% increase. D) i) NDUFA13 staining in NDUFS2 mutants in galactose media – 8-day timepoint; 34% increase ii) NDUFS3 staining in NDUFS2 mutants in galactose media – 8-day timepoint; 22% increase.

5.3.3 Maximal Complex I Activity

To further investigate the lack of effect of MOA2 upon NDUFS2 mutant fibroblasts when grown in glucose media, cells were cultured in the presence and absence of 3μM MOA2 in glucose media for four days, from which mitochondria were isolated and freeze-thawed to ensure mitochondrial membranes were fully broken. CI and CII were then assessed for activity *in vitro*. Maximal CI activity normalised to maximal CII activity, as a control for protein content (a surrogate for mitochondrial mass). The experiment was kindly carried out by clinical colleagues in The Newcastle Highly Specialised Mitochondrial Diagnostic laboratory.

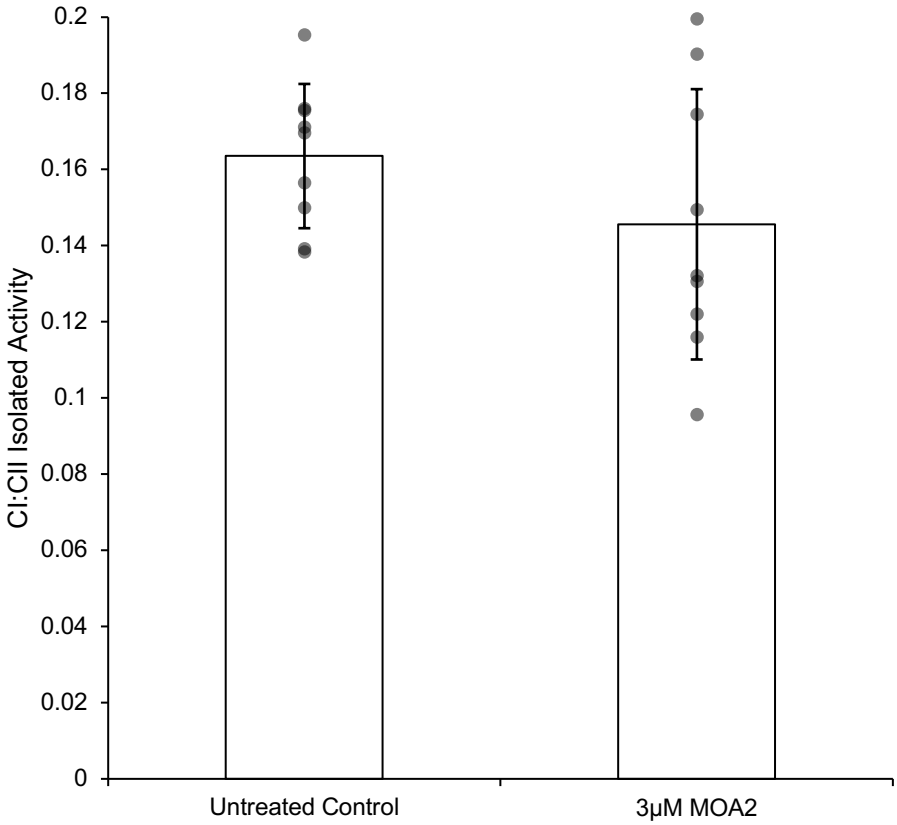

Fig 5.11. *CI:CII isolated in vitro activity ratio of NDUFS2 mutant fibroblasts cultured in glucose media for four days, with and without 3μM MOA2.* CI and CII were subject to activity assays carried out by colleagues at The Newcastle Highly Specialised Mitochondrial Diagnostic laboratory. A non-statistically significant reduction in the CI:CII activity ratio is noted with 3μM MOA2 treatment. P>0.1, n=9.

Treatment with 3μM MOA2 reduced CI:CII isolated activity ratio by 11%, relative to untreated controls, however, statistical significance was not reached (P>0.1), Fig, 5.12. This result confirmed that treatment of NDUFS2 mutant fibroblasts with 3μM MOA2 in glucose media does not result in increased CI activity, consistent with the immunofluorescent data.

5.3.4 Dose Dependency Assessment of a Lead Compound

Having confirmed the efficacy of 3μM MOA2 in increasing immuno-stained intensities of NDUFA13 and NDUFS3 in NDUFS2 mutant fibroblasts in galactose media, a serial dilution of MOA2 was next employed to assess dose dependency of this effect. The staining protocol used in section 5.3.2 was employed against NDUFS2 cells incubated in 0.1, 0.3, 1.0 and 3.0μM MOA2, alongside wild type fibroblasts without dose as a positive control for normal complex I levels. The cells were seeded in glucose media, changed to galactose media, NDUFS2 cells were then treated with MOA2 after 24 hours and incubated for 8 days with MOA2 re-application at 4 days as before. Quantification of immunofluorescent data is shown below in Fig 5.12.

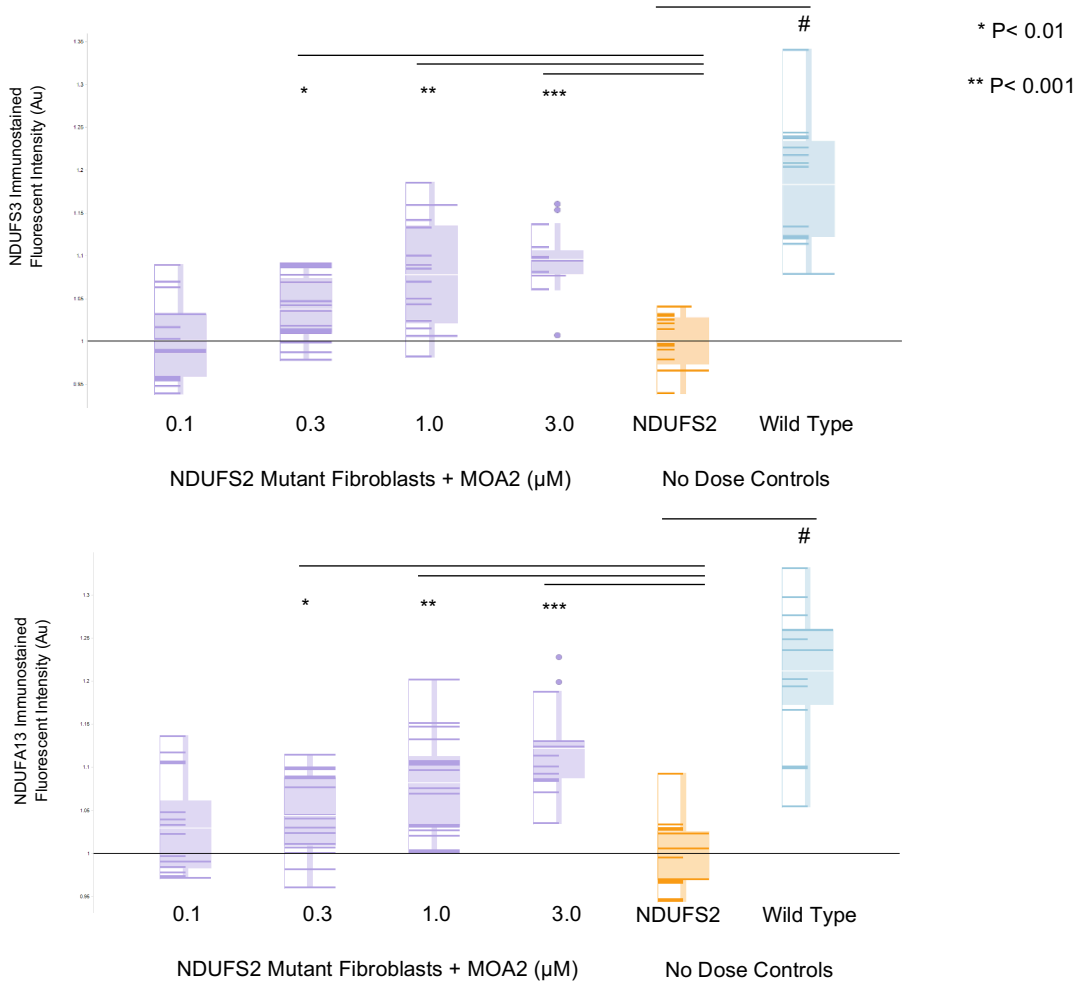

Fig 5.12. *Complex I subunits levels in NDUFS2 cells cultured in galactose media are partially rescued with MOA2 treatment in a dose dependent manner.* Immunofluorescent staining for (A) NDUFS3 staining co-stained with (B) NDUFA13 in wild type controls (blue) and NDUFS2 mutant cells subject to a serial dilution of MOA2: untreated controls (orange), 0.1, 0.3, 1.0 and 3.0μM (purple). Data presented as a box plot representing CI protein of interest immunostained fluorescent Intensity – normalised to mitochondrial area. Data presented as fold change from untreated NDUFS2 mutant fibroblasts. Contained within each box is a vertical frequency histogram, the length of horizontal lines within the box indicate the number of wells exhibiting the same fold change in protein of interest staining intensity – rounded to two decimal places.

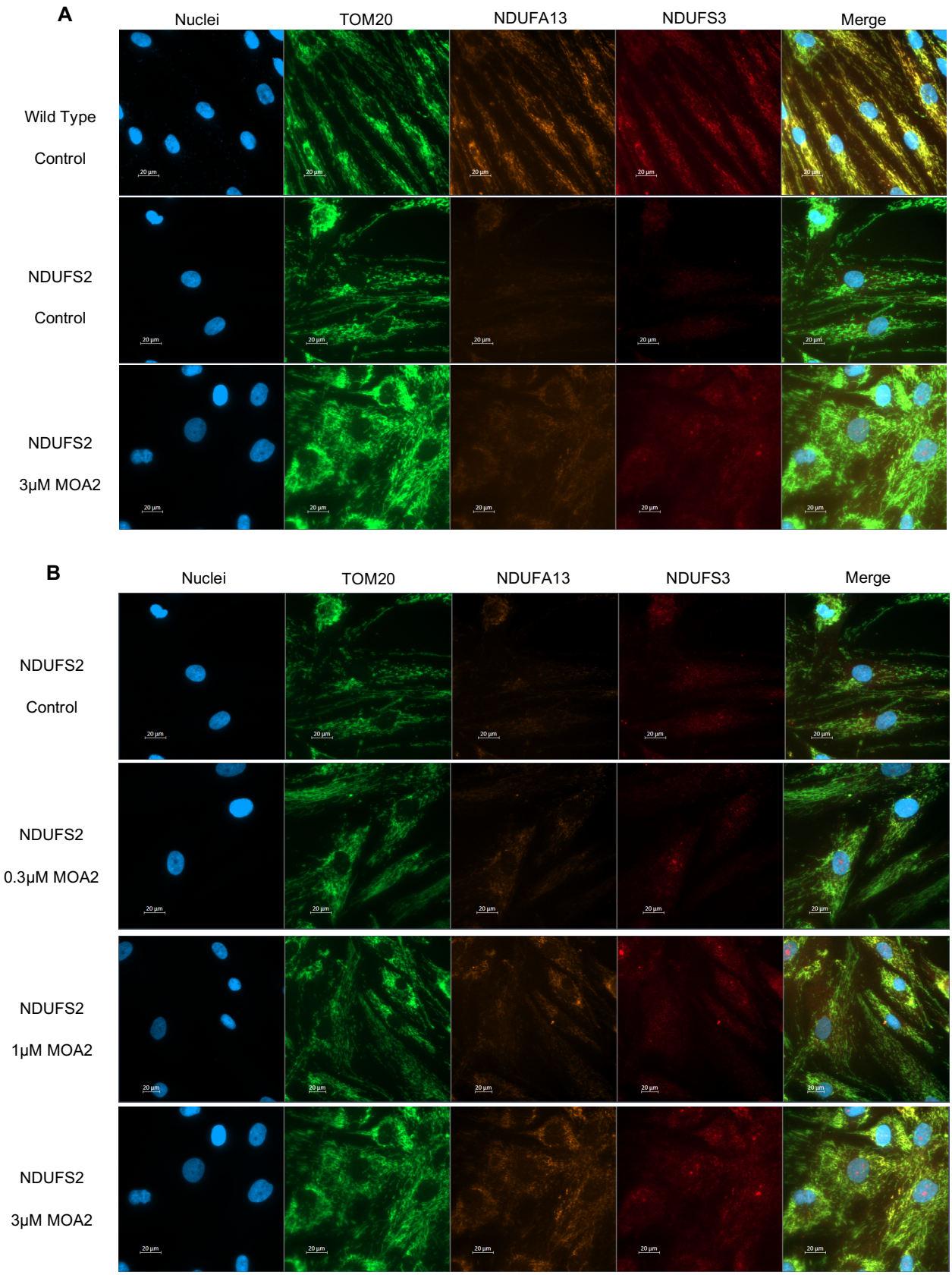

Fig 5.13. *Representative immunofluorescent images demonstrating partial rescue of CI subunits levels in NDUFS2 mutant fibroblasts, with MOA2 treatment in galactose media*. Cells were stained for TOM20, NDUFA13 and NDUFS3 in Wild Type and NDUFS2 mutant fibroblasts, in galactose media, with or without MOA2. (A) Comparison of Wild Type and untreated NDUFS2 mutant controls with NDUFS2 fibroblasts with 3μM MOA2; image display settings optimised for Wild Type controls. (B) Images showing a serial dilution of MOA2 at 0.3, 1.0 and 3.0μM MOA2 in NDUFS2 fibroblasts, image display settings optimised for NDUFS2 +3.0μM MOA2. Scale bar = 20μm.

A dose dependent increase in NDUFA13 and NDUFS3 staining intensity was noted in galactose media cultured NDUFS2 mutant fibroblasts treated with MOA2, reaching highly statistically significant ($P<0.001$) increases of 10% and 12% for NDUFS3 and NDUFA13 respectively with 3μM MOA2 treatment. Previously 0.3μM MOA2 treatment had resulted in statistically significant effects in the galactose growth assay, however, the increase was less marked in comparison to 3μM treatment. This experiment provides evidence of a stepwise improvement in CI assembly with increasing MOA2 concentrations. It is hypothesised that a threshold point of CI assembly is crossed at 3μM to improve the impaired galactose growth phenotype of NDUFS2 mutant fibroblasts. Higher concentrations of MOA2 were found to be toxic to cellular proliferation in earlier experiments (Rai, 2017).

Separate from assessing MOA2 activity, high throughput screening compatibility was determined using Z' scores. Z' scores were calculated as 0.45 and 0.43 for NDUFA13 and NDUFS3 respectively, comparing wild type and untreated NDUFS2 mutant cells. Data from wild-type cells were used in this calculation as the screen development component of the project is seeking to identify a means of restoring CI levels. As such a partial restoration of CI levels in NDUFS2 mutant cells by MOA2, a lead compound requiring further optimisation is not appropriate to use a positive control.

5.3.5 Optimisation of Protocol and Application to Automated systems

The Z' scores attained in 5.3.4., 0.45 and 0.43 for NDUFA13 and NDUFS3 respectively, fall outside the acceptable Z' range of 0.5-1.0 for a high throughput screening assay. Thus far, all sample preparation steps have been carried out manually, with the use of a multi-channel pipette. The use of liquid handling automation in appropriate steps of sample preparation, such as plate washing and reagent addition, presents as a means of further increasing sample throughput and decreasing well to well variability, which would raise the Z' score.

Experiments in glucose media (2,000 cells seeded per well, without MOA2 treatment, 24-hour culture period) were carried out to test alternative reagents and simplified iterations of methanol treatment more suited to HTS. Liquid handling systems were also used to optimise the technique for HTS. Iterations of a simpler methanol treatment was explored (methanol v/v % in dH_2O / treatment length per stage) as follows: 70%/30 minutes, 100%/30 minutes, 70%-100%/15 minutes and 70%-100%-70%/10 minutes. NDUFA13 and NDUFS3 staining intensity in cells subject to pre-methanol blocking with BSA in PBS, with and without 0.1% (v/v) TritonX100, was also assessed alongside the new reagents. Alternative reagents/methods for HTS used are presented in Table 5.1, below, alongside a brief justification for the change. Data is presented in Fig. 5.14.

Table 5.1. *Immunofluorescent reagents and their HTS alternatives*. Alterations made for the purposes of optimising an immunostaining methodology for liquid handling automation hardware, with the aim of attained a screen compatible Z' score.

Original Reagent/Method	**Purpose**	**HTS Alternative**	**Justification**
Tris-Buffered Saline (TBS)	Reagent/antibody Solvent	Phosphate-Buffered Saline	Can be purchased readily in tablet form, simpler for use and mass storage of reagent
Normal Goats Serum (NGS)	Blocking	Bovine Serum Albumin (BSA)	BSA is cheaper and easier to store
Tween20	Cell Permeabilisation	TritonX100	Harsher detergent – may synergistically improve staining with methanol treatment
Methanol Gradient	Partially disrupt target protein complexes to expose epitopes	Methanol Treatment of shorter length/fewer stages	The full methanol gradient requires six liquid changes in wells. For a single multi-well plate this poses little issue, but HTS often consists of sample numbers in the order of 10^4, requiring 25+ 384-well plates, resulting in multiple liquid changes becoming highly impractical.

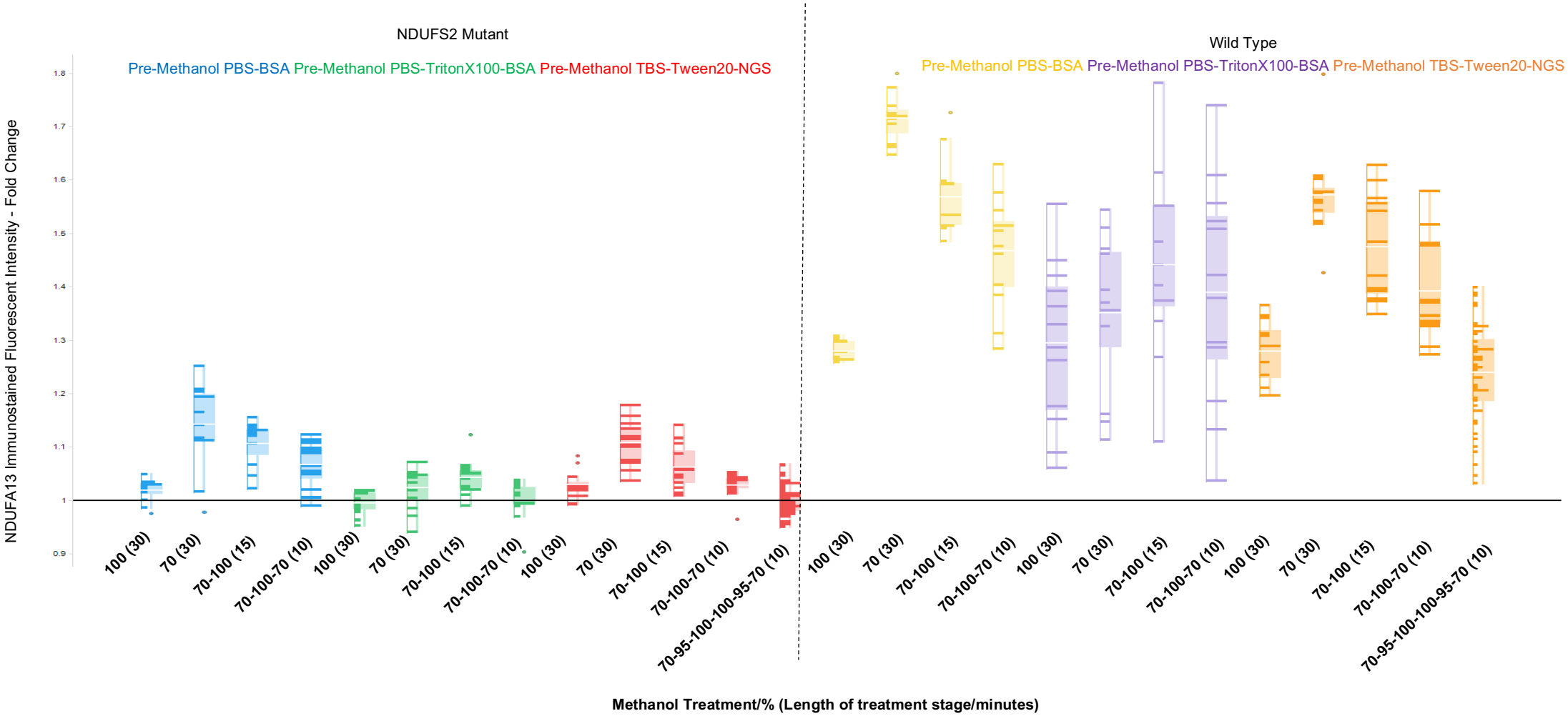

Fig. 5.14A. *Further optimisation of immunofluorescent staining of NDAUF13 using liquid handling automation and alternative HTS reagents*. Immunofluorescent stained intensity of NDUFA13 normalised to mitochondrial area, presented as fold change from NDUFS2 mutant fibroblasts subjected to the original staining protocol (TBST-NGS, methanol gradient treatment – 70-95-100-100-95-70 10 minutes per stage); the mean intensity of which is represented using a horizontal line. Data collected from Wild Type and NDUFS2 mutant fibroblasts are presented on the left and right of a dashed line, respectively. Multiple combinations of detergent and methanol treatments were explored as indicated by the colour key and x-axis.

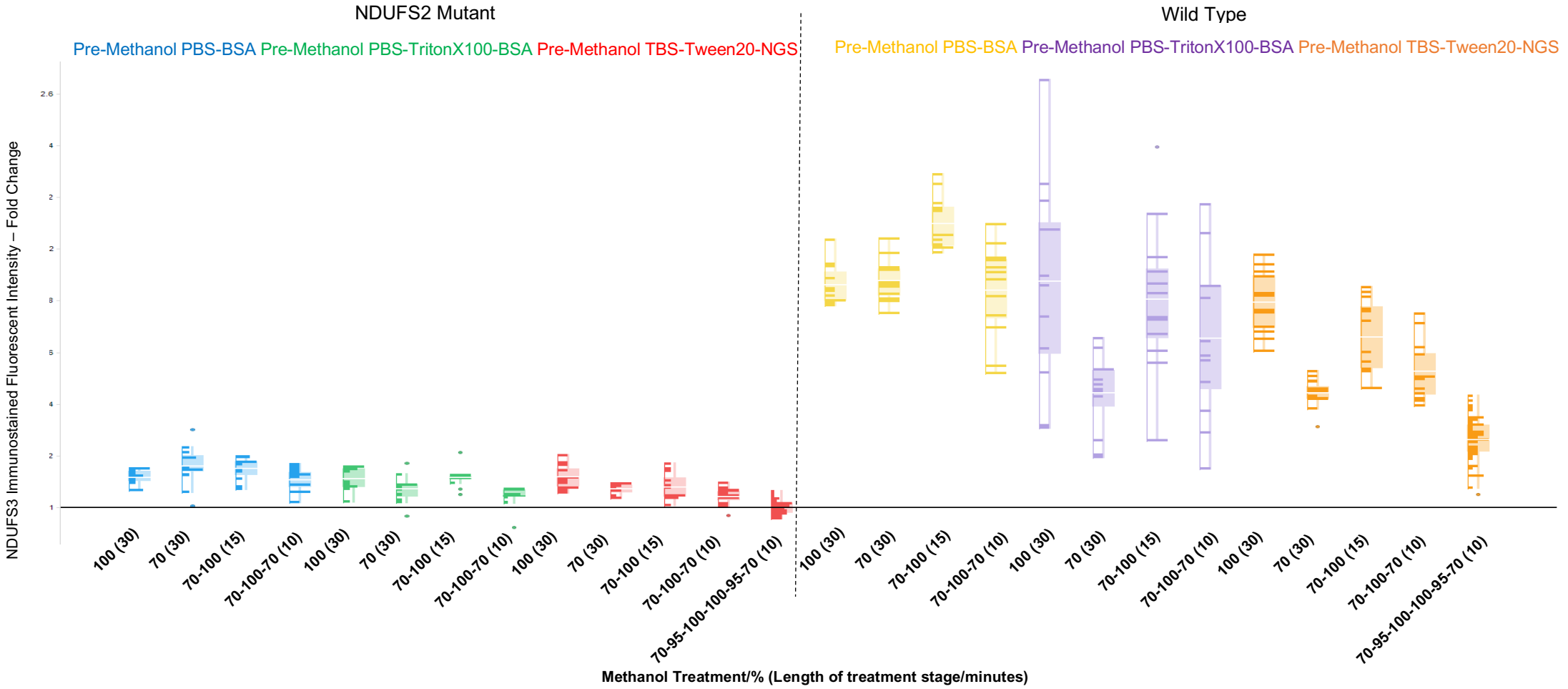

Fig. 5.14B. *Further optimisation of immunofluorescent staining of NDAUS3 using liquid handling automation and alternative HTS reagents*. Immunofluorescent stained intensity of NDUFS3 normalised to mitochondrial area, presented as fold change from NDUFS2 mutant fibroblasts subjected to the original staining protocol (TBST-NGS, methanol gradient treatment – 70-95-100-100-95-70 10 minutes per stage); the mean intensity of which is represented using a horizontal line. Data collected from Wild Type and NDUFS2 mutant fibroblasts are presented on the left and right of a dashed line, respectively. Multiple combinations of detergent and methanol treatments were explored as indicated by the colour key and x-axis.

Immunofluorescent stained intensities of NDUAF13 and NDUFS3 broadly followed similar trends. The intensity of both CI proteins in NDUFS2 mutant cells were universally below the mean for wild-type cells, however, several newly tested methods resulted in lower variance in wild-type cells than the original protocol. It was noted that the use of TritonX100 before methanol treatment in wild-type cells (purple Fig 5.14) drastically increased data variability. Shorter iterations of the methanol gradient trended towards lower well to well variability, potentially as a result of fewer in well liquid changes in the protocol.

Methods were ranked by Z' score. The best scoring protocol (Z'>0.53 for both NDUFA13 and NDUFS3) was found to be 30 minutes in PBS-1%BSA (v/v) followed by 30 minutes in 100% methanol. This is despite this method exhibiting some of the lowest observed staining intensities for NDUFA13 in wild-type cells. Though this is predicted to be a result of standard deviations contributing more greatly to Z' score than differences in mean readings. This protocol was adopted for all further immunofluorescent imaging experiments. The complete protocol can be found in section 2.5.6.

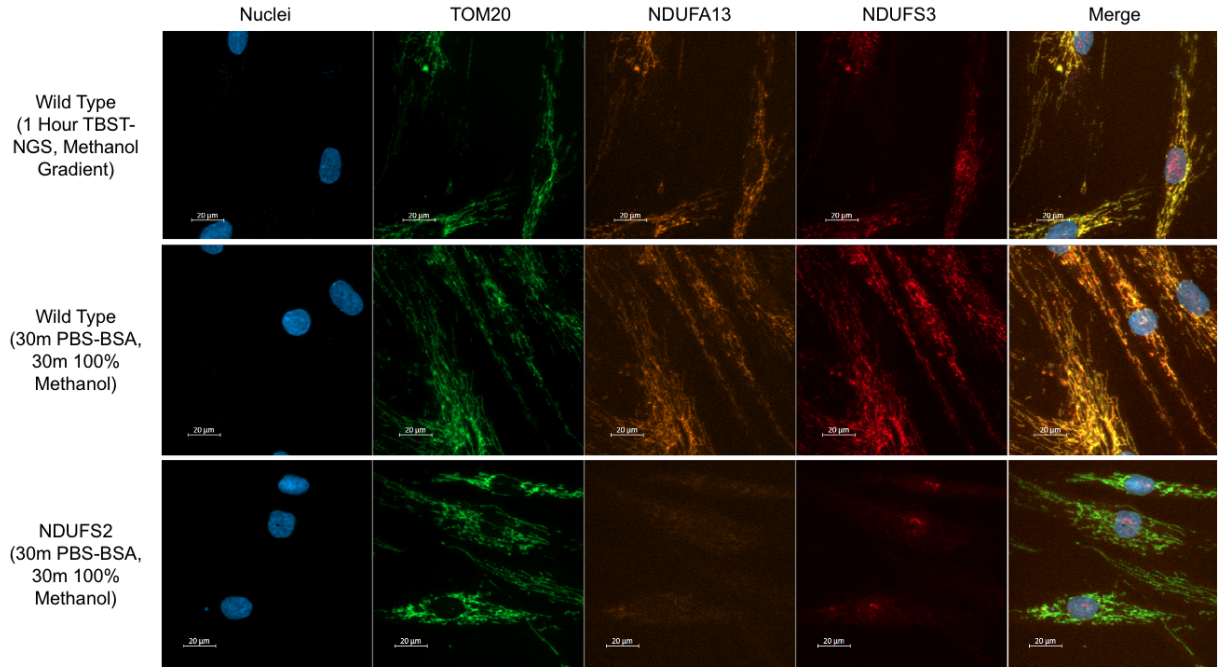

Fig 5.15. *A comparison of original and HTS optimised immunofluorescent images for staining of TOM20, NDUFA13 and NDUFS3 in Wild Type and NDUFS2 mutant fibroblasts.*

5.3.6 Establishing CIV Immunostaining

The two most common biochemical defects in mitochondrial disease are deficiencies in CI and CIV (Swalwell et al., 2011, Nouws et al., 2012, Lake et al., 2016). Having established IF staining for complex I levels using anti-NDUFA13 and anti-NDUFS3 antibodies, optimisation for CIV staining was also undertaken for the purposes of creating a high throughput means of rapidly assessing patient-derived cells for CI and CIV defects. The CIV subunit MTCOI was selected as a CIV marker due to its stability in mitochondria being dependent on its incorporation into fully assembled CIV (Dennerlein et al., 2015), and subsequent history of use as an established CIV biomarker in SDS/BN-PAGE and muscle section quadruple immunofluorescence techniques (Rocha et al., 2018, Lehmann et al., 2019).

Wild type and NDUFS2 mutant fibroblasts were immunostained with an anti-MTCOI primary antibody (0.25% v/v, 2.5µg/ml), alongside NDUFA13, using the HTS optimised protocol detailed in 2.5.6.

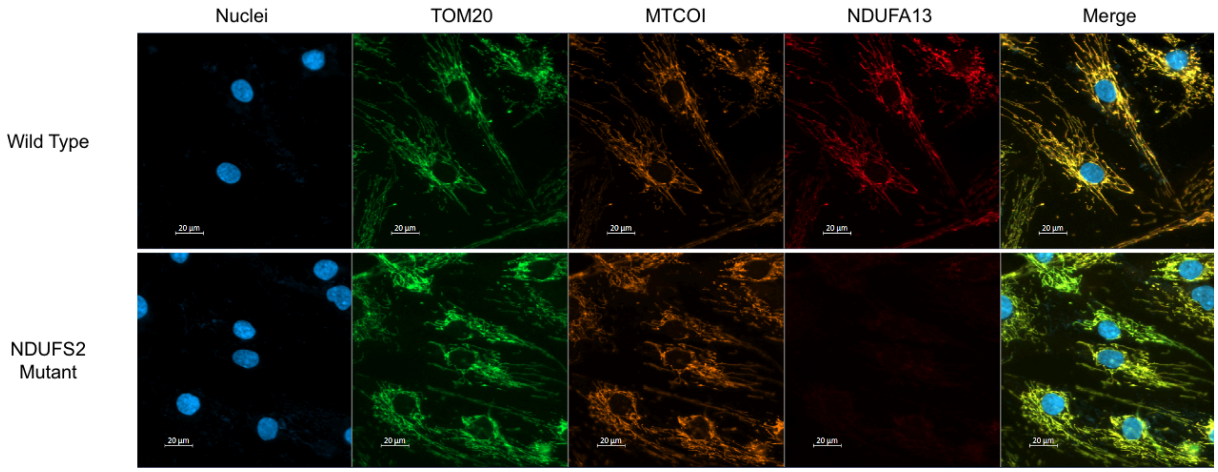

Fig 5.16. *Representative immunofluorescent images for staining of TOM20, MTCOI and NDUFA13 in Wild Type and NDUFS2 mutant fibroblasts using the HTS compatible protocol as optimised in 5.3.5, detailed in 2.5.6.*

Visual inspection of immunofluorescent images in wild type and NDUFS2 mutant fibroblasts confirms co-localisation of MTCOI staining with TOM20 staining, Fig 5.16, and a lack of NDUFA13 staining as previously noted. Staining of wild-type control fibroblasts, specifically, displayed the viability of NDUFA13/MTCOI co-staining using this protocol.

Having confirmed the efficacy of MTCOI immunostaining in wild type and NDUFS2 fibroblasts, the protocol was used against a SURF1 mutant fibroblast cell line, deficient in CIV. Additionally, to investigate the scope of the potential therapeutic activity of MOA2, SURF1 mutant fibroblasts were subjected to 8 days in galactose media, with and without 3μM MOA2 with re-application on day 4. The quantified immunofluorescent intensity of MTCOI is displayed in Fig, 5.18.

The established CIV defect was detected in untreated SURF1 mutant fibroblasts, which exhibited 45% of the total MTCOI immunostained intensity of untreated wild type controls. Staining for NDUFA13 confirmed that no CI deficiency is present in these cells and acted as a control for the staining protocol. Intriguingly, treatment with 3μM MOA2, over eight days in galactose media, resulted in the phenotypic rescue of a subset of SURF1 mutant cells, as shown in vertical frequency histograms in Fig, 5.18. Visual inspection of images, shown in Fig 5.18, confirmed the bimodal distribution of MTCOI staining in SURF1 mutant cells. This response may become more consistent across all wells with an increase in experiment duration. This effect was not pursued further in this project, as it aimed to create a high throughput means of detecting CI and CIV defects in patient-derived cells.

Taken together, experiments in wild type fibroblasts, NDUFS2 and SURF1 mutant fibroblasts, have shown that the HT immunostaining protocol (established in 5.3.5, detailed in 2.5.6) can be used to successfully quantify decreases in either complex I or IV.

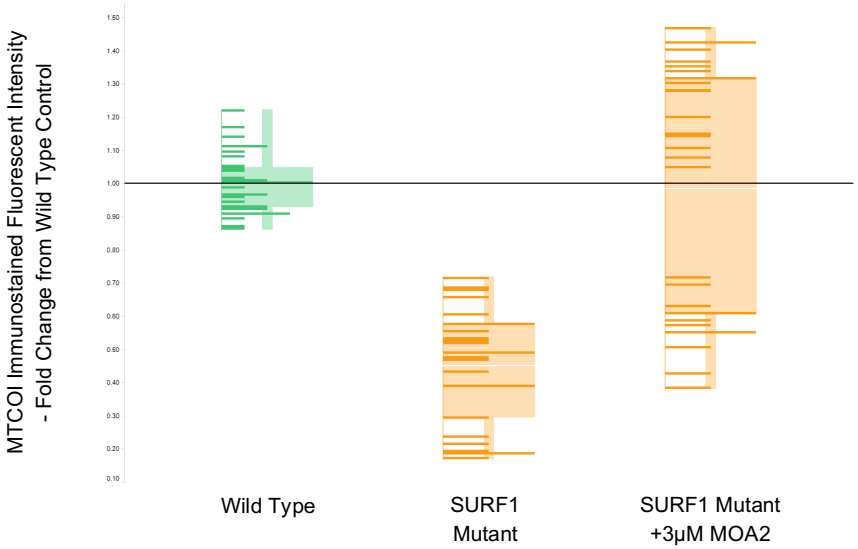

Fig 5.17. *Rescue of MTCOI staining in a CIV deficient SURF1 fibroblast cell line with MOA2 treatment*. Box plot representing MTCOI immunostained fluorescent Intensity - normalised to mitochondrial area in untreated wild type controls and SURF1 mutants, with or without 3μM MOA2. Data presented as fold change from the mean readout of untreated wild type controls (represented with a black horizontal line). Contained within each box is a vertical frequency histogram, the length of horizontal lines within the box indicate the number of wells exhibiting the same fold change in MTCOI staining intensity, allowing for the assessment of the distribution of data.

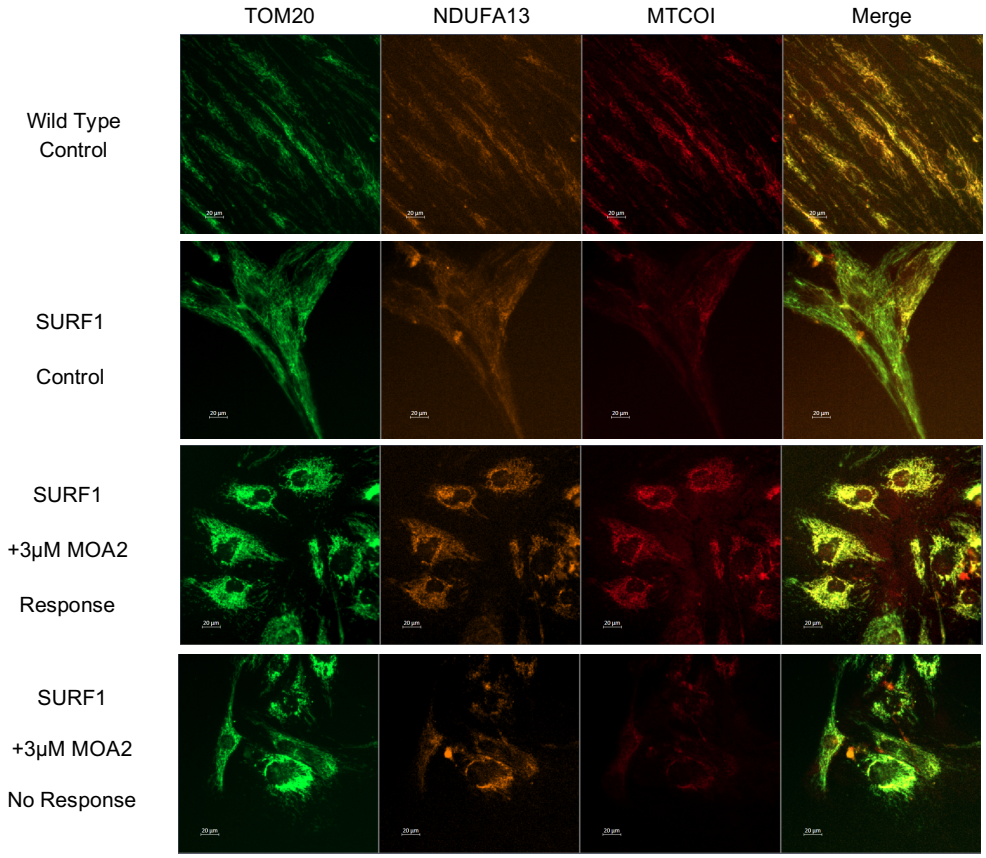

Fig 5.18. *Representative immunofluorescent images for staining of TOM20, NDUFA13 and MTCOI in Wild Type and SURF1 mutant fibroblasts, with and without 3μM MOA2 treatment*. A CIV deficiency is apparent in untreated SURF1 mutant controls, while treatment restores MTCOI staining intensity in a subset of experimental wells.

5.3.7 Quadruple Immunofluorescent Analysis of Mitochondria in Cell lines

The optimisation of quadruple immunofluorescent analysis, to facilitate the simultaneous measurement of four proteins of interest, was selected for development to increase the data yield from a single experiment. Proteins targeted were: TOM20 (mitochondrial mask for data analysis) NDUFA13 and MTCOI (previously established staining for CI and CIV) as well as immunostaining for SDHA – a CII subunit. CII presents as the only mitochondrial complex exclusively of nuclear origin, containing no mtDNA components. As such, the only mitochondrial property that its abundance is dependent upon is the maintenance of the membrane potential, such that mitochondrial protein import is maintained. It is therefore expected that reductions in levels of both CI and CIV in mitochondrial patients, but normal levels of CII, would be indicative of mtDNA depletion or impairment of mitochondrial translation machinery; for instance, the common m.3243A>G MELAS causing mutation. Defects of mtDNA count could then be followed up with specific diagnostic assays, such as qPCR to quantify mtDNA levels.

Staining for Complex II

Immunofluorescent staining for SDHA was carried out as per the HTS protocol established in 5.3.5. Three concentrations of primary antibody were explored, 0.03%, 0.13% and 0.5% v/v (0.3, 1.3 and 5µg/ml). Fig 5.19 demonstrates a stepwise increase in SDHA immunofluorescent staining intensity in wild type fibroblasts, while visual inspection of images, Fig 5.20, confirms co-localisation with TOM20 immunostaining. A control for staining, without anti-SDHA primary antibody, revealed a minimum of background signal. A concentration of 0.13% v/v (1.3µg/ml) was selected for CII immunostaining experiments as a means of generating suitable signals while conserving reagents.

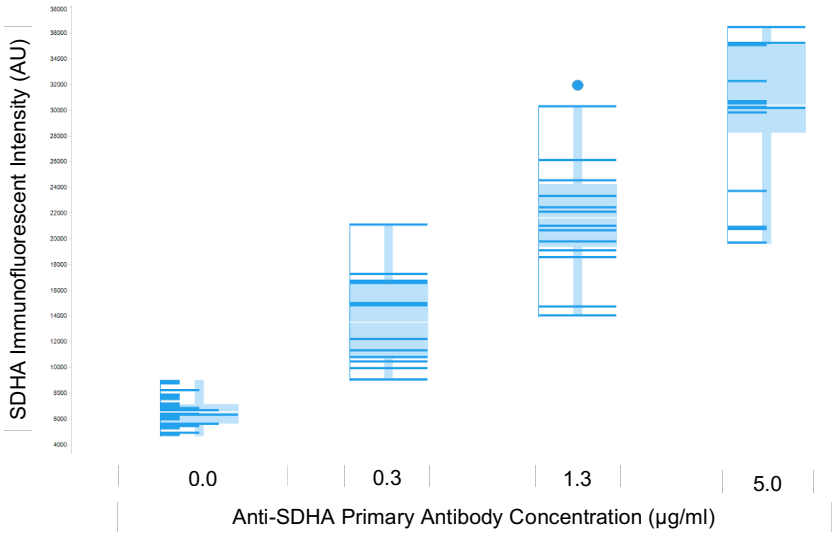

Fig 5.19. *Optimisation of SDHA immunofluorescent staining using the HTS compatible protocol*. A box plot representing SDHA immunostained fluorescent Intensity - normalised to mitochondrial area - in wild type controls. Stepwise increases in SDHA staining intensity is noted with increasing concentrations of anti-SDHA primary antibody. Contained within each box is a vertical frequency histogram, the length of horizontal lines within the box indicate the number of wells exhibiting the same fold change in SDHA staining intensity, allowing the for assessment of the distribution of data.

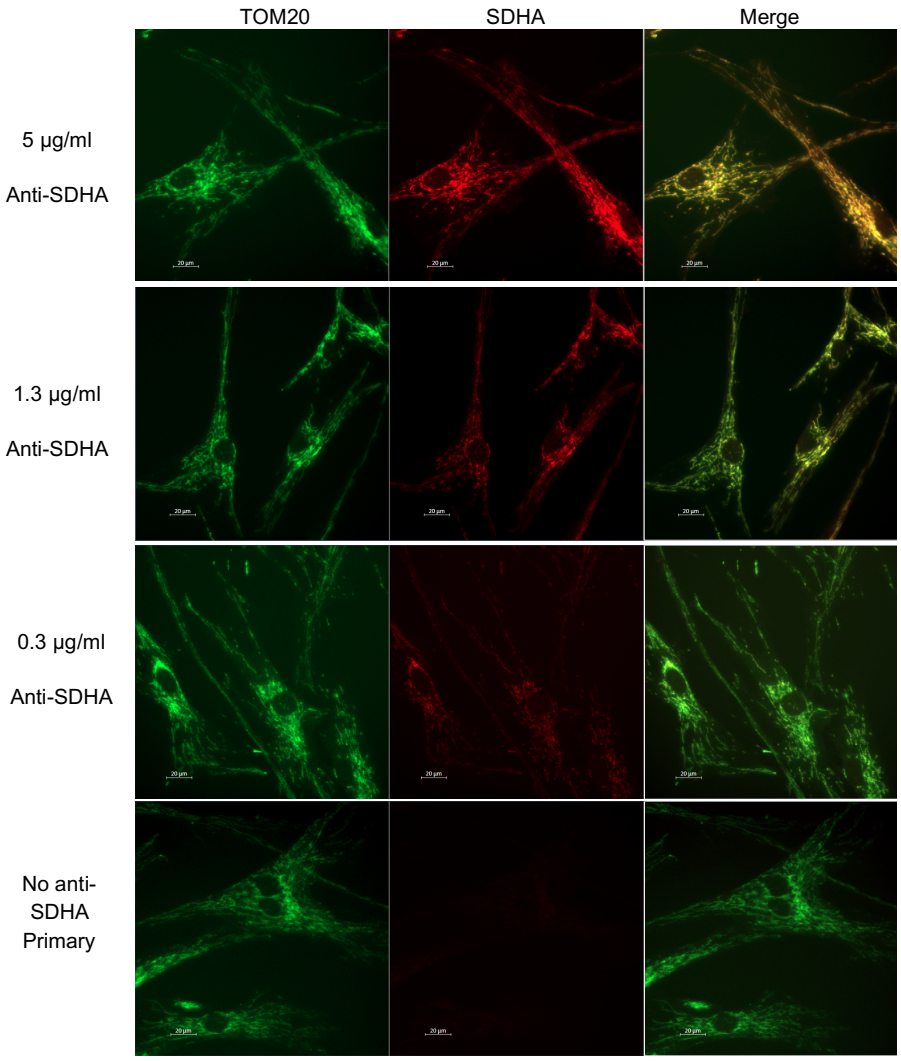

Fig 5.20. *Representative immunofluorescent images showing visible co-localisation of TOM20 and SDHA stained proteins in wild type fibroblasts*. A dilution series of anti-SDHA primary antibodies was investigated to determine suitable concentrations for use in future experiments.

Employment of Quadruple Immunofluorescent Analysis

DAPI has been previously used as a nuclear marker to serve as a means of establishing cell counts to estimate cell survivability, as used in Fig. 5.5, 5.7 and 5.8. The collection of this data is not relevant when attempting to quantify respiratory chain deficiencies within the mitochondrial network, as TOM20 is used as a means of identifying areas of interest for signal quantification and cell survival should not be impacted in high glucose media; diagnostic assays are envisaged to be carried out in standard glucose cell culture media to ensure a sufficient quantity are available for analysis. Omitting DAPI staining and using a secondary antibody, conjugated to a fluorophore of lower stimulation and emission wavelengths of light compared to those used previously, for one protein of interest, will facilitate the quadruple immunofluorescent co-staining. As such, a goat-anti-rabbit-AF405 (Rb405 – excitation peak 401nm, emission peak 422nm) secondary antibody was purchased and trialled in wild-type fibroblasts, paired with an anti-TOM20 primary antibody, as per the HTS protocol established in 5.3.5. As TOM20 was under experimental investigation, a mitochondrial mask was established using SDHA co-staining, having shown co-localisation of signals in Fig 5.21.

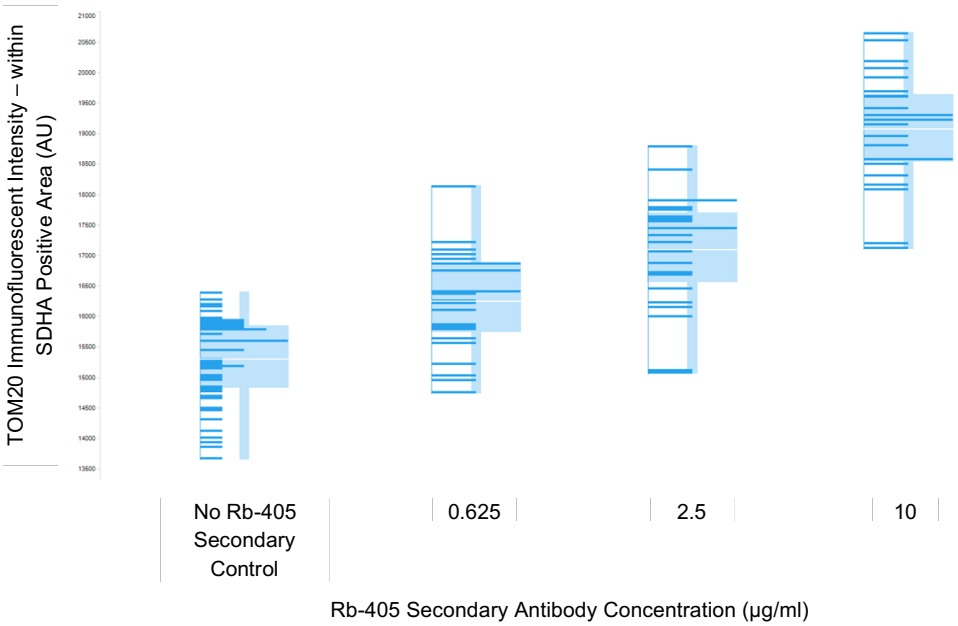

Fig 5.21. *Optimisation of TOM20 immunofluorescent staining using the HTS compatible protocol with a Goat-Anti-Rabbit-AF405 secondary antibody*. A box plot representing TOM20 immunostained fluorescent Intensity - normalised to mitochondrial area - in wild type controls using Rb405 secondary antibody. Stepwise increases in TOM20 staining intensity is noted with increasing Rb405 concentrations of. Contained within each box is a vertical frequency histogram, the length of horizontal lines within the box indicate the number of wells exhibiting the same fold change in TOM20 staining intensity, allowing for the assessment of the distribution of data.

NADH autofluorescence was considered in the selection of TOM20 for AF405 labelling. While the excitation peak of NADH is 340nm, a low level of excitation bleed from 405nm light sources would be expected due to a wide full-width at half-maximal (FWHM) reading of 60nm (Blacker and Duchen, 2016). As such, a 405nm light source stimulates NADH fluorescence to less than half the degree of a 340nm source. The emission peak of NADH is 460nm – FWHM: 100nm, which implicates the emission peak of the Rb405 secondary antibody (422nm), however, this is not expected to interfere with the experiment due to the suboptimal stimulation from 405nm light sources. All other secondary antibodies have been used at final, in well, concentrations 0.1% v/v (2µg/ml). A concentration of 0.2% v/v (4µg/ml) was selected for TOM20-Rb405 immunostaining experiments as a means of generating suitable signals while conserving reagents.

The quadruple immunofluorescent staining panel (anti-TOM20, SDHA, NDUFA13, MTCOI) was employed against wild type fibroblasts, as a means of confirming viable staining for the four targets simultaneously. A split-channel representative image is shown in Fig, 5.23.

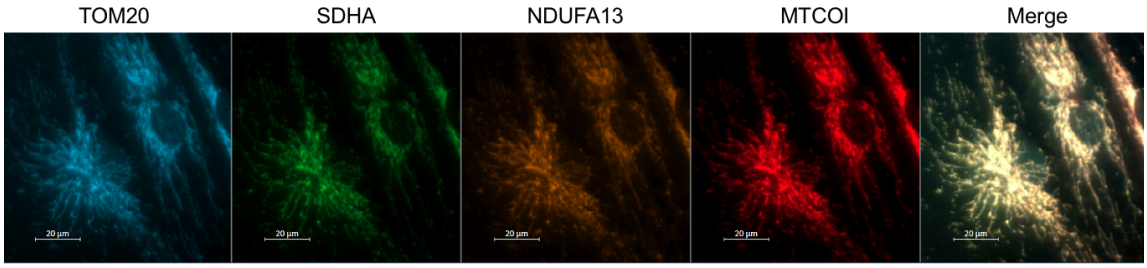

Fig 5.22. *Representative images for quadruple immunofluorescent staining of TOM20, SDHA, NDUFA13 and MTCOI in wild type fibroblasts.*

Use of Immunofluorescent Methods for the Detection of CI Deficiency in Primary Fibroblasts

To validate the immunofluorescent method as a means of quantifying mitochondrial biochemical deficiencies in diagnostically relevant samples, primary patient-derived fibroblasts were subject to immunofluorescent analysis. The cells employed had previously been subject to genome sequencing and been found to harbour a pathogenic mutation in the NDUFS6 gene. Quadruple immunofluorescent analysis of patient muscle sections had revealed a deficiency in CI, as measured by NDUFB8 immunostaining (Ahmed et al., 2017).

Immunofluorescent labelling of NDUFA13 and NDUFS3, and subsequent cell level comparative microscopy analysis, of wild type and NDUFS2 mutant cell lines alongside NDUFS6 primary fibroblasts detected a CI deficiency in the NDUFS6 mutants. Both patient-derived cell lines exhibited NDUFA13 total staining intensities at 40% of that noted in wild-type cells. A similar reduction in NDUFS3 staining is apparent in NDUFS6 primary fibroblasts, though NDUFS2 cells display 25% of the staining intensity of wild-type cells, Fig 5.23, a statistically significant reduction in comparison to the NDUFS6 mutant cells.

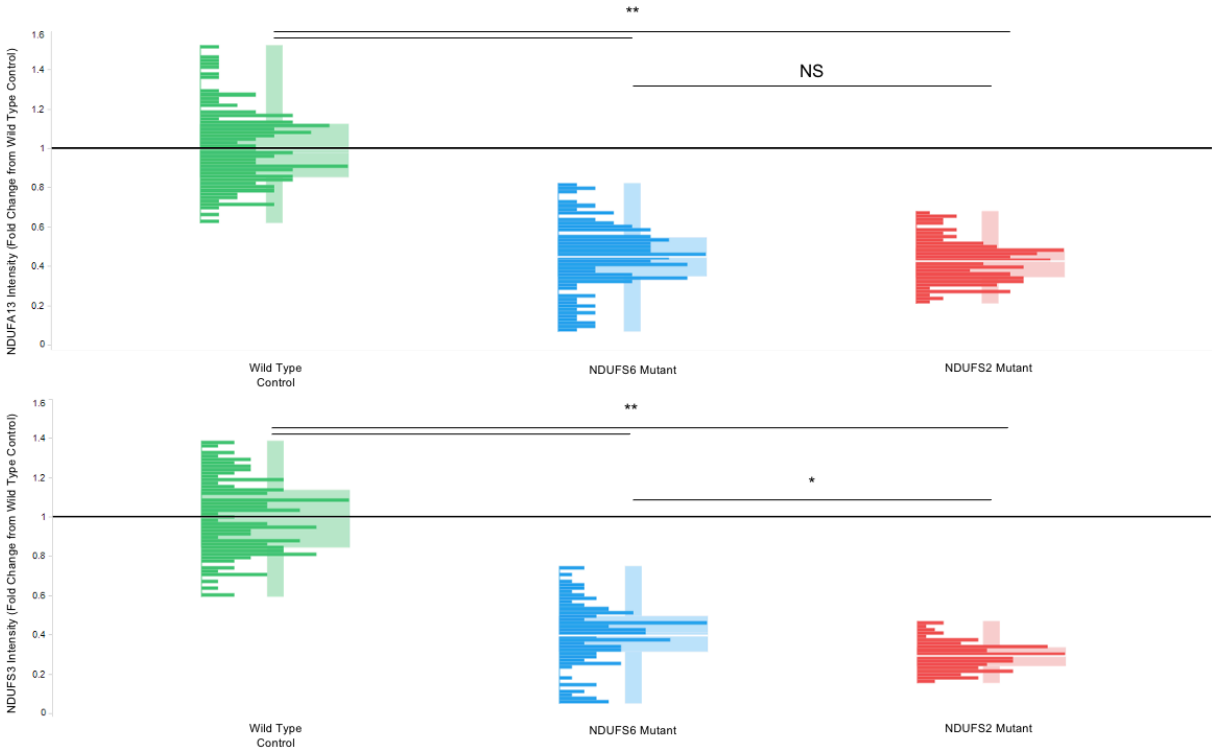

Fig 5.23. *Immunofluorescent intensities of NDUFA13 and NDUFS3 in Wild Type, NDUFS2 mutant immortalised fibroblasts and NDUFS6 mutant primary fibroblasts*. Non-Significant (NS) $P>0.05$, * $P<1x10^{-9}$, **$P<1x10^{-50}$.

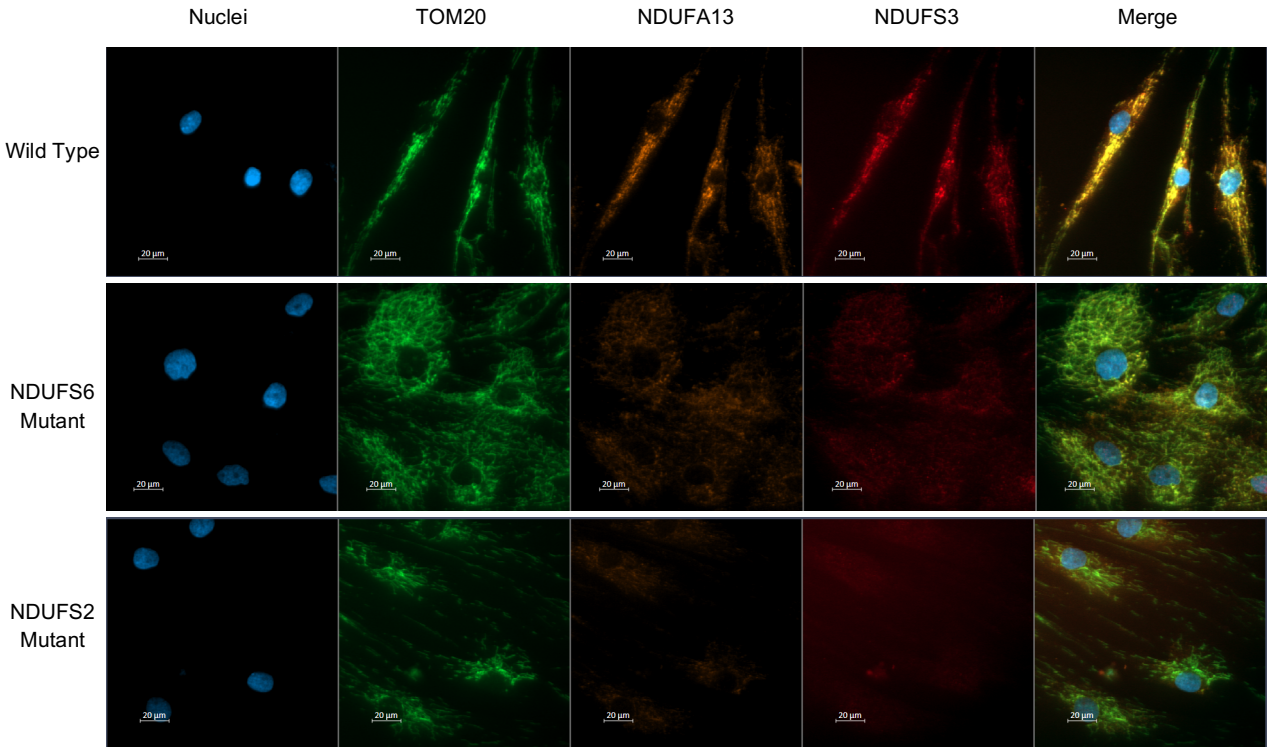

Fig 5.24. *Representative images of Wild Type, NDUFS2 mutant immortalised fibroblasts and NDUFS6 mutant primary fibroblasts immuno-stained for TOM20, NDUFA13 and NDUFS3.*

The quadruple immunofluorescent staining panel of TOM20, SDHA, NDUFA13 and MTCOI was used to compare levels of CI, CII and CIV in NDUFS6 primary cells against NDUFS2 mutant fibroblasts – as a control for CI deficiency. This method revealed no statistically significant differences in CI, CII or CIV levels between the cell populations, Fig 5.25 and 5.26.

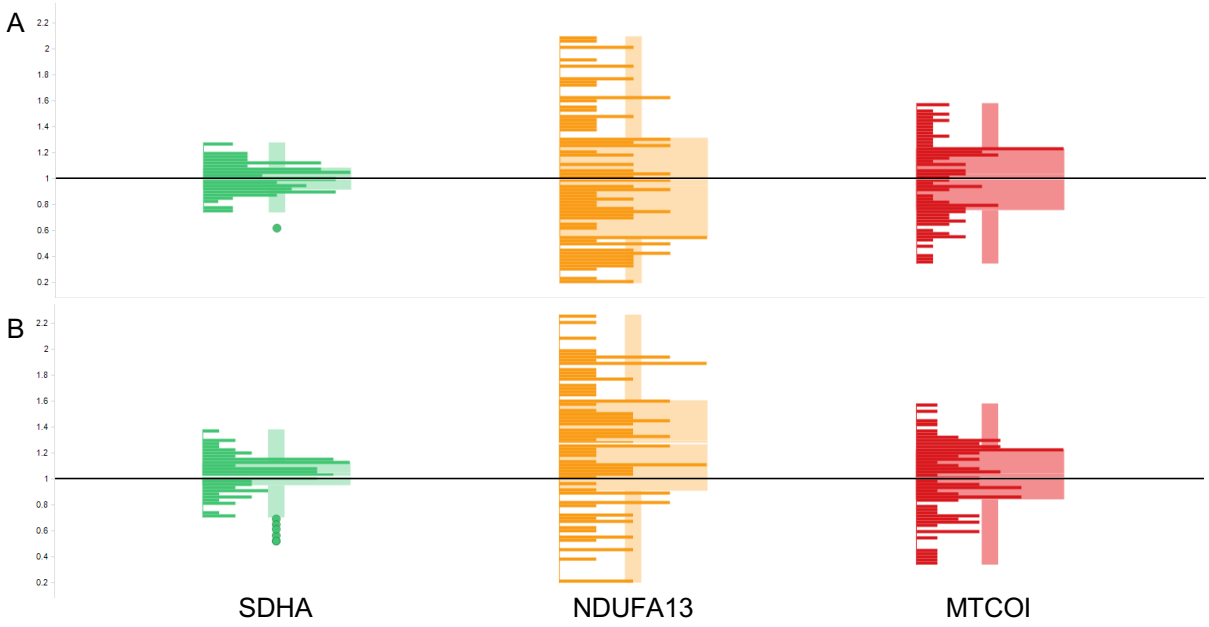

Fig 5.25. *Immunofluorescent analysis of CI, CII and CIV subunit levels in NDUFS2 and NDUFS6 mutant fibroblasts*. Total immunofluorescent staining intensity of SDHA (green), NDUFA13 (orange) and MTCOI (red), normalised to mitochondrial area, in a NDUFS2 mutant fibroblast cell line (A) and NDUFS6 mutant primary fibroblasts (B). Present as fold change from mean readings from NDUFS2 cells.

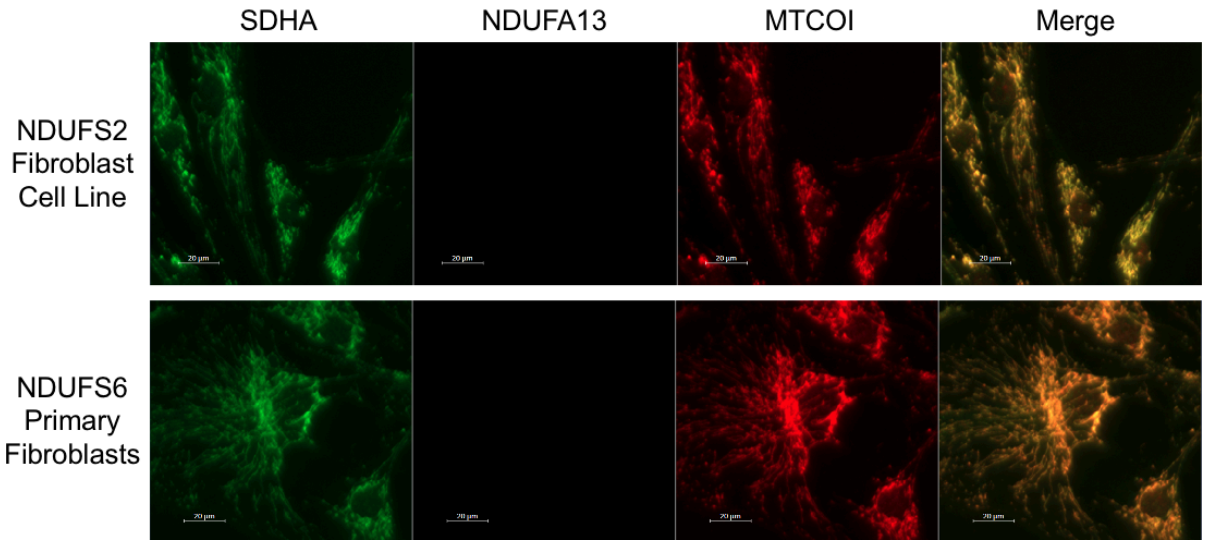

Fig 5.26. Representative immunofluorescent images *of CI, CII and CIV subunit immunostaining in NDUFS2 and NDUFS6 mutant fibroblasts*. All image display settings optimised for visualisation of SDHA staining; identical settings then applied to NDUFA13 and MTCOI channels.

The use of the well-established technique: western blotting, conducted as per 2.5.7 by Dr. S. Bell, serves as a means of confirming the above results. An antibody panel containing primary antibodies to all mitochondrial complexes was used – NDUFB8, SDHB, UQCRC2, COXII and ATPB – alongside GAPDH serving as a loading control. Western blotting confirmed the detection of CI defects in the NDUFS6 patient-derived primary fibroblasts, relative to wild-type cells, Fig 5.27. Western blotting confirms no deficiency of the remaining mitochondrial complexes in the NDUFS6 mutant cells.

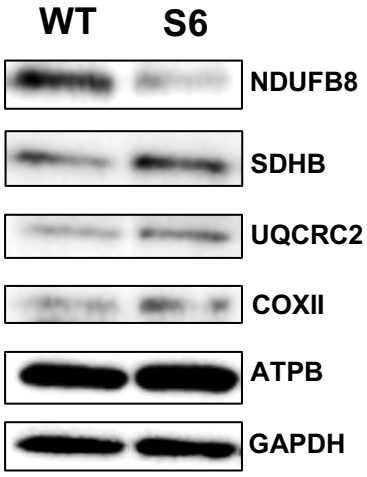

Fig 5.27. *Western blotting of cell lysates for Wild Type (WT) and NDUFS6 mutant (S6) fibroblasts*. Complex I levels are low in NDUFS6 mutant cells, compared to wild type cells. Fibroblasts were cultured and lysates were prepared as detailed in 2.5.7. Equal amounts of lysate were subjected to western blotting, section 2.5.7, with antibodies to each of the subunits shown, representing CI (NDUFB8), II (SDHB), III (UQCRC2), IV (COXII) and V (ATPB). GAPDH is used as a loading control for the total cell lysate. Experiment kindly carried out by Dr. S. Bell.

Investigation of MOA2 using TOM20, CI, CII and CIV Quadruple Immunofluorescence

Having optimised the quadruple immunofluorescent staining panel, it was finally employed against wild type and NDUFS2 mutant fibroblasts, subjected to a serial dilution of MOA2, in galactose media.

The quadruple immunofluorescent panel detected the CI defect in the NDUFS2 mutant cell line, alongside a small yet statistically significant reduction in the levels of CII. A statistically significant increase in CIV levels is also noted in the NDUFS2 mutant cell line, compared to wild-type controls. A highly significant increase in the immunofluorescent intensity of the 405nm channel (assigned to TOM20) is also apparent in NDUFS2 mutant fibroblasts, relative to the wild type control fibroblasts.

The application of MOA2 to NDUFS2 mutant cells causes further increases in the immunofluorescent intensity of TOM20 and increases CI, CII and CIV intensity are evident as MOA2 concentration increases. At 3μM, MOA2 results in 25%, 15% and 31% increases in TOM20, CII and CIV immunofluorescent intensities over wild-type controls respectively. 3μM MOA2 also increases the mean CI immunofluorescent intensity, in NDUFS2 mutant cells, from 50% of wild type controls to 87% of wild type controls. A bimodal distribution is observed in this specific data set, similar to results obtained in SURF1 mutants treated with MOA2.

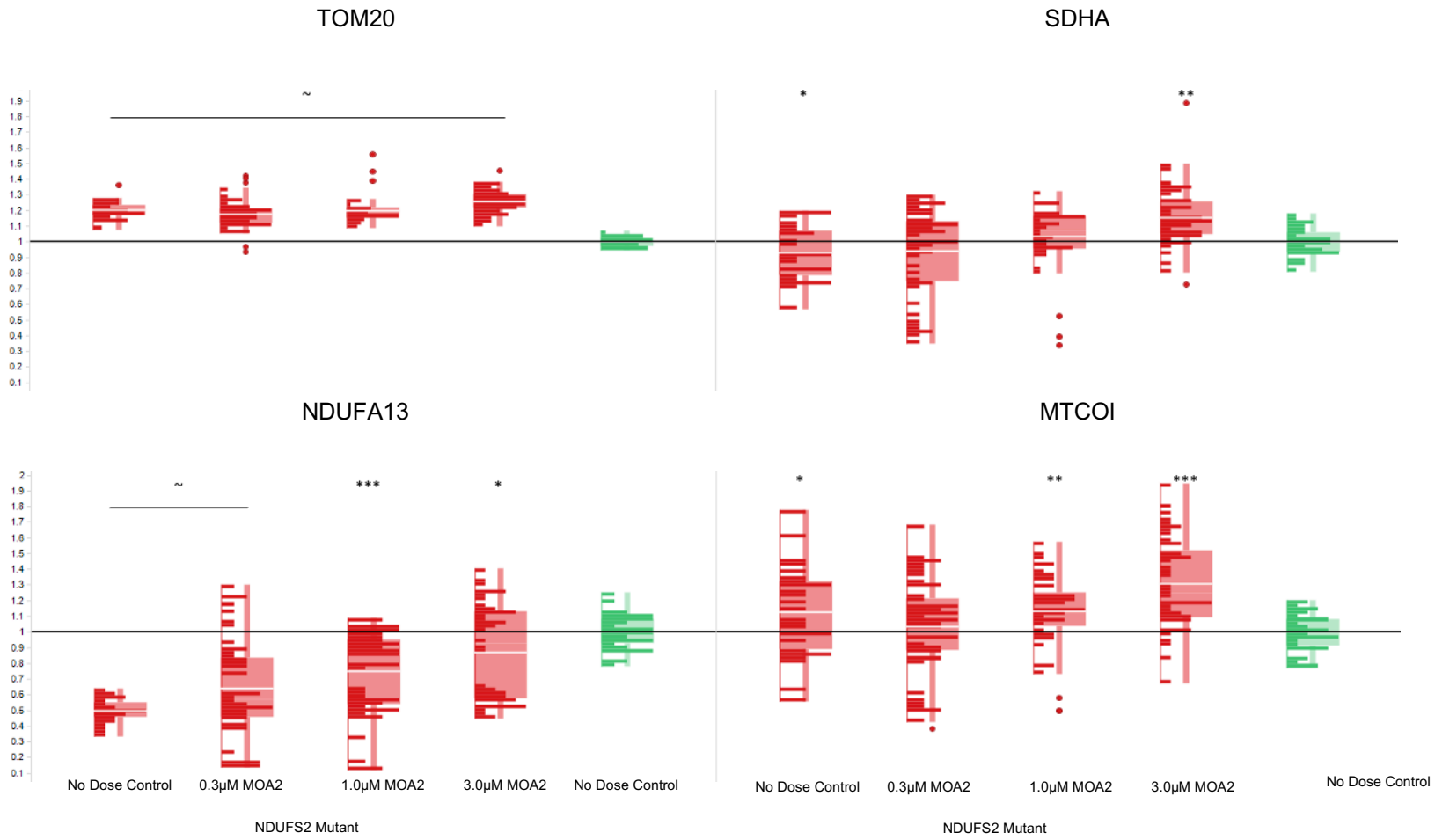

Fig 5.28. *Complex I, II and IV subunit and TOM20 immunofluorescent intensities in NDUFS2 cells cultured in galactose media with MOA2 treatment.* Immunofluorescent intensity of indicated proteins in wild type and NDUFS2 mutant cells, with and without MOA2 at 0.3, 1 and 3μM. Normalised as fold change from WT controls. N=48. * P<0.05, ** P<0.01, *** P< 10^{-5}, ~ P< 10^{-10}

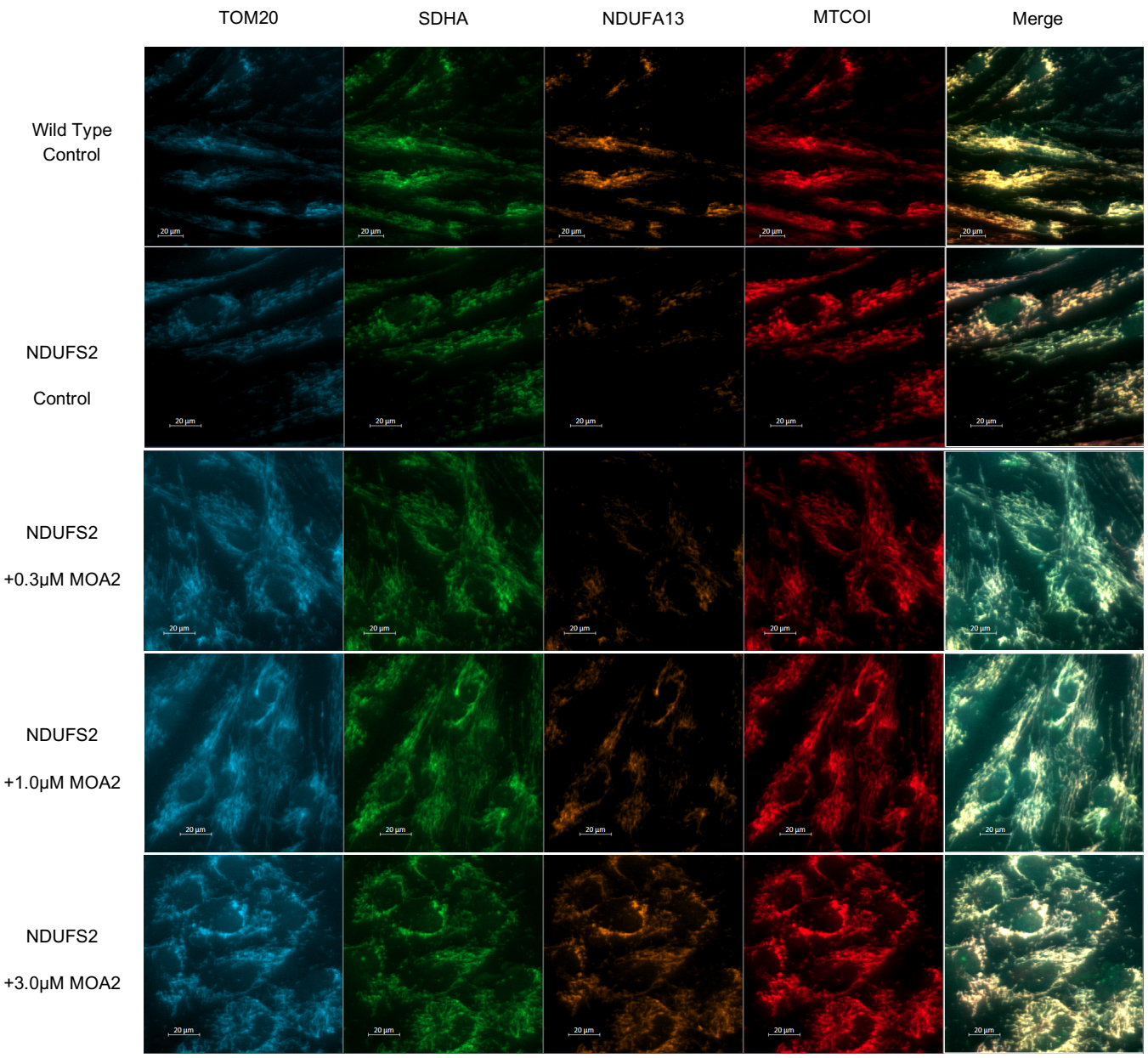

Fig 5.29. *Representative immunofluorescent images of wild type fibroblasts and NDUFS2 mutant fibroblasts, subject to treatment with a serial dilution of MOA2, immunostained for TOM20, SDHA, NDUFA13 and MTCOI.*

5.4 Discussion

5.4.1 Mitochondrial Complex I Subunit Abundancies in CI Deficient Cells

The assembly pathway of CI is complex and dynamic set of both interdependent and independent processes (Sánchez-Caballero et al., 2016, Guerrero-Castillo et al., 2017). It is dependent on the assembly of the Q module, from NDUFS2, 3 and NDUFA5 initially. Without this event, the assembly of the QP_p-a intermediate, the binding of the Q and ND1 modules, will not occur. In the absence of QP_p-a, other assembly intermediates such as P_p-b (containing ND2, 3, 4L and 6), P_D-a (ND4), P_D-b (ND5), have no binding site. In spite of their successful assembly, accumulating proteins are degraded by the mitochondrial proteosome machinery (Gerdes et al., 2012, Rendón and Shoubridge, 2012). Interestingly, the absence of mitochondrial protease activity has also been shown to result in pathogenic respiratory chain defects, in CI and CIV, as a result of dysregulated assembly (Atorino et al., 2003, Bella et al., 2010).

Investigations by Tuppen *et al.*, 2010, identified a point mutation resulting in a R118Q amino acid substitution in the NDUFS2 gene in a paediatric female with Leigh Syndrome, patient 3 (Tuppen et al., 2010). Gel-based investigations confirmed a CI assembly defect, with BN-PAGE and in-gel activity assays displaying significantly reduced levels and activity of CI in these cells respectively. SDS-PAGE and western blotting showed that fibroblast lysates exhibited reduced basal levels of NDUFA9 and NDUFB8 CI subunits, but normal levels of NDUFS3 (Tuppen et al., 2010).

Investigations by Rendón and Shoubridge, 2012, demonstrate rapid proteolytic turnover of the ND1 module in the presence of NDUFAF3 and 4 siRNA mediated knockdown (Rendón and Shoubridge, 2012). Also shown is a CI assembly defect, detected using BN-PAGE analysis with CI marked with NDUFA9 immunolabelling (Rendón and Shoubridge, 2012). While artificially induced, and stemming from deficiencies in early assembly factors, the work of Rendón and Shoubridge, 2012, confirms that impairment of Q/P_p-a assembly significantly reduces total CI assembly.

A fibroblast cell line derived from patient 3, (Tuppen et al., 2010), was used as a model for CI deficiency in the investigations of this project. Immunofluorescent microscopy analysis corroborated reduced levels of NDUFB8. BN-PAGE investigations show an absence of assembled CI, as marked by NDUFB8, however, some residual signal is seen in IF experiments, Fig, 5.6, displaying approximately 30% of the signal intensity

of wild-type cells, not zero. It is hypothesised that this signal originates from P_D-b assembly intermediates. The reduction in NDUBF8 signal intensity versus wild-type cells is proposed to be a result of the degradation of unassembled intermediates. BN-PAGE gels aiming to capture assembled CI, as shown in Tuppen *et al.*, 2010, would likely result in the P_D-b intermediate being lost to the end of the gel due to its small molecular weight in comparison to whole CI. Similar IF observations to NDUFB8 are made in the case of NDUFA13, in that the reduction in the rate of Q module assembly is present due to the pathogenic NDUFS2 mutation in these cells. This could lead to a lowering in the levels of the Q/ND1 intermediate complex – to which NDUFA13 associates to form the Q/P_p-a intermediate. As NDUFA13 directly interacts with Q and ND1 modules to form the Q/P_p-a intermediate (Guerreo-Castillo et al., 2017) it, as opposed to NDUFB8, was taken forward for further investigations. Immunostaining for NDUFS3 was employed in place of NDUFB8, to further interrogate Q module assembly in NDUFS2 mutant fibroblasts.

Using POI intensity sum per unit mitochondrial area by IF as a readout, this project consistently identified reductions in the levels of NDUFS3 in the NDUFS2 mutant cell line, contrary to the observations made by Tuppen *et al.*, 2010, in which whole cell lysates patient cells were shown to express normal levels of NDUFS3 (Tuppen *et al.*, 2010, Figure 4C). A potential explanation for this discrepancy is the mitochondrial masking carried out in the IF investigations (Appendix D). Automated data processing of IF images requires the designation of areas of interest, in which to quantify signal. In doing so any NDUFS3 present in the cytosol – newly synthesised and awaiting import - is not quantified, which would contribute to whole cell lysate readings noted in western blotting analysis.

Immunofluorescent microscopy for NDUFA13 and NDUFS3 was also able to detect CI deficiency in NDUFS6 mutant primary fibroblasts. Muscle sections of the patient had previously been analysed using quadruple immunofluorescence for laminin, porin, NDUFB8 and COXI (Ahmed et al., 2017). The investigations by Ahmed *et al.*, 2017, analysed 880 muscle fibres from the patient (patient 6), revealing a severe CI deficiency phenotype. In the CI assembly pipeline, the N module has been shown to bind the Q/P intermediate before NDUFS6 binding the resultant structure (Pereira et al., 2013, Kmita et al., 2015, Sánchez-Caballero et al., 2016, Guerreo-Castillo et al., 2017). Experiments in yeast have shown deletion of the *NUMM* gene (NDUFS6

ortholog) results in CI being unable to incorporate the N4 iron-sulphur cluster (Kmita et al., 2015). A patient exhibiting a c.343 T > C mutation (p.Cys115Arg) eliminates a Cys of the highly conserved zinc-binding domain of human NDUFS6(Rouzier et al., 2019). BN-PAGE investigations into muscle tissue and fibroblasts from this patient show severe CI deficiency using an anti-NDUFA13 antibody (Rouzier et al., 2019). It can be hypothesised that the N module binds the Q/P intermediate such that CI largely assembles in NDUFS6 mutant cells. The NDUFS6 mutation of the patient in the current project, c.316_319del (p.Glu106Glnfs*41), precludes zinc binding and mature CI assembly. It is hypothesised that this results in the turnover of the Q/P intermediate, as evidenced by deficiencies in NDUFS3 and NDUFA13, to a similar degree as noted in NDUFS2 mutant fibroblasts.

5.4.2 Effects of MOA2 and a Hypothesis for A Mechanism of Action

When untreated, the NUDFS2 mutants stop proliferating in galactose media, but do not die. Repeated media/liquid changes throughout galactose growth experiments and IF protocols with detergent (such as Tween20), used before methanol treatment in IF staining protocols, appear to wash off galactose incubated NDUFS2 fibroblasts from the well bases. Galactose growth experiments without media changes show untreated NDUFS2 fibroblasts persist to the end of the experiment, but at a greatly reduced confluence relative to MOA2 treated cells, Fig. 5.4. IF images acquired with detergent permeabilisation prior to methanol treatment exhibit reduced nuclei counts, while the removal of this detergent treatment step removes this issue. Interestingly, the presence of detergent during antibody treatment (4^{o}C overnight) does not produce this issue. It therefore follows that growth in galactose media, without MOA2, results in the weakening of well adherence of NDUFS2 fibroblasts.

A partial increase in CI assembly is noted by IF imaging with 3μM MOA2 treatment in galactose media, but not glucose media. Further investigation by colleagues in Newcastle Highly Specialised Mitochondrial Diagnostic laboratory revealed only marginal variation in CI:CII isolated activity ratio with 3μM MOA2 treatment over a four-day period. It is hypothesised that in glucose media, NDUFS2 mutants continue to utilise glycolysis for the majority of ATP generation, a phenomenon known as the Crabtree effect (Marroquin et al., 2007), regardless of MOA2 application. Providing galactose as the major carbon source results in the requirement of respiratory chain use and subsequent OXPHOS, acting as a stimulus for the transcription of new mitochondrial complex subunits to increase overall OCR and ATP production from the mitochondria (Marroquin et al., 2007, Kase et al., 2013, Liu et al., 2014, Mot et al., 2016).

A linear relationship is noted between abundancies of CI subunits, NDUFA13 and NDUFS3, with MOA2 doses ranging from 0.1μM to 3μM MOA2, Fig 5.12. Given that CI subunits are unstable when not fully assembled, increases in the steady-state levels indicate increases in complex assembly.

A statistically significant phenotypic improvement of NDUFS2 mutant fibroblasts is noted in the galactose growth assay with 0.3μM MOA2, however, this effect is blunted in comparison to 3μM MOA2 treatment, Fig. 5.4. The linear progression of increases in NDUFA13 and NDUFS3 staining intensity (in that CI markers are raised with 0.3μM MOA2 treatment) combined with this data implies a threshold effect is present for CI levels in the galactose growth assay, which, once crossed allows for improvements in proliferation rate in galactose media.

No phenotypic improvement in CI subunit levels, by IF, is seen in NDUFS2 mutant cells in glucose media over eight days, Fig 5.10 B i-ii. Additional investigations by the Highly Specialised NHS Mitochondrial Disease Diagnostic Service into the effects of MOA2 have been carried out. Maximal CI activity assays have confirmed no increase in CI activity from NDUFS2 cells cultured in glucose media for four days. It can therefore be proposed that the target of MOA2 is expressed, or is active, in NDUFS2 mutant cells as a result of increased metabolic demands, as a result of galactose media exposure. Precisely how this effect is brought about is unknown, however, it is possible that the target of MOA2 is not expressed under glycolytic conditions or that alterations to the target's action are not significant to the cellular state under these conditions, i.e., the metabolic stimulus of galactose media is required to stimulate CI subunit translation and assembly rescue is facilitated by MOA2 application.

Effects of MOA2 on other complexes of the mitochondrion have not been previously shown. Immunofluorescent staining of MTCOI in SURF1 mutant fibroblasts, treated with 3μM MOA2, demonstrate an improvement to CIV deficiency in these cells Fig 5.17. A bimodal distribution of data points is noted in 3μM MOA2 treated SURF1 mutants, it is expected that more cells will be rescued, on average, with a longer experiment duration. A phenotypic improvement in cells harbouring a pathogenic mutation in a mitochondrial complex other than CI precludes anything mechanism of action hypothesis based solely on CI assembly rescue.

Quadruple immunofluorescent analysis of NDUFS2 mutant fibroblasts revealed a minor, yet statistically significant, reduction in SDHA staining intensity relative to wild type cells. An increase of similar magnitude of MTCOI staining intensity is noted, however, with greater variance. It is hypothesised that untreated NDUFS2 mutant cells are adapting to the lack of CI activity, by modulating levels of other mitochondrial

complexes. A 20% increase in TOM20 immunostaining intensity in NDUFS2 mutant fibroblasts, compared to wild type controls, is also apparent. The increased TOM20 staining intensity is indicative of more TOM complex being present per unit area of MOM relative to wild-type controls. It is possible that CI assembly intermediates are being continually turned over in NDUFS2 mutant cells, being an early assembly defect (Rendón and Shoubridge, 2012), triggering an increase in protein import to replenish them. The cycle repeats, however, as a result of the pathogenic NDUFS2 mutation, creating a positive feedback loop for CI subunit import.

Treatment with MOA2 of increasing concentrations increases the staining intensities of SDHA, NDUFA13 and MTCOI in NDUFS2 mutant fibroblasts. This has the effect of improving the CI deficient phenotype present in NDUFS2 mutant cells, and results in the abundancies of SDHA and MTCOI proteins significantly exceeding those of wild type controls, Fig 5.28. Despite MOA2 increasing readouts for complexes not affected by the NDUFS2 mutation, results are not recapitulated in CI in wild-type fibroblasts, Fig. 5.5-5.6. Instead, a minor, yet statistically significant, reductions in the levels of NDUFB8 and NDUFA13 are noted in wild-type cells, subjected to MOA2 treatment, in galactose media. Thus, improvement of the mitochondrial state due to MOA2 treatment appears to be dependent on the presence of dysfunction and highlights the importance of maintaining cellular homeostasis.

Due to the rapid turnover rate of unassembled CI intermediates (Rendón and Shoubridge, 2012) and the increased IF signals from three CI subunits, entering the assembly pipeline of CI at three different points, and OCR improvements (Rai, 2017), it can be reasoned that MOA2 treatment improves CI assembly in NDUFS2 fibroblasts through a currently unknown mechanism of action. Partial rescue of CIV levels in CIV deficient fibroblasts, as measured by MTCOI immunofluorescence shows that the effects of MOA2 are not CI specific (section 5.3.6). It is unlikely that MOA2 serves to trigger increases in the expression of all mitochondrial subunits, in conjunction with galactose induced metabolic stress, due to a lack of such increases in wild type cells (section 5.3.2, Fig. 5.5-5.7).

A hypothesis centring on the mitochondrial proteolytic machinery has been developed. It is proposed that MOA2 acts to bind to a target, which causes the downstream reduction in the rate of complex assembly intermediate degradation. Either through the suppression of the mitochondrial protease gene transcription or through the direct inhibition of mitochondrial protease family members, such as the MIM anchored mAAA protease, responsible for the degradation of aberrant MIM proteins – such as ETC components. This reduction of aberrant complex, or free unassembled subunit, degradation could facilitate the longer time required to assemble complexes with assembly defects, for instance, the NDUFS2 and SURF1 mutations.

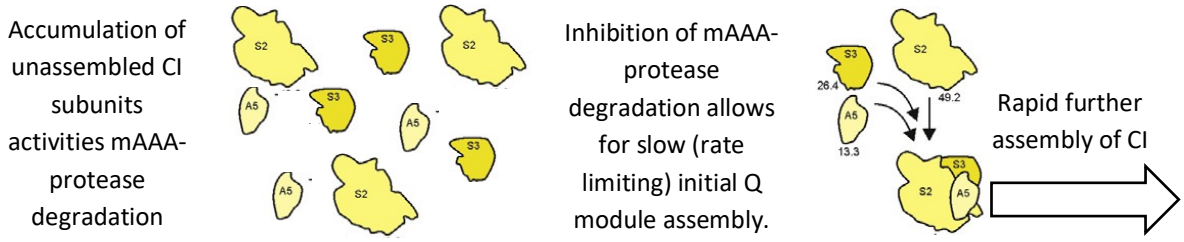

Fig 5.30. *Visual aid for the representation of a mitochondrial proteolytic machinery-based hypothesis for the mechanism of action of MOA2.* In the present of an assembly defect, subunits of the effected complex (CI used as an example) accumulate. This triggers the activation of the m-AAA protease (for example), to degrade the unassembled subunits. It is hypothesised that the inhibition of the relevant protease (or suppression of its transcription) would allow additional time for the impaired assembly process to occur, facilitate the rapid further assembly of the effected complex. Adapted from (Guerreo-Castillo et al., 2017)

The re-application requirement of MOA2 indicates that either MOA2 is rapidly metabolised by cells, or that it has a poor target affinity requiring higher concentrations for full inhibition – though concentrations higher than 3μM have previously been shown to be toxic (Rai, 2017). The requirement of 3μM MOA2, a high concentration in the field of drug development, for phenotypic improvement indicates poor cell membrane permeability or poor target affinity. The latter appears at odds with a hypothesis of covalent binding; however, the molecule may need to enter a complicated binding site (a potentially rate-limiting step) before a covalent reaction occurring.

Until the pharmacodynamics of MOA2 is improved, such that the re-application interval is lengthened, or concentration required for action significantly reduced, experiments commonly used to determine a drug target (such as protein pull-down) are not viable to carry out.

5.4.3 Phenotypic Screening

While the identification of MOA2 as a lead compound for mitochondrial complex assembly rescue is a significant step forward for mitochondrial therapeutic discovery, the high failure rate of putative therapeutics in the drug discovery pipeline necessitates the identification of an excess of lead compounds. Approximately 1.75% of academic projects yield approved therapeutics (Takebe et al., 2018) and 90% of all drug discovery projects fail (Hingorani et al., 2019). One aim of this project was to explore the phenotypes of the NDUFS2 mutant cell line to establish an HTS compatible assay.

Galactose Growth Assay

The galactose growth assay presents as a simple manner of identifying lead compounds, through the exploitation of the NDUFS2 mutant fibroblasts inability to proliferate in galactose media. A limiting factor in this method is the requirement of the NDUFS2 mutant cells to be seeded into multi-well plates in glucose media. Seeding in galactose media was explored but was not successful (data not shown). Sterile automated plate washers, permanently situated in class II microbiological safety cabinets, would be required to facilitate the glucose to galactose media change in an HTS assay. This additional process could introduce increased variability in assay results. Nevertheless, a protocol was optimised for the assessment growth rescue of NDUFS2 mutant fibroblasts with MOA2, with the view of using MOA2 as a positive control, due to NDUFS2 mutant fibroblasts dosed with MOA2 achieving similar confluences to their glucose cultured counterparts over long culture periods, Fig. 5.2.

Favourable Z' scores were obtained between untreated and treated NDUFS2 fibroblasts in galactose media, however, the requirement of MOA2 re-application, Fig. 5.4, complicates the experiment. Disturbing cells during the experiment causes a decrease in detected cell confluence and results in minor shifts in fields of view, such that the areas assessed are not consistent throughout the experiment. Designating MOA2 as a positive control for galactose growth rescue of CI deficiency is inappropriate. Despite demonstrating cell survivability in galactose media, the rate of proliferation is substantially lower than glucose cultured NDUFS2 fibroblasts. Ultimately, the long experiment duration and low sample throughput of the galactose growth assay resulted in it not being pursued for HTS protocol development.

Immunofluorescent Labelling of Mitochondrial Respiratory Complex Subunits

It was hypothesised that the partial phenotypic rescues noted in the previous assays, galactose growth and SEFA (Rai, 2017), was due to the amelioration of the CI assembly defect of the NDUFS2 mutant fibroblasts. To address this hypothesis in an HTS compatible manner, immunofluorescent microscopy using the Zeiss Cell Discoverer Series 7 high throughput widefield microscope was employed. This system allows for the rapid imaging of multiple 384 well plates.

The aims in using IF imaging was two-fold: the assessment of the effects of MOA2, establishing an HTS viable method for the identification of putative therapeutics for CI deficiency. As discussed in 5.4.2, IF methods demonstrated the multiple effects of MOA2 in rescuing CI, and subsequently CIV, defect in relevant cell lines. The method was optimised to achieve Z' scores of greater than 0.5 for immunostaining for NDUFA13 and NDUFS3 using NDUFS2 mutant fibroblasts as a model of CI deficiency. Wild-type cells were used as a positive control in this Z' calculation as MOA2 does not restore complex levels to those of wild type cells.

5.4.4 Potential for Diagnostic Applications

An additional application of the developed IF methodology was established (a potential contribution to diagnostics) due to the finding that a single immunostaining method yielded favourable results for TOM20, CI, CII and CIV co-staining.

Quadruple immunofluorescence is an established diagnostic method for the quantification of CI and CIV in muscle fibres, using NDUFB8 and MTCOI staining (Rocha et al., 2015, Ahmed et al., 2017, Alston et al., 2017). Immunological staining, on the level of cells as opposed to muscle sections, has previously been qualitatively explored in 2002 (Hanson et al., 2002), to confirm the presence of defects. The advancement of microscopy and automatic data processing technology in the last two decades now facilitates the rapid quantitative profiling of cells for diagnostic purposes.

While a phenotypic recovery of NDUFS2 cells with MOA2 treatment was observed in media using galactose as a carbon source, as opposed to glucose, biochemical defects are detectable when cells were cultured in the latter. This is highly favourable as many mitochondrial disease cells are unlikely to retain viability in a metabolically challenging environment, such as galactose media. To quantify biochemical burden, cells can be seeded into multi-well plates in glucose media and fixed 24 hours later – to allow for cell adherence to the well base. Seeding densities of 2,000 cells per well can be used in this manner, resulting in the requirement of $5x10^4$ cells, in total, for 25 replicate wells. In contrast, over ten times the number of cells are required for gel-based techniques such as SDS-PAGE and western blotting to acquire a single data point (Taanman et al., 1997, Tuppen et al., 2010). Further replicates can easily be added as required in multi-well plate-based IF methods. Cells from multiple patients can be assessed at once alongside internal controls (either wild type, positive, or a cell line with a confirmed biochemical defect, negative) for the proteins of interest.

5.5 Future Work

5.5.1 Phenotypic Screening

Immediate future work centres on the application of the IF methods optimised in this project for the identification of a new hit compound for CI rescue. While methods explored early in the project (galactose growth assay and SEFA) are unsuitable for HTS, they remain relevant for use as secondary assays of hits identified in high-throughput primary screens. Confirmation of lead compound activity is vital before extensive mechanistic elucidation work is undertaken.

5.5.2 Expansion of IF Staining Panel and Validation Against Current Methods of Mitochondrial Disease Diagnosis

Currently, muscle section methodologies, as well as the IF methods optimised in this project, focus on defects in CI and CIV, being the two most common biochemical defects in the mitochondrial disease patient population. It is envisaged that additional protein targets, such as UQCRC2 and ATP5O, can be fluorescently immunolabelled in specific cases in which rare defects in CIII and CV are suspected – pending optimisation of relevant antibodies.

Once optimised, a single analysis plate can be probed for multiple targets as a result of the compartmentalised nature of multi-well plates. For example, half of a plate can be stained for TOM20, SDHA, NDUFA13 and MTCOI, while the other could be stained for TOM20, SDHA, UQCRC2 and ATP5O. Additional segmentation of a plate could be incorporated to probe mtDNA count or a marker of gene expression, using anti-DNA or anti-TFAM antibodies. Four subsections of a 384 well plate allows for 96 wells to be used between suspected disease and control cells, facilitating 48 replicates of each. The proposed staining panels could provide an overview of mitochondrial health of a patient, quantifying subunits from every complex of the electron transport chain, CV and two mtDNA markers in high replicate numbers. This outlined analysis is projected to require approximately $4x10^5$ patient cells, when seeded at 2,000 cells per well (approximately one confluent T25 cell culture flask), in a single rapid turn-around experiment.

While this project has demonstrated the use of a novel immunofluorescent method for the quantification of deficiencies in three cell lines (two immortalised and one primary), many more validation experiments are required to confirm the complete accuracy of IF at the cellular level in detecting mitochondrial defects. It is suggested that multiple mitochondrial disease mutations are assessed in the form of cell cultures, with matched muscle biopsies, from patients diagnosed with mitochondrial disease originating from both nuclear and mtDNA mutations. In this manner, IF assessment of cell lines can be performed alongside SDS- and BN-PAGE gels with muscle section quadruple immunofluorescent and histochemical experiments. Results can then be compared to confirm, or invalidate, the application of the IF method in the diagnostic field.

While a skin punch biopsy, required for the collection of patient fibroblasts, is classified as invasive (Fernandes et al., 2016), it is less severe than open surgical muscle biopsy methods. In the future, the optimisation of immunofluorescent protocols in cells more easily collected, but still representative of patient condition, would further improve the patient experience.

5.5.3 Mass Metabolic Profiling of the Ageing Population

It is hoped that the optimised screening method will be utilised in the search for mitochondrial disease therapeutics and eventually, if fully validated, for mitochondrial disease diagnostics. However, due to its high throughput nature, it could also evolve out of this specific niche. The assessment of CI and CIV levels in the elderly could provide a means of identifying metabolic dysfunction from accumulated mitochondrial mutations (Chistiakov et al., 2014, Lane et al., 2015, Srivastava, 2017, Huang et al., 2019), a major risk factor associated with cancers (Wallace, 2012, Pavlova and Thompson, 2016), and neurodegenerative diseases (Bender et al., 2006, Lane et al., 2015, Chen et al., 2019b), to allow for early detection and intervention in diseases of advanced age.

5.5.4 Mechanistic Elucidation of MOA2

Prior to mechanistic elucidation, the pharmacodynamics of MOA2 need to be improved, as measured by a reduction in dosing interval or concentration required. An improved target binding affinity would allow for protein pull-down experiments to be conducted to identifying a target protein. Structure-activity relationship (SAR) analysis is currently underway, in collaboration with an industrial partner, with the goal of lowering the concentration required for phenotypic improvement. It is hoped that the galactose growth and IF assays developed in this project will act to accelerate the rate putative drug assessment, beyond that of previously established seahorse extracellular flux analysis assays.

5.6 Conclusion

This project has developed a high-throughput screening method for the quantification of NDUFA13 and NDUFS3 abundancies in cell lines. Further, this method was adapted into a quadruple immunofluorescent protocol for the quantification of CI, CII and CIV abundancies within a mitochondrial mask. Both techniques, CI specific and quadruple IF, were used to assess the effects of a lead compound for CI deficiency phenotypic rescue, MOA2, in an NDUFS2 mutant fibroblast cell line. Further investigations also demonstrated the potential therapeutic effects of MOA2 on CIV deficient cells. Both immunostaining protocols were also shown to be viable in primary, patient-derived, NDUFS6 mutant fibroblasts. It is hoped that the protocol undergoes further optimisation and validation for use in the mitochondrial disease diagnostic field, with potential future applications in mitochondrial health screening in the ageing population.

Chapter 6:

Final Discussion

6.1 Development of a Screening Pipeline for the Identification of Agents Capable of Inducing Mitochondrial Biogenesis

Mitochondrial biogenesis has long been hypothesised as a potential therapeutic pathway for mitochondrial diseases, with the potential relevance to a wide variety of more common human diseases (Komen and Thorburn, 2014, Lightowlers et al., 2015, Ploumi et al., 2017), see section 1.7.3. While the pathways controlling mitochondrial biogenesis have been well characterised (Scarpulla, 2002, Scarpulla, 2008, Hock and Kralli, 2009, Eichner and Giguère, 2011, Fernandez-Marcos and Auwerx, 2011, Andreux et al., 2013, Cerutti et al., 2014, Khan et al., 2014), the manner in which they interconnect and influence each other is a matter of great complexity, yet to be fully elucidated. Therefore, phenotypic screening presents as a more reliable method of lead discovery than target-directed efforts. A precise definition of what constitutes mitochondrial biogenesis has also proven troublesome to establish, due in part to the great number of parameters that can be associated with it. These include mtDNA content, mitochondrial membrane potential, mitochondrial membrane area/volume, mitochondrial protein content, oxygen consumption rate assays and protein or mRNA quantification and post-transcriptional state of key proteins involved in mitochondrial biogenesis pathways: for example, PGC-1α. This project aimed to identify agents capable of inducing mitochondrial biogenesis, in as full of a capacity as possible, through the assessment of multiple parameters listed above. In screening for improvements in multiple facets of mitochondrial biogenesis the current project increased the likelihood of identifying agents, which can elicit functional improvements and that potentially hold therapeutic value.

The project successfully optimised a high throughput flow cytometric screen for the assessment of m-GFP (mitochondrial mass) and TMRM (membrane potential) in a K652 lymphoblastoma cell line. A suspension-cultured cell line was specifically chosen for ease of use in a flow cytometry assay. A precedent for the use of both m-GFP and TMRM in the assessment of mitochondrial mass is present in the literature (Scaduto and Grotyohann, 1999, Nilsson et al., 2015). Additional assays for mtDNA count (qPCR) and immunofluorescent analysis of mean TOM20 staining intensity (an indicator of protein import and mitochondrial mass), mitochondrial area per cell and per unit cell area (physical mitochondrial network size), mean mitochondrial length (mitochondrial network interconnectivity) and TFAM immunofluorescent spot count (indictor of mtDNA and its transcription) were also employed. This project did not

explore gel-based, transcriptomic or proteomic experiments due to their incompatibility with high throughput work. During the process of establishing the assays outlined above, putative hits for mitochondrial biogenesis, from an ultra-high-throughput bacterial library screen at Nanna Therapeutics, were assessed for MB effects. The novel use of transposon mutagenesis enabled the exploration of gene overexpression, truncation or knockout, across the entire genomes of bacteria (section 3.3.1). Billions of clones were created as a result, all of which were subjected to Nanna Therapeutics unique ultra-high-throughput flow cytometry-based screening method – using TMRM fluorescence as a readout. Following secondary screening and hit selection steps, a total of ten bacterial extracts were identified to yield significant, dose-dependent, increases in multiple mitochondrial biogenesis readouts. The ten extracts were prioritised, controlling for the dose required for maximal efficacy towards mitochondria density, for future work. This future work will focus on active compound identification, purification and validation.

The primary limitation of the work presented here centres around the functional implications of hit extracts. Firstly, experiments that quantify changes in OCR or enzymatic activity were omitted from assay development experiments, due to their incongruence with high throughput work. As a result, none of the hit bacterial extracts have yet been assessed for their ability to induce functional enhancements in human cells as a result of the mitochondrial proliferation effects. Secondly, all experiments have been conducted in wild-type cells, without exposure to a mitochondrial insult. Therefore, it remains unknown whether the application of mitochondrial biogenesis inducing extracts can ameliorate deleterious phenotypes. Such experiments were purposely reserved for active compound isolates from hit bacterial extracts to expedite screening progress. Since the identification of active extracts, functional assays in disease models have not been carried out, due to the caseation of the collaboration between Nanna Therapeutics and WCMR.

Should future screening work be conducted, throughput could potentially be enhanced by incorporating anti-DNA antibody staining into immunofluorescent analysis, to mark mtDNA, in place of qPCR experiments. Doing so would essentially combine data collection presented in sections 3.3.4 and 3.3.5 into a single assay. Confirmatory qPCR analysis could later be used on cells dosed with hit extracts, to validate hit from such immunofluorescent investigations.

The immediate implications of the identification of the active bacterial extracts currently reside solely in the pre-clinical research space. Many more years of work are required to produce a full characterisation of the active component(s) of each extract identified herein. Active compounds must then pass through the rigorous clinical trial pipeline, in which the failure rate remains high (Takebe et al., 2018, Hingorani et al., 2019), to be approved for use in human patients. It is hoped that the work conducted in this project will, in time, result in the addition of numerous lead compounds to the roster of those under clinical assessment (Russell et al., 2020).

6.2 Therapeutic Prospects of Mitochondrial Turnover

As discussed in 6.1, mitochondrial biogenesis has been under investigation for several years as a potential line of inquiry for treating mitochondrial diseases. Perhaps counterintuitively, mitophagy (the degradation of mitochondria) has also recently come under investigation. To investigate the interplay between mitochondrial biogenesis and mitophagy, a pilot experiment using mitoQC expressing fibroblasts (McWilliams et al., 2016b) was employed to assess mitophagy rate, in the form of % mitophagy (Bell, 2020). The resultant imaging showed decreases in % mitophagy readouts, as a result of exposure to bacterial extracts capable of increasing net mitochondrial mass. Given the range of effects on % mitophagy by these extracts, which result in consistent mitochondrial mass increases, it can be suggested that a combination of biogenesis stimulation and mitophagy suppression is being triggered. Both extract 2.1.85, and 2.1.92, induced mitochondrial mass increases of over 30% at a 1:1 dilution in cell culture media (section 3.3.7) but caused mitophagy suppression of 76% and 26% respectively (section 4.4). The similarity of mitochondrial mass increases, but the disparity of mitophagy rates suggests different mechanisms of action for extracts 2.1.85 and 2.1.92. However, this also raises the possibility of inducing significant mitochondrial mass increases, with minor effects on mitophagy, through increased use of mitochondrial biogenesis induction over mitophagy inhibition, in extract 2.1.92 for example. Such as prospect could be used to stimulate mitochondrial mass turnover during mitochondrial biogenesis. This presents as a potential means for the selective removal of dysfunctional mitochondria, via membrane potential dependent mitophagy pathways – section 1.5.2, without lowering mitochondrial mass.

Replicate analysis of the extracts using mitoQC techniques is required to confirm the observations of the pilot experiment. It is also suggested that a series of time-course experiments are used to assess how mitophagy rate changes during, and after, extract exposure. A suggested hypothesis is that mitophagy will no longer be suppressed after extract removal, thereby mitochondrial mass would return to a basal level, necessitating continuous extract exposure to maintain the increased mitochondrial mass. Further investigations were not carried out during the current project, due to the caseation of the collaboration between Nanna Therapeutics and WCMR.

6.3 Development of an Immunofluorescent Method for Mitochondrial Defect Quantification and Phenotypic High Throughput Screening

The development of a novel immunofluorescent microscopy method, in the current project, for the high throughput assessment of CI and CIV levels within fibroblasts opens possibilities for the screening of large compound libraries for novel lead identification. It could also potentially be used in mitochondrial disease diagnosis. Whole-genome sequencing (WGS) has rapidly become the primary means of mitochondrial disease diagnosis, the rate-limiting factor for clinical diagnoses is now confirmatory assays that assess patient samples for deficiencies in mitochondrial complexes (Schon et al., 2020). Mitochondrial disease patients consult eight clinical professionals on average, during which time 70% will undergo muscle biopsy and more than half will be misdiagnosed before being correctly diagnosed with a mitochondrial disease. Furthermore, difficulty in correctly identifying the need for WGS early in the diagnostic process can also introduce delays (Grier et al., 2018). Current assays for mitochondrial complex abundancies use muscle analysis or gel-based methods, which limit sample throughput and can require invasive muscle biopsy procedures. It is envisaged that high throughput immunofluorescent techniques can aid in the diagnostic process, pending further validation against patient muscle tissue immunohistochemical analysis and other gold-standard techniques.

Should readily available cells be viably collected for analysis, the immunofluorescent analysis described in this project has the potential to be applied to the screening of the wider population, particularly in those of advanced age, to aid in the early identification of mitochondrial defects associated with common conditions of advanced age: cancers and neurodegenerative diseases.

The novel immunofluorescent method has also been applied to the development of a current lead compound of pharmaceutical interest: MOA2. The method has demonstrated the dose-dependent partial rescue of deficient complexes in CI, and CIV, deficient mitochondrial disease patient-derived cell lines. Lead optimisation experiments based on the structure of MOA2 are currently underway, to both discover a more potent lead and to contribute to the mechanism of action studies for this drug. The novel immunofluorescent method has significant potential applications in this endeavour, through being employed for the assessment of derivative compounds.

6.4 Final Conclusion

After decades of severely limited treatment options, the consistent application of innovation in the field of metabolic dysfunction, and mitochondrial disease, therapeutic discovery is expected to yield therapeutic new options in the future.

The current project has increased the pool of potential lead compounds by identifying ten bacterial extracts capable of increasing multiple parameters associated with mitochondrial mass. Active compounds within each extract require purification, activity confirmation and mechanistic elucidation, followed by pre-clinical trials before advancing to a clinical stage. It is hoped that the induction of mitochondrial biogenesis will mature into a widely relevant treatment option for those suffering from metabolic dysfunction and mitochondrial diseases.

This current project has further yielded a novel high throughput screening method for the identification of compounds capable of rescuing CI and CIV deficiencies. The method was employed against a current lead compound (MOA2) and demonstrated its ability to partially rescue CI and CIV levels, in relevant deficient cell lines. The method will next be employed in the lead optimisation of MOA2 and to aid in the elucidation of its mechanisms of action. Pending future positive pre-clinical and clinical investigations, it is hoped that a high potency derivative of MOA2 will be safely available as a treatment for biochemical defects in human patients.

Chapter 7:

Appendices

7.1. Appendix A. Analysis code used in R Studio to process all flow cytometry screening data, Chapter 3. Originally authored by Dr J. Grady, Institute of Neuroscience, Newcastle University; optimised for use in this project.

```
library(reshape2) library(plyr) library(ggplot2)

library('xlsx')

library(gridExtra)

library(grid)

library(ggplot2)

#library(lattice)

#CHANGE DESINATION FOLDER FOR EACH RUN

z <- read.csv(FILE LOCATION, stringsAsFactors = F) chans <- c('488','561')

my_theme <- theme_bw() +

theme(panel.border = element_blank())+

theme(axis.line.x = element_line(color = 'black')) +

theme(axis.line.y = element_line(color = 'black')) +

theme(text = element_text(size=16))+ theme(strip.background = element_blank())+ theme(legend.key
= element_blank())

z$ndc <- substr(z$Tube.Name, 1, 3 ) == 'NDC'

n <- subset(z, ndc == T) d <- subset(z, ndc == F)

d1 <- merge(n, d, by = c('Group'), suffix=c('.N','.D'))

dspl <- ldply(chans, function(x){ cols <- c('Group','Tube.Name.D',

paste('mean_', x,'.N',sep=''), paste('sd_', x,'.N',sep=''), paste('mean_', x,'.D',sep=''), paste('sd_',
x,'.D',sep=''))

dx <- subset(d1, select = cols)

#Correct D by N

names(dx) <- c('grp','sample','m_n','sd_n','m_d','sd_d') dx$mean <- with(dx, (m_d - m_n)/sd_n)

dx$sd <- with(dx, sd_d/sd_n)

dx$chan <- x

return (dx[,c('grp','sample','chan','mean','sd')]) })

d1 <- merge(subset(dspl, chan==chans[1]), subset(dspl, chan==chans[2]), suffix = paste('.',chans,
sep=''), by = c('grp','sample'))

d1$Compound <- as.factor(sapply(d1$sample, function(x)
return(unlist(strsplit(as.character(x),"_")[[1]][1])))

d1$Dose <- as.numeric(sapply(d1$sample, function(x)
return(unlist(strsplit(as.character(x),"_")[[1]][2])))

#CHANGE DESINATION FOLDER FOR EACH RUN

lookup <- read.csv(FILE LOCATION, stringsAsFactors=F)
```

```
d1 <- merge(d1, lookup, all.x=T)

d1$C_Name <- d1$C_Name

d1[is.na(d1$C_Name),'C_Name'] <- as.character(d1[is.na(d1$C_Name),'Compound']) int_f <-
function(x, mu1, mu2, sd1, sd2) {

f1 <- dnorm(x, mean=mu1, sd=sd1)

f2 <- dnorm(x, mean=mu2, sd=sd2)

pmax(f2 - f1,0) #If f2 > f1 then the difference between them, otherwise 0 }

figs <- list()

for (row in 1:nrow(d1)) {

intervals <- list(c(0,1),c(1,2),c(2,10),c(10,Inf))

ul <- ldply(chans, function(x){

mean_str <- paste('mean.',x,sep='')

a <- sum(unlist(lapply(intervals, function(intvl)

round(integrate(int_f, intvl[1], intvl[2], mu1=0, mu2=d1[row, mean_str] ,

sd1=1,

sd2=d1[row, paste('sd.',x,sep='')], subdivisions = 10000L )$value*100,1))))

b <- sum(unlist(lapply(intervals, function(intvl) round(integrate(int_f, -intvl[2], -intvl[1], mu1=0,

mu2=d1[row, mean_str] ,

sd1=1,

sd2=d1[row, paste('sd.',x,sep='')], subdivisions = 10000L )$value*100,1))))

return (data.frame(chan = x, upr = a, lwr=b, mean=d1[row, mean_str])) })

ul$height <- c(0.42, .46)

ul$sample <- d1[row,'sample'] ul$Compound <- d1[row,'C_Name']

ul$Dose <- d1[row,'Dose']

ul$Group <- d1[row,'grp']

p <-

ggplot(data.frame(x = c(-12, 12)), aes(x)) +

stat_function(fun=dnorm, color="darkgrey",linetype='dotted')+ theme(legend.position="none")+

my_theme +

annotate("text",x=5.8,y=0.5,hjust=1,size=5,label=paste(d1[row, 'C_Name'],d1[row, 'Dose'])) +
scale_color_manual(values=c('#00AA00','#AA0000')) + ylab('')+xlab('')+

theme(text = element_text(size=10)) + scale_y_continuous(labels = NULL)+ylim(0,0.5)

p <- p + geom_text(x=5.8,hjust=1,size=5, data=ul, aes(color=chan, y=height, label=paste(chan, ' ',
lwr,'% ',upr,'%',sep='')))

p <- p + stat_function(fun=dnorm, aes(color=chans[1]), args = list(mean=d1[row,
paste('mean.',chans[1],sep='')], sd=d1[row, paste('sd.',chans[1],sep='')]))
```

```
p <- p + stat_function(fun=dnorm, aes(color=chans[2]), args = list(mean=d1[row,
paste('mean.',chans[2],sep='')], sd=d1[row, paste('sd.',chans[2],sep='')]))

p

# p <- p + llply(chans, function(chan){})

p$ul <- ul figs[[row]] <- p }

#CHANGE DESINATION FOLDER FOR EACH RUN pdf('FILE LOCATION',width=30, height=150)
do.call("grid.arrange", c(figs, ncol=5))

dev.off()

#Scatter plot

vals <- ldply(figs, function(x){

d <- x$ul

return (d) })

vals$shift <- with(vals, upr-lwr)

data_wide <- dcast(vals, Group + Compound + Dose ~ chan, value.var="shift") names(data_wide) <-
c('Group','Compound','Dose','MTG','TMRM')

d <- data_wide d$Group<-as.factor(d$Group)

cols <- rep(c("#BF4D4D", "#BFBF4D", "#4DBF4D", "#4DBFBF", "#4D4DBF", "#BF4DBF", "#FAAABF",
"#DF5B3A","#000000", "#E69F00", "#56B4E9", "#009E73", "#F0E442", "#0072B2", "#D55E00",
"#CC79A7","#999999", "#E69F00", "#56B4E9", "#009E73", "#F0E442", "#0072B2", "#D55E00",
"#CC79A7"),10)

p <-

ggplot(data=d, aes(x=MTG,y=TMRM,color=Compound)) + geom_point(alpha=0.8,size=4,) +
#geom_text(size=3,color="black",aes(label=Compound, x=MTG.delta+.1, hjust=0))+

geom_vline(color="red",xintercept=0)+geom_hline(color="red",yintercept=0)+my_theme +
xlab("COXVIII GFP Shift")+ ylab("TMRM Shift") + xlim(-100, 100) + ylim(-100, 100)+
theme(axis.text=element_text(size=8),axis.title=element_text(size=10), legend.position="none") +
scale_shape_manual(values=c(0,1,2,3,4,5,6,7,8,9)) +

#scale_shape(solid=TRUE) + geom_text(aes(label=Dose),color="white",size=1)+
scale_colour_manual(values=cols)+coord_fixed()

#CHANGE DESINATION FOLDER FOR EACH RUN pdf('FILE LOCATION.pdf', width=15, height=10)
print(p)

dev.off()

#CHANGE DESINATION FOLDER FOR EACH RUN pdf('FILE LOCATION.pdf',width=70, height=50)

print(p +facet_wrap(~Compound, ncol=10)) dev.off()

#CHANGE DESINATION FOLDER FOR EACH RUN pdf(('FILE LOCATION.pdf',width=7.5, height=5)

histTMRM<-hist(d$TMRM, breaks=20, freq=FALSE, xlab="TMRM increase", main="Distribution of
TMRM signal")

histGFP<-hist(d$MTG, breaks=20, freq=FALSE, xlab="GFP increase", main="Distribution of GFP
signal")

dev.off()
```

```
#CHANGE DESINATION FOLDER FOR EACH RUN write.csv(d, file = "(‘FILE LOCATION.csv’", )

MTG95<- subset(d, subset=(d$MTG >quantile(d$MTG, c(0.95)))) MTG75<- subset(d, subset=(d$MTG
>quantile(d$MTG, c(0.75))))

TMRM95<- subset(d, subset=(d$TMRM >quantile(d$TMRM, c(0.95)))) TMRM75<- subset(d,
subset=(d$TMRM >quantile(d$TMRM, c(0.75)))) #CHANGE DESINATION FOLDER FOR EACH RUN

write.csv(MTG95, file = "(‘FILE LOCATION.csv’", )

write.csv(MTG75, file = "(‘FILE LOCATION.csv’", ) write.csv(TMRM95, file = "(‘FILE LOCATION.csv’",
) write.csv(TMRM75, file = "(‘FILE LOCATION.csv’", )

shapiro.test(d$TMRM) qqnorm(d$TMRM)

shapiro.test(d$MTG) qqnorm(d$MTG)
```

7.2. Appendix B – Average fold change in markers for mitochondrial mass and membrane potential for all putative hit bacterial extracts received from Nanna Therapeutics. Wells containing TMRM stained, m-GFP expressing K652 cells treated with individual extracts were prepared and subjected to flow cytometry analysis as described in section 2.3.3. Colours denote different samples within each plot, each point represents an average reading from approximately 10,000 events from a single well of a 96-well plate in biological triplicate. Plots represent data from plates 2.1-2.4, left to right.

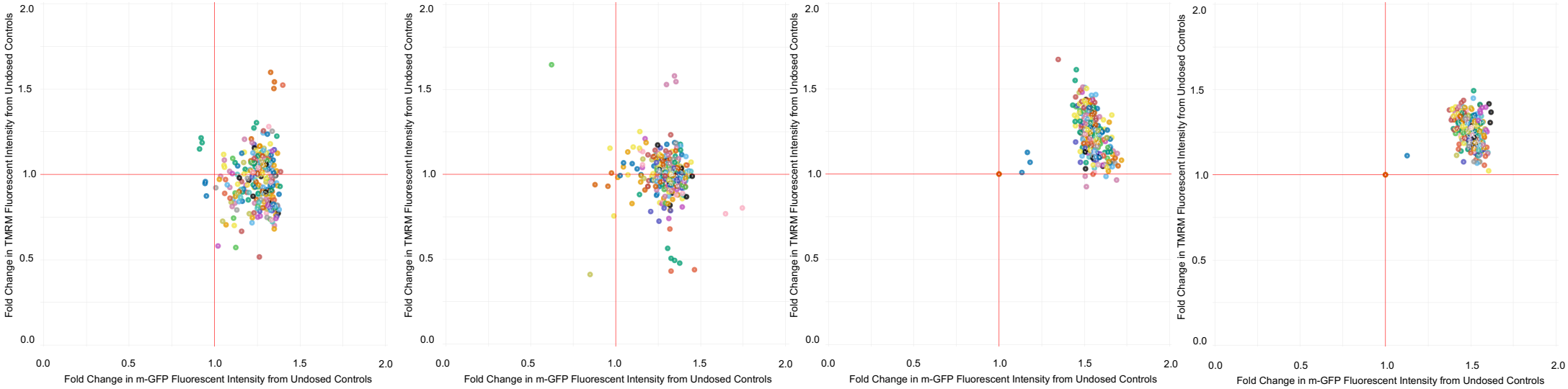

7.2. Appendix B continued – Average fold change in markers for mitochondrial mass and membrane potential for all putative hit bacterial extracts received from Nanna Therapeutics. Wells containing TMRM stained, m-GFP expressing K652 cells treated with individual extracts were prepared and subjected to flow cytometry analysis as described in section 2.3.3. Colours denote different samples within each plot, each point represents an average reading from approximately 10,000 events from a single well of a 96-well plate in biological triplicate. Plots represent data from plates 3.1-3.4, left to right.

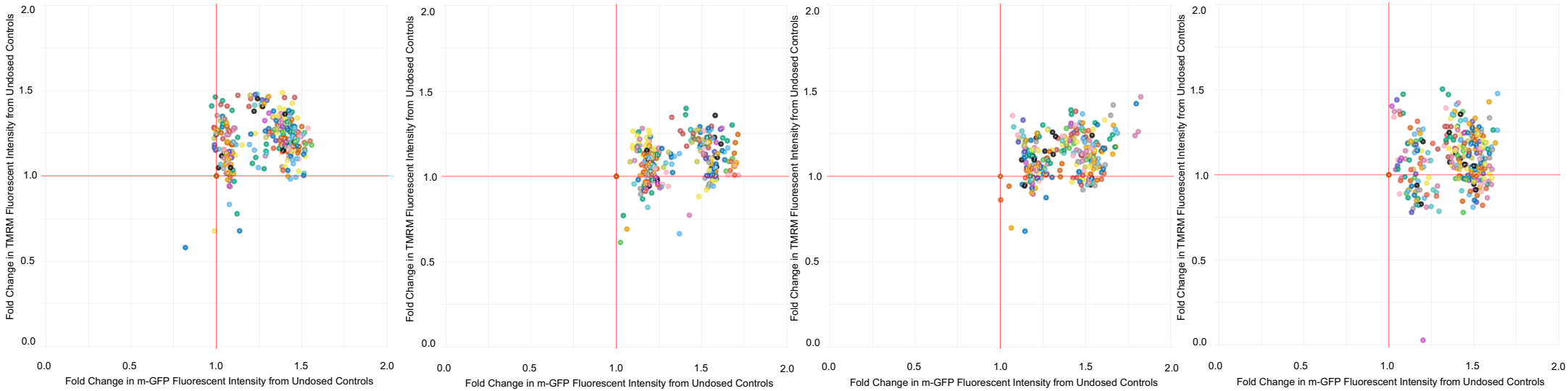

7.3. Appendix Ci Changes in parameters associated with increases in mitochondrial mass, by immunofluorescent staining, in fibroblasts incubated in hit extracts – Graphical representation of mean mitochondrial mass per unit cell area (mitochondrial density) in cells incubated in hit extracts, relative to no dose controls, n=16 images per condition. Each box within the plot panels contains a histogram (dark bars) showing the distribution values from individual images. A solid black line indicates the mean reading from no dose controls (DMEM only), dotted lines indicate the interquartile range of readings from no dose controls. All data has been normalised to the mean of no dose control cells and presented as a fold change. P<0.05: *, P<0.01: **, P<0.001: ***

7.3. Appendix Cii Changes in parameters associated with increases in mitochondrial mass, by immunofluorescent staining, in fibroblasts incubated in hit extracts – Graphical representation of mean mitochondrial mass per cell in cells incubated in hit extracts, relative to no dose controls, n=16 images per condition. Each box within the plot panels contains a histogram (dark bars) showing the distribution values from individual images. A solid black line indicates the mean reading from no dose controls (DMEM only), dotted lines indicate the interquartile range of readings from no dose controls. All data has been normalised to the mean of no dose control cells and presented as a fold change. P<0.05: *, P<0.01: **, P<0.001: ***

7.3. Appendix CIII Changes in parameters associated with increases in mitochondrial mass, by immunofluorescent staining, in fibroblasts incubated in hit extracts – Fig. 3.15. Graphical representation of TFAM immunofluorescent stained area per cell in cells incubated in hit extracts, relative to no dose controls, n=16 images per condition. Each box within the plot panels contains a histogram (dark bars) showing the distribution values from individual images. A solid black line indicates the mean reading from no dose controls (DMEM only), dotted lines indicate the interquartile range of readings from no dose controls. All data has been normalised to the mean of no dose control cells and presented as a fold change. P<0.05: *, P<0.01: **, P<0.001: ***

7.4. Appendix D - Columbus Image Quantification for Mitochondrial Area Per Unit Cell Area and TFAM Spot Count Per Cell. The default Columbus pipeline used in the quantification of TOM20 and TFAM immuno-stained areas in fibroblasts. Showing A, image import. B &C, nuclei and cytoplasm detection forming a cell mask. D & E, signal filtering of TOM20 and TFAM immuno-stained signals. F & G, detection of TOM20 and TFAM immuno-stained area. H, quantification of TOM20 immuno-stained area within cytoplasm area. I, quantification of TFAM immuno-stained area within TOM20 area. J, raw data output and normalisation to cell area and number.

A

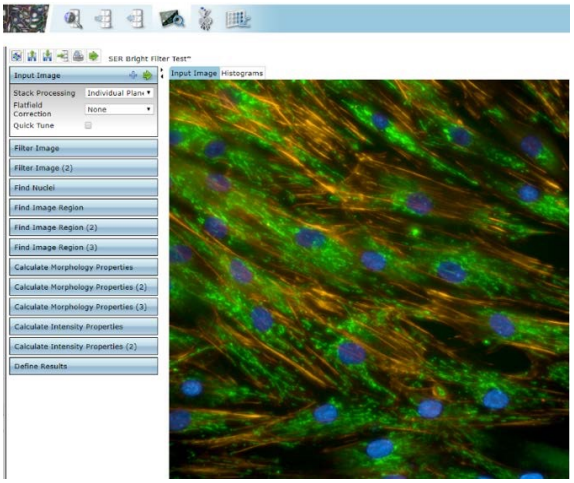

B

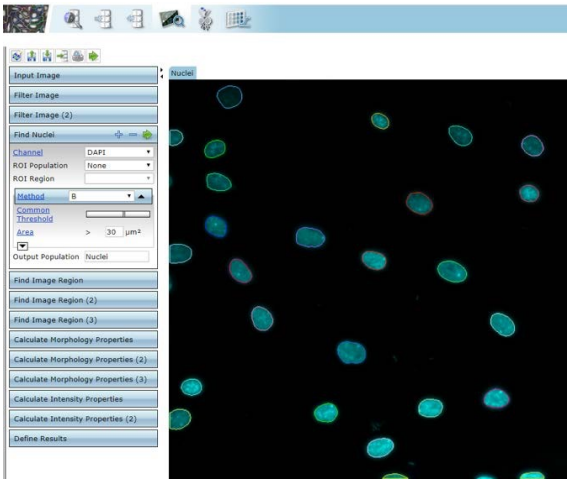

C

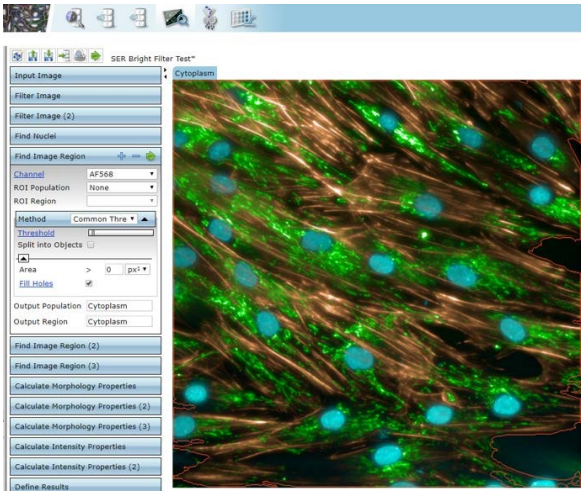

D

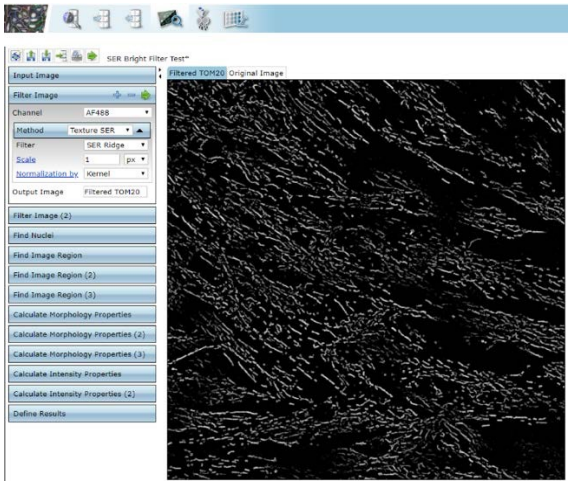

E

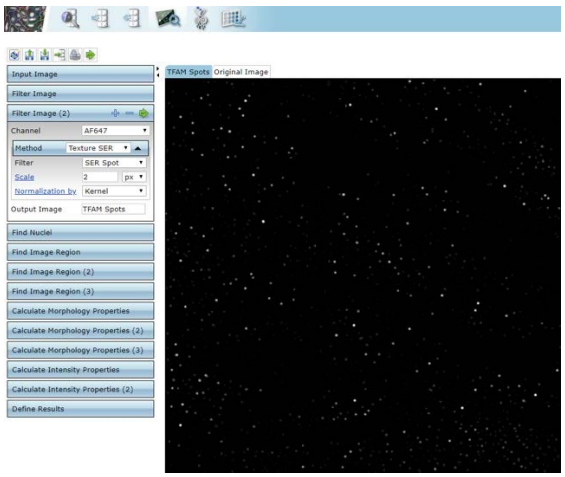

F

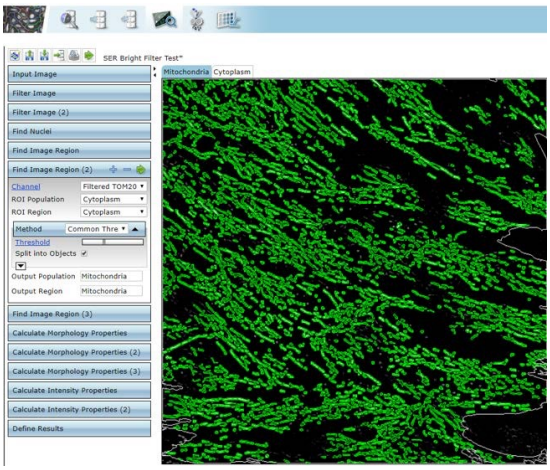
SER Bright Filter Test*
Input Image
Filter Image
Filter Image (2)
Find Nuclei
Find Image Region
Find Image Region (2)
Channel
Filtered TOM20
ROI Population
Cytoplasm
ROI Region
Cytoplasm
Method
Common Thre
Threshold
Split into Objects
Output Population
Mitochondria
Output Region
Mitochondria
Find Image Region (3)
Calculate Morphology Properties
Calculate Morphology Properties (2)
Calculate Morphology Properties (3)
Calculate Intensity Properties
Calculate Intensity Properties (2)
Define Results
Mitochondria
Cytoplasm

G

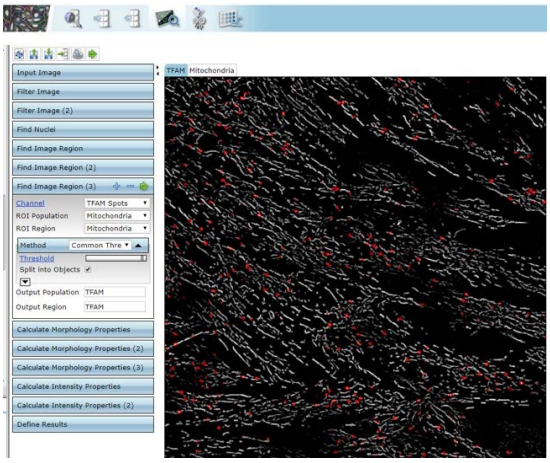
Input Image
Filter Image
Filter Image (2)
Find Nuclei
Find Image Region
Find Image Region (2)
Find Image Region (3)
Channel
TFAM Spots
ROI Population
Mitochondria
ROI Region
Mitochondria
Method
Common Thre
Threshold
Split into Objects
Output Population
TFAM
Output Region
TFAM
Calculate Morphology Properties
Calculate Morphology Properties (2)
Calculate Morphology Properties (3)
Calculate Intensity Properties
Calculate Intensity Properties (2)
Define Results
TFAM
Mitochondria

H

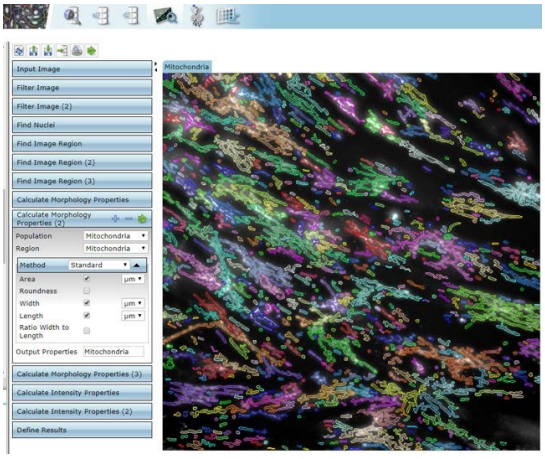
Input Image
Filter Image
Filter Image (2)
Find Nuclei
Find Image Region
Find Image Region (2)
Find Image Region (3)
Calculate Morphology Properties
Calculate Morphology Properties (2)
Population
Mitochondria
Region
Mitochondria
Method
Standard
Area
Roundness
Width
Length
Ratio Width to Length
Output Properties
Mitochondria
Calculate Morphology Properties (3)
Calculate Intensity Properties
Calculate Intensity Properties (2)
Define Results
Mitochondria

I

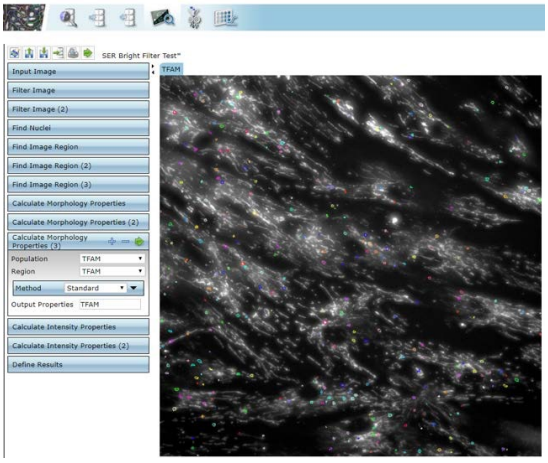
SER Bright Filter Test*
Input Image
Filter Image
Filter Image (2)
Find Nuclei
Find Image Region
Find Image Region (2)
Find Image Region (3)
Calculate Morphology Properties
Calculate Morphology Properties (2)
Calculate Morphology Properties (3)
Population
TFAM
Region
TFAM
Method
Standard
Output Properties
TFAM
Calculate Intensity Properties
Calculate Intensity Properties (2)
Define Results
TFAM

J

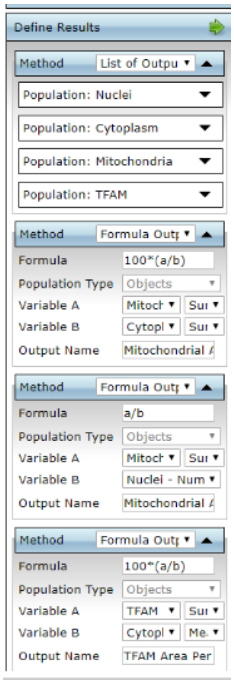

Results | Summary | Properties Nuclei

Download

Field	Nuclei - Number of Objects	Cytoplasm - Cytoplasm Area [µm²] - Sum per Well	Mitochondria - Mitochondria Area [µm²] - Sum per Well	Mitochondria - Mitochondria Width [µm] - Mean per Well	Mitochondria - Mitochondria Length [µm] - Mean per Well	Mitochondria - TOM20 Intensity Mean - Mean per Well	TFAM - Number of Objects	TFAM - TFAM Area [µm²] - Sum per Well	TFAM - TFAM Intensity Mean - Mean per Well	Mitochondrial Area Per Unit Cytoplasm (%)	Mitochondrial Area Per Cell	TFAM Area Per Unit Cytoplasm (%)	TFAM Area Per Unit Mitochondria (%)	TFAM Spots Per Nucleus
1	26	92332.355257	28275.4616057	2.30053041419	10.4506885368	3806.50230146	372	1087.93608644	4406.36824615	30.6235680082	1087.51775407	1.17828261113	7.27119955561	14.3076923077

7.5. Appendix E. Columbus Image Quantification for CI (NDUFA13), CII (SDHA), CIV (MTCOI) within TOM20 positive area (mitochondrial mask). Wild Type Fibroblasts are presented as an example. A) Input Image. TOM20 (AF405), SDHA (AF488), NDUFA13 (AF546, MTCOI (AF647). B) Imaging Filtering for Ridge Structures in Each Channel; Kernel normalisation. C) Selection of TOM20 area. Selection of POI signal within TOM20 Area. D) Quantification of Pixel Intensity Totals (sum) Selected POI Areas. E) Normalisation of Pixel Intensity Totals (sum) to Mitochondrial Area and Data reporting

A.

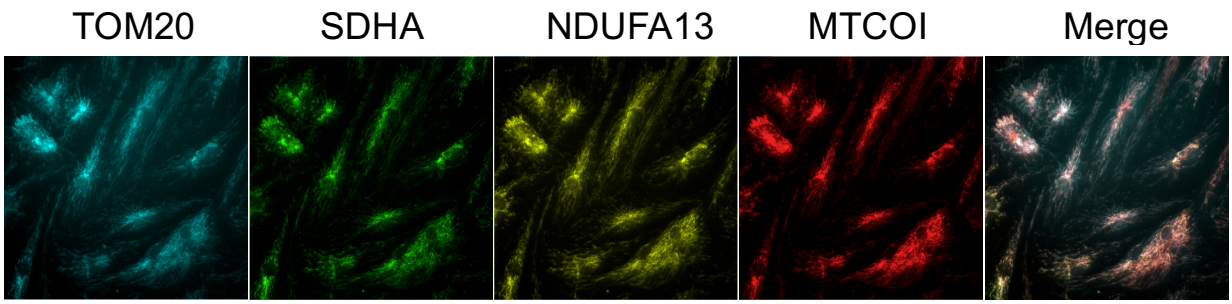

B.

C.

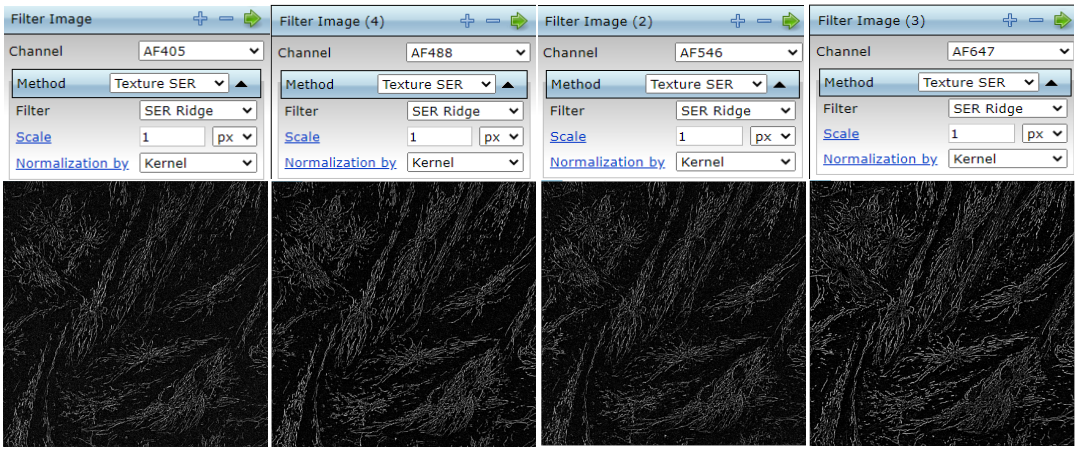

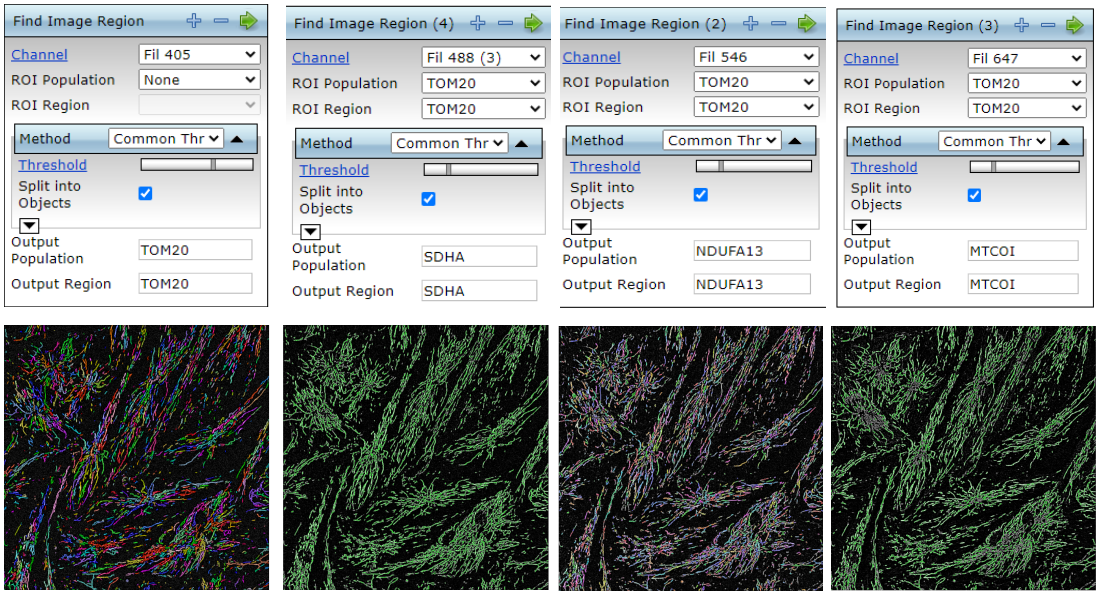

D.

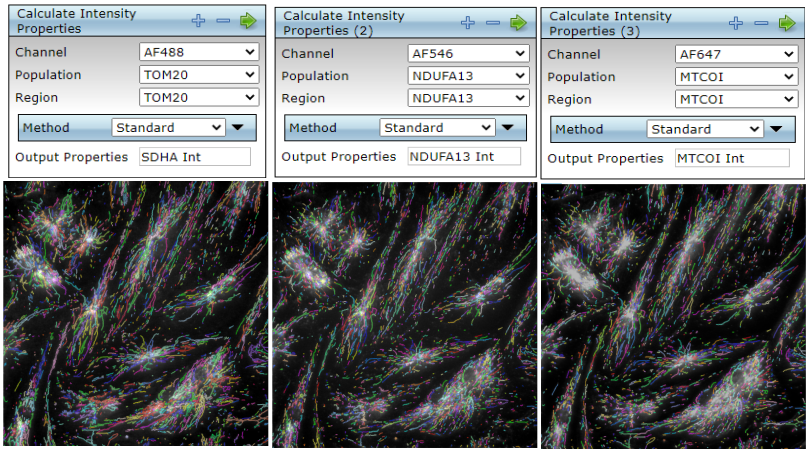
Calculate Intensity Properties
Channel AF488
Population TOM20
Region TOM20
Method Standard
Output Properties SDHA Int
Calculate Intensity Properties (2)
Channel AF546
Population NDUFA13
Region NDUFA13
Method Standard
Output Properties NDUFA13 Int
Calculate Intensity Properties (3)
Channel AF647
Population MTCOI
Region MTCOI
Method Standard
Output Properties MTCOI Int

E.

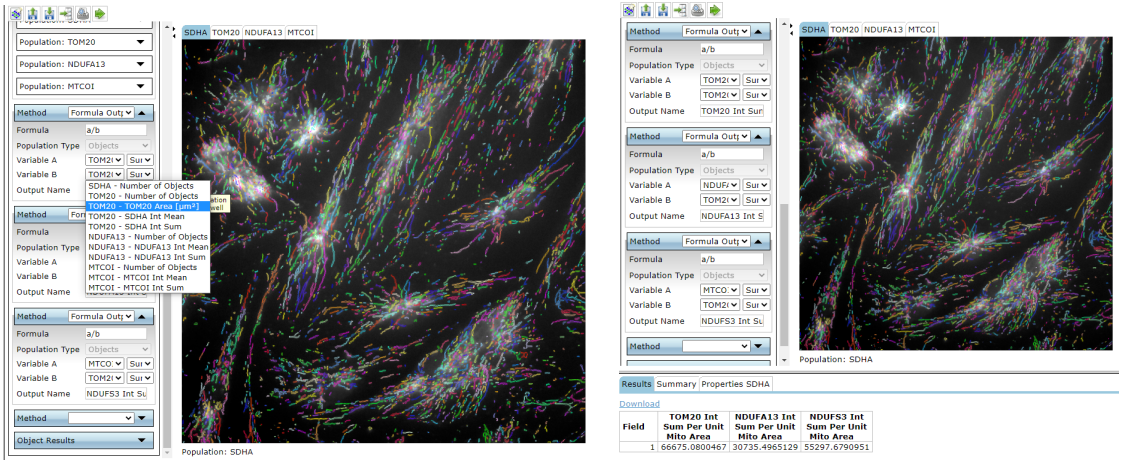
SDHA TOM20 NDUFA13 MTCOI
Population: SDHA
Results Summary Properties SDHA
Download
Field
TOM20 Int Sum Per Unit Mito Area
NDUFA13 Int Sum Per Unit Mito Area
NDUFS3 Int Sum Per Unit Mito Area
1 66675.0800467 30735.4965129 55297.6790951

Chapter 8:

References

AALTONEN, M., FRIEDMAN, J., OSMAN, C., SALIN, B., RAGO, J., NUNNARI, J., LANGER, T. & TATSUTA, T. 2016. MICOS and Phospholipid Transfer by Ups2-Mdm35 Organize Membrane Lipid Synthesis in Mitochondria. *Journal of Cell Biology,* 213**,** 525-534.

ABATE, M., FESTA, A., FALCO, M., LOMBARDI, A., LUCE, A., GRIMALDI, A., ZAPPAVIGNA, S., SPERLONGANO, P., IRACE, C., CARAGLIA, M. & MISSO, G. 2020. Mitochondria as playmakers of apoptosis, autophagy and senescence. *Seminars in Cell & Developmental Biology,* 98**,** 139-153.

ABE, Y., SHODAI, T., MUTO, T., MIHARA, K., TORIL, H. & KOHDA, D. 2000. Structural Basis of Presequence Recognition by the Mitochondrial Protein Import Receptor Tom20. *Cell,* 100**,** 551-560.

ABICHT, A., SCHARF, F., STEPHANIE, K., SCHÖN, U., HOLINSKI-FEDER, E., HORVATH, R., BENET-PAGÈS, A. & DIEBOLD, I. 2018. Mitochondrial and Nuclear Disease Panel (Mito-aND-Panel): Combined Sequencing of Mitochondrial and Nuclear DNA by a Cost-Effective and Sensitive NGS-Based Method. *Molecular Genetics & Genomic Medicine,* 6**,** 1188-1198.

ADZHUBEI, I., SCHMIDT, S., PESHKIN, L., RAMENSKY, V., GERASIMOVA, A., BORK, P., KONDRASHOV, A. & SUNYAEV, S. 2010. A Method and Server for Predicting Damaging Missense Mutations. *Nature Methods,* 7**,** 248-249.

AGARONYAN, K., MOROZOV, Y., ANIKIN, M. & TEMIAKOV, D. 2015. Mitochondrial Biology. Replication-transcription Switch in Human Mitochondria. *Science,* 347**,** 548-551.

AGIP, A., BLAZA, J., BRIDGES, H., VISCOMI, C., RAWSON, S., MUENCH, S. & HIRST, J. 2018. Cryo-EM structures of complex I from mouse heart mitochondria in two biochemically defined states. *Nature Structural and Molecular Biology,* 25**,** 548-556.

AHMED, S., ALSTON, C., HOPTON, S., HE, L., HARGREAVES, I., FALKOUS, G., OLÁHOVA, M., MCFARLAND, R., TURNBULL, D., ROCHA, M. & TAYLOR, R. 2017. Using a Quantitative Quadruple Immunofluorescent Assay to Diagnose Isolated Mitochondrial Complex I Deficiency. *Scientific Reports,* 7**,** 15676.

AHMED, S., CRAVEN, L., RUSSELL, O., TURNBULL, D. & VINCENT, A. 2018. Diagnosis and Treatment of Mitochondrial Myopathies. *Neurotherapeutics,* 15**,** 943-953.

AHTING, U., THIEFFRY, M., ENGELHARDT, H., HEGERL, R., NEUPERT, W. & NUSSBERGER, S. 2001. Tom40, the Pore-forming Component of the Protein-conducting TOM Channel in the Outer Membrane of Mitochondria. *Journal of Cell Biology,* 153**,** 1151-1160.

ALAM, T., KANKI, T., MUTA, T., UKAJI, K., ABE, Y., NAKAYAMA, H., TAKIO, K., HAMASAKI, N. & KANG, D. 2003. Human mitochondrial DNA is packaged with TFAM. *Nucleic Acids Research,* 31**,** 1640-1645.

ALLEN, M., PENNINGTON, E., PERRY, J., DADOO, S., MAKRECKA-KUKA, M., DAMBROVA, M., MOUKDAR, F., PATEL, H., HAN, X., KIDD, G., BENSON, E., RAISCH, T., POELZING, S., BROWN, D. & SHEIKH, S. 2020. The Cardiolipin-Binding Peptide Elamipretide Mitigates Fragmentation of Cristae Networks Following Cardiac Ischemia Reperfusion in Rats. *Communications Biology,* 3**,** 389.

ALPERS, B. 1931. Diffuse Progressive Degeneration of the Gray Matter of the Cerebrum. *Archives of Neurology and Psychiatry,* 25**,** 469-505.

ALSTON, C., ROCHA, M., LAX, N., TURNBULL, D. & TAYLOR, R. 2017. The Genetics and Pathology of Mitochondrial Disease. *The Journal of Pathology,* 241**,** 236-250.

ALTMANN, J., BUCHNER, B., NADAJ-PAKLEZA, A., SCHAFER, J., JACKSON, S., LEHMANN, D., DESCHAUR, M., KOPAJTICH, R., LAUTENSCHLAGER, R., KUHN, K., KARLE, K., SCHOLS, L., SCHULZ, J., WEIS, J., PROKISCH, H., KORNBLUM, C., CLAEYS, K. & KLOPSTOCK, T. 2016. Expanded Phenotypic Spectrum of the m.8344A>G "MERRF" Mutation: Data from the German mitoNET Registry. *Journal of Neurology,* 263**,** 961-972.

AMIRCHAGHMAGHI, M., DELAVARIAN, Z., IRANSHAHI, M., SHAKERI, M., MOZAFARI, P., MOHAMMADPOUR, A., FARAZI, F. & IRANSHAHY, M. 2015. A Randomised Placebo-Controlled Double Blind Clinical Trial of Quercetin for Treatment of Oral Lichen Planus. *Journal of Dental Research Dental Clinics and Dental Prospects,* 9**,** 23-28.

AMUNTS, A., BROWN, A., TOOTS, J., SCHERES, S. & RAMAKRISHNAN, V. 2015. Ribosome. The Structure of the Human Mitochondrial Ribosome. *Science,* 348**,** 95-98.

ANASTACIO, M., KANTER, E., MAKEPEACE, C., KEITH, A., ZHANG, H., SCHUESSLER, R., NICHOLS, C. & LAWTON, J. 2014. The Relationship Between Mitochondrial Matrix Volumes and Cellular

Volume in Response to Stress and The Role of the Adenosine Triphosphate Sensitive Potassium Channel. *Circulation,* 128.

ANDERSON, A. 2003. The Process of Structure-Based Drug Design. *Chemistry & Biology,* 10**,** 787-797.

ANDERSON, C. 1999. Mitochondrial Dysfunction in Diabetes Mellitis. *Drug Development Research,* 46.

ANDERSON, R., SHINDE, S., HILLE, R., ROTHERY, R., WEINER, J., RAJAGUKGUK, S., MAKLASHINA, E. & CECCHINI, G. 2014. Electron-transfer pathways in the heme and quinone-binding domain of complex II (Succinate Dehydrogenase). *Biochemistry,* 53**,** 1637-1646.

ANDERSON, S., BANKIER, A., BARRELL, B., BRUIJN, M. D., COULSON, A., DROUIN, J., EPERON, I., NIERLICH, D., ROE, B., SANGER, F., SCHREIER, P., SMITH, A., STADEN, R. & YOUNG, I. 1981. Sequence and organization of the human mitochondrial genome. *Nature,* 290**,** 457-465.

ANDREUX, P., HOUTKOOPER, R. & AUWERX, J. 2013. Pharmacological approaches to restore mitochondrial function. *Nature Reviews Drug Discovery,* 12**,** 465-483.

ANDREWS, H., NICHOLS, P., BATES, D. & TURNBULL, D. 2005. Mitochondrial Dysfunction Plays a Key Role in Progressive Axonal Loss in Multiple Sclerosis. *Medical Hypotheses,* 64**,** 669-677.

ANTONICKA, H. & SHOUBRIDGE, E. 2015. Mitochondrial RNA Granules Are Centers for Posttranscriptional RNA Processing and Ribosome Biogenesis. *Cell Reports,* 10**,** 920-932.

ANTONYUK, S., STRANGE, R., MARKLUND, S. & HASNAIN, S. 2009. The structure of human extracellular copper-zinc superoxide dismutase at 1.7 A resolution: insights into heparin and collagen binding. *Journal of Molecular Biology,* 388**,** 310-326.

ASHLEY, M., LAIPIS, P. & HAUSWIRTH, W. 1989. Rapid Segregation of Heteroplasmic Bovine Mitochondria. *Nucleic Acids Research,* 17**,** 7325-7331.

ATORINO, L., SILVESTRI, L., KOPPEN, M., CASSINA, L., CASSINA, L., BALLABIO, A., MARCONI, R., LANGER, T. & CASARI, G. 2003. Loss of m-AAA Protease in Mitochondria Causes Complex I Deficiency and Increased Sensitivity to Oxidase Stress in Hereditary Spastic Paraplegia. *The Journal of Cell Biology,* 163**,** 777-787.

AVULA, S., PARIKH, S., DEMAREST, S., KURZ, J. & GROPMAN, A. 2014. Treatment of Mitochondrial Disorders. *Current Treatment Options in Neurology,* 16**,** 292-312.

AY, M., LUO, J., LANGLEY, M., JIN, H., ANANTHARAM, V., KANTHASAMY, A. & KANTHASAMY, A. 2017. Molecular Mechanisms Underlying Protective Effects of Quercetin Against Mitochondrial Dysfunction and Progressive Dopaminergic Neurodegeneration in Cell Culture and MitoPark Transgenic Mouse Models of Parkinson's Disease. *Journal of Neurochemistry,* 141**,** 766-782.

BAAR, K., SONG, Z., SEMENKOVICH, C., JONES, T., HAN, D.-H., NOLTE, L., OJUKA, E., CHEN, M. & HOLLOSZY, J. 2003. Skeletal muscle overexpression of nuclear respiratory factor 1 increases glucose transport capacity. *The FASEB Journal,* 17.

BABCOCK, D., HERRINGTON, J., GOODWIN, P., PARK, Y. & HILLE, B. 1997. Mitochondrial Participation in the Intracellular Ca^{2+} Network. *Journal of Cell Biology,* 136**,** 833-844.

BACH, D., PICH, S., SORIANO, F., VEGA, N., BAUMGARTNER, B., ORIOLA, J., DAUGAARD, J., LLOBERAS, J., CAMPS, M., ZIERATH, J., RABASA-LHORET, R., WALLBERG-HENRILSSON, H., LAVILLE, M., PALACIN, M., VIDAL, H., RIVERA, F., BRAND, M. & ZORZANO, A. 2003. Mitofusin-2 Determines Mitochondrial Network Architecture and Mitochondrial Metabolism. *The Journal of Biological Chemistry,* 278**,** 17190-17197.

BACMAN, S., WILLIAMS, S., PINTO, M., PERALTA, S. & MORAES, C. 2013. Specific Elimination of Mutant Mitochondrial Genomes in Patient-Derived Cells by mitoTALENs. *Nature Medicine,* 19**,** 1111-1113.

BALDO, M. & VILARINHO, L. 2020. Molecular Basis of Leigh Syndrome: A Current Look. *Orphanet Journal of Rare Diseases,* 15.

BALFOUR, J. & FOSTER, R. 1999. Deferiprone: A Review of its Clinical Potential in Iron Overload β-Thalassaemia Major and Other Transfusion-Dependent Diseases. *Drugs,* 58.

BALLMOOS, C., WIEDENMANN, A. & DIMROTH, P. 2009. Essentials for ATP Synthesis by F1F0 ATP Synthases. *Annual Review of Biochemistry,* 78**,** 649-672.

BAREL, O., SHORER, Z., FLUSSER, H., OFIR, R., NARKIS, G., FINER, G., SHALEV, H., NASARA, A., SAADA, A. & BIRK, O. 2008. Mitochondrial Complex III Deficiency Associated with a Homozygous Mutation in UQCRQ. *The American Journal of Human Genetics,* 82**,** 1211-1216.

BARROW, J., BALSA, E., VERDEGUER, F., TAVARES, C., SOUSTEK, M., HOLLINGSWORTH, L., JEDRYCHOWSKI, M., VOGEL, R., PAULO, J., SMEITINK, J., GYGI, S., DOENCH, J., ROOT, D. & PUIGSERVER, P. 2016. Bromodomain Inhibitors Correct Bioenergetic Deficiency Caused by Mitochondrial Disease Complex I Mutations. *Molecular Cell,* 64**,** 163-175.

BATES, M., NEWMAN, J., JAKOVLJEVIC, D., HOLLINGSWORTH, K., ALSTON, C., ZALEWSKI, P., KLAWE, J., BLAMIRE, A., MACGOWAN, G., KEAVNEY, B., BOURKE, J., SCHAEFER, A., MCFARLAND, R., NEWTON, J., TURNBULL, D., TAYLOR, R., TRENELL, M. & GORMAN, G. 2013. Defining Cardiac Adaptation and Safety of Endurance Training in patients with m.3243A>G-Related Mitochondrial Disease. *International Journal of Cardiology,* 168**,** 3599-3608.

BELL, S. 2020. *Manipulating Mitophagy to Treat Mitochondrial Disease.* PhD, Newcastle University.

BELLA, D., LAZZARO, F., BRUSCO, A., PLUMARI, M., BATTAGLIA, G., PASTORE, A., FINARDI, A., CAGNOLI, C., TEMPIA, F., FRONTALI, M., VENEZIANO, L., SACCO, T., BODA, E., BRUSSINO, A., BONN, F., CASTELLOTTI, B., BARATTA, S., MARIOTTI, C., GELLERA, C., FRACASSO, V., MAGRI, S., LANGER, T., PLEVANI, P., DONATO, S., FALCONI, M. & TARONI, F. 2010. Mutation in the Mitochondrial Protease Gene AFG3L2 Cause Dominant Hereditary Ataxia SCA28. *Nature Genetics,* 42**,** 313-321.

BENDER, A., KRISHNAN, K., MORRIS, C., TAYLOR, G., REEVE, A., PERRY, R., JAROS, E., HERSHESON, J., BETTS, J., KLOPSTOCK, T., TAYLOR, R. & TURNBULL, D. 2006. High levels of mitochondrial DNA deletions in substantial mitra neutrons in aging and Parkinson disease. *Nature Genetics,* 38**,** 515-517.

BEREITER-HAHN, J. & VOTH, M. 1994. Dynamics of Mitochondria in Living Cells: Shape changes, Dislocations, Fusion and Fission of Mitochondria. *Microscopy Research and Technique,* 27**,** 198-219.

BESSE-PATIN, A., LEVEILLE, M., OROPEZA, D., NGUYEN, B., PRAT, A. & ESTALL, J. 2017. Estrogen Signals Through Peroxisome Proliferator-Activated Receptor-Gamma Coactivator 1-Alpha to Reduce Oxidative Damage Associated With Diet-Induced Fatty Liver Disease. *Gastroenterology,* 152**,** 243-256.

BIRK, A., LIU, S., SOONG, Y., MILLIS, W., SINGH, P., WARREN, D., SESHAN, S., PARDEE, J. & SZETO, H. 2013. The Mitochondrial-Targeted Compound SS-31 Re-Energises Ischemic Mitochondria by Interacting with Cardiolipin. *Journal of the American Society of Nephrology,* 24**,** 1250-1261.

BLACKER, T. & DUCHEN, M. 2016. Investigating Mitochondrial Redox State Using NADH and NADPH Autofluorescence. *Free Radical Biology and Medicine,* 100**,** 53-63.

BLACKSTONE, N. 2015. The impact of mitochondrial endosymbiosis on the evolution of calcium signaling. *Cell Calcium,* 57**,** 133-139.

BLAKELY, E., ALSTON, C., LECKY, B., CHAKRABARTI, B., FALKOUS, G., TURNBULL, D., TAYLOR, R. & GORMAN, G. 2014. Distal Weakness with Respiratory Insufficiency Caused by the m/8344A>G "MERRF" Mutation. *Neuromuscular Disorders,* 24**,** 533-536.

BOGENHAGEN, D. & HALEY, J. 2020. Pulse-chase SILAC-based Analysis Reveal Selective Oversynthesis and Rapid Turnover of Mitochondrial Protein Components of Respiratory Complexes. *Journal of Biological Chemsitry,* 295**,** 2544-2554.

BONEKAMP, N., PETER, B., HILLEN, H., FELSER, A., BERGBREDE, T., CHOIDAS, A., HORN, M., UNGER, A., LUCREZIA, R., ATANASSOV, I., LI, X., KOCH, U., MENNINGER, S., BOROS, J., HABENBERGER, P., GIAVALISCO, P., CRAMER, P., DENZEL, M., NUSSBAUMER, P., KLEBL, B., FALKENBERG, M., GUSTAFFSON, C. & LARSSON, N. 2020. Small-molecule inhibitors of human mitochondrial DNA transcription. *Nature,* 588**,** 712-716.

BONNET, D., RUSTIN, P., ROTIG, A., BIDOIS, J., MUNNICH, A., VOUHE, P., KACHANER, J. & SIDI, D. 2001. Heart Transplantation in Children with Mitochondrial Cardiomyopathy. *Heart,* 86**,** 570-573.

BORDT, E., CLERC, P., ROELOFS, B., SALADINO, A., TRETTER, L., ADAM-VIZI, V., CHEROK, E., KHALIL, A., YADAVA, N., GE, S., FRANCIS, C., KENNEDY, N., PICTON, L., KUMAR, T., UPPULURI, S., MILLER, A., ITOH, K., KARBOWSKI, M., SESAKI, H. & POLSTER, B. 2017. The Putative Drp1 Inhibitor mdivi-1 is a Reversible Mitochondrial Complex I Inhibitor that Modulates Reaction Oxygen Species. *Developmental Cell,* 40**,** 583-594.e6.

BORGESON, E., BORGESON, V., GODSON, C. & SHARMA, K. 2016. Therapeutic Potential of AICAR in Attenuating Obesity-Induced Metabolic, Liver and Kidney Disease. *The FASEB Journal,* 30.

BORGSTAHL, G., PARGE, H., HICKEY, M., JOHNSON, M., BOISSINOT, M., HALLEWELL, R., LEPOCK, J., CABELLI, D. & TAINER, J. 1996. Human mitochondrial manganese superoxide dismutase polymorphic variant Ile58Thr reduces activity by destabilising the tetrameter interface. *Biochemistry,* 35**,** 4287-4297.

BORRA, M., SMITH, B. & DENU, J. 2005. Mechanism of Human SIRT1 Activation by Resveratrol. *The Journal of Biological Chemistry,* 280**,** 17187-17195.

BOWMAN, S. & BREN, K. 2008. The chemistry and biochemistry of heme c: function bases for covalent attachment. *Natural Product Reports,* 25**,** 1118-1130.

BUCHET, K. & GODINOT, C. 1998. Functional F1-ATPase essential in maintaining growth and membrane potential of human mitochondrial DNA-depleted rho degrees cells. *The Journal of Biological Chemistry,* 273**,** 22983-22989.

BÉNIT, P., LEBON, S. & RUSTIN, P. 2009. Respiratory-chain Diseases Related to Complex III Deficiency. *Biochimica et Biophysica Acta - Molecular Cell Research,* 1793**,** 181-185.

BÉNIT, P., SLAMA, A., CARTAULT, F., GIURGEA, I., CHRETIEN, D., LEBON, S., MARSAC, C., MINNUCH, A., RÖTIG, A. & RUSTIN, P. 2004. Mutant NDUFS3 Subunit of Mitochondrial Complex I Causes Leigh Syndrome. *Journal of Medical Genetics,* 41**,** 14-17.

CALVO, S., CLAUSER, K. & MOOTHA, V. 2016. MitoCarta2.0: an updated inventory of mammalian mitochondrial proteins. *Nucleic Acids Research,* 44**,** 1251-1257.

CAMP, K., KROTOSKI, D., PARISR, M., GWINN, K., COHEN, B., COX, C., ENNS, G., FALK, M., GOLDSTEIN, A., SRIVASTAVA, R., GORMAN, G., HERSH, S., HIRANO, M., HOFFMAN, F., KARAA, A., MACLEOD, E., MCFARLAND, R., MOHAN, C., MULBERG, A., ODENKIRCHEN, J., PARIKH, S., RUTHERFORD, P., ANDERSON, S., TANG, W., VOCKLEY, J., WOLFE, L., YANNICELLI, S., YESKE, P. & COATES, P. 2016. Nutritional Interventions in Primary Mitochondrial Disorders: Developing an Evidence Base. *Molecular Genetics and Metabolism,* 119**,** 187-206.

CAMPBELL, G., ZIABREVA, I., REEVE, A., KRISHNAN, K., REYNOLDS, R., HOWELL, O., LASSMANN, H., TURNBULL, D. & MAHAD, D. 2011. Mitochondrial DNA Deletions and Neurodegeneration in Multiple Sclerosis. *Annuals of Neurology,* 69**,** 481-492.

CANTÓ, C. & AUWERX, J. 2009. Caloric restriction, SIRT1 and longevity. *Trends in Endocrinology & Metabolism,* 20**,** 325-331.

CAO, X., ANTONYUK, S., SEETHARAMAN, S., WHITSON, L., TAYLOR, A., HOLLOWAY, S., STRANGE, R., DOUCETTE, P., VALENTINE, J., TIWARI, A., HAYWARD, L., PADUA, S., COHLBERG, J., HASNAIN, S. & HART, P. 2008. Structures of the G85R Variant of SOD1 in Familial Amyotrophic Lateral Sclerosis. *Journal of Biological Chemistry,* 283**,** 16169-16177.

CARDENAS, C., MILLER, R., SMITH, I., BUI, T., MOLGO, J., MULLER, M., VAIS, H., CHUNG, K., YANG, J., PARKER, I., THOMPSON, C., BIRNBAUM, M., HALLOWS, K. & FOSKETT, J. 2010. Essential Regulation of Cell Bioenergetics by Constitutive $InsP_3$ receptor Ca^{2+} Transfer to Mitochondria. *Cell,* 142**,** 270-283.

CARLING, P., CREE, L. & CHINNERY, P. 2011. The Implications of Mitochondrial DNA Copy Number Regulation During Embryogenesis. *Mitochondrion,* 11**,** 686-692.

CARRARO, M., CARRER, A., URBANI, A. & BERNARDI, P. 2020. Molecular Nature and Regulation of the Mitochondrial Permeability Transition Pore(s), drug target(s) in cardioprotection. *Journal of Molecular And Cellular Cardiology,* 144**,** 76-86.

CARROLL, A., PORTER, R. & MORRICE, N. 2008. Identification of Serine Phosphorylation in Mitochondrial Uncoupling Protein 1. *Biochimica et Biophysica Acta,* 1777**,** 1060-1065.

CASSIDAY-STONE, A., CHIPUK, J., INGERMAN, E., SONG, C., YOO, C., KUWANA, T., KURTH, M., SHAW, J., HINSHAW, J., GREEN, D. & NUNNARI, J. 2008. Chemical Inhibition of the Mitochondrial Division Dynamic Reveals in Role in Bax/Bak-Dependent Mitochondrial Outer Membrane Permeabilization. *Developmental Cell,* 14**,** 193-204.

CASSIDY-STONE, A., CHIPUK, J., INGERMAN, E., SONG, C., YOO, C., KUWANA, T., KURTH, M., SHAW, J., HINSHAW, J., GREEN, D. & NUNNARI, J. 2008. Chemical Inhibition of the Mitochondrial Division Dynamin Reveals Its Role in Bax/Bak-Dependent Mitochondrial Outer Membrane Permeabilization. *Developmental Cell,* 14**,** 193-204.

CECCHINI, G. 2003. Function and structure of complex II of the respiratory chain. *Annual Review of Biochemistry,* 72**,** 77-109.

CERUTTI, R., PIRINEN, E., LAMPERTI, C., MARCHET, S., SAUVE, A., LI, W., LEONI, V., SCHON, E., DANTZER, F., AUWERX, J., VISCOMI, C. & ZEVIANI, M. 2014. NAD+-Dependent Activation of Sirt1 Corrects the Phenotype in a Mouse Model of Mitochondrial Disease. *Cell Metabolism,* 19**,** 1042-1049.

CHAN, D. 2012. Fusion and Fission: Interlinked Processes Critical for Mitochondrial Health. *Annual Review of Genetics,* 46**,** 265-287.

CHAN, S. & COPELAND, W. 2009. DNA Polymerase Gamma and Mitochondrial Disease: Understand the Consequence of POLG Mutations. *Biochimica et Biophysica Acta - Bioenergetics,* 1787**,** 312-319.

CHATFIELD, K., SPARAGNA, G., CHAU, S., PHILIPS, E., AMBARDEKAR, A., AFTAB, M., MITCHELL, M., SUCHAROV, C., MIYAMOTO, S. & STAUFFER, B. 2019. Elamipretide Improves Mitochondrial Function in the Failing Human Heart. *Journal of the American College of Cardiology: Basic to Translational Science,* 4**,** 147-157.

CHEN, C., TURNBULL, D. & REEVE, A. 2019a. Mitochondrial Dysfunction in Parkinson's Disease - Cause or Consequence. *Biology (Basel),* 8**,** 38.

CHEN, C., TURNBULL, D. & REEVE, A. 2019b. Mitochondrial Dysfunction in Parkinson's Disease - Cause or Consequence? *Biology (Basel),* 8**,** 38.

CHEN, G., HAN, Z., FENG, D., CHEN, Y., CHEN, L., WU, H., HUANG, L., ZHOU, C., CAI, X., FU, C., DUAN, L., WANG, X., LIU, L., LIU, X., SHEN, Y., ZHU, Y. & CHEN, Q. 2014. A regulatory signalling loop comprising the PGAM5 phosphatase and CK2 control receptor-mediated mitophagy. *Molecular Cell,* 54**,** 362-377.

CHEN, L. 1988. Mitochondrial Membrane Potential in Living Cells. *Annual Review of Cell and Developmental Biology,* 4**,** 155-181.

CHENG, Q., CHEN, J., GUO, H., LU, J., ZHOU, J., GUO, X., SHI, Y., ZHANG, Y., YU, S., ZHANG, Q. & DING, F. 2021. Pyrroloquinoline quinone promotes mitochondrial biogenesis in rotenone-included Parkinson's disease model via AMPK activation. *Nature APS,* 42**,** 665-678.

CHINNERY, P., ANDREWS, R., TURNBULL, D. & HOWELL, N. 2001. Leber Hereditary Optic Neuropathy: Does Heteroplasmy Influence the Inheritance and Expression of the G11778A Mitochondrial DNA Mutation. *American Journal of Medical Genetics,* 98**,** 235-243.

CHINNERY, P., HOWELL, B., LIGHTOWLERS, R. & TURNBULL, D. 1997. Molecular Pathology of MELAS and MERRF. The Relationship Between Mutation Load and Clinical Phenotypes. *Brain,* 120**,** 1713-1721.

CHISTIAKOV, D., SOBENIN, I., REVIN, V., OREKHOV, A. & BOBRYSHEV, Y. 2014. Mitochondrial Aging and Age-Related Dysfunction of Mitochondria. *BioMed Research International,* 2014.

CHOWANADISAI, W., BAUERLY, K., TCHAPRIAN, E., WONG, A., CORTOPASSI, G. & RUCKER, R. 2010. Pyrroloquinoline Quinone Stimulates Mitochondrial Biogenesis through cAMP Response Element-binding Protein Phosphorylation and Increased PGC-1α Expression. *The Journal of Biological Chemistry,* 285**,** 142-152.

CIGANA, L. & BAKOVIC, M. 2014. Formation and Regulation of Mitochondrial Membranes. *International Journal of Cell Biology,* 2014.

CIPOLAT, S., RUDKA, T., HARTMANN, D., COSTA, V., SERNEELS, L., CRAESSAERTS, K., METZGER, K., FREEZE, C., ANNAERT, W., D'ADAMIO, L., DERKS, C., DEJAEGERE, T., PELLEGRINI, L., D'HOOGE, R., SCORRANO, L. & STROOPER, B. 2006. Mitochondrial Rhomboid PARL Regulates Cytochrome c Release During Apoptosis via OPA1-Dependent Cristae Remodelling. *Cell,* 126**,** 163-175.

CIVILETTO, G., DOGAN, S., CERUTTI, R., FAGIOLARI, G., MOGGIO, M., LAMPERTI, C., BENINCA, C., VISCOMI, C. & ZEVIANI, M. 2018. Rapamycin Rescues Mitochondrial Myopathy via Coordinated Activation of Autophagy and Lysosomal Biogenesis. *EMBO Molecular Medicine,* 10**,** e8799.

CLAEYS, K., ABICHT, A., HAUSLER, M., KLEINLE, S., WIESMANN, M., SCHULZ, J., HORVATH, R. & WEIS, J. 2016. Novel Genetic and Neuropathological Insights in Neurogenic Muscle Weakness, Ataxia and Retinitis Pigmentosa (NARP). *Muscle and Nerve,* 54**,** 328-333.

CLAYTON, D. 1982. Replication of animal mitochondrial DNA. *Cell,* 28**,** 693-705.

COHEN, A., GALANELLO, R., PIGA, A., DIPALMA, A., VULLO, C. & TRICTA, F. 2000. Safety Profile of the Oral Iron Chelator Deferiprone: A Multicentre Study. *British Journal of Haematology,* 108**,** 305-312.

COHEN, B., KARAA, A., HAAS, R., GOLDSTEIN, A. & VOCKLEY, G. 2018. Effects of Elamipretide in Adults with Primary Mitochondrial Myopathy: a Phase 2 Double-Blind, Randomised, Placebo-Controlled Crossover Trial (MMPOWER-2) (S5.003). *Neurology,* 90.

COLLET, J. & MESSENS, J. 2010. Structure, Function and Mechanism of Thioredoxin Proteins. *Antioxidants & Redox Signalling,* 13**,** 1205-1216.

COTTART, C.-H., NIVET-ANTOINE, V., LAGUILLIER-MORIZOT, C. & BEAUDEUX, J.-L. 2010. Resveratrol bioavailability and toxicity in humans. *Molecular Nutrition and Food Research,* 54**,** 7-16.

CRAIG, E. 2018. Hsp70 at the membrane: driving protein translocation. *BMC Biology,* 16**,** 1.

CRAMER, W., HASAN, S. & YAMASHITA, E. 2011. The Q cycle of cytochrome b c complexes: A structure perspective. *Biochimica et Biophysica Acta - Bioenergetics,* 1807**,** 788-802.

CRAVEN, L., ALSTON, C., TAYLOR, R. & TURNBULL, D. 2017. Recent Advances in Mitochondrial Disease. *Annual Review of Genomics and Human Genetics,* 18**,** 257-275.

CRAVEN, L., HERBERT, M., MURDOCH, A., MURPHY, J., DAVIES, J. & TURNBULL, D. 2016. Research into Policy: A Brief History of Mitochondrial Donation. *Stem Cells,* 34**,** 265-267.

CRAVEN, L., MURPHY, J. & TURNBULL, D. 2020. Mitochondrial Donation - Hope for Families with Mitochondrial DNA Disease. *Emerging Topics in Life Sciences***,** ETLS20190196.

CRAVEN, L., TUPPEN, H., GREGGAINS, G., HARBOTTLE, S., MURPHY, J., CREE, L., MURDOCH, A., CHINNERY, P., TAYLOR, R., LIGHTOWLERS, R., HERBERT, M. & TURNBULL, D. 2010. Pronuclear Transfer in Human Embryos to Prevent Transmission of Mitochondrial DNA Disease. *Nature,* 465**,** 82-85.

CREE, L., SAMUELS, D., LOPES, S., RAJASIMHA, H., WONNAPINIJ, P., MANN, J., DAHL, H. & CHINNERY, P. 2008. A Reduction of Mitochondrial DNA Molecules During Embryogenesis Explains the Rapid Segregation of Genotypes. *Nature Genetics,* 40**,** 249-254.

CRUZ-BERMUDEZ, A., VICENTE-BLANCO, R., HERNANDEZ-SIERRA, R., MONTERO, M., ALVAREZ, J., MANRIQUE, M., BLAZQUEZ, A., MARTIN, M., AYUSO, C., GARESSE, R. & FERNANDEZ-MORENO, M. 2016. Functional Characterization of Three Concomitant mtDNA LHON Mutations Shows No Synergistic Effect on Mitochondrial Activity. *PLOS One,* 11**,** e0146816.

CUI, H., KONG, Y. & ZHANG, H. 2012. Oxidative Stress, Mitochondrial Dysfunction and Aging. *Journal of Signal Transduction,* 2012**,** 646354.

CUNNINGHAM, J., RODGERS, J., ARLOW, D., VAZQUES, F., MOOTHA, V. & PUIGSERVER, P. 2007. mTOR controls mitochondrial oxidative function through a YY1–PGC-1α transcriptional complex. *Nature,* 450**,** 736–740.

CZUBRYT, M., MCANALLY, J., FISHMAN, G. & OLSON, E. 2003. Regulation of peroxisome proliferator-activated receptor γ coactivator 1α (PGC-1α) and mitochondrial function by MEF2 and HDAC5. *PNAS,* 100**,** 1711-1716.

DAS, R. & CHAKRAABARTI, O. 2020. Mitochondrial Hyperfusion: A Friend or a Foe. *Biochemical Society Transactions*.

DASSA, E., DUFOUR, E., GONCALVES, S., PAUPE, V., HAKKAART, G., JACOBS, H. & RUSTIN, P. 2009. Expression of the Alternative Oxidase Complements Cytochrome C Oxidise Deficiency in Human Cells. *EMBO Molecular Medicine,* 1**,** 30-36.

DAVINELLI, S., STEFANI, D., VIVO, I. & SCAPAGNINI, G. 2020. Polyphenols as Caloric Restriction Mimetics Regulating Mitochondrial Biogenesis and Mitophagy. *Trends in Endocrinology and Metabolism,* 31**,** 526-550.

DAVIS, J., MURPHY, E., CARMICHAEL, M. & DAVIS, B. 2009. Quercetin Increases Brain and Muscle Mitochondrial Biogenesis and Exercise Tolerance. *Exercise and Respiratory Physiology,* 296**,** R1071-R1077.

DE HAAS, R., DAS, D., GARANTO, A., RENKEMA, H., GREUPINK, R., BROEK, P., PERTIJS, J., COLLIN, R., WILLEMS, P., BEYRATH, J., HEERSCHAP, A., RUSSEL, F. & SMEITINK, J. 2017. Therapeutic Effects of the Mitochondrial ROS-Redox Modulator KH176 in a Mammalian Model of Leigh Disease. *Scientific Reports,* 7**,** 11733.

DE VOS, K., ALLAN, V., GRIERSON, A. & SHEETZ, M. 2005. Mitochondrial Function and Actin

Regulate Dynamin-Related Protein 1-Dependent Mitochondrial Fission. *Current Biology,* 15**,** 678–683.

DE VOS, K., MOROTZ, G., STOICA, R., TUDOR, E., LAU, K., ACKERLEY, S., WARLEY, A., SHAW, C. & MILLER, C. 2012. VAPB Interacts With the Mitochondrial Protein PTPIP51 to Regulate Calcium Homeostasis. *Human Molecular Genetics,* 21**,** 1299-1311.

DEMINE, S., RENARD, P. & ARNOULD, T. 2019. Mitochondrial Uncoupling: A Key Controller of Biological Processes in Physiology and Diseases. *Cells,* 8**,** 795.

DENNERLEIN, S., OELJEKLAUS, S., JANS, D., HELLWIG, C., BARETH, B., JAKOBS, S., DECKERS, M., WARSCHEID, D. & REHLING, P. 2015. MITRAC7 Acts as a COX1-Specific Chaperone and Reveals a Checkpoint during Cytochrome *c* Oxidase Assembly. *Cell Reports,* 12**,** 1644-1655.

DENTON, R. & MCCORMACK, J. 1986. The calcium sensitive dehydrogenase of vertebrate mitochondria. *Cell Calcium,* 7**,** 377-386.

DIAZ, F., FUKUI, H., GARCIA, S. & MORAES, C. 2006. Cytochrome *c* Oxidase is Required for the Assembly/Stability of Respiratory Complex I in Mouse Fibroblasts. *Molecular Cell Biology,* 26**,** 48972-4881.

DILLON, L., WILLIAMS, S., HIDA, A., PEACOCK, J., PROLLA, T., LINCOLN, J. & MORAES, C. 2012. Increased Mitochondrial Biogenesis in Muscle Improves Aging Phenotypes in the mtDNA Mutator Mouse. *Human Molecular Genetics,* 21**,** 2288-2297.

DONG, J., SULIK, K. & CHEN, S.-Y. 2008. NRF2-Mediated Transcriptional Induction of Antioxidant Response in Mouse Embryos Exposed to Ethanol *in vivo*: Implications for the Prevention of Fetal Alcohol Spectrum Disorders. *Antioxidants and Redox Signalling,* 10**,** 2023-2033.

DUARTE, A., PODEROSO, C., COOKE, M., GASTON, S., MACIEL, F., GOTTIFREDI, V. & PODESTA, E. 2012. Mitochondrial fusion is essential for steroid biosynthesis. *PLoS One,* 7**,** e45829.

DUCHARLET, J., THYAGARAJAN, D., IERINO, F., MCMAHON, L. & LEE, D. 2018. Perioperative Risk Assessment for Successful Kidney Transplant in Leigh Syndrome: A Case Report. *BMC Nephrology,* 19.

DUDKINA, N., KOURIL, R., PETERS, K., BRAUN, H. & BOEKEMA, E. 2010. Structure and function of mitochondrial supercomplexes. *Biochimica et Biophysica Acta - Bioenergetics,* 1797**,** 664-670.

DUDKINA, N., SUNDERHAUS, S., BOEKEMA, E. & BRAUN, H. 2008. The Higher Level of Organisation of the Oxidative Phosphorylation System: Mitochondrial Supercomplexes. *Journal of Bioenergetics and Biomembranes,* 40**,** 419-424.

EGAN, D., SHACKELFORD, D., MIHAYLOVA, M., GELINO, S., KOHNZ, R., MAIR, W., VASQUEZ, D., JOSHI, A., GWINN, D., TAYLOR, R., ASARA, J., FITZPATRICK, J., DILLIN, A., VOILLET, B., KUNDU, M., HANSEN, M. & SHAW, R. 2011. Phosphorylation of ULK1 (hATG1) by AMP-Activated Protein Kinase Connects Energy Sensing to Mitophagy. *Science,* 331**,** 456-461.

EICHNER, L. & GIGUÈRE, V. 2011. Estrogen related receptors (ERRs): A new dawn in transcriptional control of mitochondrial gene networks. *Mitochondrion,* 11**,** 544-552.

EL-HATTAB, A., ZARANTE, A., ALMANNAI, M. & SCAGLIA, F. 2014. Therapies for mitochondrial diseases and current clinical trials. *Molecular Genetics and Metabolism,* 122**,** 1-9.

ELGASS, K., PAKAY, J., RYAN, M. & PALMER, C. 2013. Recent advances into the understanding of mitochondrial fission. *Biochimica et Biophysica Act,* 1833**,** 150-161.

ELLOUZE, S., AUGUSTIN, S., BOUAITA, A., BONNET, C., SIMONUTTI, M., FORSTER, V., PICAUD, S., SAHEL, A. & DEBRINSKI, M. 2008. Optimised Allotopic Expression of the Human Mitochondrial ND4 Prevents Blindness in a Rat Model of Mitochondrial Dysfunction. *The American Journal of Human Genetics,* 83**,** 373-387.

ELSON, J., SAMUELS, D., TURNBULL, D. & CHINNERY, P. 2001. Random Intracellular Drift Explains the Clonal Expansion of Mitochondrial DNA Mutations with Age. *The American Journal of Human Genetics,* 68**,** 802-806.

EOM, S., LEE, H., LEE, S., KANG, H., LEE, J., KIM, H. & LEE, Y. 2017. Cause of Death in Children With Mitochondrial Diseases. *Pediatric Neurology,* 66**,** 82-88.

ERNSTER, L. & DALLNER, G. 1995. Biochemical, physiological and medical aspects of ubiquinone function. *Biochimica et Biophysica Acta,* 1271.

ESPOSITO, L., MELOV, S., PANOV, A., COTTRELL, B. & WALLACE, D. 1999. Mitochondrial Disease in Mouse Results in Increased Oxidative Stress. *PNAS,* 96**,** 4820-4825.

ESTEBAN-MARTINEZ, L., SIERRA-FILARDI, E., MCGREAL, R., SALAZAR-ROA, M., MARINO, G., SECO, E., DURAND, S., ENOT, D., GRANA, O., MALUMBRES, M., CVEKL, A., CUERVO, A., KROEMER, G. &

BOYA, P. 2017. Programmed mitophagy is essential for the glycolytic switch during cell differentiation. *EMBO,* 36**,** 1688-1706.
EVANS, R., BARISH, G. & WANG, Y.-X. 2004. PPARs and the complex journey to obesity. *Nature Medicine,* 10**,** 355-361.
FALKENBERG, M. 2018. Mitochondrial DNA Replication in Mammalian Cells: Overview of the Pathway. *Essays in Biochemistry,* 62**,** 287-296.
FALKENBERG, M., GASPARI, M., RANTANEN, A., TRIFUNOVIC, A., LARSSON, N.-G. & GUSTAFSSON, C. 2002. Mitochondrial transcription factors B1 and B2 activate transcription of human mtDNA. *Nature Genetics,* 31**,** 289-294.
FALKENBERG, M., LARSSON, N. & GUSTASSON, C. 2007. DNA replication and transcription in mammalian mitochondria. *Annual Review of Biochemistry,* 76**,** 679-699.
FAN, L., KIM, S., FARR, C., SCHAEFER, K. & RANDOLPH, K. 2006. A novel processive mechanism for DNA synthesis revealed by structure, modelling and mutagenesis of the accessory subunit of human mitochondrial DNA polymerase. *Journal of Molecular Biology,* 358**,** 1229-1243.
FARACI, M., CUZZUBBO, D., MICALIZZI, C., LANINO, E., MORALE, G., DALLORSO, S., CASTAGNOLA, E., SCHIAFFINO, M., BRUNO, C., ROSSI, A., DINI, G. & CAPPELLI, B. 2007. Allogenic Bone Marrow Translation for Pearson's Syndrome. *Bone Marrow Transplantation,* 39**,** 563-565.
FASSONE, E. & RAHMAN, S. 2012. Complex I Deficiency: Clinical Features, Biochemistry and Molecular Genetics. *Journal of Medical Genetics,* 49**,** 578-590.
FAXEN, K., GLIDERSON, G., ADELROTH, P. & BRZEZINSKI, P. 2005. A mechanistic principle for proton pumping by cytochrome c oxidase. *Nature,* 437**,** 286-289.
FEIGE, J. & AUWERX, J. 2007. Transcriptional coregulators in the control of energy homeostasis. *Trends in Cell Biology,* 17**,** 292-301.
FERNANDES, I., RUSSO, F., PIGNATARI, G., EVANGELINELLIS, M., TAVOLARI, S., MUOTRI, A. & BELTRÃO-BRAGA, P. 2016. Fibroblasts Sources: Where can we get them? *Cytotechnology,* 68**,** 223-228.
FERNANDEZ-AYALA, D., SANZ, A., VARTIAINEN, S., KEMPPAINEN, K., BABUSIAK, M., MUSTALAHTI, E., COSTA, R., TUOMELA, T., ZEVIANI, M., CHUNG, J., O'DELL, K., RUSTIN , P. & JACOBS, H. 2009. Expression of the Ciona Intestinalis Alternative Oxidase (AOX) in Drosophila Complements Defects in Mitochondrial Oxidative Phosphorylation. *Cell Metabolism,* 9**,** 449-460.
FERNANDEZ-MARCOS, P. & AUWERX, J. 2011. Regulation of PGC-1α, a nodal regulator of mitochondrial biogenesis. *The American Journal of Clinical Nutrition,* 93**,** 884-890.
FERNÁNDEZ-VIZARRA, E. & ZEVIANI, M. 2015. Nuclear Gene Mutations as the Cause of Mitochondrial Complex III Deficiency. *Frontiers in Genetics,* 6.
FERRY, D., SMITH, A., MALKHANDI, J., FYFE, D., DETAKATSM, P., ANDERSON, D., BAKER, J. & KERR, D. 1996. Phase I Clinical Trial of the Flavonoid Queretin: Pharmacokinetics and Evidence for *in vivo* Tyrosine Kinase Inhibition. *Clinical Cancer Research,* 2**,** 659-668.
FIGHTAGING. 2019. *A More Serious Trial Failure for Gensight's Allotopic Expression Implementation* [Online]. https://www.fightaging.org/archives/2019/02/a-more-serious-trial-failure-for-gensights-allotopic-expression-implementation/. [Accessed 08/07/2020 2020].
FINSTERER, J. & SCORZA, F. 2017. Effects of Antiepileptic Drugs on Mitochondrial Functions, Morphology, Kinetics, Biogenesis and Survival. *Epilepsy Research,* 136**,** 5-11.
FORMOSA, L., WONG, L., RELJIC, B., SHARPE, A., JACKSON, T., BEILHARZ, T., STOIANOVSKI, D., LAZAROU, M., STROUD, D. & RYAN, M. 2020. Dissecting the Roles of Mitochondrial Complex I Intermediate Assembly Complex Factors in the Biogenesis of Complex I *Cell Reports,* 31.
FORSLUND, J., PFEIFFER, A., STOJKOVIC, G., WANROOIJ, P. & WANROOIJ, S. 2018. The Presence of rNTPs deceases the Speed of Mitochondrial DNA Replication. *PLoS Genetics,* 14.
FOSTER, K. & FINGAR, D. 2010. Mammalian Target of Rapamycin (mTOR): Conducting the Cellular Signaling Symphony. *The Journal of Biological Chemistry,* 285**,** 14071-14077.
FREDERIKS, W., KUMMERLIN, I., BOSCH, K., VREELING-SINDELAROVA, H., JONKER, A. & NOORDEN, C. 2007. NADPH Production by the Pentose Phosphate Pathway in the Zone Fasciculata of Rat Adrenal Gland. *Journal of Histochemistry & Cytochemistry,* 55**,** 975-980.
FREZZA, C., CIPOLAT, S., MARTINS DE BRITO, O., MICARONI, M., BEZNOUSSENKO, G., RUDKA, T., BARTOLI, D., POLISHUCK, R., DANIAL, N., DE STROOPER, B. & SCORRANO, L. 2006. OPA1

controls apoptotic cristae remodelling independently from mitochondrial fusion. *Cell,* 126**,** 177-189.

FRIESE, M., SCHATTLING, B. & FUGGER, L. 2014. Mechanisms of Neurodegeneration and Axonal Dysfunction in Multiple Sclerosis. *Nature Reviews Neurology,* 10**,** 225-238.

FUSS, J., TSAI, C., ISHIDA, J. & TAINER, J. 2015. Emerging Critical Roles of Fe-S Clusters in DNA Replication and Repair. *Biochimica et Biophysica Acta - Molecular Cell Research,* 1853**,** 1253-1271.

GAMMAGE, P., MORAES, C. & MINCZUK, M. 2018. Mitochondrial Genome Engineering: The Revolution May Not Be CRISPR-Ized. *Trends in Genetics,* 34**,** 101-110.

GAMMAGE, P., RORBACH, J., VINCENT, A., REBAR, E. & MINCZUK, M. 2014. Mitochondrially Targeted ZFNs for Selective Degradation of Pathogenic Mitochondrial Genomes Bearing Large-scale Deletions or Point Mutations. *EMBO Molecular Medicine,* 6**,** 458-466.

GARONE, C. & VISCOMI , C. 2018. Towards a Therapy for Mitochondrial Disease: An Update. *Biochemical Society Translations,* 46**,** 1247-1261.

GATICA, D., LAHIRI, V. & KLIONSKY, D. 2018. Cargo Recognition and Degradation by Selective Autophagy. *Nature Cell Biology,* 20**,** 233-242.

GEBERT, N., JOSHI, A., KUTIK, S., BECKER, T., MCKENZIE, M., GUAN, X., MOOGA, V., STROUD, D., KULKARNI, G., WENK, M., REHLING, P., MEISINGER, C., RYAN, M., WEIDEMANN, N., GREENBERG, M. & PFANNER, N. 2009. Mitochondrial Cardiolipin Involved in Outer Membrane Protein Biogenesis: Implications for Barth Syndrome. *Current Biology,* 19**,** 2133-2139.

GERDES, F., TATSUTA, T. & LANGER, T. 2012. Mitochondrial AAA proteases - Towards a Molecular Understanding of Membrane-Bound Proteolytic Machines. *Biochimica et Biophysica Acta - Molecular Cell Research,* 1823**,** 49-55.

GHEZZI, D. & ZEVIANI, M. 2018. Human Diseases Associated with Defects in Assembly of OXPHOS Complexes. *Essays in Biochemistry,* 62.

GIACOMELLO, M., DRAGO, I., BORTOLOZZI, M., SCORZETO, M., GIANELLE, A., PIZZO, P. & POZZAN, T. 2010. Ca^{2+} Hot Spots on the Mitochondrial Surface Are Generated by Ca^{2+} Mobilisation From Stores, but Not by Activation of Store-Operated Ca^{2+} Channels. *Molecular Cell,* 38**,** 280-290.

GIGUÈRE, V. 2008. Transcriptional Control of Energy Homeostasis by the Estrogen-Related Receptors. *Endocrine Reviews,* 29**,** 677-696.

GILES, R., BLANC, H., CANN, H. & WALLACE, D. 1980. Maternal Inheritance of Human Mitochondrial DNA. *PNAS,* 77**,** 6715-6719.

GIORGI, C., FEDERICA, B., BONONI, A., BONORA, M., MARCHI, E., MARCHI, S., MISSIROLI, S., PATERGNANI, S., RIMESSI, A., SUSKI, J., WIECKOWSKI, M. & PINTON, P. 2012. Mitochondrial Ca^{2+} and apoptosis. *Cell Calcium,* 52**,** 36-43.

GIORGI, C., MARCHI, S. & PINTON, P. 2018. The machineries, regulation and cellular functions of mitochondrial calcium. *Nature Reviews Molecular Cell Biology,* 19**,** 713-730.

GLANCY, B., WILLIS, W., CHESS, D. & BALABAN, R. 2013. Effect of Calcium on the Oxidative Phosphorylation Cascade in Skeletal Muscle Mitochondria. *Biochemistry,* 52**,** 2793-2809.

GNANDT, E., DORNER, K., STRAMPRAAD, M., VRIES, S. & FRIEDRICH, T. 2016. The multitude of iron-sulphur clusters in respiratory complex I. *Biochimica et Biophysica Acta,* 1857**,** 1068-1072.

GOLDENBERG, I., BENDERLY, M. & GOLDBOURT, U. 2008. Update on the use of fibrates: focus on bezafibrate. *Vascular Health and Risk Management,* 4**,** 131-141.

GOMES, L., BENEDETTO, G. & SCORRANO, L. 2011. During Autophagy Mitochondria Elongate, are Spared from Degradation and Sustain Cell Viability. *Nature Cell Biology,* 13**,** 589-598.

GONG, G., SONG, M., CSORDAS, G., KELLY, D., MATKOVICH, S. & DORN, G. 2015. Parkin-mediated mitophagy directs perinatal cardiac metabolic maturation in mice. *Science,* 350.

GORMAN, G., CHINNERY, P., DIMAURO, S., HIRANO, M., KOGA, Y., MCFARLAND, R., SUOMALAINEN, A., THORBURN, D., ZEVIANI, M. & TURNBULL, D. 2016. Mitochondrial Diseases. *Nature Reviews Disease Primers,* 2.

GORMAN, G., MCFARLAND, R., STEWART, J., FEENEY, C. & TURNBULL, D. 2018. Mitochondrial Donation: From Test Tube to Clinic. *The Lancet,* 392**,** 1191-1192.

GORMAN, G., SCHAEFER, A., NG, V., GOMEZ, N., BLAKELY, E., ALSTON, C., FEENEY, C., HORVATH, R., YU-WAI-MAN, P., CHINNERY, P., TAYLOR, R., TURNBULL, D. & MCFARLAND, R. 2015.

Prevalence of nuclear and mitochondrial DNA mutation related to adult mitochondrial disease. *Annuals of Neurology,* 77**,** 753-759.

GOTO, Y., NONAKA, I. & HORAI, S. 1990. A Mutation in the tRNA(Leu)(UUR) Gene Associated with the MELAS Subgroup of Mitochondrial Encephalomyopathies. *Nature,* 348**,** 651-653.

GRABHORN, E., TSIAKAS, K., HERDEN, U., FISCHER, L., FREISINGER, P., MARQUARDT, T., GANSCHOW, R., BRIEM-RICHTER, A. & SANTER, R. 2014. Long-Term Outcomes After Liver Transplantation for Deoxyguanosine Kinase Deficiency: A Single-Centre Experience and a Review of the Literature. *Liver Transplantation,* 20.

GRADY, J., PICKETT, S., NG, Y., ALSTON, C., BLAKELY, E., HARDY, S., FEENEY, C., BRIGHT, A., SCHAEGER, A., GORMAN, G., MCNALLY, R., TAYLOR, R., TURNBULL, D. & MCFARLAND, R. 2018. mtDNA Heteroplasmy Level and Copy Number Indicate Disease Burden in m.3245A>G Mitochondrial Disease. *EMBO Molecular Medicine,* 10.

GRAY, M. 2012. Mitochondrial Evolution. *Cold Spring Harbour Perspectives in Biology,* 4**,** a011403.

GRAY, M., BURGER, G. & LANG, B. F. 2001. The origin and early evolution of mitochondria. *Genome Biology,* 2.

GRAY, M., BURGER, G. & LANG, F. 1999. Mitochondiral Evolution. *Science,* 283**,** 1476-1481.

GREBER, B., BIERI, P., LEIBUNDGUT, M., LEITNER, A., AEBERSOLD, R., BOEHRINGER, D. & BAN, N. 2015. Ribosome. The Complete Structure of the 55S Mammalian Mitochondrial Ribosome. *Science,* 348**,** 303-308.

GREBER, B., BOEHRINGER, D., LEITNER, A., BIERI, P., VOIGTS-HOFFMANN, F., ERZBERGER, J., LEIBUNDGUT, M., AEBERSOLD, R. & BAN, N. 2014. Architecture of the large subunit of the mammalian mitochondrial ribosome. *Nature,* 505**,** 515-519.

GRIER, J., HIRANO, M., KARAA, A., SHEPARD, E. & THOMPSON, J. 2018. Diagnostic Odyssey of Patients with Mitochondrial Disease. *Neurology Genetics,* 4**,** e230.

GRIFFIN, E., DETMER, S. & CHAN, D. 2006. Molecular mechanism of mitochondrial membrane fusion. *Biochimica et Biophysica Acta Molecular Cell Research,* 1763**,** 482-489.

GRUNEWALD, A., RYGIEL, K., HEPPLEWHITE, P., MORRIS, C., PICARD, M. & TURNBULL, D. 2016. Mitochondrial DNA Depletion in Respiratory Chain-Deficient Parkinson Disease Neurons. *Annuals of Neurology,* 79**,** 366-378.

GUERREO-CASTILLO, S., BAERTLING, F., KOWNATZKI, D., WESSELS, H., ARNOLD, S., BRANDT, U. & NIJTMANS, L. 2017. The Assembly Pathway of Mitochondrial Respiratory Chain Complex I. *Cell Metabolism,* 25**,** 128-139.

GUERRERO-CASTILLO, S., BAERTLING, F., KOWNATZKI, D., WESSELS, H., ARNOLD, S., BRANDT, U. & NIJTIMANS, L. 2017. The Assembly Pathway of Mitochondrial Respiratory Chain Complex I. *Cell Metabolism,* 25**,** 128-139.

GUILLERY, O., MALKA, F., LANDES, T., GUILLOU, E., BLACKSTONE, C., LOMBES, A., BELENGUER, P., ARNOULT, D. & ROJO, M. 2008. Metalloprotease-mediated OPA1 processing is modulated by the mitochondrial membrane potential. *Biology of the Cell,* 100**,** 315-325.

GUO, C., CHEN, X. & ZHANG, D. 2014. Oxidative Stress, Mitochondrial Damage and Neurodegenerative Diseases. *Neural Regeneration Research,* 8**,** 2003-2014.

GURD, B., YOSHIDA, Y., LALLY, J., HOLLOWAY, G. & BONEN, A. 2009. The deacetylase enzyme SIRT1 is not associated with oxidative capacity in rat heart and skeletal muscle and its overexpression reduces mitochondrial biogenesis. *The Journal of Physiology,* 587.

GURD, B., YOSHIDA, Y., MCFARLAN, J., HOLLOWAY, G., MOYES, C., HEIGENHAUSER, G., SPRIET, L. & BONEN, A. 2011. Nuclear SIRT1 activity, but not protein content, regulates mitochondrial biogenesis in rat and human skeletal muscle. *American Journal of Physiology Regulatory, Integrative and Comparative Physiology,* 301**,** R65-R75.

GUSTAFSSON, C., FALKENBERG, M. & LARSSON, N. 2016. Maintenance and Expression of Mammalian Mitochondrial DNA. *Annual Review of Biochemistry,* 85**,** 133-160.

GUY, J., FEUER, W., DAVIS, J., PORCIATTI, V., GONZALEZ, P., KOILKONDA, R., YUAN, H., HAUSWIRTH, W. & LAM, B. 2017. Gene Therapy for Leber Hereditary Optic Neuropathy: Low- and Medium-Dose Visual Results. *Ophthalmology,* 124**,** 1621-1634.

HAAS DE MELLO, A., COSTA, A., DELLA, J., ENGEL, J. & REZIN, G. 2018. Mitochondrial Dysfunction in Obesity. *Life Sciences,* 192**,** 26-32.

HAHN, A., PAREY, K., BUBLITZ, M., MILLS, D., ZICKERMANN, V., VONCK, J., KUHLBRANDT, W. & MEIER, T. 2016. Structure of a Complete ATP Synthase Dimer Reveals the Molecular Basis of Inner Mitochondrial Membrane Morphology. *Molecular Cell,* 63**,** 445-456.

HALLBERG, M. & LARSSON, N. 2014. Making Proteins in the Powerhouse. *Cell Metabolism,* 20**,** 226-240.

HALLBERG, M., MORGANSTEIN, D., KISKINIS, E., SHAH, K., KRALLI, A., DILWORTH, S., WHITE, R., PARKER, M. & CHRISTIAN, M. 2008. A Functional Interaction between RIP140 and PGC-1α Regulates the Expression of the Lipid Droplet Protein CIDEA. *Molecular and Cellular Biology,* 28**,** 6785-6795.

HANDSCHIN, C. & SPIEGELMAN, B. 2006. Peroxisome Proliferator-Activated Receptor γ Coactivator 1 Coactivators, Energy Homeostasis, and Metabolism. *Endocrine Reviews,* 27**,** 728-735.

HANSON, B., CAPALDI, R., MARUSICH, M. & SHERWOOD, S. 2002. An Immunocytochemical Approach to Detection of Mitochondrial Disorders. *The Journal of Histochemistry and Cytochemistry,* 50**,** 1281-1288.

HARPER, J., ORDUREAU, A. & HEO, J. 2018. Building and decoding ubiquitin chains for mitophagy. *Nature Reviews Molecular Cell Biology,* 19**,** 93-108.

HARRIS, C., CHOWANADISAI, W., MISHCHUK, D., SATRE, M., SLUPSKY, C. & RUCKER, R. 2013. Dietary pyrroloquinoline quinone (PQQ) alters indicators of inflammation and mitochondrial-related metabolism in human subjects. *Journal of Nutritional Biochemistry,* 24**,** 2076-2084.

HARTL, F., SCHMIDT, B., WACHTER, E., WEISS, H. & NEUPERT, W. 1986. Transport into mitochondria and intramitochondrial sorting of the Fe/S protein of ubiquinol-cytochrome c reductase. *Cell,* 47**,** 939-951.

HASEGAWA, K., YASUDA, T., SHIRAISHI, C., FUJIWARA, K., PRZEDBORSKI, S., MOCHIZUKI, H. & YOSHIKAWA, K. 2016. Promotion of mitochondrial biogenesis by necdin protects neurons against mitochondrial insults. *Nature Communications,* 7**,** 10943.

HATTAB, A., HSU, J., EMRICK, L., WONG, L., CRAIGEN, W., JAHOOR, F. & SCAGLIA, F. 2012. Restoration of Impaired Nitric Oxide Production in MELAS Syndrome with Citrulline and Arginine Supplementation. *Molecular Genetics and Metabolism,* 105**,** 607-614.

HAUSWIRTH, W. & LAIPIS, P. 1982. Mitochondrial DNA Polymorphism in a Maternal Lineage of Holstein Cows. *PNAS,* 79**,** 4686-4690.

HAYASHI, G. & CORTOPASSI, G. 2015. Oxidative Stress in Inherited Mitochondrial Diseases. *Free Radical Biology and Medicine,* 88**,** 10-17.

HAYNES, C., PETROVA, K., BENEDETTI, C., YANG, Y. & RON, D. 2007. ClpP Mediates Acitivation of a Mitochondrial Unfolded Protein Response in *C. elegans*. *Developmental Cell,* 13**,** 467-480.

HEINDRYCKX, B., NEUPANE, J., VANDEWOESTYNE, M., CHRISTODOULOU, C., JACKERS, Y., GERRIS, J., ABBEEL, E., COSTER, R., DEFORCE, D. & SUTTER, P. 2014. Mutation-free Baby Born from a Mitochondrial Encephalopathy, Lactic Acidosis and Stroke-Like Syndrome Carrier After Blastocyst Trophectoderm Preimplantation Genetic Diagnosis. *Mitochondrion,* 18**,** 12-17.

HELLEBREKERS, D., WOFLE, R., HENDRICKX, A., COO, I., DIE, C., GERAEDTS, J., CHINNERY, P. & SMEETS, H. 2012. PGD and Heteroplasmic Mitochondrial DNA Point Mutations: A Systematic Review Estimating the Chance of Healthy Offspring. *Human Reproduction Update,* 18**,** 341-349.

HERZIG, S., LONG, F., JHALA, U., HEDRICK, S., QUINN, R., BAUER, A., RUDOLPH, D., SCHUTZ, G., YOON, C., PUIGSERVER, P., SPIEGELMAN, B. & MONTMINY, M. 2001. CREB regulates hepatic gluconeogenesis through the coactivator PGC-1. *Nature,* 413**,** 179-183.

HEZAVEH, Z., AZARKEIVAN, A., JANANI, L., HOSSEINI, S. & SHIDFAR, F. 2019. The Effect of Quercetin on Iron Overload and Inflammation in β-Thalassemia Major Patients: A Double-Blind Randomised Clinical Trial. *Complementary Therapies in Medicine,* 46**,** 24-28.

HIKMAT, O., ISOHANNI, P., SUOMALAINEN, A. & BINDOOF, L. 2019. *Diseases of DNA Polymerase Gamma In: Diagnosis and Management of Mitochondrial Disorders*, Springer.

HIKMAT, O., NAESS, K., ENGVALL, M., KLINGENBERG, C., RASMUSSEN, M., TALLAKSEN, C., BRODTKORB, E., OSTERGAARD, E., COO, I., PIAS-PELETEIRO, L., ISOHANNI, P., UUSIMAA, J., DARIN, N., RAHMAN, S. & BINDOFF, L. 2020. Simplifying the Clinical Classification of Polymerase Gamma (POLG) Disease Based on Age of Onset; Studies Using a Cohort of 155 Cases. *Journal of Inherited Metabolic Disease*.

HIKMAT, O., TZOULIS, C., CHONG, W., CHENTOUF, L., LINGENBERG, C., FRATTER, C., CARR, L., PRABHAKAR, P., KUMARAGURU, N., GISSEN, P., CROSS, J., JACQUES, T., TAANMAN, J., BINDOFF, L. & RAHMAN, S. 2017. The Clinical Spectrum and Natural History of Early-Onset Diseases Due to DNA Polymerase Gamma Mutations. *Genetics in Medicine,* 19**,** 1217-1225.

HINGORANI, A., KUAN, V., FINAN, C., KRUGER, F., GAULTON, A., CHOPPED, S., SOFAT, R., MACALLISTER, R., OVERINGTON, J., HEMINGWAY, H., DENAXAS, S., PRIETO, D. & CASAS, J. 2019. Improving the Odds of Drug Development Success Through Human Genomics: Modelling Study. *Scientific Reports,* 9**,** 18911.

HIRABAYASHI, Y., KWON, S., PAEK, H., PERNICE, W., PAUL , M., LEE, J., RACZKOWSKI, A., PETRY, D., PON, L. & POLLEUX, F. 2017. ER-mitochondria tethering by PDZD8 regularise Ca^{2+} dynamics in mammalian neurons. *Science,* 358**,** 623-630.

HIRANO, M., EMMANUELE, V. & QUINZII, C. 2018. Emerging Therapies for Mitochondrial Diseases. *Essays in Biochemistry,* 62**,** 467-481.

HIRSCH, T., MARZO, I. & KROEMER, G. 1997. Role of the Mitochondrial Permeability Transition Pore in Apoptosis. *Bioscience Reports,* 17.

HIRST, J. 2013. Mitochondrial Complex I. *Annual Review of Biochemistry,* 82**,** 551-575.

HOCK, B. & KRALLI, A. 2009. Transcriptional Control of Mitochondrial Biogenesis and Function. *The Annual Review of Physiology,* 71**,** 177-203.

HOITZING, H., JOHNSTON, I. & JONES, N. 2015. What is the Function of Mitochondrial Networks? A Theoretical Assessment for Hypothesis and Proposal for Future Research. *Bioessays,* 37**,** 687-700.

HOLMSTROM, M., GUTIERREZ, E., ZIERATH, J. & ROVES, P. 2012. Tissue-Specific Control of Mitochondrial Respiration in Obesity-Related Insulin Resistance and Diabetes. *Endocrinology and Metabolism,* 302**,** E731-E739.

HOLT, I., HARDING, A., PETTY, R. & MORGAN-HUGHES, J. 1990. A New Mitochondrial Disease Associated with Mitochondrial DNA Heteroplasmy. *American Journal of Human Genetics,* 46**,** 428-433.

HOPPINS, S., COLLINS, S., CASSIDY-STONE, A., HUMMEL, E., DEVAY, R., LACKNER, L., WESTERMANN, B., SCHULDINER, M., WEISSMAN, J. & NUNNARI, J. 2011. A mitochondrial-focused genetic interaction map reveals a scaffold-like complex required for inner membrane organization in mitochondria. *Journal of Cell Biology,* 195**,** 323-340.

HOVARTH, S., RAMPELT, H., OELJEKLAUS, S., WARSCHEID, B., VAN DER LAAN, M. & PFANNER, N. 2015. Role of membrane contact sites in protein import into mitochondria. *Protein Science,* 24**,** 277-297.

HOWELL, N., BINDOFF, L., MCCULLOUGH, D., KUBACKA, I., POULTON, J., MACKEY, D., TAYLOR, L. & TURNBULL, D. 1991. Leber Hereditary Optic Neuropathy: Identification of the Same Mitochondrial ND1 Mutation in Six Pedigrees. *American Journal of Human Genetics,* 49**,** 939-950.

HUANG, D.-D., FAN, S.-D., CHEN, X.-Y., YAN, X.-L., ZHANG, X.-Z., MA, B.-W., YU, D.-Y., XIAO, W.-Y., ZHUANG, C.-L. & YU, Z. 2019. Nrf2 deficiency exacerbates frailty and sarcopenia by impairing skeletal muscle mitochondrial biogenesis and dynamics in an age-dependent manner. *Experimental Gerontology*.

HWANG, P., MACHEK, S., CARDACI, T., WILBURN, D., KIM, C., SUEZAKI, E. & WILLOUGHBY, D. 2019. Effects of Pyrroloquinoline Quinone (PQQ) Supplementation on Aerobic Exercise Performance and Indices of Mitochondria Biogenesis in Untrained Men. *Journal of the American College of Nutrition*.

IBORRA, F., KIMURA, H. & COOK, P. 2004. The Functional Organisation of Mitochondrial Genomes in Human Cells. *BMC Biology,* 2.

IMAI, A., FUJITA, S., KISHITA, Y., KOHDA, M., TOKUZAWA, Y., HIRATA, T., MIZUNO, Y., HARASHIMA, H., NAKAYA, A., SAKATA, Y., TAKEDA, A., MORI, M., MURAYAMA, K., OHTAKE, A. & OKAZAKI, Y. 2016. Rapidly Progressive Infantile Cardiomyopathy with Mitochondrial Respiratory Chain Complex V Deficiency Due to Loss of ATPase 6 and 8 Protein. *International Journal of Cardiology,* 207**,** 203-205.

ISSOP, L., RONE, M. & PAPADOPOULOS, V. 2013. Organelle plasticity and interactions in cholesterol transport and steroid biosynthesis. *Molecular and Cellular Endocrinology,* 371**,** 34-46.

IVATT, R. & WHITWORTH, A. 2014. The Many Faces of Mitophagy. *EMBO Reports,* 15**,** 5-6.

JACKSON, C., HAHN, D., SCHRÖTER, B., RICHTER, U., BATTERSBY, B., SCHMITT-MECHELKE, T., MARTTINEN, P., NUOFFER, J. & SCHALLER, A. 2017. A Novel Mitochondrial ATP6 Framshift Mutation Causing Isolated Complex V Deficiency, Ataxia and Encephalomyopathy. *European Journal of Medical Genetics,* 60**,** 345-351.

JANSSEN, M., KOENE, S., LAAT, P., HEMELAAR, P., PICKKERS, P., SPAANS, E., BEUKEMA, R., BEYRATH, J., GROOTHUIS, J., VERHAAK, C. & SMEITINK, J. 2018. The KHENERGY Study: Safety and Efficacy of KH 176 in Mitochondrial m.3243A>G Spectrum Disorders. *Clinical Pharmacology and Theraputics,* 105.

JAOKAR, T., SHARMA, R. & SURESCH, C. 2013. Structural Effects of Leigh Syndrome Mutations on the Function of Human Mitochondrial Complex-I Q module. *Biochemistry and Physiology,* S2.

JEMT, E., PERSSON, O., SHI, Y., MEHMEDOVIC, M., UHLER, J., LOPEZ, M., FREYER, C., GUSTAFSSON, C., SAMUELSSON, T. & FALKENBERG, M. 2015. Regulation of DNA Replication at the End of the Mitochondria D-Loop Involves the Helicase TWINKLE and a Conserved Sequence Element. *Nucleic Acids Research,* 30**,** 9262-9275.

JENINGA, E., SCHOONJANS, K. & AUWERX, J. 2010. Reversible acetylation of PGC-1: connecting energy sensors and effectors to guarantee metabolic flexibility. *Oncogene,* 29**,** 4617-4624.

JEPPESEN, T., AL-HASHIMI, N., DUNO, M., WIBRAND, F., ANDERSEN, G. & VISSING, J. 2017. Mitochondrial DNA Mutation Load in a Family with the m.8344A>G Point Mutation and Lipomas: A Case Study. *Clinical Case Reports,* 5.

JEPPESEN, T., SCHWARTZ, M., OLSEN, D., WIBRAND, F., KRAG, T., DUNO, M., HAUERSLEV, S. & VISSING, J. 2006. Aerobic Training is Safe and Improves Exercise Capacity in Patients with Mitochondrial Myopathy. *Brain,* 129**,** 3402-3412.

JOHNS, D., NEUFELD, M. & PARK, R. 1992. An ND-6 Mitochondrial DNA Mutation Associated With Leber Hereditary Optic Neuropathy. *Biochemical and Biophysical Research Communications,* 187**,** 1551-1557.

JOHNSON, S., YANOS, M., KAYSER, E., QUINTANA, A., SANGESLAND, M., CASTANZA, A., UHDE, L., HUI, J., WALL, V., GAGNIDZE, A., OH, K., WAS, B., RAMOS, F., PALMITER, R., RABINOVITCH, P., MORGAN, P., SEDENSKY, M. & KAEBERLEIN, M. 2013. mTOR Inhibition Alleviates Mitochondrial Disease in a Mouse Model of Leigh Syndrome. *Science,* 342**,** 1524-1528.

JONAS, E., PORTER, G., BEUTNER, G., MNATSAKANYAN, B., PARK, H., MEHTA, N., CHEN, R. & ALAVIAN, K. 2017. *The Mitochondrial Permeability Transition Pore: Molecular Structure and Function in Health and Disease*.

JONCKHEERE, A., SMEITINK, J. & RODENBURG, R. 2012a. Mitochondrial ATP Synthase: Architecture, Function and Pathology. *Journal of Inherited Metabolic Disease,* 35**,** 211-225.

JONCKHEERE, A., SMEITINK, J. & RODENBURG, R. 2012b. Mitochondrial ATP synthase: architecture, function and pathology. *Journal of Inherited Metabolic Disease,* 35**,** 211-225.

JORNAYVAZ, F. & SHULMAN, G. 2010. Regulation of mitochondrial biogenesis. *Essays Biochem,* 47.

JOSEPH, A. & HOOD, D. 2012. Plasticity of TOM Complex Assembly in Skeletal Muscle Mitochondria in Response to Chronic Contractile Activity. *Mitochondrion,* 12**,** 305-312.

JOURDAIN, A., BOEHM, E., MAUNDRELL, K. & MARTINOU, J. 2016. Mitochondrial RNA granules: Compartmentalizing mitochondrial gene expression. *Journal of Cell Biology,* 212**,** 611-614.

JOURDAIN, A., KOPPEN, M., HYDRO, M., RODLEY, C., LIGHTOWLERS, R., CHRZANOWSKA-LIGHTOWLERS, Z. & MARTINOU, J. 2013. GRSF1 Regulates RNA Processing in Mitochondrial RNA Granules. *Cell Metabolism,* 17**,** 399-410.

JOURDIAN, A., BOEHM, E., MAUNDRELL, K. & MARTINOU, J. 2016. Mitochondrial RNA granules: Compartmentalizing mitochondrial gene expression. *Journal of Cell Biology,* 212**,** 611-614.

KADOWAKI, T., KADOWAKI, H., MORI, Y., TOBE, K., SAKUTA, R., SUZUKI, Y., TANABE, Y., SAKURA, H., AWATA, T., GOTO, Y., HAYAKAWA, T., MATSUOKA, K., KARAMORI, R., KAMADA, T., HORAI, S., NONAKA, I., HAGURA, R., AKANUMA, Y. & YAZAKI, Y. 1994. A Subtype of Diabetes Mellitus Associated with a Mutation of Mitochondrial DNA. *The New England Journal of Medicine,* 330**,** 962-968.

KAEBERLEIN, M. 2013. mTOR Inhibition: From Aging to Autism and Beyond. *Scientifica,* 2013**,** 849186.
KANG, P., OSTERMANN, J., SHILLING, J., NEUPERT, W., CRAIG, E. & PFANNER, N. 1990. Requirement of Hsp70 in the mitochondrial matrix for translocation and folding of precursor proteins. *Nature,* 348**,** 137-143.
KAPP, L. & LORSCH, J. 2004. The Molecular Mechanics of Eukaryotic Translation. *Annual Review of Biochemistry,* 73**,** 657-704.
KASE, E., NIKOLIC, N., BAKKE, S., BOGEN, K., AAS, V., THORESEN, G. & RUSTAN, A. 2013. Remodelling of Oxidative Energy Metabolism by Galactose Improves Glucose Handling and Metabolic Switching in Human Skeletal Muscle Cells. *PLoS One,* 8**,** e59972.
KENNEDY, E. 1958. The Biosynthesis of Phospholipids. *The American Journal of Clinical Nutrition,* 6**,** 216-220.
KHAN, N., NIKKANEN, J., YATSUGA, S., JACKSON, C., WANG, L., PRADHAN, S., KIVELA, R., PESSIA, A., VELAGAPUDI, V. & SOUMALAINEN, A. 2017. mTORC1 Regulates Mitochondrial Integrated Stress Response and Mitochondrial Myopathy Progression. *Cell Metabolism,* 26**,** 419-428.e5.
KHAN, N. A., AURANEN, M., PAETAU, I., PIRINEN, E., EURO, L., FORSSTRÖM, S., PASILA, L., VELAGAPUDI, V., CARROLL, C. J., AUWERX, J. & SUOMALAINEN, A. 2014. Effective treatment of mitochondrial myopathy by nicotinamide riboside, a vitamin B3. *EMBO Molecular Medicine,* 6.
KIM, C., KWON, Y., CHOE, S., HONG, S., YOO, H., GOTO, T., KAWADA, T., CHOI, H., JOE, Y., CHUNG, H. & YU, R. 2015. Quercetin Reduces Obesity-Induced Hepatosteasosis by Enhancing Mitochondrial Oxidative Metabolism via Heme Oxygenase-1. *Nutrition and Metabolism,* 12**,** 33.
KIRINO, Y., YASUKAWA, T., OHTA, S., AKIRA, S., ISHIHARA, K., WATANABE, K. & SUZUKI, T. 2004. Condon-specific Translational Defect Caused by a Wobble Modification Deficiency in Mutant tRNA from a Human Mitochondrial Disease. *PNAS,* 101**,** 15070-15075.
KLEELE, T., REY, T., WINTER, J., ZAGANELLI, S., MAHECIC, D., LAMBERT, H., RUBERTO, F., NEMIR, M., WAI, T., PEDRAZZINI, T. & MANLEY, S. 2021. Distinct Fission Signatures Predict Mitochondrial Degradation or Biogenesis. *Nature*.
KLEIN, A., ISRAEL, L., S, L., NARGANG, F. & IMHOF, A. 2012. Characterisation of the inserts for B-barrel proteins of the outer mitochondrial membrane. *Journal of Cell Biology,* 199**,** 599-611.
KLOPSTOCK, T., METZ, G., YU-WAI-MAN, P., BUCHNER, B., GALLENMULLER, C., BAILIE, M., NWALI, B., GRIFFITHS, P., LIVONIUS, B., REZNICEK, L., ROULEAU, J., COPPARD, N., MEIER, T. & CHINNERY, P. 2013. Persistence of the Treatment Effect of Idebenone in Leber's Hereditary Optic Neuropathy. *Brain,* 136**,** e230.
KLOPSTOCK, T., YU-WAI-MAN, P., DIMITRIADIS, K., ROULEAU, J., HECK, S., BAILIE, M., ATAWAN, A., CHATTOPADHYAY, S., SCHUBERT, M., GARIP, A., KERNT, M., PETRAKI, D., RUMMERY, C., LEINONEN, M., METZ, G., GRIFFITHS, P., MEIER, T. & CHINNERY, P. 2011. A Randomized Placebo-controlled Trial of Idebenone in Leber's Hereditary Optic Neuropathy. *Brain,* 134**,** 2677-2686.
KLUCKOVA, K., BEZAWORK-GELETA, A., ROHLENA, J., DONG, L. & NEUZIL, J. 2013. Mitochondrial Complex II, a novel target for anti-cancer agents. *Biochimica et Biophysica Act - Bioenergetics,* 1827**,** 552-564.
KMITA, K., WIRTH, C., WARNAU, J., GUERRERO-CASTILLO, S., HUNTE, C., HUMMER, G., KAILA, V., ZWICKER, K., BRANDT, U. & ZICKERMANN, V. 2015. Accessory NUMM (NDUFS6) Subunit Harbours a Zn-Binding Site and is Essential for Biogenesis of Mitochondrial Complex I. *Proceedings of the Natural Academy of Science USA,* 112**,** 5685-5690.
KOGA, Y., AKITA, Y., NISHIOKA, S., YATSUGA, S., POVALKO, N., TANABE, Y., FUGIMOTO, S. & MATSUISHI, T. 2005. L-Arginine Improves the Symptoms of Strokelike Episodes in MELAS. *Neurology,* 64.
KOHLER, R., MOONEY, R., MILLS, D., LANDICK, R. & CRAMER, P. 2017. Architecture of a Transcribing-translating Expressome. *Science,* 356**,** 194-197.
KOMEN, J. & THORBURN, D. 2014. Turn up the power – pharmacological activation of mitochondrial biogenesis in mouse models. *British Journal of Pharmacology,* 171**,** 1818-1836.
KONDADI, A., ANAND, R., HANSCH, S., URBACH, J., ZOBEL, T., WOLF, D., SEGAWA, M., LIESA, M., SHIRIHAI, O., WEIDTKAMP-PETERS, S. & REICHERT, A. 2020. Cristae undergo continuous cycles of membrane remodelling in a MICOS-dependent manner. *EMBO Reports,* 21.

KOOPMAN, W., BEYRATH, J., FUN, C., KOENE, S., RODENBURG, R., WILLEMS, P. & SMEITINK, J. 2016. Mitochondrial Disorders in Children: Toward Development of Small-Molecule Treatment Strategies. *EMBO Molecular Medicine,* 8**,** 311-327.

KOOSHYAR, M., MOZAFARI, P., AMIRCHAGHMAGHI, M., PAKFETRAT, A., KAROSS, P., MOHASEL, M., ORAFAI, H. & AZARIAN, A. 2017. A Randomised Placebo-Controlled Double Blind Clinical Trial of Quercetin in the Prevention and Treatment of Chemotherapy-Induced Oral Mucositis. *Journal of Clinical and Diagnostic Research,* 11**,** ZC46-ZC50.

KORHONEN, J., PHAM, X., PELLEGRINI, M. & FALKENBERG, M. 2004. Reconstitution of a minimal mtDNA replisome in vitro. *EMBO J,* 23**,** 2423-2429.

KOSHIBA, T., DETMER, S., KAISER, J., CHEN, H., MCCAFFERY, J. & CHAN, D. 2004. Structural Basis of Mitochondrial Tethering by mitofusin complexes. *Science,* 305**,** 858-862.

KOSTIC, M., RAJKOVIC, J., FLORANOVIC, M., DIMOV, I. & PAVLOVIC, D. 2013. Multiple sclerosis and oxidative stress - a clinical perspective. *Clinical Neurochemistry,* 7**,** 76-86.

KOZIN, M., KULAKOVA, O. & FAVOROVA, O. 2018. Involvement of Mitochondria in Neurodegeneration in Multiple Sclerosis. *Biochemistry,* 83**,** 813-830.

KUJOTH, G., HIONA, A., PUGH, T., SOMEYA, S., PANZER, K., WOHLGEMUTH, S., HOFER, T., SEO, A., SULLIVAN, R., JOBLING, W., MORROW, J., REMMEN, H., SEDIVY, J., YAMASOBA, T., TANOKURA, M., WEINDRUCH, R., LEEUWENBURGH, C. & PROLLA, T. 2005. Mitochondrial DNA Mutations, Oxidative Stress and Apoptosis in Mammalian Aging. *Science,* 309**,** 481-484.

KWONG, J. & MOLKENTIN, J. 2016. Physiological and Pathological Role of the Mitochondrial Permeability Transition Pore in the Heart. *Cell Metabolism,* 21**,** 206-214.

LADOUKAKIS, E. & ZOUROS, E. 2017. Evolution and Inheritance of Animal Mitochondrial DNA: Rules and Exceptions. *Journal of Biological Research,* 24.

LAGOUGE, M., ARGMANN, C., GERHART-HINES, Z., MEZIANE, H., LERIN, C., DAUSSIN, F., MESSADEQ, N., MILNE, J., LAMBERT, P., ELLIOTT, P., GENY, B., LAAKSO, M., PUIGSERVER, P. & AUWERX, J. 2006. Resveratrol Improves Mitochondrial Function and Protects against Metabolic Disease by Activating SIRT1 and PGC-1α. *Cell,* 127**,** 1109-1122.

LAKE, N., COMPTON, A., RAHMAN, S. & THORBURN, D. 2016. Leigh Syndrome: One Disorder, More than 75 Monogenic Causes. *Annals of Neurology,* 79.

LAMBERT, A. & BRAND, M. 2009. *Reactive Oxygen Species Production by Mitochondria,* Humana Press.

LANE, N. & MARTIN, W. 2010. The energetics of genome complexity. *Nature,* 467**,** 929-934.

LANE, R., HILSABECK, T. & REA, S. 2015. The Role of Mitochondrial Dysfunction in Age-Related Diseases. *Biochimica et Biophysica Acta - Bioenergetics,* 1847**,** 1387-1400.

LAX, N., GRADY, J., LAUDE, A., CHAN, F., HEPPLEWHITE, P., GORMAN, G., WHITTAKER, R., NG, Y., CUNNINGHAM, M. & TURNBULL, D. 2016. Extensive Respiratory Chain Defects in Inhibitory Interneurones in Patients with Mitochondrial Disease. *Neuropathology and Applied Neurobiology,* 42**,** 180-193.

LEARY, S. 2012. Blue Native Polyacrylamide Gel Electrophoresis: A Powerful Diagnostic Tool for the Detection of Assembly Defects in the Enzyme Complexes of Oxidative Phosphorylation. *Mitochondrial Disorders,* 837**,** 195-206.

LEE, C., CAUDAL, A., ABELL, L., GOWDA, G. & TIAN, R. 2019. Targeting NAD^+ Metabolism as Interventions for Mitochondrial Disease. *Scientific Reports,* 9**,** 3073.

LEE, H., SHIN, S., CHOI, C., LEE, Y. & LEE, S. 2002. Formation and Removal of α-synuclein Aggregates in Cells Exposed to Mitochondrial Inhibitors. *The Journal of Biological Chemistry,* 277**,** 5411-5417.

LEE, I., CAO, L., MOSTOSLAVSKY, R., LOMBARD, D., LIU, J., BRUNS, N., TSOKO, M., ALT, F. & FINKEL, T. 2008. A Role of the NAD-Dependent Deacetylase SIRT1 in the Regulation of Autophagy. *PNAS,* 105.

LEE, M. & KIM, Y. 2018. Effects of Isorhamnetin on Adipocyte Mitochondrial Biogenesis and AMPK Activation. *Molecules,* 23**,** 1853.

LEE, T. & YOUNG, R. 2000. Transcription of Eukaryotic Protein-Coding Genes. *Annual Review of Genetics,* 34**,** 77-137.

LEHMAN, J., BARGER, P., KOVACS, A., SAFFITZ, J., MEDEIROS, D. & KELLY, D. 2000. Peroxisome proliferator-activated receptor gamma coactivator-1 promotes cardiac mitochondrial biogenesis. *Journal of Clinical Investigation,* 106**,** 847-856.

LEHMANN, D., TUPPEN, H., CAMPBELLL, G., ALSTON, C., LAWLESS, C., ROSA, H., ROCHA, M., REEVE, A., NICHOLLS, T., DESCHAUER, M., ZIERZ, S., TAYLOR, R., TURNBULL, D. & VINCENT, A. 2019. Understanding Mitochondrial DNA Maintenance Disorders at the Single Muscle Fibre Level. *Nucleic Acids Research,* 47**,** 7430-7443.

LELOIR, F. 1951. The Enzymatic Transformation of Uridine Diphosphate Glucose into a Galactose Derivative. *Archives of Biochemistry and Biophysics,* 33**,** 186-190.

LEONHARD, K., HERRMANN, J., STUART, R., MANNHAUPT, G., NEUPERT, W. & LANGER, T. 1996. AAA Processes with Catalytic Sites on Opposite Membrane Surfaces Comprise a Proteolytic System for the ATP-dependent Degradation of Inner Membrane Proteins in Mitochondria. *EMBO J,* 15**,** 4218-4229.

LERIN, C., RODGERS, J., KALUME, D., KIM, S.-H., PANDEY, A. & PUIGSERVER, P. 2006. GCN5 acetyltransferase complex controls glucose metabolism through transcriptional repression of PGC-1α. *Cell Metabolism,* 3**,** 429-438.

LETTS, J. & SAZANOV, L. 2017. Clarifying the Supercomplex: The Higher-Order Organisation of the Mitochondrial Electron Transport Chain. *Nature Structural and Molecular Biology,* 24**,** 800-808.

LI, P., NIJHAWAN, D., BUDIHARDJO, I., SRINIVASULA, S., AHMAD, M., ALNERMRI, E. & WANG, X. 1997. Cytochrome C and dATP-dependent Formation of Apaf-1/caspase-9 Complex Initiates an Apoptotic Protease Cascade. *Cell,* 91**,** 479-489.

LI, X., WANG, H., GAO, Y., LI, L., TANG, C., WEN, G., ZHOU, Y., ZHOU, M., MAO, L. & FAN, Y. 2016. Protective Effects of Quercetin on Mitochondrial Biogenesis in Experimental Traumatic Brain Injury via the NRF2 Signalling Pathway. *PLoS ONE,* 11.

LIBERTHAL, W., MENZA, S. & LEVINE, J. 1998. Graded ATP Depletion Can Cause Necrosis or Apoptosis of Cultured Mouse Proximal Tubular Cells. *American Journal of Physiology,* 274**,** F315-F327.

LIESA, M. & SHIRIHAI, O. 2013. Mitochondrial Dynamics in the Regulation of Nutrient Utilisation and Energy Expenditure. *Cell Metabolism,* 17**,** 491-506.

LIGHTOWLERS, R., ROZANSKA, A. & CHRZANOWSKA-LIGHTOWLERS, Z. 2014. Mitochondrial protein synthesis: Figuring the fundamentals, complexities and complications, of mammalian mitochondrial translation. *FEBS Letters,* 588**,** 2496-2503.

LIGHTOWLERS, R., TAYLOR, R. & TURNBULL, D. 2015. Mutations causing mitochondrial disease: What is new and what challenges remain? *Science,* 349**,** 1494-1499.

LILL, R. & FREIBERT, S. 2020. Mechanisms of Mitochondrial Iron-Sulphur Protein Biogenesis. *Annual Review of Biochemistry,* 89.

LIN, D., HUANG, Y., HO, C., HUNG, P., HSU, M., WANG, T., WU, T., LEE, T., HUANG, Z., CHANG, P. & CHIANG, M. 2019. Oxidative Insults and Mitochondrial DNA Mutation Promote Enhanced Autophagy and Mitophagy Compromising Cell Viability in Pluripotent Cell Model of Mitochondrial Disease. *Cells,* 8**,** 65.

LIN, J., WU, H., TARR, P., ZHANG, C.-Y., WU, Z., BOSS, O., MICHAEL, L., PUIGSERVER, P., ISOTANI, E., OLSON, E., LOWELL, B. B., BASSEL-DUBY, R. & SPIEGELMAN, B. 2002. Transcriptional co-activator PGC-1α drives the formation of slow-twitch muscle fibres. *Nature,* 418**,** 797-801.

LIU, J., MCINTYRE, R., G, J. & HOUTKOOPER, R. 2020. Mitochondrial fission and fusion: A dynamic role in aging and potential target for age-related disease. *Mechanisms of Ageing and Development,* 186.

LIU, L., FENG, D., CHEN, G., CHEN, M., ZHENG, Q., SONG, P., MA, Q., ZHU, C., WANG, R., QI, W., HUANG, L., XUE, P., LI, B., WANG, X., JIN, H., WANG, J., YANG, F., LIU, P., ZHU, Y., SUI, S. & CHEN, Q. 2012. Mitochondrial outer-membrane protein FUNDC1 mediates hypoxia-induced mitophagy in mammalian cells. *Nature Cell Biology,* 14**,** 177-185.

LIU, L., MINWOO, N., FAN, W., AKIE, T., HOAGLIN, D., GAO, G., KEANEY, J. & COPPER, M. 2014. Nutrient Sensing by the Mitochondrial Transcription Machinery Dictates Oxidative Phosphorylation. *Journal of Clinical Investigations,* 124.

LIU, P., LIN, H., XU, Y., ZHOU, F., WANG, J., LIU, J., ZHU, X., GUO, X., TANG, Y. & YAO, P. 2018. Frataxin-Mediated PINK1-Parkin-Dependent Mitophagy in Hepatic Steatosis: The Protective Effects of Quercetin. *Molecular Nutrition and Food Research,* 62**,** 1800164-1800175.

LOPEZ-OTIN, C., BLASCO, M., PARTRIDGE, L., SERRANO, M. & KROEMER, G. 2013. The Hallmarks of Aging. *Cell,* 153**,** 1194-1217.

LOTT, M., LEIPZIG, J., DERBENEVA, O., XIE, H., CHALKIA, D., SARMADY, M., PROCACCIO, V. & WALLACE, D. 2013. mtDNA Variation and Analysis Using Mitomap and Mitomaster. *Current Protocols in Bioinformatics,* 44**,** 1.23.1-1.23.26.

LY, J., GRUBB, D. & LAWEN, A. 2003. The Mitochondrial Membrane Potential (**$\Delta\psi_m$) in Apoptosis; An Update**. *Apoptosis,* 8**,** 115-128.

LYNCH, D., FARMER, J., HAUSER, L., BLAIR, I., WANG, Q., MESAROS, C., SNYDER, N., BOESCH, S., CHIN, M., DELATYCKI, M., GIUNTI, P., GOLDSBERRY, A., HOYLE, C., MCBRIDE, M., NACHBAUER, W., O'GRADY, M., PERLMAN, S., SUBRAMONY, S., WILMOT, G., ZESIEWICZ, T. & MEYER, C. 2019. Safety, Pharmacodynamics, and Potential Benefit of Omaveloxolone in Friedreich Ataxia. *Annals of Clinical and Translation Neurology,* 6**,** 15-26.

LYNCH, D., FARMER, J., WILSON, R. & BALCER, L. 2005. Performance Measure in Friedrich Ataxia: Potential Utility as Clinical Outcome Tools. *Movement Disorders,* 20.

MA, J., CAMPBELL, A. & KARLIN, S. 2002. Correlations between Shine-Dalgarno Sequences and Gene Features Such as Predicted Expression Levels and Operon Structures. *Journal of Bacteriology,* 184**,** 5733-5745.

MA, J., ZHAL, Y., CHEN, M., ZHANG, K., CHEN, Q., PANG, X. & SUN, F. 2019. New interfaces on MiD51 for Drp1 Recruitment and Regulation. *PLoS One,* 14**,** e0211459.

MAACK, C. & O'ROURKE, B. 2007. Excitation-contraction coupling and mitochondrial energetics. *Basic Research in Cardiology,* 102**,** 369-392.

MACAO, B., UHLER, J., SIIBAK, T., ZHU, X., SHI, Y., SHENG, W., OLSSON, M., STEWART, J., GUSTAFSSON, C. & FALKENBERG, M. 2015. The exonuclease activity of DNA polymerase γ is required for ligation during mitochondrial DNA replication. *Nature Communications,* 6**,** 7303.

MACKENZIE, M. & RYAN, M. 2010. Assembly factors of human mitochondrial complex I and their defects in disease. *IUBMB Life,* 62.

MADSEN, K., BUCH, A., COHEN, B., FALK, M., GOLDSBERRY, A., GOLDSTEIN, A., KARAA, A., KOENIG, M., MURARESKU, C., MEYER, C., O'GRADY, M., SCAGLIA, F., SHIEH, P., VOCKLEY, J., ZOLKIPLI-CINNINGHAM, Z., HALLER, R. & VISSING, J. 2020. Safety and Efficacy of Omaveloxolone in Patients with Mitochondrial Myoptahy MOTOR Trial. *Neurology,* 94**,** e687-e698.

MAHAD, D., TRAPP, B. & LASSMANN, H. 2015. Pathological Mechanisms in Progressive Multiple Sclerosis. *Lancet Neurology,* 14**,** 183-193.

MAILLOUX, R. 2020. An Update on Mitochondrial Reactive Oxygen Species Production. *Antioxidants,* 9**,** 472.

MAN, P., GRIFFITHS, P. & CHINNERY, P. 2011. Mitochondrial Optic Neuropathies - Disease Mechanism and Therapeutic Strategies. *Progress in Retinal and Eye Research,* 30**,** 81-114.

MANWARING, N., JONES, M., WANG, J., ROCHTCHINA, E., HOWARD, C., MITCHELL, P. & SUE, C. 2007. Population Prevalence of the MELAS A3243G Mutation. *Mitochondrion,* 7**,** 230-233.

MARCHI, S., PATERGNANI, S., MISSIROLI, S., MORCIANO, G., RIMESSI, A., WEICKOWSKI, M., GIORGI, C. & PINTON, P. 2018. Mitochondrial and endoplasmic reticulum calcium homeostasis and cell death. *Cell Calcium,* 69**,** 62-72.

MARGULIS, L. 1971. SYMBIOSIS AND EVOLUTION. *Scientific American,* 225**,** 48-61.

MARROQUIN, L., HYNES, J., DYKENS, J., JAMIESON, J. & WILL, Y. 2007. Circumventing the Crabtree effect: Replacing Media Glucose with Galactose Increases Susceptibility of HepG2 cells to Mitochondrial Toxicants. *Toxicology Sciences,* 97**,** 539-547.

MARTIN, J., MAHLKE, K. & PFANNER, N. 1991. Role of an Energized Inner Membrane Mitochondrial Protein Import. *The Journal of Biological Chemistry,* 266**,** 18051-18057.

MARTIN, W., GARG, S. & ZIMORSKI, V. 2015. Endosymbiotic theories for eukaryote origin. *Philosophical Transactions of the Royal Society of London. Series B,* 370**,** 20140330.

MARTINELLI, P., MATTINA, V., BERNACCHIA, A., MAGNONI, R., CERRI, F., COX, G., QUATTRINI, A., CASARI, G. & RUGARLI, E. 2009. Genetic Interaction Between the m-AAAprotease Isoenzymes Reveals Novel Roles in Cerebellar Degeneration. *Human Molecular Genetics,* 18**,** 2001-2013.

MASTERS, B., STOHL, L. & CLAYTON, D. 1987. Yeast mitochondrial RNA polymerase is homologous to those encoded by bacteriophages T3 and T7. *Cell,* 51**,** 89-99.

MASUCCI, J., DAVIDSON, M., KOGA, Y., SCHON, E. & KING, M. 1995. In Vitro Analysis of Mutations Causing Myoclonus Epilepsy with Ragged-Reg Fibers in the Mitochondrial $tRNA^{Lys}$ Gene: Two Genotypes Produce Similar Phenotypes. *Molecular and Cellular Biology,* 15**,** 2872–2881.

MCCULLOCH, V., SEIDEL-ROGOL, B. & SHADEI, G. 2002. A Human Mitochondrial Transcription Factor Is Related to RNA Adenine Methyltransferases and Binds *S*-Adenosylmethionine. *Molecular and Cellular Biology,* 22**,** 1116-1125.

MCFARLAND, R. & TURNBULL, D. 2009. Batteries not Included: Diagnosis and Management of Mitochondrial Disease. *Journal of Internal Medicine,* 265**,** 210-228.

MCKENZIE, M., LIOLISTSA, D., AKINSHINA, B., CAMPANELLA, M., SISODIYA, S., HARGREAVES, I., NIRMALANANTHAN, N., SWEENEY, M., ABOU-SLEIMAN, P., WOOD, N., HANNA, M. & DUCHEN, M. 2007. Mitochondrial ND5 Gene Variation Associated with Encephalomyopathy and Mitochondrial ATP Consumption. *Journal of Biological Chemistry,* 282.

MCKENZIE, M. & RYAN, M. 2010. Assembly factors of human mitochondrial complex I and their defects in disease. *IUBMB Life,* 62.

MCMILLAN, R., STEWART, S., BUDNICK, J., CASWELL, C., HULVER, M., MUKHERJEE, K. & SRIVASTAVA, S. 2019. Quantitative Variation in m.3243A>G Mutation Produce Discrete Changes in Energy Metabolism. *Scientific Reports,* 9.

MCWILLIAMS, T., PRESCOTT, A., ALLEN, G., TAMJAR, J., MUNSON, M., THOMSON, C., MUQIT, M. & GANLEY, I. 2016a. *mito*-QC Illuminates Mitophagy and Mitochondrial Architecture *in vivo*. *Journal of Cell Biology,* 214**,** 333-345.

MCWILLIAMS, T. G., PRESCOTT, A. R., ALLEN, G. F. G., TAMJAR, J., MUNSON, M. J., THOMSON, C., MUQIT, M. M. K. & GANLEY, I. G. 2016b. mito-QC illuminates mitophagy and mitochondrial architecture in vivo. *The Journal of Cell Biology,* 214**,** 333-345.

MELSER, S., CHATELAIN, E., LAVIE, J., MAHFOUF, W., JOSE, C., OBRE, E., GOORDEN, S., PRIAULT, M., ELGERSMA, Y., REZVANI, H., ROSSIGNOL, R. & BENARD, G. 2013. Rheb Regulates Mitophagy Induced Mitochondrial Energetic Status. *Cell Metabolism,* 17**,** 719-730.

MERMIGKIS, C., BOULOUKAKI, I., MASTORODEMOS, V., A, P., ALOGDIANAKIS, V., SIAFAKAS, N. & SCHIZA, S. 2013. Medical Treatment with Thiamine, Coenzyme Q, Vitamins E and C and Carnitine Improved Obstructive Sleep Apnea in an Adult Case of Leigh Disease. *Sleep and Breathing,* 17**,** 1129-1135.

MESECKE, N., TERZIYSKA, N., KOZANY, C., BAUMANN, F. & NEUPERT, W. 2005. A disulphide relay system in the intermembrane space of mitochondria that mediates protein import. *Cell,* 121**,** 1059-1069.

MILEYKOVSKAYA, E. & DOWHAN, W. 2014. Cardiolipin-Dependent Formation of Mitochondrial respiratory Supercomplexes. *Chemistry and Physics of Lipids,* 179**,** 42-48.

MILLER, W. 1988. Molecular Biology of Steroid Hormone Synthesis. *Endocrine Reviews,* 9**,** 295-318.

MIMAKI, M., WANG, X., MCKENZIE, M., THORBURN, D. & RYAN, M. 2012. Understanding Mitochondrial Complex I Assembly in Health and Disease. *Biochimica et Biophysica Acta - Bioenergetics,* 1817**,** 851-862.

MINCZUK, M., PAPWORTH, M., KOLASINSKA, P., MURPHY, M. & KLUG, A. 2006. Sequence-specific Modification of Mitochondria DNA Using a Chimeric Zinc Finger Methylase. *PNAS,* 103**,** 19689-16694.

MINCZUK, M., PAPWORTH, M., MILLER, J., MURPHY, M. & KLUG, A. 2008. Development of a Single-chain, Quasi-dimeric Zinc-finger Nuclease for the Selective Degradation of Mutated Human Mitochondrial DNA. *Nucleic Acids Research,* 36**,** 3925-3938.

MIRALLES FUSTE, J., SHI, Y., ZHU, X. & JEMT, E. 2014. In vivo occupancy of mitochondrial single-stranded DNA binding protein supports the strand displacement mode of DNA replication. *PLOS Genetics,* 10**,** e1004832.

MIRSHAFIEY, A. & MOHSENZADEGAN, M. 2008. Antioxidant Therapy in Multiple Sclerosis. *Immunopharmacology and Immunotoxicology,* 2008.

MISHRA, P. & CHAN, D. 2014. Mitochondrial Dynamics and Inheritance During Cell Division, Development and Disease. *Nature Reviews Molecular Cell Biology,* 15**,** 634-646.

MITCHELL, A., JONES, A., MERCER, R. & RUCKER, R. 1999. Characterization of Pyrroloquinoline Quinone Amino Acid Derivatives by Electrospray Ionization Mass Spectrometry and Detection in Human Milk. *Analytical Biochemistry,* 269**,** 317-325.

MITRA, K., WUNDER, C., ROYSAM, B., LIN, G. & LIPPINCOTT-SCHWARTZ, J. 2009. A Hyperfused Mitochondrial State Achieved at G_1-S Regulates Cyclin E Buildup and Entry into S Phase. *PNAS,* 106**,** 11960-11965.

MOK, B., MORAES, M., ZENG, J., BOSCH, D., KOTRYS, A., RAGURAM, A., HSU, F., RADEY, M., PETERSON, B., MOOTHA, V., MOUGOUS, J. & LIU, D. 2020. A Bacterial Cytidine Deaminase Toxin Enables CRISPR-Free Mitochondrial Base Editing. *Nature,* 583**,** 631-637.

MONNOT, S., GIGAREL, N., SAMUELS, D., BURLET, P., HESTERS, L., FRYDMAN, N., FRYDMAN, R., KERBRAT, V., FUNALOT, B., MARTINOVIC, J., BENCH, A., FEINGOLD, J., MUNNICH, A., BONNEFONT, J. & STEFFANN, J. 2011. Segregation of mtDNA Throughout Human Embryofetal Development: m.3243A>G as a Model System. *Human Mutation,* 32**,** 116-125.

MORENO-ULLOA, A., CID, A., RUBI-GAYOSSO, I., CEBALLOS, G., VILLARREAL, F. & RAMIREZ-SANCHEZ, I. 2013. Effects of (−)-epicatechin and derivatives on nitric oxide mediated induction of mitochondrial proteins. *Bioorganic & Medicinal Chemistry Letters,* 23**,** 4441-4446.

MORGAN, S., GROOTENDORST, P., LEXCHIN, J., CUNNINGHAM, C. & GREYSON, D. 2011. The Cost of Drug Development: A Systematic Review. *Health Policy,* 100**,** 4-17.

MOT, A., LIDDELL, J., WHITE, A. & CROUCH, P. 2016. Circumventing the Crabtree Effect: A Method to Induce Lactate Consumption and Increase Oxidative Phosphorylation in Cell Culture. *The International Journal of Biochemistry and Cell Biology,* 79**,** 128-138.

MURARESKU, C., MCCORMICK, E. & FALK, M. 2018. Mitochondrial Disease: Advances in Clinical Diagnosis, Management, Therapeutic Development and Preventative Strategies. *Current Genetic Medicine Reports,* 6**,** 62-72.

MURPHY, M. 2008. How Mitochondria Produce Reactive Oxygen Species. *Biochemical Journal,* 417**,** 1-13.

MURPHY, M. 2013. Mitochondrial Dysfunction Indirectly Elevates ROS Production by the Endoplasmic Reticulum. *Cell Metabolism,* 18**,** 145-146.

NAON, D., ZANINELLO, M., GIACOMELLO, M., VARANITA, T., GRESPI, F., LAKSHMINARANAYAN, S., SERAFINI, A., SEMENZATO, M., HERKENNE, S., HERNANDEZ-ALVAREZ, M., ZORZANO, A., DE STEFANI, D., DORN, G. & SCORRANO, L. 2016. Critical reappraisal confirms that Mitofusin 2 is an endoplasmic reticulum-mitochondrial tether. *PNAS,* 113**,** 11249-11254.

NARESH, N. & HAYNES, C. 2019. Signalling and Regulation of the Mitochondrial Unfolded Protein Response. *Cold Spring Harbor Perspectives in Biology,* 11**,** a033944.

NEWELL, C., KHAN, A., SINASAC, D., SHOFFNER, J., FRIEDERICH, M., VAN HOVE, J., HUME, S., SHEARER, J. & SOSOVA, I. 2019. Hybrid Gel Electrophoresis Using Skin Fibroblasts to Aid in Diagnosing Mitochondrial Disease. *Nature Genetics,* 5**,** e336.

NEWMAN, J., GALNA, B., JAKOVLJEVIC, D., BATES, M., SCHAEFER, A., MCFARLAND, R., TURNBULL, D., TRENELL, M., TAYLOR, R., ROCHESTER, L. & GORMAN, G. 2015. Preliminary Evaluation of Clinician Rated Outcome Measure in Mitochondrial Disease. *Journal of Neuromuscular Diseases,* 2**,** 151-155.

NEYMOTIN, A., CALINGASAN, N., WILLE, E., NASERI, N., PETRI, S., DAMIANO, M., LIBY, K., RISINGSONG, R., SPORN, M., BEAL, M. F. & KIAEI, M. 2011. Neuroprotective effect of Nrf2/ARE Activators, CDDO-ethylamide and CDDO-trifluoroethylamide in a Mouse Model of Amyotrophic Lateral Sclerosis. *Free Radical Biology and Medicine,* 51**,** 88-96.

NG, Y., BINDOFF, L., GORMAN, G., KLOPSTOCK, T., KORNBLUM, C., MANCUSO, M., MCFARLAND, R., SUE, C., SUOMALAINEN, A., TAYLOR, R., THORBURN, D. & TURNBULL, D. 2021. Mitochondrial Disease in Adults: Recent Advances and Future Promise. *The Lancet Neurology,* 20**,** 573-584.

NG, Y. & TURNBULL, D. 2016. Mitochondrial Disease: Genetics and Management. *Journal of Neurology,* 263**,** 179-191.

NGU, L., LIJTMANS, L., DISTELMAIER, F., VENSELAAR, H., VRIES, S., BRAND, M., STOLTENBORG, B., WINTJES, L., WILLEMS, P., HEUVEL, L., SMEITINK, J. & RODENBURG, R. 2012. A Catalytic Defect in Mitochondrial Respiratory Chain Complex I due to a Mutation in NDUFS2 in a Patient With Leigh Syndrome. *Biochimica et Biophysica Acta - Molecular Basis of Disease,* 1822**,** 168-175.

NICHOLLS, T. & GUSTAFSSON, C. 2018. Separating and Segregating the Human Mitochondrial Genome. *Trends in Biochemical Sciences,* 43**,** 869-881.

NICHOLLS, T., NADALUTTI, C., MOTORI, E., SOMMERVILLE, E., GORMAN, G., BASU, S., HOBERY, E., TURNBULL, D., CHINNERY, P., LASSON, N., LARSSON, E., FALKENBERG, M., TAYLOR, R., GRIFFITH, J. & GUSTAFSSON, C. 2018. Topoisomerase 3**α is Required for Decatenation and Segregation of Human mtDNA**. *Molecular Cell,* 69**,** 9-23.e6.

NICKEL, C., HORNEFF, R., HEERMANN, R., NEUMANN, B., JUNG, K., SOLL, J. & SCHWENKERT, S. 2019. Phosphorylation of the outer membrane mitochondrial protein OM64 influences protein import into mitochondria. *Mitochondrion,* 44**,** 93-102.

NIEMAN, D., WILLIAMS, A., ANDREW, S., JIN, F., MCANULTY, S., TRIPLETT, T., AUSTIN, M. & HENSON, D. 2010. Quercetin's Influence on Exercise Performance and Muscle Mitochondrial Biogenesis. *Medicine and Science in Sports and Exercise,* 42**,** 338-345.

NILSSON, L., PETTERSEN, I., NIKOLAISEN, J., MICKLEM, D., DALE, H., RØSLAND, G., LORENS, J. & TRONSTAD, K. 2015. A new live-cell reporter strategy to simultaneously monitor mitochondrial biogenesis and morphology. *Scientific Reports,* 5**,** 17217.

NIMSE, S. & PAL, D. 2015. Free radicals, natural antioxidants, and their reaction mechanisms. *RSC Advances,* 5**,** 27986-28006.

NISOLI, E., CLEMENTI, E., PAOLUCCI, C., COZZI, V., TONELLO, C., SCIORATI, C., BRACALE, R., VALERIO, A., FRANCOLINI, M., MONCADA, S. & CARRUBA, M. 2003. Mitochondrial Biogenesis in Mammals: The Role of Endogenous Nitric Oxide. *Science,* 299**,** 896-899.

NISOLI, E., TONELLO, C., CARDILE, A., COZZI, V., BRACALE, R., TEDESCO, L., FALCONE, S., VALERIO, A., CANTONI, O., CLEMENTI, E., MONCADA, S. & CARRUBA, M. 2005. Calorie Restriction Promotes Mitochondrial Biogenesis by Inducing the Expression of eNOS. *Science Reports,* 310**,** 314-317.

NISSANKA, N. & MORAES, C. 2020. Mitochondrial DNA Heteroplasmy in Disease and Targeted Nuclease-Based Theraputics Approaches. *EMBO Reports,* 21**,** e49612.

NOGALES, E., LOUDER, R. & HE, Y. 2017. Structural Insights into the Eukaryotic Transcription Initiation Machinery. *Annual Review of Biophysics,* 46**,** 59-83.

NOGUEIRA, L., RAMIREZ‐SANCHEZ, I., PERKINS, G., MURPHY, A., TAUB, P., CEBALLOS, G., VILLARREAL, F., HOGAN, M. & MALEK, M. 2011. (–)‐Epicatechin enhances fatigue resistance and oxidative capacity in mouse muscle. *The Journal of Physiology,* 589.

NORTON, M., NG, A., BAIRD, S., DUMOULIN, A., SHUTT, T., MAH, N., ANDRADE-NAVARRO, M., MCBRIDE, H. & SCREATON, R. 2014. ROMO1 Is an Essential Redox-Dependent Regulator of Mitochondrial Dynamics. *Science Signalling,* 7**,** ra10.

NOUWS, J., NIJTMANS, L., SMEITINK, J. & VOGEL, R. 2012. Assembly Factors as a New Class of Disease Genes for Mitochondrial Complex I Deficiency: Cause, Pathology and Treatment Groups. *Brain,* 135**,** 12-22.

OGAWA, E., SHIMURA, M., FUSHIMI, T., TAJIKA, M., ICHIMOTO, K., MATSUNAGA, A., TSURUOKA, T., ISHIGE, M., FUCHIGAMI, T., YAMAZAKI, T., MORI, M., KOHDA, M., KISHITA, Y., OKAZAKI, Y., TAKAHASHI, S., OHTAKE, A. & MURAYAMA, K. 2017. Clinical validity of biochemical and molecular analysis in diagnosing Leigh Syndrome: a study of 106 Japanese patients. *Journal of Inherited Metabolic Disease,* 40**,** 685-693.

OHNISHI, T. 1998. Iron-Sulfur clusters/semiquinones in Complex I. *Biochimica et Biophysica Acta - Bioenergetics,* 1364**,** 186-206.

OKAMOTO, T. 2005. Safety of Quercetin for Clinical Application. *International Journal of Molecular Medicine,* 16**,** 275-278.

OKUNO, D., IINO, R. & NOJI, H. 2011. Rotation and structure of FoF1-ATP synthase. *The Journal of Biochemistry,* 149**,** 655-664.

OLIVEIRA, V., MOREIRA, G., BRESSAN, F., MARIANO, C., ROBALLO, K., CHARPENTIER, M., CONCORDET, J., MEIRELLES, F. & C, A. 2019. Edition of TFAM Gene by CRISPR/Cas9 Technology in Bovine Model. *PLOS ONE,* 14**,** e0213376.

ORDUREAU, A., SARRAF, S., DUDA, D., HEO, J., JEDRYCHOWSKI, M., SVIDERSKIY, V., OLSZEWSKI, J., KOERBER, J., XIE, T., BEAUSOLEIL, S., WELLS, J., GYGI, S., SCHULMAN, B. & HARPER, J. 2014. Quantitative proteomics reveal a feedforward mechanism for mitochondrial PARKIN translocation and ubiquitin chain synthesis. *Molecular Cell,* 56**,** 360-375.

ORTIZ-FLORES, M., PORTILLA-MARTINEZ, A., CABRERA-PEREZ, F., NAJERA, N., MEANEY, E., VILLARREAL, F., PEREZ-DURAN, J. & CEBALLOS, G. 2020. PXR is a Target of (-)-Epicatechin in Skeletal Muscle. *Heliyon,* 6**,** e05357.

OSMAN, C., VOELKER, D. & LANGER, T. 2011. Making heads or tails of phospholipids in mitochondria. *Journal of Cell Biology,* 192**,** 7-16.

OSTERMANN, J., HORWICH, A., NEUPERT, W. & HARTL, F. 1999. Protein folding in mitochondria requires complex formation with Hsp60 and ATP hydrolysis *Nature,* 34**,** 125-130.

PACHOLEC, M., BLEASDALE, J. E., CHRUNYK, B., CUNNINGHAM, D., FLYNN, D., GAROFALO, R. S., GRIFFITH, D., GRIFFOR, M., LOULAKIS, P., PABST, B., QIU, X., STOCKMAN, B., THANABAL, V., VARGHESE, A., WARD, J., WITHKA, J. & AHN, K. 2010. SRT1720, SRT2183, SRT1460, and Resveratrol Are Not Direct Activators of SIRT1. *Journal of Biological Chemistry,* 285**,** 8340-8351.

PAGNIEZ-MAMMERI, H., LOUBLIER, S., LEGRAND, A., BENIT, P., RUSTIN, P. & SLAMA, A. 2011. Mitochondrial Complex I Deficiency of Nuclear Origin I Structural Genes. *Molecular Genetics and Metabolism,* 105**,** 163-172.

PAILLUSSON, S., GOMEZ-SUAGA, P., STOICA, R., LITTLE, D., GISSEN, P., DEVINE, M., NOBLE, W., HANGER, D. & MILLER, C. 2017. α-Synuclein Binds to the ER-Mitochondrial Tethering Protein VAPB to Disrupt Ca 2^{+} Homeostasis and Mitochondrial ATP Production. *Acta Neuropathologica,* 134**,** 129-149.

PALIKARAS, K., LIONAKI, E. & TAVERNARAKIS, N. 2015. Balancing Mitochondrial Biogenesis and Mitophagy to Maintain Energy Metabolism Homeostasis. *Cell Death & Differentiation,* 22**,** 1399-1401.

PALIKARAS, K., LIONAKI, E. & TAVERNARAKIS, N. 2018. Mechanisms of mitophagy in cellular homeostasis, physiology and pathology. *Nature Cell Biology,* 20**,** 1013-1022.

PARADIES, G., PARADIES, V., BENEDICTIS, V., RUGGIERO, F. & PETROSILLO, G. 2014. Functional role of cardiolipin in mitochondrial bioenergetics. *Biochimica et Biophysica Acta - Bioenergetics,* 1837**,** 408-417.

PARIKH, S., KARAA, A., GOLDSTEIN, A., NG, Y., GORMAN, G., FEIGENBAUM, A., CHISTODOULOU, J., HAAS, R., TARNOPOLSKY, M., COHEN, B., DIMMOCK, D., FEYMA, T., KOENIG, M., MUNDY, H., NIYAZOV, D., SANETO, R., WAINWRIGHT, M., WUSTHOOF, C., MCFARLAND, R. & SCAGLIA, F. 2016. Solid Organ Transplantation in Primary Mitochondrial Disease: Proceed with Caution. *Molecular Genetics and Metabolism,* 118**,** 178-184.

PARIKH, S., SANETO, R., FALK, M., ANSELM, I., COHEN, B. & HAAS, R. 2013. A Modern Approach to the Treatment of Mitochondrial Disease. *Current Treatment Options in Neurology,* 11**,** 414-430.

PATEL, S., VELINGKAAR, N. & KONDRATOV, R. 2014. Transcriptional Clock of Antioxidant Defence by the Circadian Clock. *Antioxidant Redox Signalling,* 20**,** 2997-3006.

PAVLOVA, N. & THOMPSON, C. 2016. The Emerging Hallmarks of Cancer Metabolism. *Cell Metabolism,* 23**,** 27-47.

PAZ, M., COTAN, D., GARRIDO-MARAVER, J., CORDERO, M., OROPESA-AVILA, M., MATA, M., PAVON, A., LAVERA, I., ALCOCER-GOMEZ, E. & SANCHEZ-ALCAZAR, J. 2016. Targeting Autophagy and Mitophagy for Mitochondrial Diseases Treatment. *Expert Opinion on Therapeutic Targets,* 20**,** 487-500.

PEARCE, S., REBELO-GUIOMAR, P., D'SOUZA, A., POWELL, C., HAUTE, L. & MINCZUK, M. 2017. Regulation of Mammalian Mitochondrial Gene Expression: Recent Advances. *Trends in Biochemical Science,* 42**,** 625-639.

PEIXOTO DE BARCELOS, I., TROXELL, R. & GRAVES, J. 2019. Mitochondrial Dysfunction and Multiple Sclerosis. *Biology,* 8**,** 37.

PEREIRA, B., VIDEIERA, A. & DUARTE, M. 2013. Novel Insights into the Role of Neurospora crassa NDUFAF2, an Evolutionarily Conserved Mitochondrial Complex I Assembly Factor. *Molecular Cell Biology,* 33**,** 2623-2634.

PEREZ, R., BAFALUY, M., SILVA, P., LOSHUERTOS, R., MARTOS, A., BRUNO, C., MORAES, C. & ENRIQUEZ, J. 2004. Respiratory Complex III is Required to Maintain Complex I in Mammalian Mitochondria. *Molecular Cell,* 13**,** 805-815.

PFEIFFER, K., GOHIL, V., STUART, R., HUNTE, C., BRANDT, U., GREENBERG, M. & SCHAGGER, H. 2003. Cardiolipin Stabilizes Respiratory Chain Supercomplexes. *Journal of Biological Chemistry,* 278**,** 52873-52880.

PICHAUD, N., BÉRUBE, R., CÖTÉ, G., BELZILE, C., DUFRESNE, F., MORROW, G., TANGUAY, R., RAND, D. & BLIER, P. 2019. Age Dependent Dysfunction of Mitochondrial and ROS Metabolism Induced by Mitonuclear Mismatch. *Frontiers in Genetics,* 20**,** 130.

PIQUEREAU, J., BOET, A., PECHOUX, C., ANTIGNY, F., LAMBERT, M., GRESSETTE, M., RANCHOUX, B., GAMBARYAN, N., DOMERGUE, V., MUMBY, S., MONTANI, D., ADCOCK, I., HUMBERT, M., GARNIER, A., RUCKER-MARTIN, C. & PERROS, F. 2019. The BET Bromodomain Inhibitor I-BET-151 Induces Structural and Functional Alternation of the Heart Mitochondrial in Healthy Male Mice and Rats. *International Journal of Molecular Sciences,* 20**,** 1527.

PIRINEN, E., AURANEN, M., KHAN, N., BRILHANTE, V., URHO, N., PESSIA, A., HAKKARAINEN, A., KUULA, J., HEINONEN, U., SCHMIDT, M., HAIMILAHTI, K., PIIRILA, P., LUNDBOM, N., TASKINEN, M., BRENNER, C., VELAGAPUDI, V., PIETILAINEN, K. & SUOMALAINEN, A. 2020. Niacin Cures Systemic NAD^+ Deficiency and Improves Muscle Performance in Adult-Onset Mitochondrial Myopathy. *Cell Metabolism,* 31**,** 1078-1090.e5.

PLOUMI, C., DASKALAKI, I. & TAVERNARAKIS, N. 2017. Mitochondrial biogenesis and clearance: a balancing act. *The FEBS Journal,* 284**,** 183-195.

POTTER, M., NEWPORT, E. & MORTEN, K. 2016. The Warburg Effect: 80 Years on. *Biochemical Society Transactions,* 44**,** 1499-1505.

POWELKA, A., SETH, A., VIRBASIUS, J., KISKINIS, E., NICOLORO, S., GUILHERME, A., TANG, X., STRAUBHAAR, J., CHERNIACK, A., PARKER, M. & CZECH, M. 2006. Suppression of oxidative metabolism and mitochondrial biogenesis by the transcriptional corepressor RIP140 in mouse adipocytes. *The Journal of Clinical Investigation,* 116**,** 125-136.

PRNEWSWIRE. 2019. *Stealth BioTherapeutics Provides Update on Phase 3 Trial of Elamipretide in Primary Mitochondrial Myopathy* [Online]. Available: https://www.prnewswire.com/news-releases/stealth-biotherapeutics-provides-update-on-phase-3-trial-of-elamipretide-in-primary-mitochondrial-myopathy-300978082.html [Accessed].

PRUDENT, J. & MCBRIDE, H. 2016. Mitochondrial Dynamics: ER Actin Tightens the Drp1 Noose. *Current Biology,* 26**,** R207-R209.

QIAN, W., WANG, J., ROGINSKAYA, V., MCDERMOTT, L., EDWARDS, R., STOLZ, D., LAMB, F., GREEN, D. & HOUTEN, B. 2014. Novel Combination of Mitochondrial Division Inhibitor 1 (mdivi-1) and Platinum Agents Produces Synergistic Pre-Apoptotic Effect in Drug Resistant Tumour Cells. *Oncotarget,* 5**,** 4180-4194.

QUIROS, P., ESPANOL, Y., ACIN-PEREZ, R., RODRIGUEZ, F., BARCENA, C., WATANABE, K., CALVO, E., LOUREIRO, M., FERNANDEZ-GARCIA, M., FUEYO, A., VAZQUEZ, J., ENRIQUEZ, J. & LOPEZ-OTIN, C. 2014. ATP-Dependent Lon Protease Controls Tumor Bioenergetics by Reprogramming Mitochondrial Activity. *Cell Reports,* 8**,** 542-556.

RAFELSKI, S. 2013. Mitochondrial network morphology: building an integrative, geometrical view. *BMC Biology,* 11.

RAHMAN, J., NORONHA, A., THIELE, I. & RAHMAN, S. 2017. Leigh map: A Novel Computational Diagnostic Resource for Mitochondrial Disease. *Annals of Neurology,* 81**,** 9-16.

RAHMAN, S. 2020. Mitochondrial Disease in Children. *Journal of Internal Medicine,* 287**,** 609-633.

RAHMAN, S., BLOK, R., DAHL, H., DANKS, D., KIRBY, D., CHOW, C., CHRISTODOULOU, J. & THORBURN, D. 1996. Leigh Syndrome: Clinical Features and Biochemical and DNA Abnormalities. *Annals of Neurology,* 39.

RAI, P. 2017. *Development of Cell Based Assays to Discover Pharmacological Therapies for the Treatment of Mitochondrial Disease.* Doctor of Philosophy, Newcastle University.

RAI, P., RUSSELL, O., LIGHTOWLERS, R. & TURNBULL, D. 2015. Potential compounds for the treatment of mitochondrial disease. *British Molecular Bulletin,* 116**,** 5-18.

RAMPELT H, ZERBES, R., LAAN, M. & PFANNER, N. 2017. Role of the mitochondrial contact site and cristae organizing system in membrane architecture and dynamics. *Biochimica et Biophysica Acta - Molecular Cell Research,* 1864**,** 737-746.

RANIERI, M., BRAJKOVIC, S., RIBOLDI, G., RONCHI, D., RIZZO, F., BRESOLIN, N., CORTI, S. & COMI, G. 2013. Mitochondrial Fusion Proteins and Human Diseases. *Neurology Research International,* 2013.

RAO, N., FELTON, S., HUENNEKENS, F. & MACKLER, B. 1963. Flavin Mononucleotide: The Coenzyme of Reduced Diphosphopyridine Nucleotide Dehydrogenase. *The Journal of Biological Chemistry,* 238**,** 449-455.

RATH, S., STARMA, R., GUPTA, R., AST, T., CHAN, C., DURHAM, T., GOODMAN, R., GRABAREK, Z., HASS, M., HUNG, W., JOSHI, P., JOURDAIN, A., KIM, S., KOTRYS, A., LAM, S., MCCOY, J., MEISEL, J., MIRANDA, M., PANDA, A., PATGIRI, A., ROGERS, R., SADRE, S., SHAH, H., SKINNER, O., TO, T., MALKER, M., WANG, H., WARD, P., WENGROD, J., YUAN, C., CALVO, S. & MOOTHA, V. 2021. MitoCarta3.0: an updated mitochondrial proteome now with sub-organelle localization and pathway annotations. *Nucleic Acids Research,* 8**,** D1541-D1547.

RAYAMAJHI, N., KIM, S., GO, H., JOE, Y., CALLAWAY, Z., KANG, J., RYTER, S. & CHUNG, H. 2013. Quercetin Induces Mitochondrial Biogenesis Through Activation of HO-1 in HepG2 Cells. *Oxidate Medicine and Cellular Longevity,* 2013.

REDZA-DUTORDOIR, M. & AVERILL-BATES, D. 2016. Activation of apoptosis signalling pathways by reactive oxygen species. *Biochimica et Biophysica Acta - Molecular Cell Research,* 1863**,** 2977-2992.

REHLING, P., MODEL, K., BRANDER, K., KOVERMANN, P. & SICKMANN, A. 2003. Protein insertion into the mitochondrial inner membrane by twin-pore translocase. *Science,* 299**,** 1747-1751.

REISMAN, S., LEE, C., MEYER, C., PROKSCH, J. & WARD, K. 2014. Topical Application of the Synthetic Triterpenoid RTA 408 Activates NRF2 and Induces Cytoprotective Genes in Rat Skin. *Archives of Dermatological Research,* 306**,** 447-454.

RENDÓN, O. & SHOUBRIDGE, E. 2012. Early Complex I Assembly Defects Result in Rapid Turnover of the ND1 Subunit. *Human Molecular Genetics,* 21**,** 3815-3824.

REYNIER, P., MAY-PANLOUP, P., CHRETIEN, M., MORGAN, C., JEAN, M., SAVAGNER, F., BARRIERE, P. & MALTHIERY, Y. 2001. Mitochondrial DNA content affects the fertilisability of human oocytes. *Molecular Human Reproduction,* 7**,** 425-429.

RIEHLE, C. & ABEL, E. 2012. PGC-1 Proteins and Heart Failure. *Trends in Cardiovascular Medicine,* 22**,** 98-105.

ROBBERSON, D., KASAMATSU, H. & VINOGRAD, J. 1972. Replication of Mitochondrial DNA. Circular Replicative Intermediates in Mouse L Cells. *PNAS,* 69**,** 737-741.

ROBINSON, J., INMAN, L., SUMEGI, B. & SRERE, P. 1987. F**urther Characterization of the Krebs Tricaboxylic Acid Cycle Metabolon**. *The Journal of Biological Chemistry,* 262**,** 1786-1790.

ROCHA, A. & DANCIS, A. 2015. Life without Fe-S clusters. *Molecular Microbiology,* 99.

ROCHA, M., GRADY, J., GRÜNEWALD, A., VINCENT, A., DOBSON, P., TAYLOR, R., TURNBULL, D. & RYGIEL, K. 2015. A Novel Immunofluorescent Assay to Investigate Oxidative Phosphorylation Deficiency in Mitochondrial Myopathy: Understanding Mechanisms and Improving Diagnosis. *Scientific Reports,* 5**,** 15037.

ROCHA, M., ROSA, H., GRADY, J., BLAKELY, E., HE, L., ROMAIN, N., HALLER, R., NEWMAN, J., MCFARLAND, R., NG, Y., GORMAN, G., SCHAEFER, A., TUPPEN, H., TAYLOR, R. & TURNBULL, D. 2018. Pathological Mechanisms Underlying Single Large-Scale Mitochondrial DNA Deletions. *Annuals of Neurology,* 83**,** 115-130.

RODGERS, J., LERIN, C., HAAS, W., GYGI, S., SPIEGELMAN, B. & PUIGSERVER, P. 2005. Nutrient control of glucose homeostasis through a complex of PGC-1a and SIRT1. *Nature,* 434**,** 113-118.

RODNINA, M. 2018. Translation in Prokaryotes. *Cold Spring Harb Perspect Med,* 10.

ROGGE, M. 2009. The Role of Impaired Mitochondrial Lipid Oxidation in Obesity. *Biological Research for Nursing,* 10**,** 356-373.

ROJO, E., STUART, R. & NEUPERT, W. 1995. Conservative sorting of F0-ATPase subunit 9; export from matrix requires **ΔpH across inner membrane and matrix ATP**. *EMBO,* 14**,** 3445-3451.

ROODYN, D., REIS, P. & WORK, T. 1961. Protein synthesis in mitochondria. Requirements for the incorporation of radioactive amino acids into mitochondrial protein. *Biochemical Journal,* 80**,** 9-21.

ROSS, J. 2011. Visualization of Mitochondrial Respiratory Function Using Cytochrome C Oxidase/Succinate Dehydrogenase (COX/SDH) Double-labeling Histochemistry. *Journal of Visualized Experiments,* 57**,** 3266.

ROSSI, A., PIZZO, R. & FILED, R. 2019. Calcium, mitochondria and cell metabolism: A function triangle in bioenergetics. *Biochimica et Biophysica Acta (BBA)- Molecular Cell Research,* 1866**,** 1068-1078.

ROSSIGNOL, R., FAUSTIN, B., ROCHER, C., MALGAT, M., MAZAT, J. & LETELLIER, T. 2003. Mitochondrial Threshold Effects. *Biochemical Journal,* 370**,** 751-762.

ROUZIER, C., CHAUSSENOT, A., K, F., SERRE, V., MKADEM, S., RUCHELME, C., FLUCKINGER, V. & BANNWARTH, S. 2019. NDUFS6 Related Leigh Syndrome:A Case Report and Review of the Literature. *Journal of Human Genetics,* 64**,** 637-645.

RUDOLPH, G., DIMITRAIADIS, K., BUCHNER, B., HECK, S., AL-TAMAMI, J., SEIDENSTICKER, F., RUMMEY, C., LEINONEN, M., MEIER, T. & KLOPSTOCK, T. 2013. Effects of Idebenone on Colour Vision in Patients with Leber Hereditary Optic Neuropathy. *Journal of Neurology-Ophthalmology,* 33**,** 30-36.

RUEGSEGGER, G. & BOOTH, F. 2018. Health Benefits of Exercise. *Cold Spring Harbor Perspectives in Medicine,* 8**,** a029694.

RUSSELL, L., MANSFIELD, C., LEHMAN, J., KOVACS, A., COURTOIS, M., SAFFITZ, J., MEDEIROS, D., VALENCIK, M., MCDONALD, J. & KELLY, D. 2004. Cardiac-specific induction of the transcriptional coactivator peroxisome proliferator-activated receptor gamma coactivator-1alpha promotes mitochondrial biogenesis and reversible cardiomyopathy in a developmental stage-dependent manner. *Circulatory Research,* 94**,** 525-533.

RUSSELL, O. 2013. *Development and Discovery of Treatments for Mitochondrial Disease.* PhD, Newcastle University.

RUSSELL, O., GORMAN, G., LIGHTOWLERS, R. & TURNBULL, D. 2020. Mitochondrial Diseases: Hope for the Future. *Cell,* 181**,** 168-188.

RYGIEL, K., GRADY, J., TAYLOR, R., TUPPEN, H. & TURNBULL, D. 2015. Triplex real-time PCR–an improved method to detect a wide spectrum of mitochondrial DNA deletions in single cells. *Nature Scientific Reports,* 5.

RÖCKL, K., WITCZAK, C. & GOODYEAR, L. 2008. Signaling Mechanisms in Skeletal Muscle: Acute Responses and Chronic Adaptations to Exercise. *IUBMB Life,* 60**,** 145-153.

SABOUNY, R., FRAUNBERGER, E., GEOFFRION, M., NG, A., BAIRD, S., SCREATON, R., MILNE, R., MCBRIDE, H. & SHUTT, T. 2017. The Keap1-NRF2 Stress Response Pathway Promotes Mitochondrial Hyperfusion Through Degradation of the Mitochondrial Fission Protein Drp1. *Antioxidants & Redox Signaling,* 27.

SAIHARA, K., KAMIKUBO, R., IKEMOTO, K., UCHIDA, K. & AKAGAWA, M. 2017. Pyrroloquinoline Quinone, a Redox-Active o-Quinone, Stimulates Mitochondrial Biogenesis by Activating the SIRT1/PGC-1α Signaling Pathway. *Biochemistry,* 56**,** 6615-6625.

SAJISH, M. & SCHIMMEL, P. 2015. A human tRNA synthetase is a potent PARP1-activating effector target for resveratrol. *Nature,* 519**,** 370-373.

SALLEVELT, S., DREESEN, J., DRUSEDAU, M., SPIRITS, S., COONEN, E., TIENEN, F., GOLDE, R., COO, I., GERADETS, J., DIE-SMULDERS, C. & SMEETS, H. 2013. Preimplantation Genetic Diagnosis in Mitochondrial DNA Disorders: Challenge and Success. *Journal of Medical Genetics,* 50**,** 125-132.

SALMA, N., SONG, J., ARANY, Z. & FISHER, D. 2015. Transcription Factor Tfe3 Directly Regulates Pgc-1alpha in Muscle. *Journal of Cellular Physiology,* 230**,** 2330-2336.

SANCAK, Y., MARKHARD, A., KITAMI, T., KOVACS-BOGDAN, E., KAMER, K., UDESHI, N., CARR, S., CHAUDHURI, D., CLAPHAM, D., LI, A., CALVO, S., GOLDBERGER, O. & MOOTHA, V. 2013. EMRE is an Essential Component of the Mitochondrial Calcium Uniporter Complex. *Science,* 342**,** 1379-1382.

SANDERS, C., TURKARSIAN, S., LEE, D. & DALDAL, F. 2010. Cytochrome c biogenesis: the Ccm system. *Trends in Microbiology,* 18**,** 266-274.

SANDERSON, J. 2006. The Steroid Hormone Biosynthesis Pathway as a Target for Endocrine-Distrupting Chemicals. *Toxicological Sciences,* 94**,** 3-21.

SANDOVAL, H., THIAGARAJAN, P., DASGUPTA, S., SCHUMACHER, A., PRCHAL, J., CHEN, M. & WANG, J. 2008. Essential role for NIX in autophagy maturation of erythroid cells. *Nature,* 454**,** 232-235.

SARKAR, N. 1997. Polyadenylation of mRNA in Prokaryotes. *Annual Review of Biochemistry,* 66**,** 173-197.

SASAKI, K., SAKAMOTO, S., UCHIDA, H., NARUMOTO, S., SHIGETA, T., FUKUDA, A., ITO, R., IRIE, R., YOSHIOKA, T., MURAYAMA, K. & KASAHARA, M. 2017. Liver Transplantation for Mitochondrial Respiratory Chain Disorder: A Single-Centre Experience and Excellent Marker of Differential Diagnosis. *Transplant Proceedings,* 49**,** 1097-1102.

SCADUTO, R. & GROTYOHANN, L. 1999. Measurement of mitochondrial membrane potential using fluorescent rhodamine derivatives. *Biophysical Journal,* 76**,** 469-477.

SCARPULLA, R. 2002. Nuclear activators and coactivators in mammalian mitochondrial biogenesis. *Biochem Biophys Acta,* 1576**,** 1-14.

SCARPULLA, R. 2008. Transcriptional Paradigms in Mammalian Mitochondrial Biogenesis and Function. *Physiol Rev,* 88**,** 611-638.

SCARPULLA, R., VEGA, R. & KELLY, D. 2012. Transcriptional integration of mitochondrial biogenesis. *Trends Endocrinol Metab,* 23**,** 459-466.

SCHAEFER, A., MCFARLAND, R., BLAKELY, E., HE, L., WHITTAER, R., TAYLOR, R., CHINNERY, P. & TURNBULL, D. 2008. Prevalence of Mitochondrial DNA Disease in Adults. *Annals of Neurology,* 63**,** 35-39.

SCHAEFER, A., PHOENIX, C., ELSON, J., MCFARLAND, R., CHINNERY, P. & TURNBULL, D. 2006. Mitochondrial Disease in Adults: A Scale to Monitor Progression and Treatment. *Neurology,* 66**,** 1932-1934.

SCHAEFER, A., WALKER, M., TURNBULL, D. & TAYLOR, R. 2013. Endocrine Disorders in Mitochondrial Disease. *Molecular and Cellular Endocrinology,* 379**,** 2-11.

SCHAFER, E., SEELERT, H., REIFSCHNEIDER, N., KRAUSE, F., DENCHER, N. & VONCK, J. 2006. Architecture of Active Mammalian Respiratory Chain Supercomplexes. *Journal of Biological Chemistry,* 281**,** 15370-15375.

SCHAGGER, H. & PFEIFFER, K. 2000. Supercomplexes in the Respiratory Chains of Yeast and Mammalian Mitochondria. *EMBO J,* 19**,** 1777-1783.

SCHENKEL , L. & BAKOVIC, M. 2014. Formation and Regulation of Mitochondrial Membranes. *International Journal of Cell Biology,* 2014.

SCHIEKE, S., PHILLIPS, D., JR, P. M., APONTE, A., SHEN, R.-F., BALABAN, R. & FINKEL, T. 2006. The Mammalian Target of Rapamycin (mTOR) Pathway Regulates Mitochondrial Oxygen Consumption and Oxidative Capacity. *The Journal of Biological Chemistry,* 281**,** 27643-27652.

SCHON, E., DIMAURO, S., HIRANO, M. & GILKERSON, R. 2010. Therapeutic prospects for mitochondrial disease. *Trends in Molecular Medicine,* 16**,** 268-276.

SCHON, E. & MANFREDI, G. 2003. Neuronal Degeneration and Mitochondrial Dysfunction. *The Journal of Clinical Investigation,* 111**,** 303-312.

SCHON, E., RIZZUTO, R., MORAES, C., NAKASE, H., ZEVIANI, M. & DIMAURO, S. 1989. A Direct Repeat is a Hotspot for Large-Scale Deletions in Human Mitochondrial DNA. *Science,* 244**,** 346-349.

SCHON, K., RATNAIKE, T., AMEELE, J., HORVATH, R. & CHINNERY, P. 2020. Mitochondrial Diseases: A Diagnostic Revolution. *Trends in Genetics,* 36.

SCHREIBER, S., EMTER, R., HOCK, B., KNUTTI, D., CARDENAS, J., PODVINEC, M., OAKELEY, E. & KRALLI, A. 2004. The estrogen-related receptor α (ERRα) functions in PPAR coactivator 1α (PGC-1α)-induced mitochondrial biogenesis. *PNAS,* 101**,** 6472-6477.

SCHROEDER, M., ATHERTON, H., BALL, D., COLE, M., HEATHER, L., GRIFFIN, J., CLARKE, K., RADDA, G. & TYLER, D. 2009. Real-time assessment of Krebs cycle metabolism using hyperpolarized 13 C magnetic resonance spectroscopy. *FASEB,* 23**,** 2529-2538.

SCHWARZ, N., BLAHNIK, Z., PRAHADEESWARAN, S., MCKINLEY-BARNARD, S., HOLDEN, S. & WALDHELM, A. 2018. (-)-Epicatechin Supplementation Inhibits Aerobic Adaptations to Cycling Exercise in Humans. *Frontiers in Nutrition,* 5**,** 132.

SCORRANO, L., ASHIYA, M., BUTTLE, K., WEILER, S., OAKES, S., MANNELLA, C. & KORSMEYER, S. 2002. A Distinct Pathway Remodels Mitochondrial Cristae and Mobilises Cytochrome C During Apoptosis. *Developmental Cell,* 2.

SEARS, I., MACGINNITIE, M., KOVACS, L. & GRAVES, R. 1996. Differentiation-dependent expression of the brown adipocyte uncapping protein gene: regulation by peroxisome proliferator-activated receptor gamma. *American Society for Microbiology,* 16.

SEKINE, S. & YOULE, R. 2018. PINK1 import regulation; a fine system to convey mitochondrial stress to the cytosol. *BMC Biology,* 16.

SETH, A., STEEL, J., NICHOL, D., POCOCK, V., KUMARAN, M., FRITAH, A., MOBBERLEY, M., RYDER, T., ROWLERSON, A., SCOTT, J., POUTANEN, M., WHITE, R. & PARKER, M. 2007. The Transcriptional Corepressor RIP140 Regulates Oxidative Metabolism in Skeletal Muscle. *Cell Metabolism,* 6**,** 236-245.

SGARBI, G., BARACCA, A., LENAZ, G., VALENTINO, L., CARELLI, V. & SOLAINI, G. 2006. Inefficient Coupling Between Proton Transport and ATP Synthesis May Be the Pathogenic Mechanism for NARP and Leigh Syndrome Resulting Form the T8993G Mutation in mtDNA. *Biochemical Journal,* 395**,** 493-500.

SHARMA, L., TIWARI, M., RAI, N. & BAI, Y. 2019. Mitophagy Activation Repairs Leber's Hereditary Optic Neuropathy-Associated Mitochondrial Dysfunction and Improves Cell Survival. *Human Molecular Genetics,* 28**,** 422-433.

SHARMA, M., KOC, E., DATTA, P., BOOTH, T., SPREMULLI, L. & AGRAWAL, R. 2003. Structure of the Mammalian Mitochondrial Ribosome Reveals an Expanded Function Role for Its Component Proteins. *Cell,* 115**,** 97-108.

SHIMIZU, H., SCHREDELSEKER, J., HUANG, J., LU, K., NAGHDI, S., LU, F., FRANKLIN, S., FIJI, H., WANG, K., ZHU, H., TIAN, C., LIN, B., NAKANO, H., EHRLICH, A., NAKAI, J., STEIG, A., GIMZEWSKI, J., NAKANO, A., GOLDHABER, J., VONDRISKA, T., HAJNOCZKY, G., KWON, O. & CHEN, J. 2015. Mitochondrial Ca^{2+} Uptake by the Voltage Dependent Anion Channel 2 Regulates Cardiac Rhythmicity. *eLife***,** e04801.

SHIRIHAI, O., SONG, M. & DORN, G. 2015. How Mitochondrial Dynamism Orchestrates Mitophagy. *Circulation Research,* 116**,** 1835-1849.

SHOFFNER, J., LOTT, M., LEZZA, A., SEIBEL, P., BALLINGER, S. & WALLACE, D. 1990. Myoclonic Epilepsy and Ragged-Red Fiber Disease (MERRF) Is Associated with a Mitochondrial DNA $tRNA^{Lys}$ Mutation. *Cell,* 61**,** 931-937.

SHOFFNER, J. & WALLACE, D. 1992. Mitochondrial Genetics: Principles and Practice. *American Journal of Human Genetics,* 51**,** 1179-1186.

SHOSHAN-BARMATZ, V., DE PINTO, V., ZWECKSTETTER, M., RAVIV, Z., KEINAN, N. & ARBEL, N. 2010. VDAC, a multi-function mitochondrial protein regulating cell life and death. *Molecular Aspects of Medicine,* 31.

SHUTT, T. & GRAY, M. 2006. Bacteriophage origins of mitochondrial replication and transcription proteins. *Trends in Genetics,* 22**,** 90-95.

SIGNES, A. & FERNANDEZ-VIZARRA, E. 2018. Assembly of Mammalian Oxidative Phosphorylation Complexes I-V and Supercomplexes. *Essays in Biochemistry,* 62**,** 255-270.

SILVA-PINHEIRO, P., CERUTTI, R., LUNA-SANCHEZ, M., ZEVIANI, M. & VISCOMI, C. 2020. A Single Intravenous Injection of AAV-PHP.B-*hNDUFS4* Ameliorates the Phenotype of *NDUFS4*$^{-/-}$ Mice. *Molecular Therapy: Methods & Clinical Development,* 17**,** 1071-1078.

SMEETS, H., SALLEVELT, S., DREESEN, J., DIE-SMULDERS, C. & COO, I. 2015. Preventing the Transmission of Mitochondrial DNA Disorders Using Prenatal or Preimplantation Genetic Diagnosis. *Annals of the New York Academy of Sciences,* 1350**,** 29-36.

SOFOU, K., COO, I., ISOHANNI, P., OSTERGAARD, E., NAESS, K., MEIRLEIR, L., TZOULIS, C., UUSIMAA, J., ANGST, I., LONNQVIST, T., PIHKO, H., MANKINEN, K., BINDOFF, L., TULINIUS, M. & DARIN, N. 2014. A Multicenter Study on Leigh Syndrome: Disease Course and Predictors of Survival. *Orphanet Journal of Rare Diseases,* 9.

SOLMAZ, S. & HUNTE, C. 2008. Structure of Complex III with Bound Cytochrome c in Reduced State and Definition of a Minimal Core Interface for Electron Transfer. *The Journal of Biological Chemistry,* 283**,** 17542-17549.

SONG, Z., GHOCHANI, M., MCCAFFERY, J., FREY, T. & CHAN, D. 2009. Mitofusins and POA1 mediate sequential steps in mitochondrial membrane fusion. *Molecular Biology of the Cell,* 20**,** 3525-3532.

SPIKES, T., MONTGOMERY, M. & WALKER, J. 2020. Structure of the dimeric ATP Synthase from Bovine Mitochondria. *PNAS***,** 202013998.

SRIVASTAVA, S. 2017. The Mitochondrial Basis of Aging and Age-Related Disorders. *Genes (Basel),* 8**,** 398.

ST-PIERRE, J., DRORI, S., ULDRY, M., SILVAGGI, J., RHEE, J., JÄGER, S., HANDSCHIN, C., ZHENG, K., LIN, J., YANG, W., SIMON, D., BACHOO, R. & SPIEGELMAN, B. 2006. Suppression of Reactive Oxygen Species and Neurodegeneration by the PGC-1 Transcriptional Coactivators. *Cell,* 127**,** 397-408.

STEELE, H., HORVATH, R., LYON, J. & CHINNERY, P. 2017. Monitoring Clinical Progression with Mitochondrial Disease Biomarkers. *Brain,* 140**,** 2530-2540.

STEFELY, J. & PAGLIARINI, D. 2017. Biochemistry of Mitochondrial Coenzyme Q Biosynthesis. *Trends in Biochemical Sciences,* 42**,** 824-843.

STEPHAN T, ROESCH, A., RIEDEL, D. & JAKOBS, S. 2019. Live-cell STED Nanoscopy of Mitochondrial Cristae. *Scientific Reports,* 9.

STEPHAN, T., ROESCH, A., RIEDEL, D. & JAKOBS, S. 2019. Live-cell STED Nanoscopy of Mitochondrial Cristae. *Scientific Reports,* 9.

STOICA, R., VOS, K., PAILLUSSON, S., MUELLER, S., SANCHO, R., LAU, K., VIZCAY-BARRENA, G., LIN, W., XU, Y., LEWIS, J., DICKSON, D., PETRUCELLI , L., MITCHELL, J., SHAW, C. & MILLER, C. 2014. ER-Mitochondrial Associations are Regulated by the VAPB-PTPIP51 Interaction and are Disrupted by ALS/FTD-Associated TDP-43. *Nature Communications,* 3**,** 3996.

STRAUSS, M., HOFHAUS, G., SCHRODER, R. & KUHLBRANDT, W. 2008. Dimer Ribbons of ATP Synthase Shape the Inner Mitochondrial Membrane. *EMBO J,* 27**,** 1154-1160.

STROUD, D., SURGENOR, E., FORMOSA, L., RELJIC, B., FRAZIER, A., DIBLEY, M., OSELLAME, L., STAIT, T., BEILHARZ, T., THORBURN, D., SALIM, A. & RYAN, M. 2016. Accessory subunits are integral for assembly and function of human mitochondrial complex I. *Nature,* 538**,** 123-126.

SUKHORUKOV, V., DIKVO, D., REICHERT, A. & MEYER-HERMANN, M. 2012. Emergence of the Mitochondrial Reticulum from Fission and Fusion Dynamics. *PLOS Computational Biology,* 8**,** e1002745.

SUTOVSKY, P., MORENO, R., RAMALHO-SANTOS, J., DOMINKO, T., SIMPLY, C. & SCHATTEN, G. 1999. Ubiquitin Tag for Sperm Mitochondria. *Nature,* 402**,** 371-372.

SWALWELL, H., KIRBY, S., BLAKELY, E., MITCHELL, A., SALEMI, R., SUGIANA, C., COMPTON, A., TUCKER, E., KE, B., LAMONT, P., TURNBULL, D., MCFARLAND, R., TAYLOR, R. & THORBURN, D. 2011. Respiratory Chain Complex I Deficiency Caused by Mitochondrial DNA Mutations. *European Journal of Human Genetics,* 19**,** 769-775.

SWINDELLS, N., WHITE, P. & FINDLAY, J. 1978. The X-ray crystal structure of rapamycin, C51H79NO13. *Canadian Journal of Chemistry,* 56**,** 2491-2492.

SZCZEPANOWSKA, J., MALINSKA, D., WIECKOWSKI, M. & DUSZYNSKI, J. 2012. Effect of mtDNA Point Mutations on Cellular Bioenergetics. *Biochimica et Biophysica Acta - Bioenergetics,* 1817**,** 1740-1746.

SÁNCHEZ-CABALLERO, L., GUERRERO-CASTILLO, S. & NIJTMANS, L. 2016. Unraveling the Complexity of Mitochondrial Complex I Assembly: A Dynamic Process. *Biochimica et Biophysica Acta,* 1857**,** 980-990.

TAANMAN, J., BODNAR, A., COOPER, J., MORRIS, A., CLAYTON, P., LEONARD, J. & SCHAPIRA, A. 1997. Molecular Mechanisms in Mitochondrial DNA Depletion Syndrome. *Human Molecular Genetics,* 6**,** 935-942.

TAIVASSALO, T., SHOUBRIDGE, E., CHEN, J., KENNAWAY, N., DIMAURO, S., ARNOLD, D. & HALLER, R. 2001. Aerobic Conditioning in Patients with Mitochondrial Myopathies: Physiological, Biochemical and Genetic Effects. *Annals of Neurology,* 50**,** 133-141.

TAKAHASHI, M., CHESLEY, A., FREYSSENET, D. & HOOD, D. 1998. Contractile Activity-Induced Adaptations in the Mitochondrial Protein Import System. *American Journal of Physiology Cell Physiology,* 274**,** C1380-C1387.

TAKEBE, T., IMAI, R. & ONO, S. 2018. The Current Status of Drug Discovery and Development as Originated in United States Academia: The Influence of Industrial and Academic Collaboration on Drug Discovery and Development. *Clinical and Translational Science,* 11**,** 597-606.

TANIDA, I., UENO, T. & KOMINAMI, E. 2004. LC3 Conjugation System in Mammalian Autophagy. *The International Journal of Biochemistry and Cell Biology,* 36**,** 2503-2518.

TANIDA, I., UENO, T. & KOMINAMI, E. 2008. *LC3 and Autophagy*, Humana Press.

TATSUTA, T. & LANGER, T. 2009. AAA Proteases in Mitochondria: Diverse Function of Membrane-Bound Proteolytic Machines. *Research in Microbiology,* 160**,** 711-717.

TAUBER, J., DLASKOVA, A., SANTOROVA, J., SMOLKOVA, K., ALAN, L., SPACEK, T., PLECITA-HLAVATA, L., JABUREK, M. & JEZEK, P. 2013. Distribution of mitochondrial nucleoids upon mitochondrial network fragmentation and network reintegration in HEPG2 cells. *The International Journal of Biochemistry & Cell Biology,* 45**,** 593-603.

TEMPERLEY, R., WYDRO, M., LIGHTOWLERS, R. & CHRZANOWSKA-LIGHTOWLERS, Z. 2010. Human mitochondrial mRNAs—like members of all families, similar but different. *Biochimica et Biophysica Acta,* 1797**,** 1081-1085.

TENENBAUM, A., MOTRO, M. & FISMAN, E. 2005. Dual and pan-peroxisome proliferator-activated receptors (PPAR) co-agonism: the bezafibrate lessons. *Cardiovascular Diabetology,* 4.

TERRITO, P., MOOTHA, V., FRENCH, S. & BALABAN, R. 2000. Ca^{2+} activation of heart mitochondrial oxidative phosphorylation: role of the F_0/F_1-ATPase. *Cell Physiology,* 278.

THANNICKAL, V. & FANBURG, B. 2000. Reactive Oxygen Species in Cell Signaling. *American Journal of Physiology,* 279**,** 1005-1028.

THORBURN, D., RAHMAN, J. & RAHMAN, S. 2003. *Mitochondrial DNA-Associated Leigh Syndrome and NARP* [Online]. Seattle (WA): University of Washington. Available: https://www.ncbi.nlm.nih.gov/books/NBK1173/ [Accessed June 2020].

TITRANTI, V., SAVOIA, A., FORTI, F., D'APOLITO, M.-F., CENTRA, M., ROCCHI, M. & ZEVIANI, M. 1997. Identification of the Gene Encoding the Human Mitochondrial RNA Polymerase (h-mtRPOL) by Cyberscreening of the Expressed Sequence Tags Database. *Human Molecular Genetics,* 6**,** 615-625.

TOMÉ-CARNEIRO, J., LARROSA, M., GONZÁLEZ-SARRÍAS, A., TOMÁS-BARBERÁN, F., GARCÍA-CONESA, M. T. & ESPÍN, J. C. 2013. Resveratrol and Clinical Trials: The Crossroad from In Vitro Studies to Human Evidence. *Current Pharmaceutical Design,* 19**,** 6040-6093.

TRIFUNOVIC, A., WREDENBERG, A., FALKENBERG, M., SPELBRINK, J., ROVIO, A., BRUDER, C., BOHLOOLY-Y, M., GIDLOF, S., OLDFORS, A., WIBOM, R., TORNELL, J., JACOBS, H. & LARSSON, N. 2004. Premature Ageing In Mice Expressing Defective Mitochondrial DNA Polymerase. *Nature,* 429**,** 417-423.

TSUKIHARA, T., AOYAMA, H., YAMASHITA, E., TOMIZAKI, T., YAMAGUCHI, H., SHINZAWA-ITOH, K., NAKASHIMA, R., YAONO, R. & YOSHIKAWA, S. 1996. The whole structure of the 13-subunit oxidised cytochrome c oxidase at 2.8 A. *Science,* 272**,** 1136-1144.

TUFEKCI, K., BAYIN, E., GENC, S. & GENC, K. 2011. The Nrf2/ARE Pathway: A Promising Target to Counteract Mitochondrial Dysfunction in Parkinson's Disease. *Mitochondria and Parkinson's Disease,* 2011.

TUPPEN, H., HOGAN, V., HE, L., BLAKELY, E., WORGAN, L., AL-DOSARY, M., SARETZKI, G., ALSTON, C., MORRIS, A., CLARKE, M., JONES, S., DEVLIN, A., MANSOUR, S., CHRZANOWSKA-LIGHTOWLERS, Z., THORBURN, D., MCFARLAND, R. & TAYLOR, R. 2010. The p.M292T NDUFS2 mutation causes complex I-deficient Leigh syndrome in multiple families. *Brain,* 133**,** 2952-2963.

TWIG, G. & SHIRIHAI, O. 2011. The Interplay Between Mitochondrial Dynamics and Mitophagy. *Antioxidants and Redox Signalling,* 116**,** 1835-1849.

TYYNISMAA, H., MJOSUND, K., WANROOIJ, S., ILSE, L., YLIKALLIO, E., JALANKO, A., SPELBRINK, J., PAETAU, A. & SUOMALANINEN, A. 2005. Mutant Mitochondrial Helicase Twinkle Causes Multiple mtDNA Deletions and Late-Onset Mitochondrial Disease in Mice. *PNAS,* 102**,** 17687-17692.

TZOULIS, C., NECKELMANN, G., MORK, S., ENGELSEN, B., VISCOMI, C., MOEN, G., ERSLAND, L., ZEVIANI, M. & BINDOFF, L. 2010. Localised Cerebral Energy Failure in DNA Polymerase Gamma-Associated Encephalopathy Syndromes. *Brain,* 133**,** 1428-1437.

VARANITA, T., SORIANO, M., ROMANELLO, V., ZAGLIA, T., CABRERA, R., SEMENZATO, M., MENABO, R., COSTA, V., CIVILETTO, G., PESCE, P., VISCOMI, C., ZEVIANI, M., LISA, F., MONGILLO, M., SANDRI,

M. & SCORRANO, L. 2015. The OPA1-dependent Mitochondrial Cristae Remodelling Pathway Controls Atrophic, Apoptotic and Ischemic Tissue Damage. *Cell Metabolism,* 21**,** 834-844.

VAZQUEZ, A. 2018. *Overflow Metabolism: From Yeast to Marathon Runners,* Academic Press.

VERHAAK, C., LAAT, P., KOENE, S., TIBOSCH, M., RODENBURG, R., GROOT, I., KNOOP, H., JANSSEN, M. & SMEITINK, J. 2016. Quality of Life, Fatigue and Mental Health in Patients with the m.3243A>G Mutation and its Correlates with Genetic Characteristics and Disease Manifestation. *Orphanet Journal of Rare Diseases,* 11.

VERMULST, M., WANAGAT, J., KUJOTH, G., BIELAS, J., RABINOVITCH, P., PROLLA, T. & LOEB, L. 2008. DNA Deletions and Clonal Mutations Drive Premature Aging in Mitochondrial Mutator Mice. *Nature Genetics,* 40**,** 392-394.

VINCENT, A., ROSA, H., PABIS, K., LAWLESS, C., CHEN, C., GRUNEWALD, A., RYGIEL, K., ROCHA, M., REEVE, A., FALKOUS, G., PERISSI, V., WHITE, K., DAVEY, T., PETROF, B., SAYER, A., COOPER, C., DEEHAN, D., TAYLOR, R., TURNBULL, D. & PICARD, M. 2018. Subcellular Origin of Mitochondrial DNA Deletions in Human Skeletal Muscle. *Annals of Neurology,* 84**,** 289-301.

VISCOMI, C., BOTTANI, E., CIVILETTO, G., CERUTTI, R., MOGGIO, M., FAGIOLARI, G., SCHON, E., LAMPERTI, C. & ZEVIANI, M. 2011. In Vivo Correction of COX Deficiency by Activation of the AMPK/PGC-1α Axis. *Cell Metabolism,* 14**,** 80-90.

VOGEL, F., BORNHOVD, C., NEUPUERT, W. & REICHERT, S. 2006. Dynamic subcompartmentalization of the mitochondrial inner membrane. *Journal of Cell Biology,* 175**,** 237-247.

VOGEL, R., DIETEREN, C., HEUVEL, L., WILLEMS, P., SMEITINK, J., KOOPMAN, W. & NIJTMANS, L. 2007. Identification of Mitochondrial Complex I Assembly Intermediates by Tracing Tagged NDUFS3 Demonstrates the Entry Point of Mitochondrial Subunits. *Journal of Biological Chemistry,* 282**,** 7582-7590.

VÉZINA, C., KUDELSKI, A. & SEHGAL, S. 1975. Rapamycin (AY-22,989), a new antifungal antibiotic. I. Taxonomy of the producing streptomycete and isolation of the active principle. *J Antibiot,* 28**,** 721-726.

WAI, T., TEOLI, D. & SHOUBRIDGE, E. 2008. The Mitochondrial DNA Genetic Bottleneck Results from Replication of a Subpopulation of Genomes. *Nature Genetics,* 40**,** 1484-1488.

WALLACE, D. 2012. Mitochondria and Cancer. *Nature Reviews Cancer,* 12**,** 685-698.

WALLACE, D., FAN, W. & PROCACCIO, V. 2010. Mitochondrial energetics and therapeutics. *Annu Rev Pathol,* 5**,** 297–348.

WALLACE, D., SINGH, G., LOTT, M., HODGE, J., SCHURR, T., LEZZA, A., ELSAS, L. & NIKOSKELAINEN, E. 1988. Mitochondrial DNA Mutation Associated with Leber's Hereditary Optic Neuropathy. *Science,* 242**,** 1427-1430.

WANG, C. & YOULE, R. 2016. The Role of Mitochondria in Apoptosis. *Annual Review of Genetics,* 43**,** 95-118.

WANG, K., LIU, R., LI, J., MAO, J., LEI, Y., WU, J., ZENG, J., ZHANG, T., WU, H., CHEN, L., HUANG, C. & WEI, Y. 2011a. Quercetin Induces Protective Autophagy in Gastic Cancer Cells: Involvement of Akt-mTOR and Hypoxia-Induced Factor 1-Alpha-Mediated Signalling. *Autophagy,* 7**,** 966-978.

WANG, W., YANG, B., QU, Y., LIU, X. & SU, W. 2011b. FeS/S/FeS(2) redox system and its oxidoreductase-like chemistry in the iron-sulphur world. *Astrobiology,* 11**,** 471-476.

WATT, I., MONTGOMERY, M., RUNSWICK, M., LESLIE, A. & WALKER, J. 2010. Bioenergetic cost of making an adenosine triphosphate molecule in animal mitochondria. *PNAS,* 107**,** 16823-16827.

WEDATILAKE, Y., BROWN, R., MCFARLAND, R., YAPLITO-LEE, J., MORRIS, A., CHAMPION, M., JARDINE, P., CLARKE, A., THORBURN, D., TAYLOR, R., LAND, J., FORREST, K., DOBBIE, A., SIMMONS, L., AASHEIM, E., KETTERIDIGE, D., HANRAHAN, D., CHAKRAPANI, A., BROWN, G. & RAHMAN, S. 2013. SURF1 Deficiency: A Multi-Centre Natural History Study. *Orphanet Journal of Rare Diseases,* 8.

WEI, W. & CHINNERY, P. 2020. Inheritance of mitochondrial DNA in humans: implications for rare and common diseases. *Journal of Internal Medicine,* 287**,** 634-644.

WEI, W., TUNA, S., KEOGH, M., SMITH, K., AITMAN, T., BEALES, P., BENNET, D., GALE, D., BITNER-GLINDZICZ, M., BLACK, G., BRENNAN, P., ELLIOTT, P., FLINTER, F., FLOTO, R., HOULDEN, H., IRVING, M., KOZIELL, A., MAHER, E., MARKUS, H., MORRELL, N., NEWMAN, W., ROBERTS, I., SAYER, J., SMITH, K., TAYLOR, J., WATKINS, H., WEBSTER, A., WILKIE, A., WILLIAMSON, C.,

DISEASES, N. B.-R., 100, G. P.-R. D. P., ASHFORD, S., PENKETT, C., STIRRUPS, K., RENDON, A., OUWEHAND, W., BRADLEY, J., RAYMOND, F., CAULFIELD, M., TURRO, E. & CHINNERY, P. 2019. Germline Selection Shapes Human Mitochondrial DNA Diversity. *Science,* 364.

WEIL, B., ABARBANELL, A., HERRMANN, J., WANG, Y. & MELDRUM, D. 2009. High Glucose Concentration in Cell Culture Medium does not Acutely Affect Human Mesenchymal Stem Cell Growth Factor Production of Proliferation. *American Journal of Physiology. Regulatory, integrative and comparative physiology.,* 296**,** R1735-1743.

WEINDRUCH, R. & SOHAL, R. 1997. Caloric Intake and Aging. *The New England Journal of Medicine,* 337**,** 986-994.

WEINER, J., LAMBERT, A., THURM, C., HALL, M., SOSLOW, J., REIMSCHISEL, Y., BEARL, D., DODD, D., FEINGOLD, B. & GODOWN, J. 2020. Heart Transplantation in Children with Mitochondrial Disease. *The Journal of Pediatrics,* 217**,** 46-51.e4.

WIEDEMANN, N. & PFANNER, N. 2017. Mitochondrial Machineries for Protein Import and Assembly. *Annual Review of Biochemistry,* 86**,** 685-714.

WIEDEMANN, N., PFANNER, N. & RYAN, M. 2001. The the modules of ADP/ATP carrier cooperate in receptor recruitment and translocation into mitochondria. *EMBO J,* 20**,** 951-960.

WIKSTROM, J., TWIG, G. & SHIRIHAI, O. 2009. What an mitochondrial heterogeneity tell us about mitochondrial dynamics and autophagy? *The International Journal of Biochemistry & Cell Biology,* 41**,** 1914-1927.

WILKINS, H., CARL, S. & SWERDLOW, R. 2014. Cytoplasmic Hybrid (Cybrid) Cell Liunes as a Practical Model for Mitochondriopathies. *Redox Biology,* 2**,** 619-631.

WILLIS, S., FLETCHER, J., KAUFMANN, T., DELFT, M., CHEN, L., CRABOTAR, P., IERINO, H., LEE, E., FAIRLIE, W., BOUILLET, P., STRASSER, A., KLUCK, R., ADAMS, J. & HUANG, D. 2007. Apoptosis Initiated When BH3 Ligands Engage Multiple Bcl-2 Homologs, Not Bax or Bak. *Science,* 315**,** 856-859.

WIRTH, C., BRANDT, U., HUNTE, C. & ZICKERMANN, V. 2016. Structure and function of mitochondrial complex I. *Biochimica et Biophysica Acta,* 1857**,** 902-914.

WITTE, M., NIJLAND, P., DREXHAGE, J., GERRITSEN, W., GEERTS, D., HET HOF, B., REIJERKERK, A., VRIES, H., VALK, P. & HORSSEN, J. 2013. Reduced Expression of PGC-1 α partly underlies mitochondrial changes and correlates with neuronal loss in multiple sclerosis cortex. *Acta Neuropathology,* 125**,** 231-243.

WOLF, D., SEGAWA, M., KONDADI, A., ANAND, R., BAILEY, S., REICHERT, A., BLIEK, A., SHACKELFORD, D., LIESA, M. & SHIRIHAI, O. 2019. Individual cristae within the same mitochondrion display different membrane potentials and are functionally independent. *EMBO,* 38**,** e 101056.

WRIGHT, C., FITZPATRICK, D. & FIRTH, H. 2018. Paediatric Genomics: Diagnosing Rare Disease in Children. *Nature Reviews Genetics,* 19**,** 253-268.

WU, H., KANATOUS, S., THURMOND, F., GALLARDO, T., ISOTANI, E., BASSEL-DUBY, R. & WILLIAMS, R. 2002. Regulation of Mitochondrial Biogenesis in Skeletal Muscle by CaMK. *Science,* 296.

XIA, D., YU, C., XIA, J., KACHURIN, A., ZHANG, L., YU, L. & DIESENHOFER, J. 1997. Crystal structure of the cytochrome bc1 complex from bovine heart mitochondria. *Science,* 277**,** 60-66.

YAMAMOTO, H., WILLIAMS, E., MOUCHIROUD, L., CANTÓ, C., FAN, W., DOWNES, M., HÉLIGON, C., BARISH, G., DESVERGNE, B., EVANS, R., SCHOONJANS, K. & AUWERX, J. 2011. NCoR1 Is a Conserved Physiological Modulator of Muscle Mass and Oxidative Function. *Cell,* 147**,** 827-839.

YANG, S., MA, S., WAN, X., HE, H., PEI, H., ZHAO, M., CHEN, C., WANG, D., DONG, X., YUAN, J. & LI, B. 2016. Long-term Outcomes of Gene Therapy for the Treatment of Leber's Hereditary. *EBioMedicine,* 10**,** 258-268.

YARIBEYGI, H., ATKIN, S. & SAHEBKAR, A. 2018. Mitochondrial Dysfunction in Diabetes and the Regulatory Roles of Antidiabetic Agents on the Mitochondrial Function. *Journal of Cellular Physiology,* 234**,** 8402-8410.

YASUKAWA, T., SUZUKI, T., ISHII, N., OHTA, S. & WATANABE, K. 2001. Wobble Modification Defect in tRNA Disturbs Codon-Anticodon Interaction in a Mitochondrial Disease. *EMBO J,* 20**,** 4794-4802.

YATSUGA, S. & SUOMALAINEN, A. 2011. Effect of bezafibrate treatment on late-onset mitochondrial myopathy in mice. *Human Molecular Genetics,* 21**,** 526–535.

YIN, X., LANZA, I., SWAIN, J., SARR, M., NAIR, S. & JENSEN, M. 2014. Adipocyte Mitochondrial Function is Reduced in Human Obesity Independent of Fat Cell Size. *The Journal of Clinical Endocrinology and Metabolism,* 99**,** E209-E216.

YOULE, R. & BLIEK, A. V. D. 2012. Mitochondrial Fission, Fusion, and Stress. *Science,* 337**,** 1062-1065.

YU, S. 2003. Na^+, K^+-ATPase: The New Face of an Old Player in Pathogenesis and Apoptotic/Hybrid Cell Death. *Biochemical Pharmacology,* 66**,** 1601-1609.

YU, X., XU, Y., ZHANG, S., SUN, J., LIU, P., XIAO, L., TANG, Y., LIU, L. & YAO, P. 2016. Quercetin Attenuates Chronic Ethanol-Induced Hepatic Mitochondrial Damage Through Enhanced Mitophagy. *Nutrients,* 8.

ZAHEDI, M., GHIASVAND, R., FEIZI, A., ASGARI, G. & DARVISH, L. 2013. Does Quercetin Improve Cardiovascular Risk Factors and Inflammatory Biomarkers in Women with Type 2 Diabetes: A Double-Blind Randomised Controlled Clinical Trial. *International Journal of Preventative Medicine,* 4**,** 777-785.

ZHANG, J., GUO, J., FANG, W., JUN, Q. & SHI, K. 2015a. Clinical Features of MELAS and its Relation with A3243G Gene Point Mutation. *International Journal of Clinical and Experimental Pathology,* 8**,** 13411-13415.

ZHANG, J., MERUVU, S., BEDI, Y. S., CHAU, J., ARGUELLES, A., RUCKER, R. & CHOUDHURY, M. 2015b. Pyrroloquinoline quinone increases the expression and activity of Sirt1 and -3 genes in HepG2 cells. *Nutrition Research,* 35**,** 844-849.

ZHANG, M., ZHENG, J., NUSSINOV, R. & MA, B. 2017a. Release of Cytochrome C from Bad Pores at the Mitochondrial Membrane. *Nature Scientific Reports,* 7.

ZHANG, P., LEHMANN, B., SAMUELS, D., ZHAO, S., ZHAO, Y.-Y., SHYR, Y. & GUO, Y. 2017b. Estimating relative mitochondrial DNA copy number using high throughput sequencing data. *Genomics,* 109**,** 457-462.

ZHANG, T., XUE, L., LI, L., TANG, C., WAN, Z., WANG, R., TAN, J., TAN, Y., HAN, H., TIAN, R., BILLIAR, T., TAO, W. & ZHANG, Z. 2016. BNIP3 Protein Suppresses PINK1 Kinase Proteolytic Cleavage to Promote Mitophagy. *Journal of Biological Chemistry,* 291**,** 21616-21629.

ZHANG, Y. & MARTIN, S. G. 2014. Redox Proteins and Radiotherapy. *Clinical oncology.,* 26**,** 289-300.

ZHAO, Z. & PU, Y. 2019. Lixisenatide enhances mitochondrial biogenesis and function throughregulating the CREB/PGC-1a pathway. *Biochemical and Biophysical Research Communications,* 508**,** 1120-1125.

ZHOU, J., LI, G., ZHENG, Y., SHEN, H., HU, X., MING, Q., HUANG, C., LI, P. & GAO, N. 2015. A novel autophagy/mitochagy inhibitor liensinine sensitises great cancer cells to chemotherapy through DNM1L-mediated mitochondrial fission. *Autophagy,* 11**,** 1259-1279.

ZHU, J., WANG, K. & CHU, C. 2013. After the Banquet: Mitochondrial Biogenesis, Mitophagy and Cell Survival. *Autophagy,* 9**,** 1663-1676.

ZINSER, E., SPERKA-GOTTLIEB, C., FASCH, E., KOHLWEIN, S., PALTAUF, F. & DAUM, G. 1991. Phospholipid Synthesis and Lipid Composition of Subcellular Membranes in the Unicellular Eukaryote *Saccharomyces cerevisiae*. *Journal of Bacteriology,* 173**,** 2026-2034.

ZORKAU, M., ALBUS, C., BERLINGUER-PALMINI, R., CHRZANOWSKA-LIGHTOWLERS, Z. & LIGHTOWLERS, R. 2021. High-Resolution Imaging Reveals Compartmentalisation of Mitochondrial Protein Synthesis in Cultured Human Cells. *PNAS,* 118**,** e2008778118.

ZOROV, D., JUHASZOVA, M. & SOLLOTT, S. 2014. Mitochondrial Reactive Oxygen Species (ROS) and ROS-Induced ROS Release. *Physiological Reviews,* 94**,** 909-950.